DOTTORATO DI RICERCA IN INGEGNERIA GEOTECNICA

Consorzio tra:
Università di Napoli Federico II, Università di Napoli Parthenope, Seconda Università di Napoli, Università di Salerno, Università del Sannio

DOTTORATO DI RICERCA IN
INGEGNERIA GEOTECNICA (XXVI CICLO)

An Innovative Ground Treatment Approach for Seismic Risk Mitigation of Existing Structures

A thesis submitted for the degree of Dottore di Ricerca

Ph. D. Student:
Daniele Lombardi

tutor:
prof. Alessandro Flora

co-tutor:
prof. Francesco Silvestri

Odio gli indifferenti. Credo che vivere voglia dire essere partigiani. Chi vive veramente non può non essere cittadino e partigiano. L’indifferenza è abulia, è parassitismo, è vigliaccheria, non è vita. Perciò odio gli indifferenti. L’indifferenza è il peso morto della storia.

L’indifferenza opera potentemente nella storia. Opera passivamente, ma opera. È la fatalità; è ciò su cui non si può contare; è ciò che sconvolge i programmi, che rovescia i piani meglio costruiti; è la materia bruta che strozza l’intelligenza. Ciò che succede, il male che si abbatte su tutti, avviene perché la massa degli uomini abdica alla sua volontà, lascia promulgare le leggi che solo la rivolta potrà abrogare, lascia salire al potere uomini che poi solo un ammutinamento potrà rovesciare. Tra l’assenteismo e l’indifferenza poche mani, non sorvegliate da alcun controllo, tessono la tela della vita collettiva, e la massa ignora, perché non se ne preoccupa; e allora sembra sia la fatalità a travolgere tutto e tutti, sembra che la storia non sia altro che un enorme fenomeno naturale, un’eruzione, un terremoto del quale rimangono vittime tutti, chi ha voluto e chi non ha voluto, chi sapeva e chi non sapeva, chi era stato attivo e chi indifferente. Alcuni piagnucolano pietosamente, altri bestemmiano oscenamente, ma nessuno o pochi si domandano: se avessi fatto anch’io il mio dovere, se avessi cercato di far valere la mia volontà, sarebbe successo ciò che è successo? Odio gli indifferenti anche per questo: perché mi dà fastidio il loro piagnisteo da eterni innocenti. Chiedo conto a ognuno di loro del come ha svolto il compito che la vita gli ha posto e gli pone quotidianamente, di ciò che ha fatto e specialmente di ciò che non ha fatto. E sento di poter essere inesorabile, di non dover sprecare la mia pietà, di non dover spartire con loro le mie lacrime. Sono partigiano, vivo, sento nelle coscienze della mia parte già pulsare l’attività della città future che la mia parte sta costruendo. E in essa la catena sociale non pesa su pochi, in essa ogni cosa che succede non è dovuta al caso, alla fatalità, ma è intelligente opera dei cittadini. Non c’è in essa nessuno che stia alla finestra a guardare mentre i pochi si sacrificano, si svenano. Vivo, sono partigiano. Perciò odio chi non parteggia, odio gli indifferenti.

I hate the indifferent. I believe that living means taking sides. Those who really live cannot help being a citizen and a partisan. Indifference and apathy are parasitism, perversion, not life. That is why I hate the indifferent. The indifference is the deadweight of history. The indifference operates with great power on history. The indifference operates passively, but it operates. It is fate, that which cannot be counted on. It twists programs and ruins the best-conceived plans. It is the raw material that ruins intelligence. That what happens, the evil that weighs upon all, happens because the human mass abdicates to their will; allows laws to be promulgated that only the revolt could nullify, and leaves men that only a mutiny will be able to overthrow to achieve the power. The mass ignores because it is careless and then it seems like it is the product of fate that runs over everything and everyone: the one who consents as well as the one who dissents; the one who knew as well as the one who didn’t know; the active as well as the indifferent. Some whimper piously, others curse obscenely, but nobody, or very few ask themselves: If I had tried to impose my will, would this have happened? I also hate the indifferent because of that: because their whimpering of eternally innocent ones annoys me. I make each one liable: how they have tackled with the task that life has given and gives them every day, what have they done, and especially, what they have not done. And I feel I have the right to be inexorable and not squander my compassion, of not sharing my tears with them. I am a partisan, I am alive, I feel the pulse of the activity of the future city that those on my side are building is alive in their conscience. And in it, the social chain does not rest on a few; nothing of what happens in it is a matter of luck, nor the product of fate, but the intelligent work of the citizens. Nobody in it is looking from the window of the sacrifice and the drain of a few. Alive, I am a partisan. That is why I hate the ones that don’t take sides, I hate the indifferent.

Antonio Gramsci, 11th February 1917

Summary

1. Introduction 3
  1.1. Historical examples 5
  1.2. Modern examples 10
  1.3. Idea and objectives 11
  1.4. Waves in an infinite, homogeneous, isotropic, elastic medium 28
  1.5. Basic waves properties 35
  1.6. Elastic waves approaching discontinuity surfaces 39
  1.7. Phenomena of stress waves attenuation 45
  1.8. Seismic site response 49
  1.9. Synthetic parameters used to describe the results 58
  1.10. References 62
2. Dynamic Analyses 68
  2.1. Input motions 68
    2.1.1. Natural signals 68
    2.1.2. Risker Wavelets 71
  2.2. 1D Analyses 73
    2.2.1. Introduction to 1D Analyses 73
    2.2.2. First 1D analyses on soil column 80
  2.3. Dynamic 2D analyses 105
    2.3.1. Description of the numerical modelling 105
    2.3.2. Preliminary 2D analyses with vertical and horizontal diaphragms 112
    2.3.3. Soft Caisson: rectangular section 127
    2.3.4. Soft Caisson: inclined injections 193
  2.4. References 224
3. Static analyses 226
  3.1. Characteristics of the software Plaxis2D 226
    3.1.1. 1st phase: input 226
    3.1.2. 2nd phase: calculation 228
    3.1.3. 3rd phase: output results 228
    3.1.4. Geometrical configurations 230
    3.1.5. Effect of the treatment on the ultimate load value 246
  3.2. References 249
4. Laboratory tests 250
  4.1. Laboratory activity on a polyurethane foam 251
  4.2. Laboratory activity on a Super Absorbent Polymer (SAP) 253
    4.2.1. Tests on Sand 253
    4.2.2. Tests on Poly (acrylic acid) partial sodium salt (SAP) 262
    4.2.3. References 277
5. Results and future perspectives 278
  5.1. Dynamic Analyses 278
    5.1.1. 1D analyses 278
    5.1.2. 2D analyses 279
  5.2. Static analyses 282
  5.3. Laboratory activity 283
  5.4. Final Considerations 284
List of Symbols 286

1. Introduction

This thesis focuses on an innovative approach to deal with one of the biggest challenges for civil engineers, i.e. the seismic risk (R).

The seismic risk can be formally defined as:

$$R = H \cdot V \cdot E \tag{1.1}$$

where:

- H is called hazard, that is the probability of exceedance of a given level of a selected strong ground motion parameter in a given time interval;
- V is the vulnerability, that is the probability of exceeding a given damage level due to the occurrence of a given ground motion level;
- E is the exposure, a qualitative and quantitative estimation of the elements at risk.

In time, a certain number of techniques have been developed to tackle seismic risk out, with reference both to existing and new buildings.

In principle, risk mitigation can be attempted using two different approaches: lowering the site-specific hazard, or reducing the vulnerability. The former option (lowering the hazard) corresponds to limiting the external action (i.e. the so called "demand"), the latter to increasing the "capacity" of the structure. Theoretically, the two approaches should be joined in order to obtain the best possible mitigation effect (Dolce, 2010).

Indeed, in the geotechnical field, the first strategy is possible and currently pursued when facing those natural hazards, like slope instability, for which the probability of happening of a critical natural mechanism can be reduced by designing stabilization interventions, such as drainages, supporting structures, etc..

Dealing with seismic hazard, common sense suggests that there is nothing that the technical community can do to reduce it, and so it is widely accepted that the mitigation of seismic risk cannot be carried out without reducing the building vulnerability through structural reinforcement. Nowadays, for instance, it is common practice on new buildings to design seismic resistant structures or, marginally, to use specific structural elements to protect them from seismic shaking (seismic isolators) and to the damp the incoming energy (seismic dampers). For existing structures, the seismic resistance can be enhanced with specific structural strengthening interventions, whose effectiveness however is still a matter of concern. Sometimes, superficial grouting to strengthen the soil is carried out too (e.g. Lirer et al., 2006), but its effectiveness in seismic isolation is difficult to assess (Lombardi et al., 2012, 2013). Furthermore, for buildings of historical or architectonical relevance, which poses tighter constraints to seismic upgrading design (caused by the need to respect their formal and material integrity), structural strengthening cannot be considered satisfactory, the building possibly needing to be preserved as it is. As a consequence, the increase of structural capacity cannot be pursued for such cases.

As it is formulated, seismic risk mitigation for existing buildings, especially if historically or artistically relevant, seems a problem which allows no completely satisfactory solution.

This thesis presents an innovative research activity in progress at the University of Napoli Federico II (Italy), conceived to overcome this apparent lack of solution. The idea is to concentrate the seismic protection in the subsoil, far enough from the structure to be protected, using a suitable grout to attenuate site seismic amplification. Actually, the soil plays, when overpassed by a seismic wave, a relevant role in defining the characteristics of the ground surface motion (Kramer, 1996) and so our research is basically thought to investigate the way in which the site amplification can be varied by discrete modifications into the soil.

In the following chapters, our original approach will be described in detail.

1. In the first chapter, some literature examples of alternative systems based on passive seismic protection, i.e. systems that do not provide any form of energy to the structure to defend, will be shown, with short descriptions on their functionality and features. In the same chapter, the general purposes of seismic wave transmission trough soil layers will be described, with specific remarks on phenomena of reflection, refraction and diffraction (scattering).
2. In the second chapter, some observations will be made on 1D propagation waves through a discontinuity at a certain position into an infinite bar; such observations are outstanding to recognise the whole phenomenon. In this chapter some examples will be reported of 1D propagation scheme, useful to understand some important features by propagating through certain treated and untreated soil columns both accelerograms and wavelets. In the second chapter, the propagation schemes will be extended to 2D analyses too, considering treatments with different geometrical features: soft caissons with a rectangular section or made by inclined injections into soil layers.
3. In the third chapter, the static consequences of the proposed soil treatment will be described; some considerations will be made on the static interaction between the

maximum displacements compatible with the presence of a structure at the ground level with the use of this kind of mitigation system.

4. In the fourth chapter, the involved laboratory activity will be described; some results on a polyurethanic foam and a super adsorbent polymer will be shown in order to individuate a material useful for the soft grout.
5. In the fifth chapter, some synthetic considerations will be reported on the thesis activities and its developments, with a view on the obtained results and the future advances.

1.1. Historical examples.

Recent earthquakes like those occurred in Haiti in 2010 (316000 fatalities) or in the Northern Sumatra in 2004 (227898 fatalities) or in the region of Wenchuan in 2008 (87587 fatalities) (United States Geological Survey's Largest and Deadliest Earthquakes by Year 1990 - 2011 USGS http://earthquake.usgs.gov/earthquakes/eqarchives/year/byyear.php) have reminded us of the cruel power of earthquakes, above all when these events happen in urban cities where fragile buildings and infrastructure prevail, with the consequence of inevitable severe devastation and high death tolls. This is remarkable in the case both of developing countries, where in the past decades an important urbanization has commonly occurred with the breakdown of the rural economy and the consequential migration of rural population to urban areas (Lovisolo, 2006), and in historical centres, where the seismic vulnerability is due to the absence of well-known anti-seismic strategies on the existing structures.

Both recently and in the past, entire societies and their progress have been influenced by important crisis due to damages caused by earthquakes. Actually, historical researches and archaeological campaigns, have shown (Giovannardi, 2013; Naderzadeh, 2009) that ancient civilizations had well-known the necessity to construct structures able to resist to earthquakes. The intuition of our ancestors and the experimental observations of observed collapses make them sensitive to features to be useful in preventing great damages on buildings. Without any scientific knowledge on structural and geotechnical aspects, they understood that a feasible solution was possible regarding the composition of the structure, but also the foundation soil, with an astonishing first preliminary approach to the concepts of isolation and ductility. The buildings of many ancient civilizations, mostly those with important social features, have survived to several earthquakes because their builders understood the importance of incorporating "elements" that had the function to mitigate the effects produced by earthquakes.

In the ancient Crete (2000 to 1200 BC), for example, archaeologists have discovered symmetrical buildings with walls made of stone blocks connected by wooden elements with the aim to ensure the connection between the blocks and to provide plasticity to the whole structure, compensating, at the same time, the fragility of the stone. The buildings were also placed on a layer of sand and loose gravel, for levelling the irregularities of the ground surface and for filtering soil vibrations during the earthquakes.

According to the archaeologist Carl Blegen, in the construction of the great walls of Troy (1500 BC), a layer of compacted ground was deliberately left under the foundations of the great wall between the ground and the rock foundation base, with similarities with the technique used, more than a thousand years later, in the three Doric temples of Paestum (273 BC; see Figure 1.1.1a), whose foundations are separated from the underneath rock by a layer of sand.

In the ancient Greece and Persia, builders commonly interposed, between the soil and the foundations of temples, some layers of material useful to allow the translation of the building with respect to the underneath layer during an earthquake. In some cases, a stratum of lead had been placed under the columns; in other cases, the walls foundations were put on layers of ceramic and clay, where the ceramic layer was used to protect clay from moisture and de-hydration, maintaining over time the plastic properties and the high plasticity of the clay useful for damping the vibration of the ground during an earthquake.

Another example of a pre-scientific seismic isolation system consists in placing between the foundation and the masonry structure a horizontal joint made of mortar and sand, to let the building slip. A similar method, with a foundation composed of several layers of smoothed rocks, has been discovered in the Mausoleum of Cyrus the Great in Pasargadae (Saiful Islam, 2011), shown in Figure 1.1.1b, southeast Iran , built in 550 BC. Similar considerations can be made for the Parthenon, where metallic connections had been placed between the elements of the tall columns.

(a)

(b)

Figure 1.1.1 *Temple of Cerere in Paestum (a) and mausoleum of Cyrus the Great in Pasargadae (b).*

There is a thought-provoking citation from Pliny the Elder in his “Naturalis Historia”, since it is the only classical source in which the use of a seismic device is explicitly mentioned in antiquity.

Pliny the Elder has actually reported an example of a sort of isolation system for the Diana Temple of Ephesus (see Figures 1.1.2):

“Graecae magnificentiae vera admiratio exstat templum Ephesiae Dianae CXX annis factum a tota Asia. In solo id palustri fecere, ne terrae motus sentiret aut hiatus timeret, rursus ne in lubrico atque instabili fundamenta tantae molis locarentur, calcatis ea substravere carbonicus, dein velleribus lanae.”

“The temple of Diana at Ephesus, which still exists, is an example of the Greek grandiosity, which is worthy of the authentic wonder. Its construction has engaged all Asia for 120 years. It was built it in a marshy area, because it does not suffer earthquakes or fear cracks in the soil; on the other hand, because they did not want that the foundation of such an impressive building was posed on a soil deposit so slippery and unstable, a layer of fragments of coal and another of fleeces of wool was placed under it.”

Figures 1.1.2 *Temple of Diana at Ephesus.*

The Buddhist temple in Sanjusangendo (Kyoto) (see Figures 1.1.4), founded in 1164, is another example of pre-scientific anti-seismic application. It holds 1001 gold-plated statues, and these statues, with the entire temple, have survived without excessive ruptures to incredibly strong earthquakes, like the earthquake of Hyogoken-Nambu (1995) when only some damages to four statues were observed. In this structure, a trellis of beams connects the wooden pillars and the spread footing is founded on a compacted soil made of alternated layers of sand and clay to guarantee respectively stiffness and damping.

Figure 1.1.4 *Buddhist temple in Sanjusangendo (Kyoto).*

In modern times, the first patent linked to a seismic isolation system was made in 1870 by Jules Touaillon (see Figure 1.1.5), with spherical roller bearings in special niches between the superstructure and foundation, facilitating the return to the initial position by the elliptical geometry of the housing system , but without any practical real application.

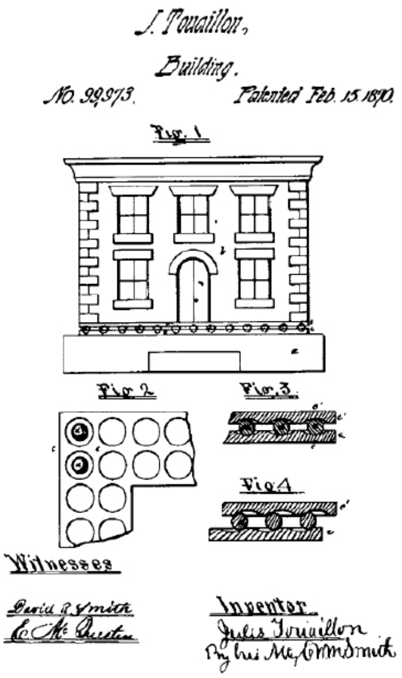

Figure 1.1.5 *First idea in the field of seismic isolation (Jules Touaillon, 1870).*

Generally speaking, research in the field of seismic isolation has then continued by referring the methodology to structural elements, concentrating all modifications into the structures of either the over-structure or the foundation, without any variation of the undelaying soil.

The first researcher that had rediscovered the idea to use soft ground layers as a cushion to tackle the effects of the earthquake was Frank Lloyd Wright, who applied this concept to the design of the Imperial Hotel in Tokyo. The site had rather unfavourable geological characteristics: a layer of 18 ÷ 20m of muddy silts below a compacted surface layer only 2.5m thick.

The architect used the layer of silt as "a good cushion to relieve the terrible shocks", above which the building would behave "as a battleship floats on water" (Walker, 1982). Actually, the structure famously survived the Great Kantō earthquake of 1923 (7.9 on the Moment magnitude scale, M_W), but one of the building's critical issue was indeed its foundation. Wright had intended the hotel to float on the site's alluvial mud; this was accomplished by making it shallow, with broad footings, supposing that a similar system should allow the building to float during an earthquake. However, the foundation was an inadequate support and did nothing to prevent the building from sinking into the mud to such a magnitude that it had to be demolished decades later. This example is indicative of a fact: it should be given a great importance to the seismic adequacy without forgetting the relevance of the static performance.

1.2. **Modern examples.**

In recent years, a number of techniques have been developed in time to deal with seismic hazard both with reference to existing or new buildings.

As far as the latter are concerned, structural engineers, as previously reported, have nowadays developed refined technical elements to protect structures from seismic shaking (for example seismic isolators and dampers), able to dissipate most of the seismic energy, thus preserving the structure. Geotechnical engineers have also developed new analytical approaches to design shallow and deep foundations taking into account the kinematic and inertial effects of the seismic action (Gazetas, 1991), thus giving a relevant contribution to a safe and reliable design of seismic resistant structures. As a consequence, with reference to new structures, there certainly exist a number of reliable solutions, currently adopted in practice, to tackle seismic hazard.

On the contrary, the seismic protection of existing buildings, which have not been designed following the latest refined dynamic or pseudo-static approaches, is still a matter of great concern for geotechnical and structural engineers. In countries like Italy, with a high seismic hazard and old or very old towns, with frequent cases in which most of the buildings in the centre of the towns are hundreds of years old, this is one of the most relevant problems for the protection of both population and cultural heritage (Costanzo et al., 2007). The recent tragedy of the city of L'Aquila (Abruzzo, Italy), whose historical centre almost completely collapsed after the M_W 6.3 earthquake of 6.IV.2009, is paradigmatic in this sense. Such a key concern needs to be faced, especially in the case of strategic buildings, as for instance ancient monuments, historical buildings, hospitals, schools and so on.

In some and rare cases, existing structures have been seismically isolated with passive structural systems installed underneath the buildings with a complex procedure of partial uplifts and setting of isolators and dampers (see for instance Martelli, 2009; Alterio, 2012). Examples of such complex procedures are: the Salt Lake City & County Building (USA), the San Francisco City Hall (USA), the Maritime Museum of Auckland (New Zealand), the Church of San Giovanni in Carife (Italy), the Los Angeles City Hall (see Figures 1.2.1).

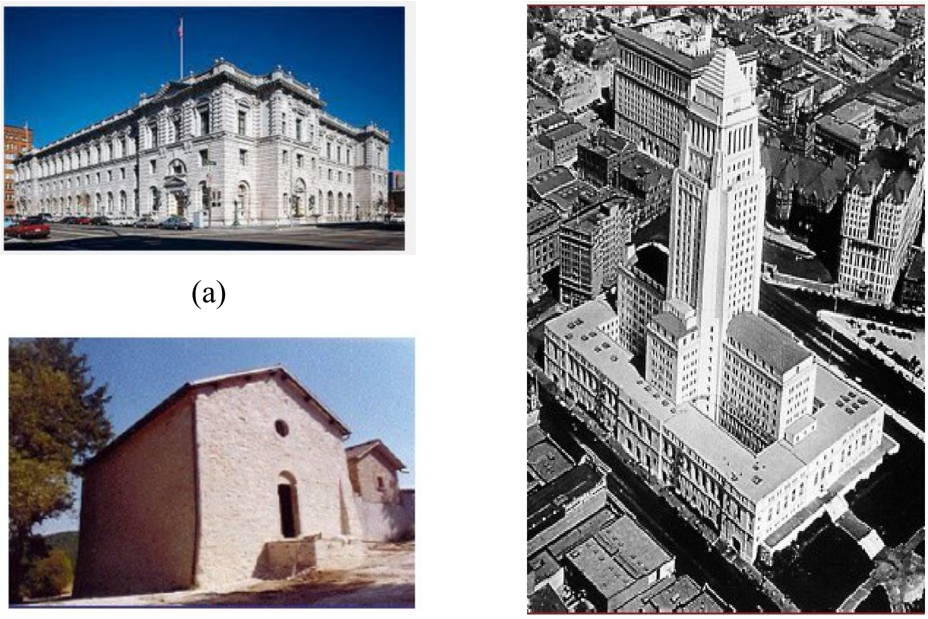

(a)

(b)

(c)

Figure 1.2.1 *San Francisco City Hall, San Francisco, CA, USA (a); Church of San Giovanni in Carife (Italy) (b);Los AngelesCity Hall, CA, USA (c).*

These procedures are very expensive, and not always feasible, depending especially on the structural behaviour of the building. Furthermore, the installation, for instance, of seismic isolators in structures of artistic or historical relevance may alter their original configuration in a way which cannot be accepted in the light of the most recent rules of conservation and retrofitting, as stated for instance by the so called Venice Charter (1964), which is the reference document for the ICOMOS (*International Council of Monuments and Sites*) of UNESCO.

1.3. Idea and objectives.

Generally speaking, earthquakes generate seismic waves that radiate away from the source and travel through the earth crust, eventually reaching the ground surface and producing shaking, possibly causing damage to existing structures. Such a damage results from the complex soil-foundation-structure interaction mechanisms due either to the transient ground motion, or, in peculiar conditions (loose saturated granular soils), caused by soil liquefaction. The shaking caused by the waves depends on some general characteristics of the earthquake (size and location, and therefore distance from the site to be protected) and on the characteristics of the site, in terms of subsoil conditions and morphology. Soil characteristics play a relevant role in waves propagation, as soil deposits tend to act as "filters" to seismic waves: considering a complex signal, as it is always the case in nature, some frequencies may be attenuated passing through the soils, some may be amplified (Richart et al., 1970; Aki, 1988; Kramer, 1996; Chavez-Garcia, 2011). Nowadays, analytical tools are available to accurately carry out local seismic amplification analyses taking into account the effects of soil stratigraphy and ground morphology (Lanzo et al., 2011; Evangelista et al., 2011). The idea supporting the proposed research activity is to control the subsoil filtering action by artificially modifying the mechanical and physical characteristics of a small part of the foundation subsoil underneath the building to be protected. The research is, therefore, aimed to find a completely new and unconventional way to protect, for instance, existing strategic constructions from earthquakes, respecting their integrity in the most possible meaning (structural, artistic, historical): seismic protection will be obtained by adopting a peculiar grouting technique to adequately modify the mechanical and physical properties of a limited volume of soil, far enough from the structure to be protected. In particular, the idea to be developed consists in introducing into the ground (displacing or permeating it, or both) a new grouting mixture able to completely modify the mechanical response of the treated soil to seismic excitation. The proposed unusual soil grouting should be injected in a small portion of the subsoil, at a suitable depth, not directly beneath the structure to be protected. The depth and thickness of grouting have to be optimized on the basis of the soil properties, the characteristics of the building to be protected, and the expected seismic action.

As previously stated, such an approach is best suited for existing structures, since there are nowadays simpler and more practical alternatives to be implemented in the design of new structures. For existing structures, on the contrary, it is in principle the least invasive and likely the most effective, if properly conceived.

The idea of a "screen barrier" in the ground has been already proposed in literature. For example, different vibration mitigation measures (for vibrations caused by vehicle and rail-bound traffic generally complex and difficult to analyse) can be used near the source, in the soil layers or close to the buildings to be protected, remembering that the most efficient mitigation methods should be proposed at the design stage of a project. Some authors (Chouw, 1992; Kellezi, 2011) have proposed an approach that is thought to isolate building foundations from steady-state or transient soil vibrations by placing a stiff layer, such as an artificial bedrock, under the building's foundation. Vibration at the soil surface depends on the soft layer thickness, its material properties and the frequency content of the dynamic source; the aim is to artificially reduce the wave propagation in the top layer thanks to a virtual rigid base at an appropriate depth (see Figure 1.3.1), because if the excitation frequency is less than the lowest eigen-frequency of the layer, the waves spreading into the layer will be impeded, reducing foundation excitation and structural response (Kellezi, 2011).

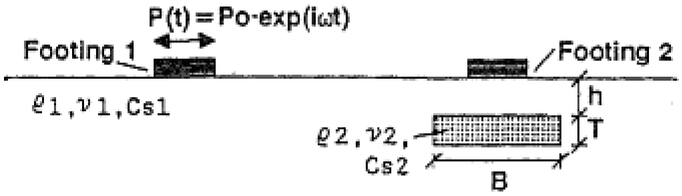

Figure 1.3.1 *Screen barrier for superficial waves.*

The dynamic response of buildings can also be improved by installing wave lateral barriers like open, in-filled (walls) or gas cushion trenches (Massarsc, 2004, 2005) close to the vibration source. The most efficient isolation barrier is an open trench in the ground; open or liquid-filled trenches are unfortunately difficult to use in practice, above all in built up areas, also because rain or percolating water can fill up the trench, reducing the impedance difference relatively to the ground significantly (Andersen and Augustesen, 2009); so light-weight in-filled trenches are generally placed. When subjected to compressive stresses due to the lateral earth pressure after installation in the ground, however, these light-weight materials change their dynamic properties and loose much of their vibration isolation effect. As a matter of fact, in order to achieve vibration isolation from artificial vibrations, it is necessary to create an abrupt change of impedance in the ground; density as well as stiffness increase by increasing pressure and so a lateral trench should resist the high lateral earth pressure without changing its impedance. So gas cushions in-filled trenches are also used to create a flexible barrier to great depths, with a very low impedance (low density and low wave velocity). Such barriers are able to resist the later earth pressure, creating a flexible barrier with a vibration isolation capacity comparable to an open trench.

As an alternative approach, nowadays soil grouting is sometimes used for earthquake hazard mitigation, but with little or no ability to truly mitigate seismic hazard.

As a matter of fact, during the last years, an increasing number of researchers have been studying treated ground dynamic properties in order to understand and control the modifications introduced by various treatments to the mechanical and dynamical ground properties (Saxena et al., 1987; Chepkoit and Aggour, 2000; Cai and Liang, 2003; Spencer, 2010). However, these studies have an approach completely different from the one herein proposed, and usually study grouted soils which are stiffer and stronger than the original soil, while this will not be the goal of our research project, whose aim is to introduce a less stiff grouted layer.

In some cases, engineering applications of conventional superficial grouting have been proposed in literature as a mean to mitigate seismic actions, but always considering cemented (and therefore improved) soils in the topmost part of the subsoil. Numerical one-dimensional site response analyses proved that stiffening the uppermost soil layers by grouting reduces the overall ground motion, but has little or no effect on the high-frequency content of the seismic motion transmitted to the surface, which can therefore still be potentially dangerous to stiff massive buildings to be protected (D'Onofrio et al., 1999).

Two-dimensional FEM analyses have proved that the use of vertical stiff barriers of grouted soil may even amplify the seismic acceleration amplitudes due to the internal reflections of waves under the building foundations (Di Prisco and Serra, 1996). In other words, while static vertical and lateral ground displacements may be somehow reduced by the conventional shallow soil grouting techniques, these latter do not guarantee an appropriate mitigation of seismic inertial forces in the buildings.

So, stiffening the uppermost soil by grouting certainly reduces seismically induced ground motion, but may have little or no effect on the energy transmitted to the structure to be protected, which can still be very high and therefore potentially dangerous. So, ground displacements may be somehow reduced by this conventional superficial soil grouting because of increasing soil stiffness, but this does not guarantee that the seismic hazard has been properly mitigated.

The approach proposed in this research is similar to the ones previously exposed for lateral trenches used to preserve from superficial vibrations. In fact, the proposed solution tends to explore the possibility to create a full screen barrier for seismic risk mitigation. Since there are only very few references in literature on this topic (Kirtas, 2009), this research is innovative and, in case applicable, it would give rise to new activities both in the research and application fields.

The isolation mechanism that this thesis will analyse takes advantage of few experiences reported in literature. One of those is the one, reported by Dietz and Woods (2006), who shows series of shaking table tests, made to evaluate the seismic response of a caisson modelled at 1/30 scale, using a shear stack (that is a flexible-walled hollow box designed and built to enable geotechnical modelling in conjunction with the shaking table).

The mitigation scheme studied by Dietz and Woods involved the construction of a soft caisson around and beneath an existing foundation , made by inserting a horizontal slip layer at a moderate depth (authors suggests around 10m) and also inserting soft trenches around the foundation (see Figure 1.3.2). The weak layer had a low value of the friction angle, thanks to the use of the roller bearings, which the experimental box sits on, whereas soft trenches (made with cylinders of neoprene) offered negligible shear stiffness.

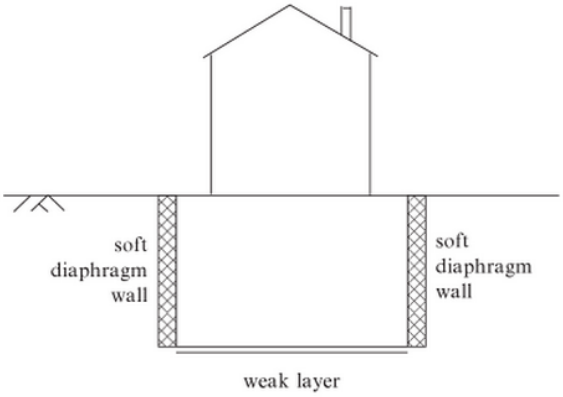

Figure 1.3.2 *Scheme adopted by Wood (2006) for his isolation typology.*

The shaking table tests, performed by applying different accelerograms to the system, demonstrated that this isolation scheme, installed within the ground underlying a vulnerable structure, can improve its seismic performance, but the inclusions are successful only when the frequency content of the input motion lies above the resonance frequency of the modified system. Thus, for maximising their benefit and widening their range of application, the stiffness and the friction angle of the whole treated mass should be minimised; this is an important, critical theoretical topic, because the frequency content of the expected earthquake motion is not previously known.

There are several studies on base-isolating low-rise buildings by placing liners beneath the foundation slab, thanks to the slip coefficients that are function of axial load, number of cycles and velocity and that has been obtained with both standard and modified surfaces. Many authors have studied slip layer beneath a building slab foundation to provide base isolation.

On the basis of shake table tests on sand deposit and analytical tests, Yegian and Kadakal (2004) proposed to place a smooth synthetic material beneath building foundations (see

Figure 1.3.3) in order to provide a slip layer by using a geo-textile placed over an ultra-high molecular weight polyethylene sheet. The concept was that the liner placed in a curved shape penetrating the soil profile would dissipate energy through slip displacement (Yegian, 2004), transmitting significantly reduced motions to the overlying isolated soil layer and any structure founded on it. This system is useful in decreasing both peak as well as spectral responses measured at the surface and in the central isolated mass than the motion below the isolating liner, but, as a consequence, slip displacements were recorded along the perimeter of the isolated soil layer. Because of the restoring force, effect of the gravitational weight of the isolated soil layer, the slip displacements are small in the central zone, but, near the edges of the isolated region, it's necessary to study the effects on utilities and similar.

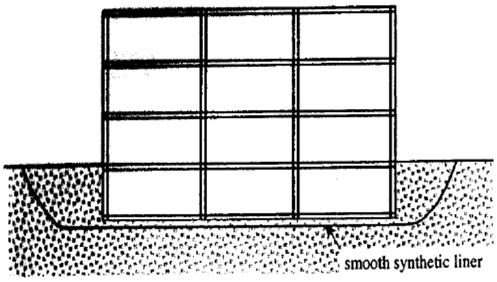

Figure 1.3.3 *Isolating scheme with smooth synthetic material beneath building foundation (Yegian and Kadakal, 2004).*

Doudomis et al (2002) proposed placing soil layers with low shearing resistance beneath buildings, to let building slip under the action of strong seismic motions (see Figure 1.3.4). According to the authors, the low shearing layer should be provided by suitable natural materials, such as granular products from rocks containing low friction materials (talc, chlorite, serpentine, etc.) with an adequate strength in compression or high plasticity clays (monmorillonitic clays and similar). The great disadvantages of this system are the doubtful constructability, and the design problems. The coefficient of friction of 0.2 proposed by the authors does not guarantee large force reductions.

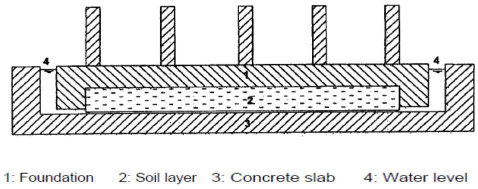

Figure 1.3.4 *Scheme proposed by Doudomis et al (2002) with an artificial soil layer.*

A similar approach has been made by Taskov et al. (2004). A liquid storage tank whose base has been isolated by the ALSC (which means: “Almost Lifted Structure Concept”) system has been modelled. In this system, the foundation of the structure is placed on a sliding plate positioned on a recess containing oil under pressure, which has the purpose of lowering the sliding resistance between the foundation and the ground. By using shacking table test, the modified structure is hit by a certain vibration; structure moves with no foundation shear resistance, because this resistance is quite totally decreased by the uplift oil pressure force. The movements are opposed by springs at the sides of the ALSC system, which have to break down the maximum displacements and refocus the foundation to its original position when oscillations end. Tests with this typology of system have been made on a reduced scale test of the model of St. Nicholas church (Tashkov et al., 2010) (see Figure 1.3.5a). The system shows a very effective reduction of input energy transmission and keeps the structure out of resonance within a broad frequency range of the excitation force, deleting bending and shear forces in the main structure and relative story drifts; moreover, this system is not sensitive to vertical excitation component. ALSC system seems to be a good retrofit system, because it does not change the aesthetic appearance of the structure and it is limited to foundation intervention; it is also reversible, because, for coming back to the original condition, oil pressure can be set equal to zero (Figure 1.3.5 b).

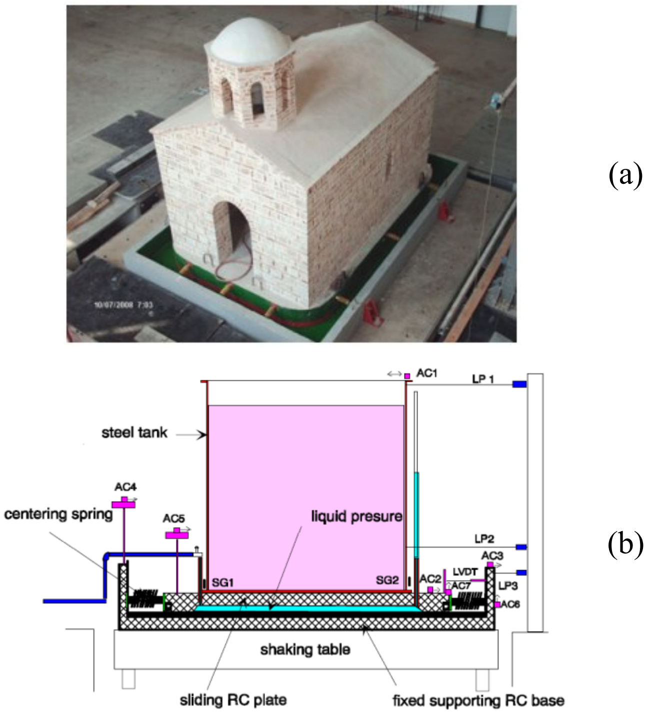

Figure 1.3.5 *St. Nicholas church model to the scale of 1/3.5 tested on the seismic shaking table (a); ALSC instrumentation set up (b).*

On the other hand, an alternative possibility should be to increase the damping of the foundation soil beneath the building to protect. In this sense, rubber soil mixtures (whose acronym is “RSM”) placed around the foundation of a building have been proposed (Tsang et al, 2007, 2011; see Figure 1.3.6) for adsorbing seismic energy and exerting a function similar to that of a cushion. Rubber has important damping properties used for many years in structural isolating system. According to Tsang (2007), the soil layers surrounding foundation (considered having G=222MPa at a confining pressure of 345kPa; Vs ≈ 350m/s) can be replaced by a medium which is made up of soil mixed with a designed proportion of rubber and sand (G=7,5MPa at a confining pressure of 345kPa; Vs ≈ 90m/s), with both an important increase in damping and a decrease in shear stiffness. Using this system, the authors predict an average reduction of 40÷60% in horizontal accelerations, above all for wider buildings (low to medium rise buildings) with a remarkable increase in the foundamental structural period. The effectiveness of the proposed RSM system has been shown by a preliminary parametric study using three recorded earthquake ground motions. An important issue that has not been explored is the amount of induced vertical displacements, which could be relevant for a building placed at ground surface.

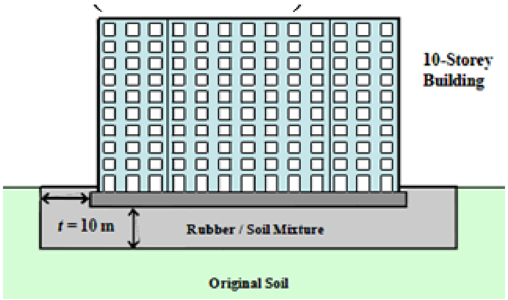

Figure 1.3.6 *RSM system around the foundation of a building (Tsang et al, 2007, 2011).*

However, the principal topic is not achieved, that is: “How is it possible to apply this method to an existing structure? How could the foundation system be easily modified in order to place such a system?”

In order to answer these questions, the research activity to be carried out should be both theoretical and experimental and should consider the treatment at depth of a thin layer of soil.

In this sense, Kirtas (2009) has studied, numerically and by using centrifuge equipment, the inclusion of different stiff and soft treatments into a soil deposit, considering the presence of a SDOF (Single Degree of Freedom) at ground surface simulating the case of structures with surface foundations. Actually, he has studied the insertion of horizontal layers beneath the foundation, vertical diaphragms next to the foundation and caissons, which are the combination of two vertical diaphragms and one horizontal layer to form an isolated soil-structure area; any modification of the foundation soil properties may affect the structural response through soil-structure interaction mechanisms in a beneficial or a detrimental way, as reported by Wood (2006). Evaluation of foundation subsoil stiffening and stiff diaphragm intervention effects has revealed that the specific approaches are not efficient in reducing the seismic part of the structural response. On the contrary, the seismic acceleration for several soil-structure combinations could increase after the intervention compared to the initial system, although the adequacy of the methods in soil strength enhancement and excessive settlement reduction is not under question.

In Kirtas (2009) several structural mass and height combinations are examined, since they both enhance soil-structure interaction phenomena leading to different dynamic response. Normalized values of structural mass and height are used according to the expressions:

$$m_{norm} = \frac{m_{str}}{\rho \cdot B^3} \tag{1.3.1}$$

$$h_{norm} = \frac{h_{str}}{B} \tag{1.3.2}$$

where:

- m_{str} is the superstructure mass;
- h_{str} is the superstructure height;
- ρ is the soil density;
- B is the characteristic foundation dimension (half the foundation width for strip foundation type).

Results are generally depicted in the frequency domain, introducing the term ‘‘response ratio’’. This is the ratio of the Fourier transform of the response time-histories in selected locations of the modified system to the corresponding response of the initial unmodified system. Thus, values of the response ratio below unity are indicative of the mitigation efficiency of the structural response in the examined frequencies, whereas for ratios exceeding unity it is possible that the intervention has a detrimental effect on the system’s seismic performance.

According to Kirtas (2009) incorporating a short-length soft horizontal layer in the foundation subsoil does not affect significantly the structural seismic response (see Figure 1.3.7, where T_{str} is the SDOF natural period).

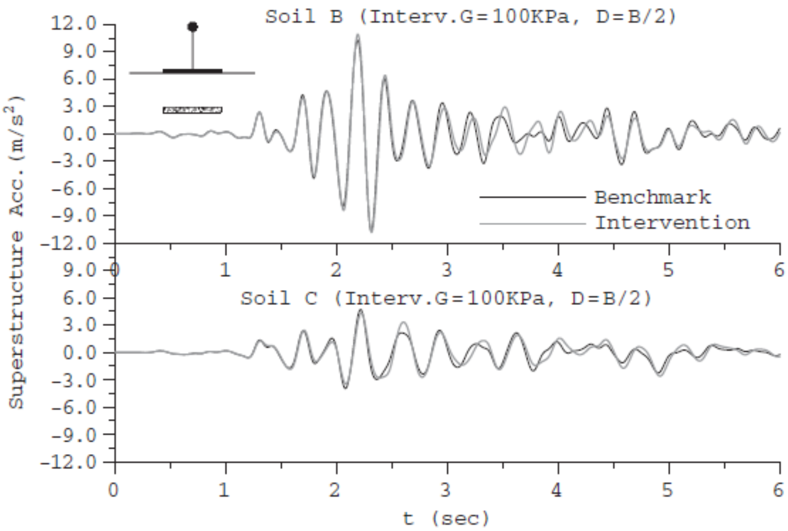

Figure 1.3.7 *Soft horizontal layer: acceleration time-histories (T_{str}=0.2s; m_{nom}=2).*

Construction of flexible vertical diaphragms next to the foundation could aim at isolating a soil mass underneath the foundation and the superstructure, in order to reduce the induced ground shaking and allow independent oscillation from the surrounding soil.

Unlike the previously examined methods, the superstructure acceleration ratio in the case of the ‘‘soft diaphragms’’ presents a wide range of values below unity near the fundamental effective period of the structure, indicating an efficient mitigation of the seismic response (see Figures 1.3.8).

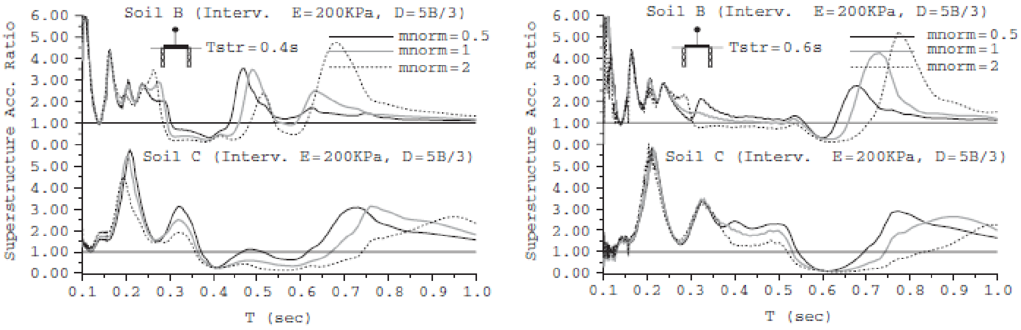

(a) (b)

Figure 1.3.8 *Soft diaphragms: superstructure ratios for T_{str}= 0.4s (a) and T_{str}=0.6s (b).*

The superstructure accelerations in the time-domain (see Figure 1.3.9) for the structure with T_{str}=0.6s and two different excitations verify the mitigation efficiency of the intervention (the excitations are: EQ1with predominant period between 0.15s÷0.40s and EQ2 with a wide range of frequencies with an important frequency content for T=0.6s÷0.8s, a period range near to the structural effective period).

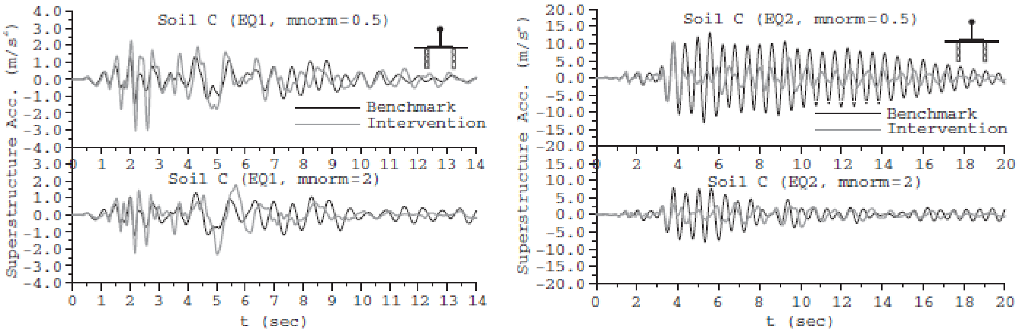

(a) (b)

Figure 1.3.9 *Soft diaphragms: acceleration time-histories for excitations EQ1 (a) and EQ2 (b) (T_{str}=0.6s).*

The increase of the dynamic response due to the presence of the proposed system during the EQ1 excitation is of minor importance since the structure is out of resonance with the seismic motion, which is obvious considering the low level of the superstructure acceleration developed in the initial system. On the other hand, applying the EQ2 input motion where resonance phenomena occur, the soft diaphragms induce a significant reduction of structural response. The efficiency of the intervention increases with increasing structural mass, as depicted in both the time and frequency domains. Because of the significant deformability of the implemented intervention compared to the initial foundation subsoil conditions, it is reasonable to expect an increase of the seismic displacements of the system. Yet, displacement ratios (see Figure 1.3.10a) indicate the possibility of either increased or reduced displacements, depending on the frequency content of the imposed seismic motion. For instance, in the case of EQ1 input motion of low predominant frequency, the displacement of the structure having T_{str}=0.6s is only slightly increased (see Figure 1.3.10 b), confirming the displacement ratio predictions.

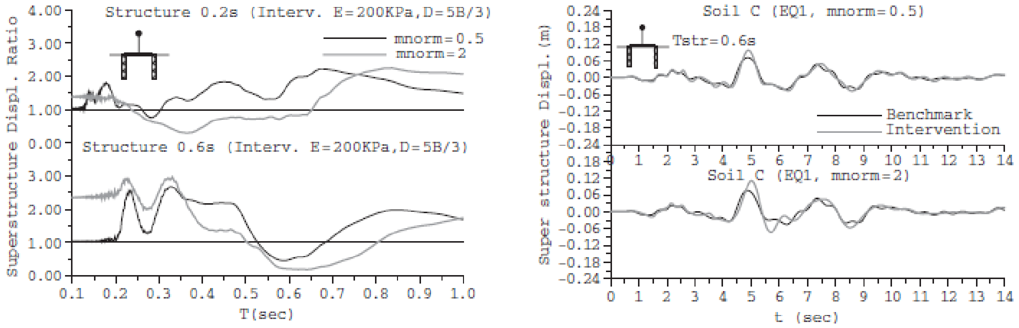

(a) (b)

Figure 1.3.10 *Soft diaphragms: superstructure displacement ratios (a) and corresponding time-histories for EQ1 (T_{str}=0.6s).*

However, when this layer is combined with flexible diaphragms forming a soft caisson, a reduction of the soil-structure's seismic loading levels could be achieved (see Figure 1.3.11). The dynamic characteristics and especially the fundamental period of this system seem to dominate the response, shifting it to higher periods, out of the frequency content range of common earthquakes.

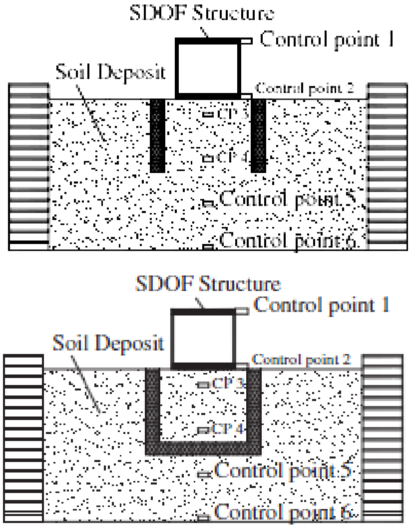

Figure 1.3.11 *Some of the schemes adopted by Kirtas (2009).*

According to authors, significant alteration of the dynamic properties of the system shifts the SDOF response to higher period values, out of the frequency range of common earthquake records, resulting in beneficial effect of the implemented intervention (see Figures 1.3.12 a and b). The response ratios in Figure 1.3.12 c and d are plotted for periods up to 2.0s, highlighting the significant modification of the system's dynamic properties. The existence of a wide range of ratio values below unity is evident near the fundamental period of the oscillating systems with T_{str}=0.2s and 0.6s, indicating a substantial reduction of the structural seismic response. These findings are also verified by the important reduction of the acceleration time-histories at the top of the structure in Figures 1.3.12 c and d.

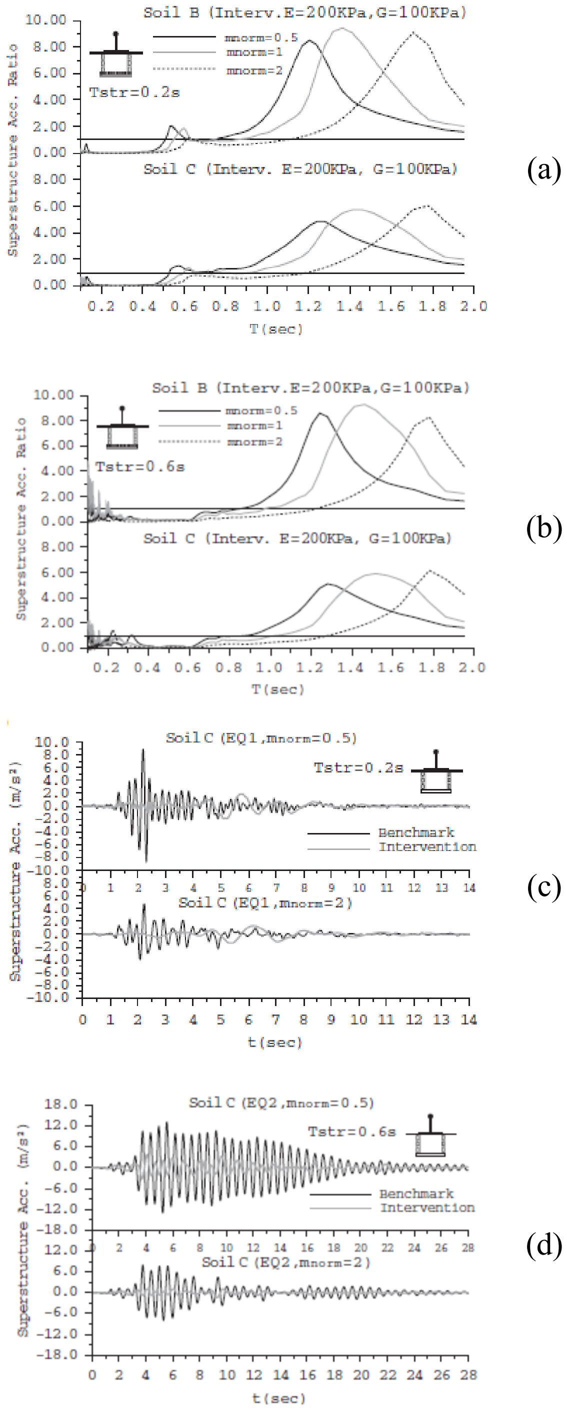

Figure 1.3.12 *Soft caisson: superstructure ratios for* T_{str}*=0.2s (a) and* T_{str}*=0.6s (b); superstructure acceleration time-histories for* T_{str}*=0.2s (c) and* T_{str}*=0.6s (d) (Kirtas (2009).*

However, according to Kirtas (2009), by considering such a system, increase of the soil deformations and structural displacements are expected and should be handled appropriately considering the specific nature of the implicated materials (see Figure 1.3.13).

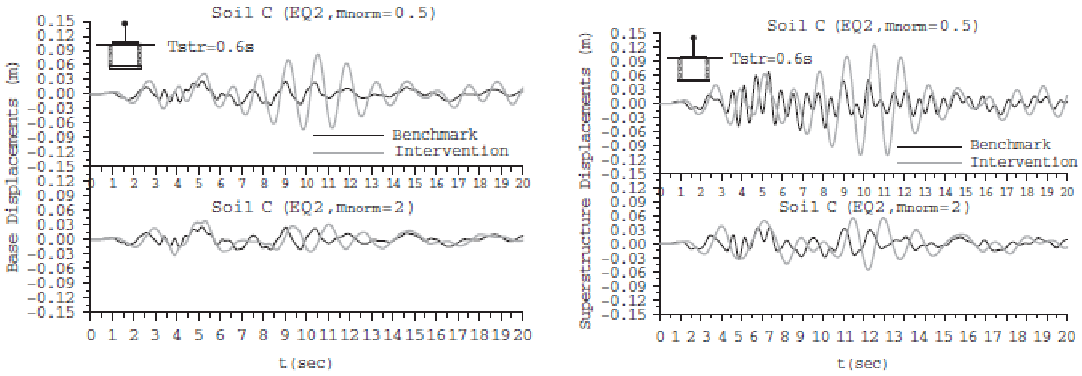

(a) (b)

Figure 1.3.13 *Soft caisson: base (a) and superstructure (b) displacements time-histories.*

Generally speaking, after a review of literature cases, as it is formulated as the product of hazard, vulnerability and exposure, the seismic risk mitigation above all for existing and historical buildings seems to be an unresolved problem which allows no completely satisfactory solution.

It has been decided to continue in investigating in the direction of the previously reported works. Together with the seismic isolation method being investigated in this thesis, the aforementioned seismic isolation methods have been collectively named as “geotechnical seismic isolation systems” (whose acronym is “GSI”; Tsang, 2009).

A GSI system can be defined as a seismic isolation system that involves the direct interaction with the natural soil and/or man-made reinforced soil materials, in contrast to the commonly well-known structural seismic isolation system, in which the flexible or sliding interface is positioned between a structure and its foundation.

The GSI method proposed in this thesis could be explained by referring to the performance-based design approach; the two key elements for a seismic safety assessment of a building (Figures 1.3.14) are the seismic demand and the capacity curve.

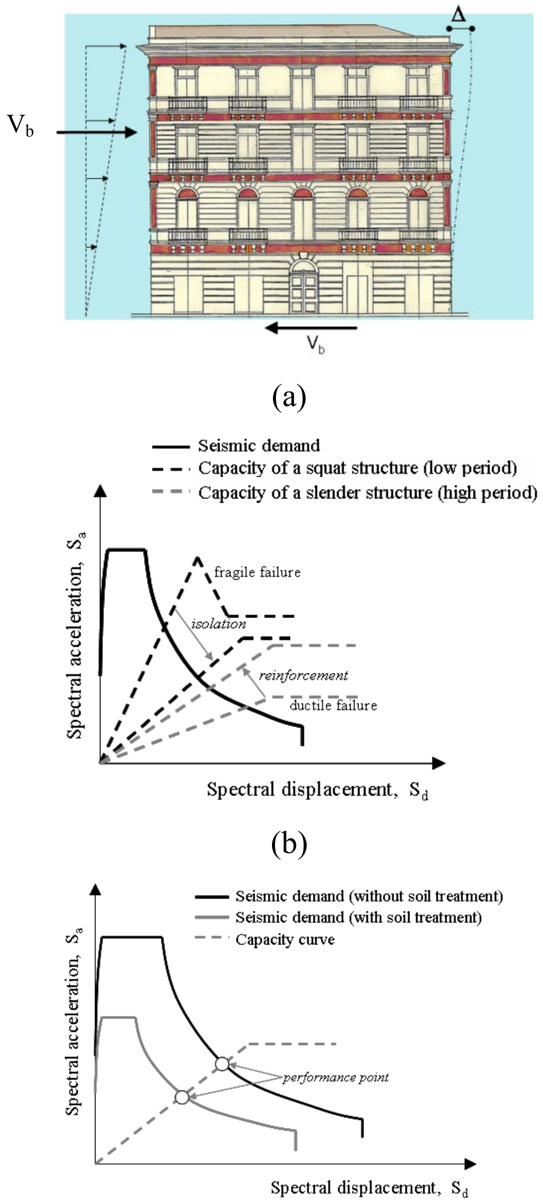

(a)

(b)

(c)

Figure 1.3.14 *Seismic safety assessment procedure (Lombardi et al. 2013).*

This latter is often referred to as a “pushover curve”, relating the base shear force V_b, to a reference horizontal displacement Δ, for instance at the top of the building (see Figure 1.3.14 a). The seismic demand for the pseudo-static analysis of a rigid system can be typically defined in terms of a seismic coefficient (proportional to the design peak ground acceleration a_{max}); for deformable systems, the most conventional way to express it is by using the spectral acceleration $S_a(T)$, the spectral displacement $S_d(T)$, or both (Figure1.3.14 b). For a structure with a given fundamental period, T, $S_a(T)$ and $S_d(T)$ can be viewed as proportional to the above defined shear force and displacement, respectively.

As a consequence, they represent a convenient and synthetic way to analyse seismic demand. $S_a(T)$ and $S_d(T)$ depend on the regional seismic hazard, the seismic site response and the system ductility. The safety assessment can be therefore expressed by comparing demand and capacity, individuating a "performance point" at the intersection of the curves (Figures 1.3.14 b and c). If such a performance point does not exist (i.e. the capacity is lower than the demand, and safety cannot be guaranteed) or it is too close to the limit capacity (i.e. the safety margins are not sufficient or do not respect Codes of Practice specifications), seismic risk mitigation interventions are necessary. In principle, this can be achieved by changing either the capacity curve or the seismic demand, with the final goal to have a performance point with higher safety margins. As previously mentioned, it is common practice to work on the capacity, i.e. on the pushover curve. For new structures, this can be done with base isolation techniques, reducing the fragility and increasing the ductility in the structural capacity, thus shifting the capacity curve to the right in the plot of Figure1.3.14b. This is certainly beneficial in terms of safety margins at the performance point, as the limit capacity can be assumed to be similar to that of the less ductile structure without isolation. An alternative is the reinforcement of the structure, obtained by increasing both the stiffness and the strength of the building (Figure 1.3.14b). In such a way, even though the capacity curve is shifted to the left in the plot of Figure1.3.14 b, safety margins may be increased.

In the case of existing constructions and in special case for those having historical value, both this approaches may be incompatible with the need to preserve its original state (integrity). If neither the building ductility can be increased nor a base isolation system can be adopted, it would be desirable to change the seismic demand. Since seismic demand depends on seismic site response, the only way to change it consists of artificially modifying soil stratification.

The modification can be obtained by grouting activities, and must be dimensioned in order to shrink the seismic demand curve (Figure1.3.14c), thus resulting into a performance point which, being constant the capacity curve of the building, has larger safety margins against structural failure. Grouting has therefore the function of artificially modifying the mechanism of propagation of the seismic waves in the uppermost part of the subsoil, in such a way to attenuate seismic effects at ground level. Since it may be impossible to reach this goal for any period T, soil treatment has to be tuned to be effective in the range of periods typical of the structures to be preserved. The basic idea of the research work described in this thesis, therefore, is to consider a grouted layer installed at a suitable depth with a suited shape, by injecting a material with a specific dynamic impedance η much lower than that of the surrounding soil ($\eta=\rho\cdot V_S$, where ρ is the material density and V_S the velocity of shear waves), possibly being able to dissipate part of the incoming seismic energy too. As typical in soil dynamics, the ability of a soil to dissipate energy is usually calculated via the damping ratio D. Since, as previously said, dynamic impedance depends on material density as well, the grouted material may be conceived as having the lowest possible density too. By placing a thin layer with a low dynamic impedance, it is expected that most of the seismically induced effects will concentrate within the layer, and very little will be transmitted to the soil on top. Then, a strongly reduced seismic action will reach the building or the structure to be preserved and smaller or nil damage will occur. This kind of seismic isolation could be called "soil worsening" instead of soil improvement, as it is actually aimed to locally worsen the mechanical behaviour of the soil.

The relevant - and not trivial - issues to be addressed in proposing the adoption of seismic isolation grouted layers are:

- the depth and the geometrical configuration of the grouted layer.
- the choice of the best suited grout to be injected.

The grouted curtain should be deep enough to avoid measurable static settlements and to exclude a reduction of the foundation bearing capacity. This requirement can be guaranteed by grouting at depths high enough that no interaction must be expected with the structure to be protected; on the other hand, the grouting depth should be not so high to make the installation procedure not affordable or the attenuation of seismic energy not effective. Different geometrical schemes of the grouted curtain can be taken into account (see Figures 1.3.15) in order to individuate the best solution in terms of cost-benefits balance between effectiveness and feasibility on site.

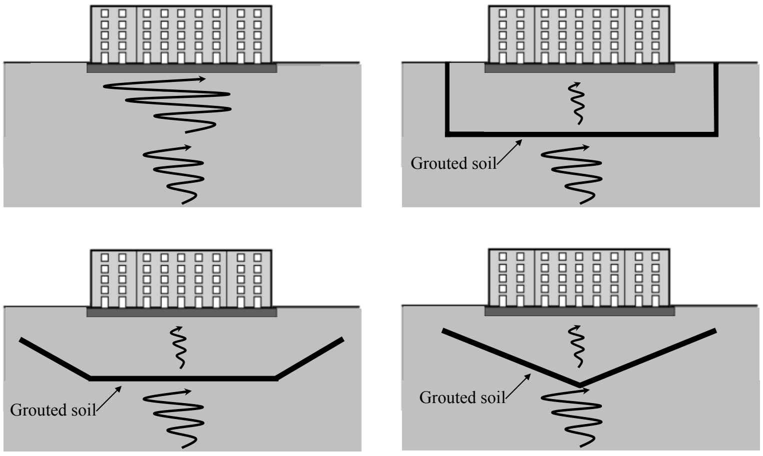

Figure 1.3.15 *Scheme with no grouted layer and possible geometrical configurations of the isolating grouted layer.*

The execution under an existing building of a horizontal continuous barrier may be extremely difficult, while sloping layers may be more easily realized with a number of closely placed injections, which can be done with inclined drilling and injection, multiple local injections or even with directional drilling and injection.

1.4. Waves in an infinite, homogeneous, isotropic, elastic medium.

In order to derive the equations of motion for an elastic medium the equilibrium of a small element is considered, as shown in Figure 1.4.1, where the variations in force of this element are reported (Richart, 1970). The stresses on each face are represented by sets of orthogonal vectors; the solid vectors act on the visible faces, the dotted ones on the hidden faces.

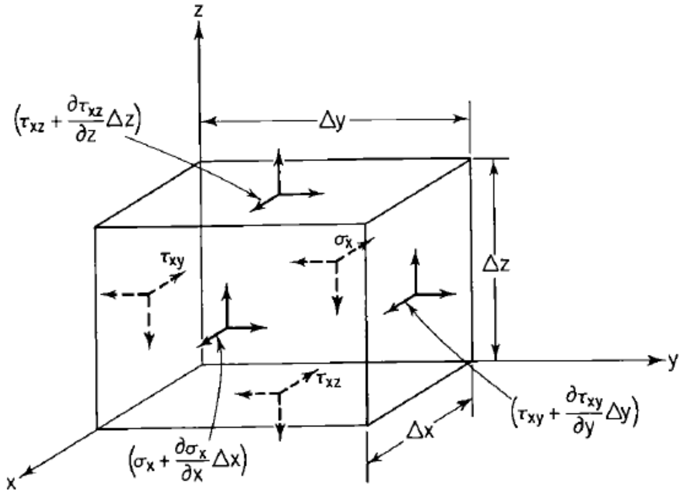

Figure 1.4.1 *Stress on small element of an infinite elastic medium.*

Neglecting body forces and applying Newton's second law in the three directions, three equations of motion in terms of stresses are obtained:

$$\begin{aligned}
\rho \cdot \frac{\partial^2 u}{\partial t^2} &= \frac{\partial \sigma_x}{\partial x} + \frac{\partial \tau_{xy}}{\partial y} + \frac{\partial \tau_{xz}}{\partial z} \\
\rho \cdot \frac{\partial^2 v}{\partial t^2} &= \frac{\partial \tau_{yx}}{\partial x} + \frac{\partial \sigma_y}{\partial y} + \frac{\partial \tau_{yz}}{\partial z} \\
\rho \cdot \frac{\partial^2 w}{\partial t^2} &= \frac{\partial \tau_{zx}}{\partial x} + \frac{\partial \tau_{zy}}{\partial y} + \frac{\partial \sigma_z}{\partial z}
\end{aligned} \tag{1.4.1}$$

where u, v and w are the displacements, respectively, in the x, y and z-directions. The right sides of the three equations can be expressed by using the Poisson ratio υ and the Lamé's constants λ and G (also called shear stiffness modulus):

$$
\begin{aligned}
&\sigma_x = \lambda \cdot \varepsilon_v + 2 \cdot G \cdot \varepsilon_x \\
&\sigma_y = \lambda \cdot \varepsilon_v + 2 \cdot G \cdot \varepsilon_y \\
&\sigma_z = \lambda \cdot \varepsilon_v + 2 \cdot G \cdot \varepsilon_z \\
&\tau_{xy} = \tau_{yx} = G \cdot \gamma_{xy} \\
&\tau_{yz} = \tau_{zy} = G \cdot \gamma_{yz} \\
&\tau_{zx} = \tau_{xz} = G \cdot \gamma_{zx} \\
&G = \frac{E}{2 \cdot (1+\upsilon)} \\
&\lambda = \frac{\upsilon \cdot E}{(1+\upsilon) \cdot (1-2\cdot\upsilon)}
\end{aligned}
\tag{1.4.2}
$$

E is the Young Modulus, ε_v is the volumetric deformation defined by $\varepsilon_v = \varepsilon_x + \varepsilon_y + \varepsilon_z$.

It is needed the following relationships for strain and rotation in terms of displacements:

$$
\begin{aligned}
&\varepsilon_x = \frac{\partial u}{\partial x} \quad \gamma_{xy} = \frac{\partial v}{\partial x} + \frac{\partial u}{\partial y} \quad 2 \cdot \omega_x = \frac{\partial w}{\partial y} - \frac{\partial v}{\partial z} \\
&\varepsilon_y = \frac{\partial v}{\partial y} \quad \gamma_{yz} = \frac{\partial w}{\partial y} + \frac{\partial v}{\partial z} \quad 2 \cdot \omega_y = \frac{\partial u}{\partial z} - \frac{\partial w}{\partial x} \\
&\varepsilon_z = \frac{\partial w}{\partial z} \quad \gamma_{zx} = \frac{\partial u}{\partial z} + \frac{\partial w}{\partial x} \quad 2 \cdot \omega_z = \frac{\partial v}{\partial x} - \frac{\partial u}{\partial y}
\end{aligned}
\tag{1.4.3}
$$

where ω_x , ω_y . ω_z are the rotations around each axis. Combining the eq.s (1.4.2) and (1.4.3):

$$
\begin{aligned}
&\rho \cdot \frac{\partial^2 u}{\partial t^2} = (\lambda + G)\frac{\partial \varepsilon_v}{\partial x} + G \cdot \nabla^2 u \\
&\rho \cdot \frac{\partial^2 v}{\partial t^2} = (\lambda + G)\frac{\partial \varepsilon_v}{\partial y} + G \cdot \nabla^2 v \\
&\rho \cdot \frac{\partial^2 w}{\partial t^2} = (\lambda + G)\frac{\partial \varepsilon_v}{\partial z} + G \cdot \nabla^2 w
\end{aligned}
\tag{1.4.4}
$$

where ∇^2 is the Laplacian operator in Cartesian coordinates:

$$
\nabla^2 = \frac{\partial^2}{\partial x^2} + \frac{\partial^2}{\partial y^2} + \frac{\partial^2}{\partial z^2}
\tag{1.4.5}
$$

The equations of motions have two solutions: the former describes the propagation of a wave of volumetric deformation (irrotational wave); the latter describes the propagation of a wave of pure rotation (equivoluminal wave). The velocity of these waves can be written as:

$$\frac{\partial^2 \varepsilon_v}{\partial t^2} = V_P^2 \cdot \nabla^2 \varepsilon_v \tag{1.4.6}$$

in which:

$$V_P = \sqrt{\frac{\lambda + 2 \cdot G}{\rho}} \tag{1.4.7}$$

and:

$$\frac{\partial^2 \omega_i}{\partial t^2} = v_s^2 \cdot \nabla^2 \omega_i \quad i = x, y, z \tag{1.4.8}$$

where:

$$V_S = \sqrt{\frac{G}{\rho}} \tag{1.4.9}$$

The induced volumetric deformation ε_V, therefore, propagates at a velocity V_P, whereas rotations propagate with velocity V_S. An infinite elastic medium can thus sustain two kinds of waves with different velocities, representing different types of body motions. The two waves are generally named:

1) dilatational waves (primary waves, P-waves, compression waves, irrotational waves), propagating with a velocity V_P. They are transmitted in the form of volumetric strain (contractions and extensions) of the propagation medium and are characterized by particle motion in the direction of propagation of the waves themselves. It is also said that the wave is polarized longitudinally. In an incompressible medium ($\nu = 0.5$), the P-wave velocity tends to infinity.

2) distortional waves (secondary waves, S-waves, shear waves, equi-voluminal waves), propagating with a velocity V_S. S-waves are transmitted in the form of distortional deformations, i.e. without producing changes in volume, and are characterized by particle motion perpendicular to the direction of propagation of the wave. They can be conveniently separated into two components, to consider the energy partition when they touch an interface between two materials (Figure 1.4.2). It is possible to distinguish between transverse waves of type SV, if the vibrations are polarized in the vertical plane, and of type SH, if vibrations are confined in a horizontal plane (see Figures 1.4.2). A generic shear wave characterized by any one direction of vibration of the particles can be represented as the vector sum of two components SV and SH.

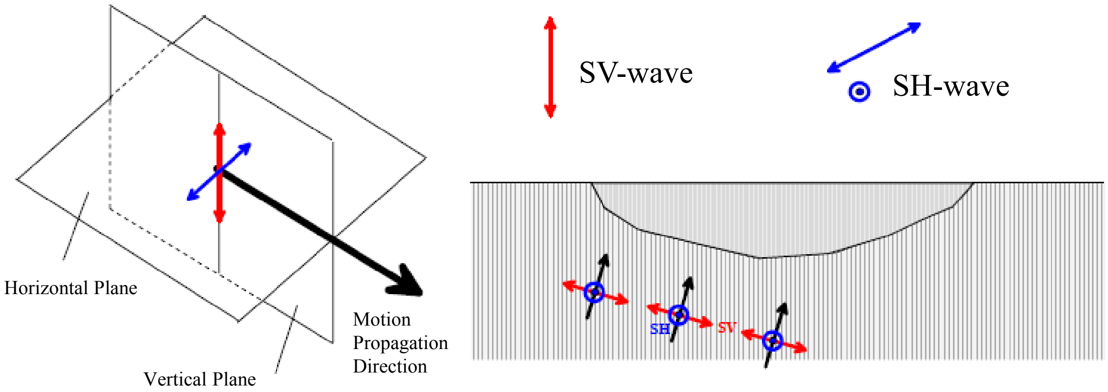

Figure 1.4.2 *Possible polarization of the shear waves: SV-wave and SH-wave.*

From eq.s (1.4.7) and (1.4.9) it can be observed that P-wave are always faster than S-wave; from this observation the names primary and secondary waves have been derived. The ratio between the two velocities is:

$$\frac{V_P}{V_S} = \sqrt{\frac{2 \cdot (1-\upsilon)}{(1-2\cdot\upsilon)}} \tag{1.4.10}$$

In an elastic half-space, it is possible to find a third solution for the equation of motion, which corresponds to a wave, called Rayleigh wave, whose motion in confined to a zone near the boundary of the half-space. A wave with these characteristics can be obtained starting from eq.s (1.4.1) imposing the appropriate boundary conditions, i.e. no stress at the surface, and, a plane wave travelling in the x-direction with particle displacements independent of the y-direction, $\sigma_z=0$ and $\tau_{zx}=0$ is considered. Displacements can be written by using two potential functions Φ and Ψ, chosen such that the former is associated with dilatation and the latter with rotation of the medium.

$$\begin{aligned}
u &= \frac{\partial \Phi}{\partial x} + \frac{\partial \Psi}{\partial z} \\
w &= \frac{\partial \Phi}{\partial z} - \frac{\partial \Psi}{\partial x} \\
\varepsilon_v &= \nabla^2 \Phi \\
2 \cdot \omega_y &= \nabla^2 \Psi
\end{aligned} \tag{1.4.11}$$

Substituting into eq.s (1.4.4), it is obtained:

$$\begin{aligned}
\frac{\partial^2 \Phi}{\partial x^2} &= \frac{\lambda + 2 \cdot G}{\rho} \cdot \nabla^2 \Phi = V_P^2 \cdot \nabla^2 \Phi \\
\frac{\partial^2 \Psi}{\partial x^2} &= \left(\frac{G}{\rho} \right) \cdot \nabla^2 \Psi = V_S^2 \cdot \nabla^2 \Psi
\end{aligned} \tag{1.4.12}$$

Expanding these equations and with the suitable boundary conditions, and assuming a sinusoidal wave travelling in the positive x-direction:

$$\begin{aligned}
\Phi &= F(z) \cdot \exp\left[i \cdot (\omega \cdot t - N \cdot x)\right] \\
\Psi &= G(z) \cdot \exp\left[i \cdot (\omega \cdot t - N \cdot x)\right]
\end{aligned} \tag{1.4.13}$$

where F(z) and G(z) describe the variation in amplitude of the wave as a function of depth, and N is the wave number defined by:

$$N = \frac{2 \cdot \pi}{L_w} \tag{1.4.14}$$

Where L_w is the wavelength, it is obtained:

$$16 \cdot \left(1 - \frac{V_R^2}{V_P^2} \right) \cdot \left(1 - \frac{V_R^2}{V_S^2} \right) = \left(2 - \frac{V_R^2}{V_S^2} \right)^2 \cdot \left(2 - \frac{\lambda + 2 \cdot G}{G} \cdot \frac{V_R^2}{V_P^2} \right)^2 \tag{1.4.15}$$

Eq. (1.4.15) is a cubic equation in V_R^2/V_P^2 and real valued solutions could be found for given values of ν. From this solution, it is understood that V_R^2/V_P^2 is independent with respect to the frequency of the wave. Therefore, the velocity of a surface wave in a half-space in independent of the frequency and is non-dispersive. Curves of the ratio between V_R and V_S are shown in Figure 1.4.3.

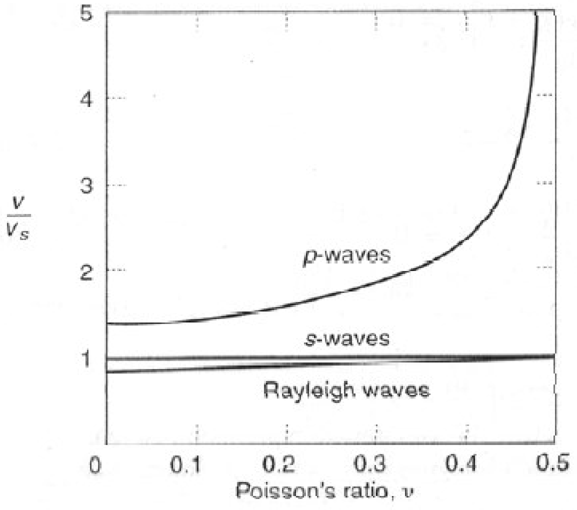

Figure 1.4.3 *Variations of Rayleigh and body waves velocities with respect to the Poisson ratio, ν.*

The following curves (see Figure1.4.4) show the variation of the two components U(z) and W(z) with depth. Rayleigh wave amplitude rapidly decreases with depth; generally, it tends to 10% of the surface value at a depth of 1.5 times the wavelength.

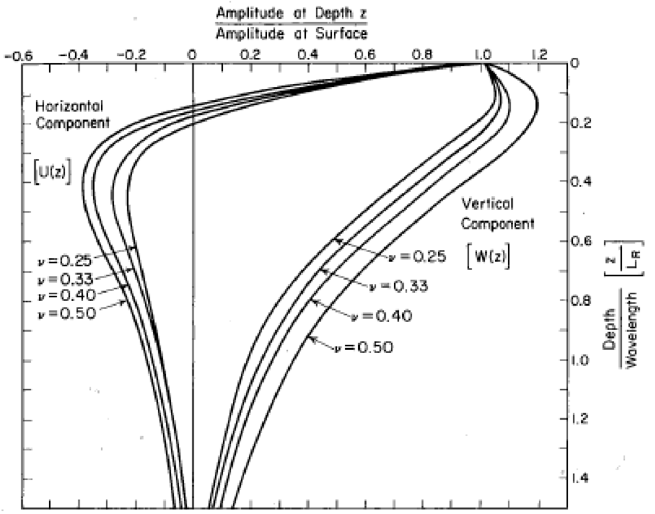

Figure 1.4.4 *Amplitude ratio with respect to the dimensionless depth for Rayleigh wave (Richart, 1970).*

By combining the horizontal and the vertical components of particle motion (see Figure 1.4.5), the path of the particle motion describes a retrograde ellipse; therefore, the Rayleigh wave can be considered as made of a vertical component and a transversal one with vertical polarization (SV).

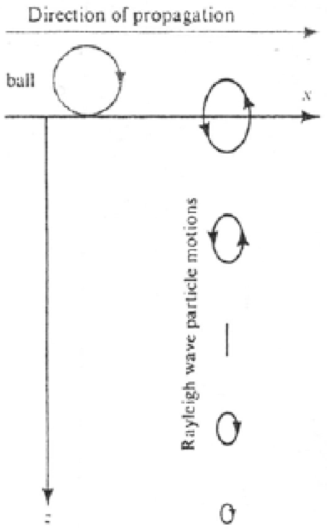

Figure 1.4.5 *Paths described by a particle at different depths into the soil layer due to the propagation of a Rayleigh wave (Aki and Richart, 1980).*

In the case of a layered medium bounded by a free surface, the mathematical solution is more complex and other boundary conditions should be imposed, such as the continuity of displacements and forces at the interfaces between materials with different mechanical characteristics (Aki and Richards, 1980).

The analytical solution indicates that, in this case, the Rayleigh waves show the phenomenon of dispersion, i.e. the speed also depends on the frequency. Since the law with which varies the phase velocity depends on the geometrical features of the layers near the surface and the elastic characteristics of the same layers, the dispersive properties of the Rayleigh waves are used in geophysical surveys (e.g. the test SASW) to determine the profile of the V_S and damping in a soil deposit.

In the case of a layered medium, the analytical developments also show the existence of another type of surface wave: the wave of Love. Due to the passage of this wave, the particles of the medium oscillate on a horizontal plane with a direction normal to that of the wave propagation (Figure 1.4.6). Love waves appear in the case of incidence of SH waves on a surface layer less rigid lying on a substrate and propagate due to multiple reflections of the transverse waves within the layer itself. In other words, Love waves consist of a package of

SH waves, which are entrapped for multiple reflections within the layer with the lower stiffness and propagate parallel to it. The Love wave amplitude varies sinusoidally with the depth in the surface layer, while decays exponentially in the underlying half-space.

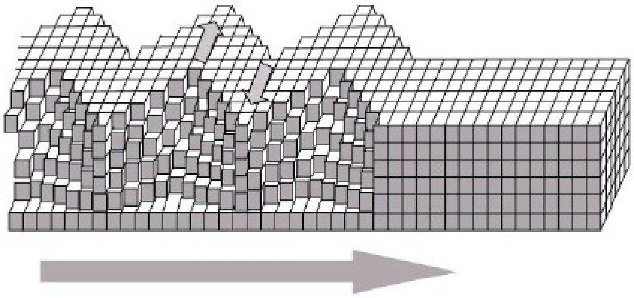

Figure 1.4.6 *Direction of oscillation of particles due to the propagation of Love superficial wave; the grey arrow represents the direction of propagation of the waves.*

In the case of a homogeneous layer of depth H and shear velocity V_{S1} based on an homogeneous half-space with $V_{S2}>V_{S1}$, the velocity of the Love V_L wave satisfies the equation:

$$\frac{G_1 \cdot \sqrt{1-\frac{V_L^2}{V_{S1}^2}}}{G_2 \cdot \sqrt{\frac{V_L^2}{V_{s2}^2}-1}} = \tan\left(N \cdot H \cdot \sqrt{\frac{V_L^2}{V_{s2}^2}-1} \right) \tag{1.4.16}$$

where $N=\omega/V_L$ is the wave number and ω is the angular frequency of the harmonic wave. This typology of wave is dispersive, because V_L depends on the frequency. V_L takes values in the range between V_{S1} of the upper layer and V_{S2} of the half-space.

1.5. Basic waves properties.

It is of interest to recall some fundamental definitions, which will be used for waves, above all to describe their temporal and spatial evolution. In order to describe the spatial properties of a wave, it is useful making reference to the concepts of wavefront and seismic radius. The wavefront is the locus of the points energized by the same wave at a certain time. If the perturbation propagates in every direction of the elastic continuum with identical characteristic, a spherical wavefront will be defined. Huygens' Principle provides a quick method to predict the propagation of a wavefront through, for example, a spherical wavefront that will remain spherical as the energy of the wave is carried away equally in all directions.

Such directions of energy flow, which are always perpendicular to the wavefront, are called seismic rays, which are the directions of propagation of the elastic perturbation.

The simplest form of a wavefront is the plane wave, where the rays are parallel to one another. Considering the temporal evolution of a wave, a distinction between periodic and non-periodic waves can be made. A periodic motion is of the type such that the displacement-time relationship repeats itself. Mathematically a wave u(t) could be defined periodic if there is a period T for which:

$$u(t + T) = u(t) \tag{1.5.1}$$

Harmonic or sinusoidal motion is the simplest form of vibratory motion; for this typology of wave displacement, velocity and acceleration vary in a sinusoidal manner with time. A wave is non-periodical when it does not repeat identically after constant time increments. It could be due to impulsive shock (such as explosions) or transient-type actions (such as earthquake or traffic). To introduce the fundamental features of a wave, the solution of the one-dimensional equation of motion can be considered, taking into account the propagation of a wave in the x-direction. The one-dimensional wave expression is a partial differential equation of the form (Kramer, 1996):

$$\frac{\partial^2 u}{\partial t^2} = V^2 \cdot \frac{\partial^2 u}{\partial x^2} \tag{1.5.2}$$

where V is the wave propagation velocity corresponding to the type of stress wave of interest. The solution of such an equation can be written in the form:

$$u(x,t) = f(V \cdot t - x) + g(V \cdot t + x) \tag{1.5.3}$$

where f and g can be arbitrary functions of (V•t-x) and (V•t+x) that satisfy equation (1.5.1). The argument of f remains constant when x increases with time at velocity V, and the argument of g remains constant when x decreases with time. So the solution of the previous equation describes a displacement wave f(V•t-x) travelling at velocity v in the positive x-direction and another one g(V•t-x) travelling at the same speed in the negative x-direction. It implies that the shape of the waves do not change with position or time. If a rod is subjected to a steady–state harmonic stress:

$$\sigma(t) = \sigma_0 \cdot \cos(\overline{\omega} \cdot t) \tag{1.5.4}$$

where σ_0 is the stress wave amplitude and $\overline{\omega}$ is the circular frequency of the applied loading, the solution can be expressed as:

$$u(x,t) = A \cdot \cos(\overline{\omega} \cdot t - N \cdot x) + B \cos(\overline{\omega} \cdot t + N \cdot x) \tag{1.5.5}$$

where:

$$N = \frac{\overline{\omega}}{V} \tag{1.5.6}$$

is the wave number, and A and B are the amplitudes of the two harmonic waves propagating in the positive and negative x-direction. Equation (1.5.5) indicates that the displacement varies harmonically with respect to both time and position (see Figures 1.5.1).

The period of the applied loading $\overline{T}$ is:

$$\overline{T} = \frac{1}{\overline{f}} = \frac{2 \cdot \pi}{\overline{\omega}} \tag{1.5.7}$$

It represents the time leg between two consecutive crests of the wave, whereas the analogue parameter in the space is the wavelength L_w:

$$L_w = \frac{2 \cdot \pi}{N} = v \cdot \overline{T} = \frac{v}{\overline{f}} = \frac{2 \cdot \pi}{\overline{\omega}} \cdot v = \frac{2 \cdot \pi}{N} \tag{1.5.8}$$

and expresses the spatial distance between two maximum values of the harmonic perturbation. At a given frequency, the wavelength increases with increasing the wave propagation velocity, so with the stiffness of the material.

For an assigned stiffness, L_w increases with the period of the harmonic wave.

(a) (b)

Figure 1.5.1 *Particle displacements as a function of time (a), and as a function of the position along the rod (b).*

Another important parameter is the phase angle ϕ of a harmonic wave, which describes the amount of time by which the peaks (and zero points) are shifted from those of a pure sine function (see Figure 1.5.2). The displacement will be zero when $\omega\cdot t+\phi=0$ or, consequently, when $t=-\phi/\omega$. In its simple form, simple harmonic motion can be expressed in terms of a displacement u(t), using the trigonometric expression:

$$u(t)=A\cdot\sin(\omega\cdot t+\phi) \tag{1.5.9}$$

where A is the amplitude, ω is the circular frequency describing the rate of oscillation in terms of radians per unit time.

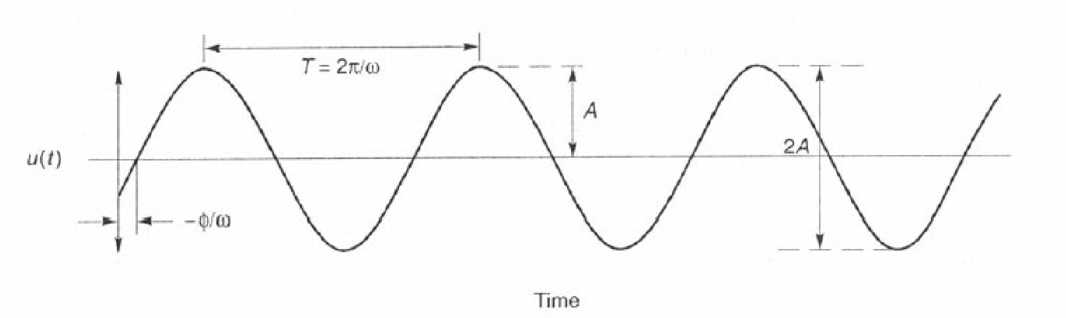

Figure 1.5.2 *Influence of the phase angle on the position of sinusoid; a positive phase angle indicate that the motion leads the sine function; it lags the sine function if the phase angle is negative.*

Harmonic waves are extremely useful in seismology and earthquake engineering because every periodic signal could be expressed by using Fourier series, as a sum of a series of sinusoids of different amplitudes, frequencies and phase angles:

$$X(t) = A_0 + \sum_{n=1}^{\infty} A_n \cdot \sin(2 \cdot \pi \cdot n \cdot f_0 \cdot t + \phi_n) \tag{1.5.10}$$

where A_0 is the medium value of the signal, A_n and ϕ_n are respectively amplitude and phase angle of the harmonic wave of frequency equal to $f_n = n \cdot f_0$. A plot of A_n versus $n \cdot f_0$ is known as a Fourier amplitude spectrum; a plot of ϕ_n versus f_n gives a Fourier Phase Spectrum.

1.6. Elastic waves approaching discontinuity surfaces.

The simplest discontinuity consists of a layer limited by a unique boundary that is the topographic surface. This boundary separates the layer where the propagation is mechanically possible (made of rock or soil) from air, unable to transmit waves. Generally speaking, waves propagate through a medium made of a certain number of discontinuities, which separate materials with different properties; when a wave intercepts a different layer, some modifications in amplitude and direction of wave, possible modal conversion phenomena and the generation of new typology of waves occur.

When a body wave travelling in an elastic medium encounters an interface with another elastic medium, some of the incident wave energy will be reflected into the first medium and some energy will be transmitted into the second medium.

Furthermore, there is another phenomenon called “mode conversion” for which the reflected waves and the transmitted ones generated at the interface could be either of the same type of the incident waves or of different typology.

Using the elastic theory, Zoeppritz (1919) determined the nature of the reflected and transmitted waves and the distribution of energy between these waves (Richart, 1970). For an incident P-wave (P) (see Figure 1.6.1a) there will be four resultant waves:

1) a reflected P-wave (P-P1)
2) a reflected SV-wave (P-SV1)
3) a refracted P-wave (P-P1)
4) a refracted SV-wave (P-SV2)

For an incident SV-wave (SV) (see Figure 1.6.1b) there will be four resultant waves too:

1) a reflected SV-wave (SV-SV1)
2) a reflected P-wave (SV-P1)
3) a refracted SV-wave (SV-SV2)
4) a refracted P-wave (SV-P2)

An incident SH-wave (SH) (see Figure 1.6.1c) produces only:

1) a reflected SH-wave (SH-SH1)

2) a refracted SH-wave (SH-SH2)

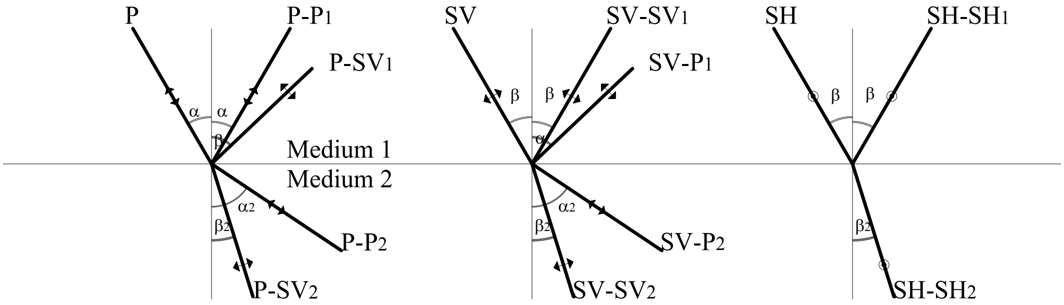

(a) Incident P-Wave (b) Incident SV-wave (c) Incident SH-wave

Figure 1.6.1 *Partition of the elastic wave at the interface between two elastic media.*

The angle, at which a resultant wave leaves the interface, depends on the angle at which the incident wave approaches the interface and the ratio of wave velocities of the media. Exit angles for all waves can be found from Snell's law:

$$\frac{\sin\alpha}{v_{P1}} = \frac{\sin\beta}{v_{S1}} = \frac{\sin\alpha_2}{v_{P2}} = \frac{\sin\beta_2}{v_{S2}} = \text{constant} \qquad (1.6.1)$$

Where the angles α, α_2, β, β_2 are measured from the normal to the interface and are defined in Figure 1.6.1, and V_{P1}, V_{S1}, V_{P2}, V_{S2} are, respectively, the velocities of the P-wave and S-wave in the first medium and the velocities of P-wave and S-wave in the second one. The eq. (1.6.1) underlines that:

1) the reflecting angle is identical to the incident one, both for S-wave and P-wave;

2) the refracting angle is linked to the incident angle by the velocity of propagation of the waves into the two materials divided by interface.

Actually, if the waves are travelling into a material and intercept a less stiff material, the refracted wave will be closer to the normal at interface, i.e. waves propagating toward the surface, throughout layers with decreasing stiffness, are refracted to a direction tending to the vertical. In the analyses performed in this thesis, waves are consequently propagated vertically to the surface, without considering any deviation in direction.

At the interface, it is not observed only a variation in the propagation direction and modal conversion phenomena, but also a variation in the wave amplitude. The amplitude of the reflected and refracted waves could be expressed as a function of the incident wave amplitude imposing the conditions of continuity of the displacements and tensions at interface.

Zoeppritz (1919) expressed the distribution of energy among the resultant waves in terms of incident and resultant wave amplitudes (see Figures 1.6.2 and 1.6.3), using the notation reported in the following:

A=amplitude of P-wave;
B=amplitude of incident S-wave;
C=amplitude of reflected P-wave;
D=amplitude of reflected S-wave;
E=amplitude of refracted P-wave;
F=amplitude of refracted S-wave;
ρ_1=density of medium 1;
ρ_2=density of medium 2.

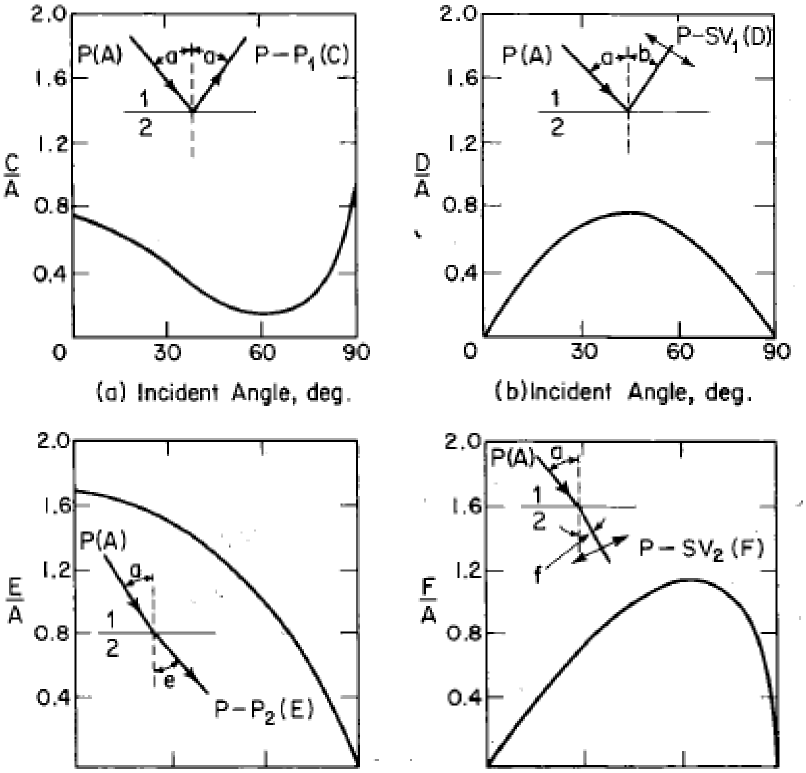

Figure 1.6.2 *Amplitude ratio with respect to the incident angle for P-wave (Richart, 1970).*

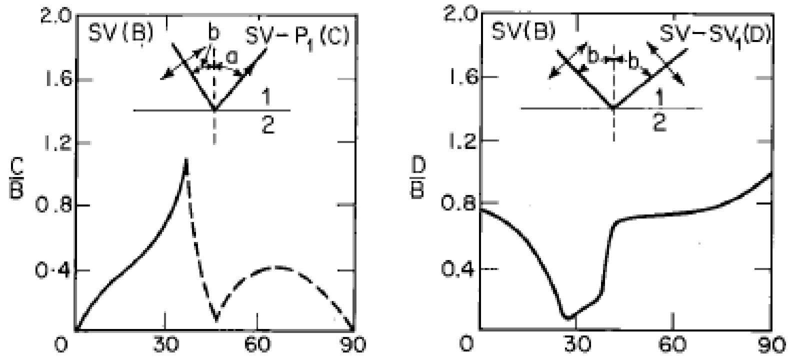

(a) Incident Angle, deg.   (b) Incident Angle, deg.

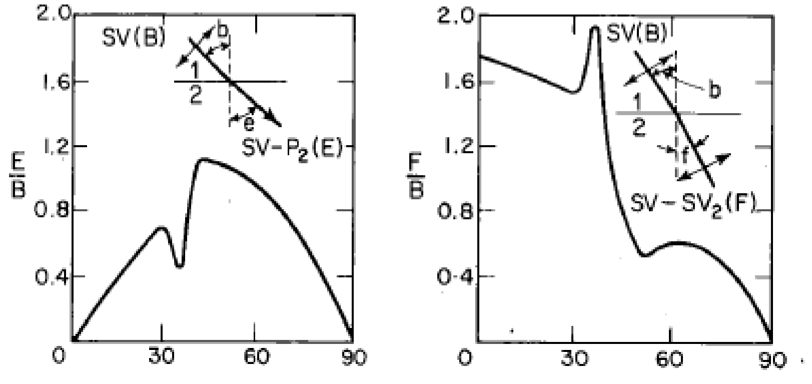

(c) Incident Angle, deg.   (d) Incident Angle, deg.

Figure 1.6.3 *Amplitude ratio with respect to he incident angle for SV-wave (Richart, 1970).*

When the interface is not plane, all the considerations previously reported are useful if the curvature radius is large enough with respect to the wavelength. When the curvatures are smaller, i.e. the characteristic lengths of the discontinuity surface are comparable with the incident wavelength, the wavefront is extremely modified by a diffraction phenomenon, a modification in the wave path due to the interception with an interface between two different materials, which differs from reflection and refraction phenomena (Sanchez-Sesma, 1987).

In order to explain the diffraction phenomenon, it could be reminded the Huygens' Principle which states that every point on a wave surface becomes in turn a source for a new disturbance, and so every point may be considered the source of a secondary wave; the successive wavefront is the tangential envelope of the secondary wavesfronts.

If a scheme with a plane wavefront generated by a certain source, interacting with a semi-infinite length rigid screen (see Figure 1.6.4), is considered, when the direct wave interacts with the edge, as previously reported by the Huygens' Principle, the points on the edge become vibration sources and generate spherical waves. The envelope of these spherical waves is a wave with a cylindrical front whose amplitude is function of the distance from the edge, of the incident angle, of the angle formed by the normal to the screen and the propagation direction, and of the wavelength. In Figure 1.6.4 the amplitude of the wave for the different propagation direction is schematically represented by the length of the segments that describe the diffracted wavefront.

The diffraction is also named scattering, term used principally to indicate all the modifies at which an incident wavefront may be submitted due to the presence of a discontinuity.

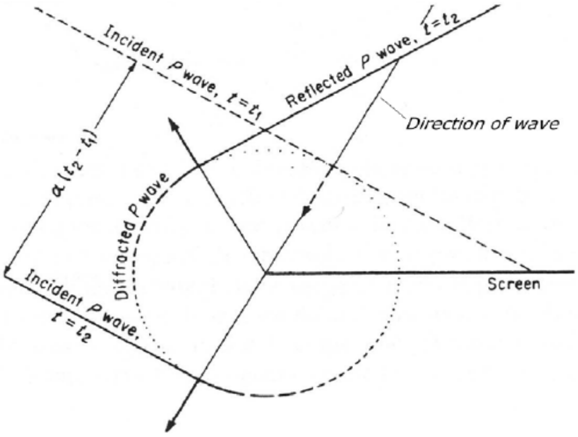

Figure 1.6.4 *Diffraction of a plane wave due to a semi-infinite rigid screen (Grant and West, 1965).*

Generally speaking, when a wave approaches an interface, there is a change in the propagation direction, associated to the generation of typologies of waves which differ from the incident one. The amplitude of the generated waves can be expressed as a function of the incident wave one, imposing the appropriate continuity conditions on displacements and tensions. It has just reported an overview of how complex is the matter if a generic incident angle is considered. It becomes easier for a vertical incident wave, because there are not at all mode conversion phenomena. For instance, if a P-wave orthogonally touches a discontinuity surface, only compression stresses will be generated. In this case, if A_I is the amplitude of the incident wave and A_R and A_T are respectively the reflected and refracted (transmitted) amplitude, the following two non- dimensional parameters can be defined as:

$$\begin{aligned} c_r &= \frac{A_R}{A_I} = \frac{1-\alpha}{1+\alpha} \\ c_t &= \frac{A_T}{A_I} = \frac{2}{1+\alpha} \end{aligned} \tag{1.6.2}$$

where α is the dynamic impedance ratio, defined as:

$$\alpha = \frac{\rho_2 \cdot V_2}{\rho_1 \cdot V_1} \tag{1.6.3}$$

where ρ_1 and V_1 , as well as ρ_2 and V_2 are couples of values representing respectively the density and the velocity of the medium from which the waves come (1) and the density and the velocity of the medium the wave is coming to (2). The two ratios previously reported are generally named respectively coefficients of reflexion and of transmission, and their variation depends on the dynamic impedance ratio α (Figure 1.6.5). If the waves travel from a stiffer medium to a softer one ($\alpha < 1$) the transmitted wave amplitude increases with respect to the incident wave amplitude ($c_t > 1$). Lowering the stiffness of the incoming media, the wave amplitude increases. If a wave touches a medium infinitely stiff with respect to the outcoming one (α tends to ∞) the reflection coefficient c_r tends to -1, while the transmission coefficient tends to 0, actually the wave will be completely reflected into the outcoming medium. An example of alteration on the motion field due to a discontinuity is reported in Figure 1.6.5.

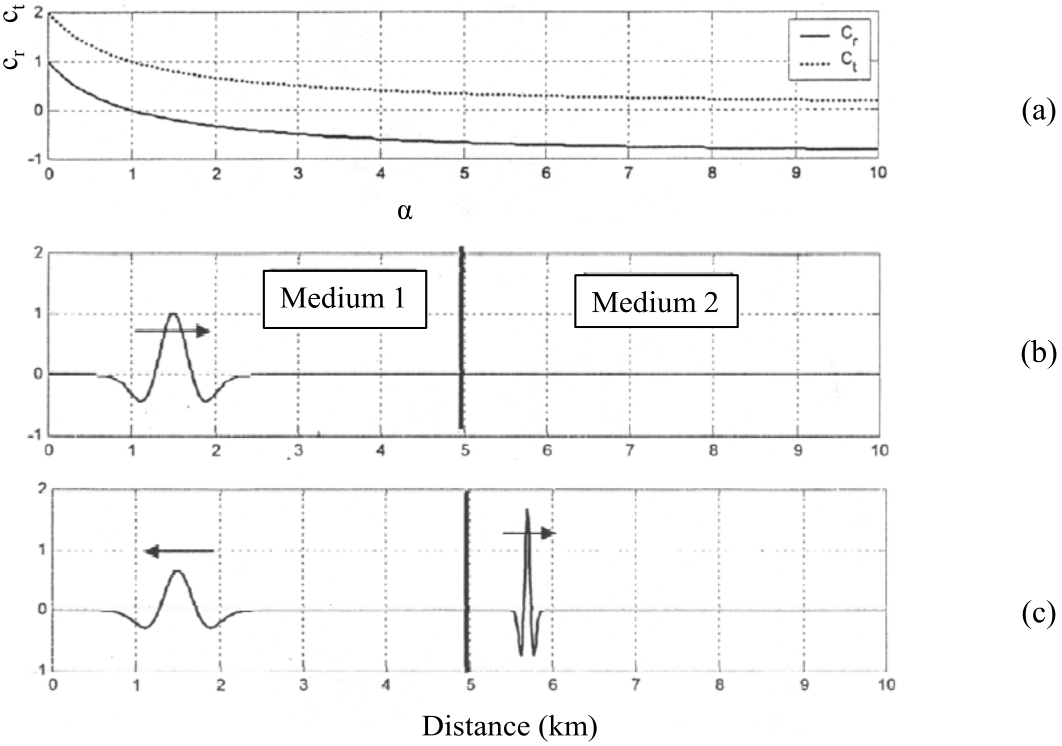

Figure 1.6.5 *Reflection and transmission coefficients for a wave travelling from a medium 1 to a medium 2, approaching normally to an interface placed at 5km from the origin; the velocities are V_{S1}=5000m/s V_{S2}=1000 m/s and the media have equal densities (a); variations of c_r and c_t with respect to α: displacements field at a certain time at which wave hasn't approached interface yet (b); displacements field after 1.4 seconds, with the propagation of a reflected wave into medium 1 and a transmitted wave into medium 2 (c) (Faccioli e Paolucci, 2005).*

Generally speaking, the amplitudes of reflecting and refracted waves hardly depend on the incident angle and the impedance ratio between adjacent materials.

1.7. Phenomena of stress waves attenuation.

In the previous paragraphs, only the propagation of waves in homogeneous linear elastic materials has been considered, where waves travel indefinitely without any change in amplitude; this is an unrealistic condition in real materials, in which it is well known that the amplitude attenuates with distance. This attenuation can be attributed to two causes: one depends on the properties of the materials through which the waves travel; the second involves the geometrical features of the problem. From the engineering point of view, the most significant waves for structural verification purposes are those associated with the horizontal propagation of S-waves, because the volumetric strains produced by P-waves are generally negligible compared to distorsional ones due to S-waves (Kramer, 1996).

The mechanical behaviour of soils has been consequently studied substantially investigating the conditions due to cyclic simple shear, i.e. with reference to a cyclic shear increment $\tau(t)$ load, starting from the geostatic conditions (σ'_{v0} , σ'_{h0}).

Laboratory tests have shown that soil stiffness and damping are influenced by the cyclic strain amplitude, the density and the mean principal effective stress for a coarse grained soil, the plasticity index and the overconsolidation ratio for fine grained soil, and the number of loading cycles (Kramer, 1996; Silvestri, 1991; Srbulov, 2008). A typical relationship between applied shear stress and induced shear strain exhibits a hysteretic loop (see Figures 1.7.1).

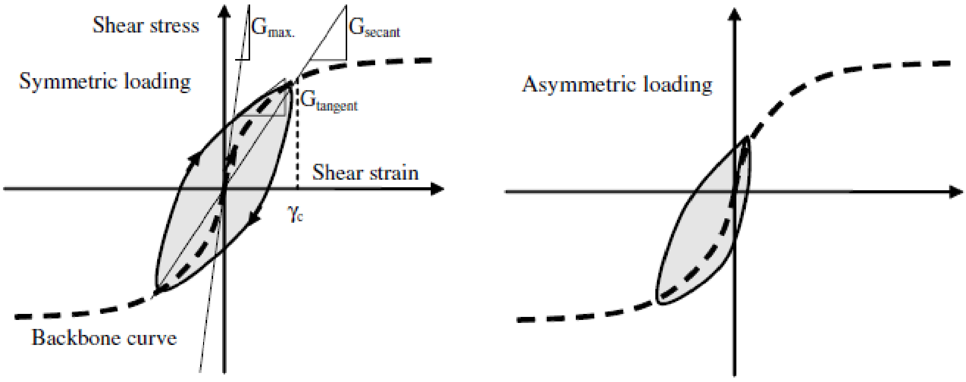

(a) (b)

Figure 1.7.1 *A hysteretic loop in one cycle of soil shearing, within soil under symmetric cyclic loading (a) and for the case of a non-symmetrical cyclic loading (b).*

The behaviour depicted in Figures 1.7.1 obviously stems from the fact that the soil has a non-linear, non-reversible (i.e. dissipative) and stress-dependent mechanical behaviour. The mechanical behaviour of the soil during a process of loading – unloading - reloading can be effectively represented by the parameters:

- shear modulus G
- damping ratio D.

Due to the non-linear behaviour of the soil, these parameters vary with the level of shear deformation γ ($G(\gamma)$, $D(\gamma)$). Three fields of behaviour are typically identified, respectively, related to: small, medium and large deformations (Figures 1.7.2).

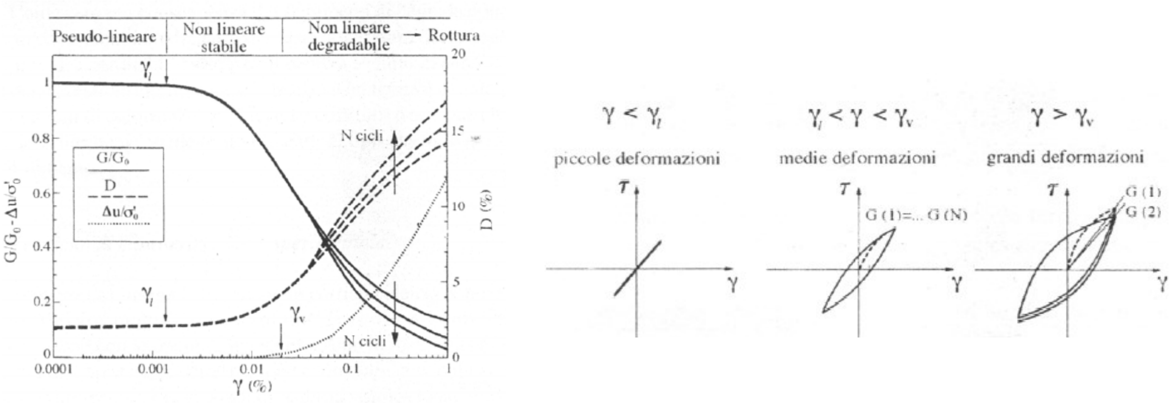

Figure 1.7.2 *Typical mechanical behaviour fields for a soil subjected to cyclic shear tests.*

The shear modulus G is a ratio between incremental shear stress and shear strain. Several different measurements of shear modulus are shown in Figures 1.7.1. When the increments are related to the origin (zero values), then the so-called secant modulus G_{secant} is obtained. If the increments are related to the change in values from previous values then the tangent modulus $G_{tangent}$ is obtained.

The area of the hysteretic loop A_{loop} is a measure of the internal energy dissipation, which involves the transformation of energy or work into heat, by particles friction due to their movements. The damping ratio ξ is frequently used as a measure of the energy dissipation (e.g. Kramer, 1996):

$$\xi = \frac{W_D}{4\cdot\pi\cdot W_s} = \frac{1}{2\cdot\pi}\cdot\frac{A_{loop}}{G_{secant}\cdot\gamma_c^2} \tag{1.7.1}$$

where W_D is the dissipated energy, W_S is the maximum strain energy, i.e. the area of the triangle in Figure 1.7.1 bordered by the G_{secant} line, the vertical at γ_c and the shear strain axis, and A_{loop} is the area of the hysteretic loop. Soil parameters G_{secant} and ξ are often referred to as equivalent linear soil parameters.

With the increase in shear stress and strain, slippage between grains causes a weakening of the soil structure, and a decrease of its shear strength and stiffness (Srbulov, 2008). This process results in rotation of the hysteretic loop towards the horizontal axis. The locus of points corresponding to the tips of hysteretic loops of various cyclic strain amplitudes is called a backbone (or skeleton) curve (e.g. Kramer, 1996). It should be noted that the backbone curve shown in Figure 1.7.2 is for one cycle of loading/unloading. A backbone curve for greater number of cycles may change if soil strength and stiffness change (decrease) with an increase in the number of cycles or with an excess pore water pressure increment. For elastic materials, the hysteretic loop and the backbone curve are straight and coincidental lines.

At very small shear strains, hysteresis is negligible, and the behaviour of the soil is often considered as linear-elastic. For strains smaller than a linear threshold (γ_l) the G modulus too is almost constant (G_0). This threshold takes values in the order of 0.0001% and 0.001%, in function of the granulometric and microstructural features of the soil, and is conventionally put in correspondence of a value of G equal to $G(\gamma)=0.95\cdot G_0$ (Silvestri et al, 1992).

The damping ratio ξ, also called D (at low shear strain D_0), has low value; D_0 assumes values of almost 1÷2% for sands and higher values for clays (2-4%) depending on the typology of clay. In this strain range, soil may be modelled according to a linear elastic constitutive criterion or viscous-elastic one.

When the soil behaves as an isotropic linear elastic body, the shear modulus G_0 is related to other quantities by:

$$G_0 = \rho \cdot V_S^2 \tag{1.7.2}$$

where ρ is soil unit density (kg/m^3) and V_S is the soil transversal wave velocity.

For higher mobilized shear strains, the soil maintains a stable behaviour, independent from the loading history and, after various repetition of the same cyclic stress path of constant amplitude; soil tends to follow the same cycle stress-strain: the soil exhibits a medium deformation behaviour. In this field, the soil can be modelled with an equivalent linear constitutive law by defining for each value of γ a pair of equivalent dynamic parameters G and D.

Growing the amplitude of the tangential deformations, it is possible to identify a further deformation level (volumetric threshold γ_v), exceeding γ_l of one or two orders of magnitude. When a soil exceeds this strain level, it is affected by irreversible deformations. Soil is in the field of high strains behaviour. At each cyclic cycle, non-negligible residual values of volumetric strain (if the solicitation occurs in drained conditions) or important values of neutral overpressure Δu (if the solicitation occurs in undrained conditions) are associated.

The soil retains memory of previous stress and strain-paths showing a behaviour that evolves with the number of cycles N; such behaviour is generally named "cyclic degradation", a term that reflects the structural changes of the soil skeleton. In this strain field, soil requires a constitutive law such as a hardening non-linear elasto-plastic model.

Material damping adsorbs part of the elastic energy of a stress wave, so the specific energy, i.e. the elastic energy per unit volume, decreases as the wave travels through a material. This specific energy decreases by another mechanism and so with the distance. Even though energy is conserved, there is a reduction in amplitude due to spreading of the energy over a greater volume of material, with a mechanism called radiation damping or geometric damping or geometric attenuation. When energy is released from a fault below the ground surface, body waves travel away from the source in all directions (see Figure 1.7.3). If the rupture zone can be assumed as a point source, the wavefronts will be spherical and the geometric attenuation will cause the amplitude to decrease at a rate of 1/r. The attenuation is larger if the waves travel next to the surface rather than in the medium, where the rate of attenuation is proportional to $1/r^2$.

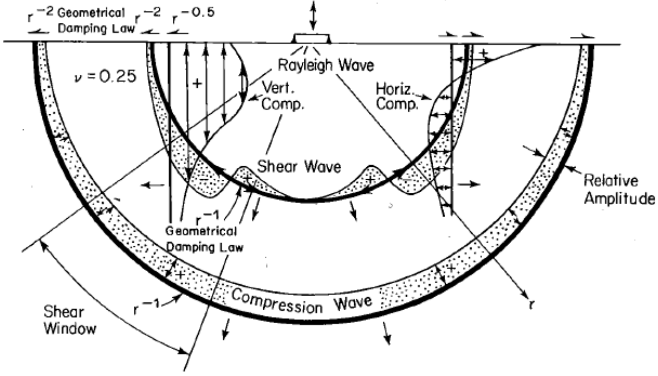

Figure 1.7.3 *Geometrical attenuation of body waves and Rayleigh waves.*

Rayleigh waves, having a cylindrical wavefront, attenuate with a rate of $1/r^{0.5}$. Surface waves attenuate geometrically more slowly than body waves, and so this explain the greater proportion of surface wave motion relative to body wave motion that is commonly observed at large epicentral distances. If the attenuation due to the dissipative properties of the material is considered, in the case of an harmonic wavefront with angular frequency equal to ω, it will lead to:

$$A_1 = A \cdot \frac{r}{r_1} \cdot e^{-\frac{\omega}{2 \cdot Q_f \cdot V}(r_1 - r)} \tag{1.7.3}$$

where V is the wave velocity and Q_f the quality factor, used in seismology to define the dissipative properties of a material:

$$Q_f = \sqrt{\frac{1 + D^2}{2 \cdot D}} \tag{1.7.4}$$

where D is the damping ratio. The previous expression shows that the high frequency components attenuate much more rapidly with the distance, explaining why at large distances seismograms have low dominant frequencies.

1.8. Seismic site response

The seismic motion generated by an earthquake at the free surface of a certain site (free-field condition) depends on different phenomena synthetizing in: source mechanism, wave propagation from the source to the site, and site effects. The first two phenomena define the input motion at the site, whereas the site effect cause modifies due to the interaction between the seismic waves and the site conditions i.e. the morphologic and the stratigraphic characteristics of the site and the physical and mechanical properties of the materials.

The total amount of modifies of the input seismic motion in terms of amplitude, frequency content and duration is called “site effects”.

The site effects result from a certain amount of physical phenomena like multiple reflexions, diffractions, focalization, resonance, etc, whose waves are subjected due to discontinuities or topographic irregularities. As a function of the different physical phenomena involved into the site effect, it is possible to distinguish between:

- stratigraphic effects (1D);
- topographic and basin effects (2D).

Practically, the site effects are valued with respect to a reference motion site. This motion could be that of a planar rock outcrop. The seismic motion, calculated by using numerical or experimental methods, is so faced to the motion on the bedrock (called rock outcropping motion).

The seismic site response indicates the stratigraphic or one-dimensional (1D) effects, i.e. the changes occurred to a seismic motion propagating almost vertically through a soil deposit with a horizontal free surface level, characterized by a substantially horizontal stratification and negligible lateral variations. From a physical point of view, the hypothesis of horizontal stratification, free horizontal surface and vertical body waves propagation involve the absence of surface waves and the exclusion of phenomena of mode conversion.

As reported by Rogriguez-Marek (2000), significant damage and loss of life has been directly related to the effect of local site conditions in various earthquakes, such as the Mexico City (1985), Loma Prieta (1989), Northridge (1994), and Kobe (1995) earthquakes (e.g. Seed et al. 1987; Chang et al. 1996). The amplification of the ground motion due to the local site conditions plays an important part in increasing seismic damage; the correlation between site effects and building damage is dramatically illustrated in Figure 1.8.1 for the Caracas earthquake (1967). Larger amounts of damage had occurred when the natural periods of the buildings and the site were closely matched. These observations suggest that a correct quantification of site effects is necessary for a complete assessment of the seismic hazard.

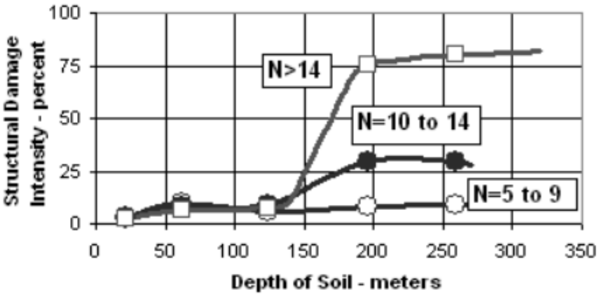

Figure 1.8.1 *Relationship between structural damage intensity and soil depth in the Caracas earthquake of 1967; N=number of stories (from Seed and Alonso, 1974).*

Referring to a 1D analyses, when waves are propagated from the base to the upper part through a soil layer, at the ground level the whole amount of energy is retransmitted into the medium, because the atmosphere has zero dynamic impedance (see §1.6). Waves travel through the soil and, when they touch the base of the soil column, are partially reflected, and partially transmitted into the base soil, according to the mutual impedance ratio. The amount of reflected energy is proportional to the impedance ratio: the higher the dynamic impedance of the base with respect to the soil layer, the higher the energy retransmitted into the soil. The total reflection at surface and the reflection at the base may cause a wave entrapment into the soil layer. The loss of energy by transmission to the base is named radiative damping.

To sum up, the effects of site stratigraphy are mostly attributable to phenomena of:

- "entrapment" of seismic waves, as a result of multiple reflections due to the impedance contrast between the soil constituting the deposit and the underlying bedrock;
- resonance between incident and reflected seismic waves , depending on the condition of the subsurface stratigraphy, the physical-mechanical properties of the soils and the predominant frequency content of the seismic motion .

A description of a seismic motion can be made either in the time domain or in the frequency domain. In the time domain , the most significantly parameters used to describe the features of a certain earthquake are the maximum value (called “peak”) of acceleration or velocity or displacement and the duration; in the frequency domain the most useful are the Fourier spectrum and the response spectrum in acceleration or velocity or displacement.

The response spectrum represents the law of variation of the maximum amplitude in terms of acceleration, velocity or displacement of the motion produced by a signal (F(t)) applied at the base of a simple oscillator with a certain mass m, an elastic stiffness k and a damping c, described by the equation:

$$m \cdot \ddot{u} + c \cdot \dot{u} + k \cdot u = F(t) \qquad (1.8.1)$$

with a certain damping ratio $\xi = c / c_c = c / \left(2 \cdot \sqrt{k \cdot m}\right)$, and a natural period defined by:

$$T = 2 \cdot \pi \cdot \sqrt{\frac{m}{k}} \qquad (1.8.2)$$

Then, the variation of the seismic motion can be efficiently evaluated by comparing the parameters of the motion at the surface of the soil to those at the bedrock (site reference motion), in the time and frequency domain. In the former the most practical parameter is the ratio between the maximum acceleration at the surface ($a_{max,s}$) and the maximum one at the bedrock ($a_{max,b}$), called amplification factor. This factor may be also less than unity when the site effects produce a deamplification of the motion amplitude passing into soil layer.

The description of a seismic motion cannot be only limited to the variations in terms of maximum amplitude, because modifications in the frequency content of the signal are possible too. The soil works as a filter, increasing the amplitude of the motion on some frequencies, and reducing them for other ones. To evaluate the filter effect of the soil is so necessary take in account the frequency domain, by using the amplification function A(f). Any amplitude of the transferring function is the ratio between the amplitude of the Fourier spectrum of the motion at the surface and at the bedrock, considering a certain frequency. By varying the value of the frequencies, the different ratios define the profile of the transferring function. This methodology can be applied only in the case of linear elasticity for the soil. In this hypothesis, the amplification function is a property of the site and can be expressed as a function of the geometry and mechanical properties of the soil.

The essential characteristics of the stratigraphic effect may be understood by referring to a simple mono-dimensional scheme made of an isotropic, linear elastic, homogenous soil, with a given thickness H, placed on a bedrock subjected to harmonic horizontal shear waves, which vertically propagate upwards in the overlying soil. The soil is supposed having a viscous-linear elastic behaviour, a density ρ_s, a shear wave velocity $V_{s,s}$ and a damping ratio D_s; the corresponding bedrock parameters are named ρ_b, $V_{s,b}$ and D_b.

If the incident shear waves are sinusoidal, the accelerations through the layer will be sinusoidal too (Kramer, 1996; Lanzo and Silvestri, 1999). If $D_b=0$, the amplification factor, which depend on the harmonic input signal, the soil damping D_s and the seismic impedance between the bedrock and the soil $\alpha = (\rho_b \cdot V_{s,b})/(\rho_s \cdot V_{s,s})$, has a variation as reported in Figure 1.8.2:

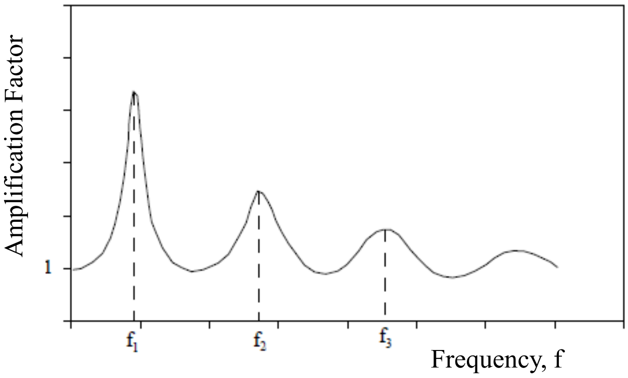

Figure 1.8.2 *Typical 1D amplification function.*

The motion is amplified at certain frequencies called natural vibration frequencies f_n of the soil deposit, equal to:

$$f_n = \frac{1}{T_n} = \frac{V_{s,s} \cdot (2 \cdot n - 1)}{4 \cdot H} \qquad n = 1,2,...,\infty \tag{1.8.3}$$

The maximum value of A(f) is:

$$A_{\max,n} \approx \frac{1}{\frac{1}{\alpha} + (2 \cdot n - 1) \cdot \frac{\pi \cdot D_s}{2}} \qquad n = 1,2,...,\infty \tag{1.8.4}$$

The peak values of the amplification function depend on the impedance ratio and damping ratio, and their maximum value is related to the fundamental frequency (i.e. for: n=1):

$$A_{\max,1} \approx \frac{1}{\frac{1}{\alpha} + \frac{\pi \cdot D_s}{2}} \qquad n = 1 \tag{1.8.5}$$

at a frequency equal to:

$$f_1 = \frac{V_s}{4 \cdot H} \qquad n = 1 \tag{1.8.6}$$

$A_{\max,1}$ can be appreciated as a function of α, by varying the damping ratio D_s (see Figure 1.8.3).

Cause the maximum value of the amplification ratio is related to the fundamental frequency (i.e. for: n=1), in the following chapters (especially in §2), the reported values of f_n and T_n are implicitly referred to n=1.

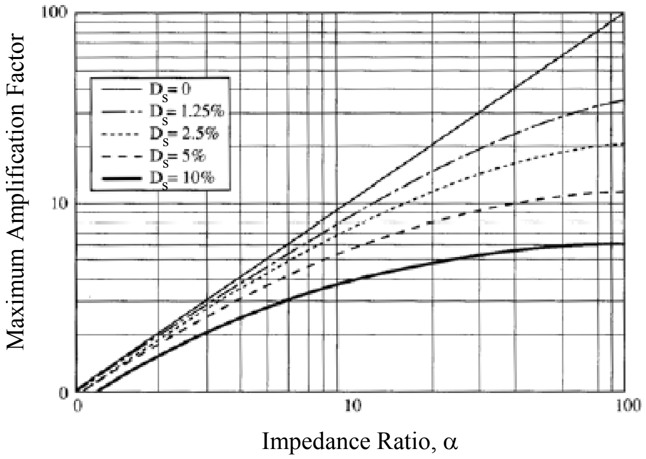

Figure 1.8.3 *Influence of the impedance ratio α and the damping ratio D_s on the maximum amplification related to the fundamental frequency, for a homogenous visco-elastic layer placed on a deformable basement.*

Therefore, the amplitude peaks depend on n, α and D_s. The impedance ratio has an effect on A(f) which is similar to the effect due to the damping: a sort of effective damping ratio can be defined as:

$$D_{ef} = D_s + D_r = D_s + \frac{2}{\pi \cdot \alpha} \tag{1.8.7}$$

where the first term (D_s) is the damping of the soil, the second one (D_r) depends on α, and represents the damping linked to the loss of energy for radiation. The expression of the amplitude peaks relative to the first fundamental frequency becomes:

$$A_{\max,a} \approx \frac{2}{\pi \cdot D_{ef}} \tag{1.8.8}$$

In their simplicity, these expressions are useful, because, considering a certain layer as made of an equivalent homogeneous stratum, they give a first indication on the range of frequencies in which the natural frequencies belong to. Above all, they underline the most important geotechnical parameters governing the site amplification phenomena: shear wave velocity, geometric feature. Typically (Pagliaroli, 2006) the fundamental frequency may vary between 0.2Hz (large depth layers, such as for the Los Angeles or Tokyo layers, or extremely soft soil layer such as for Mexico City soil deposits) and 10Hz (much thin layers and stiffer soils).

By increasing the intensity of the seismic input, the shear strains come across the linear behaviour, and the seismic site response is influenced by the soil non-linearity; generally speaking, increasing the non-linear effects, the fundamental frequency goes down, cause to the decrement in shear stiffness due to the shear strain increments. At the same time, the peak amplification goes down thanks to the increment in damping; therefore, the amplification function is not a property of the layer, but it depends on the amplitude and the frequency of the seismic motion too and the soil non-linear behaviour. For lower strain amplitude, the peak acceleration at surface generally increases with respect to the bedrock motion; actually, for higher peak acceleration amplitudes on rock, it is observed a reverse response, with decreasing values along the soil layer (see Figures 1.8.4: Seed et al, 1976; Idriss, 1990).

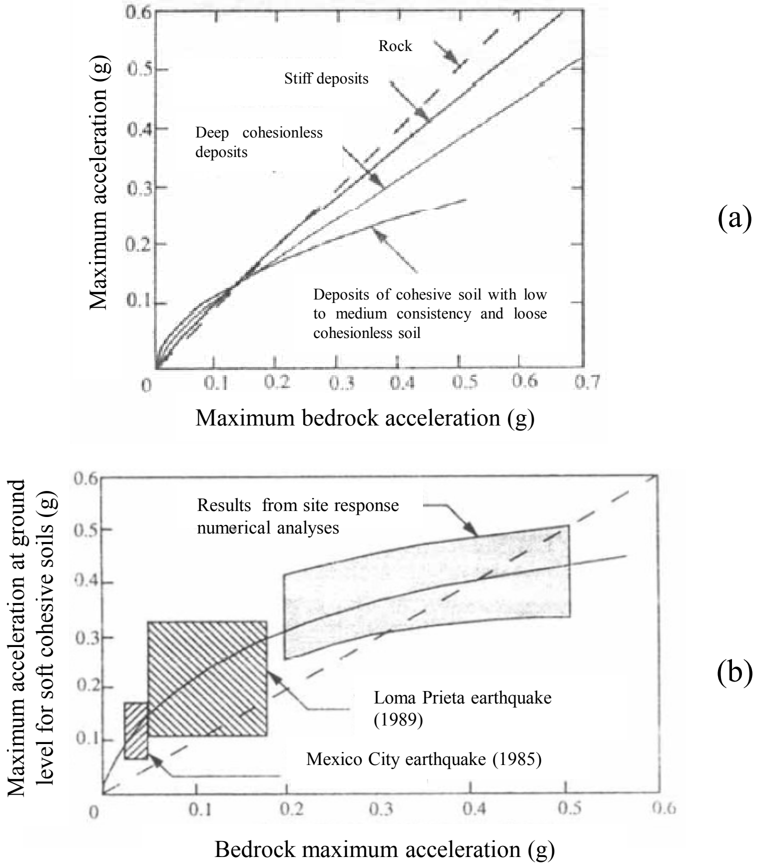

Figure 1.8.4 *Maximum acceleration variation at surface with respect to the maximum acceleration at bedrock for various deposits (a) (Seed et al, 1976; Lanzo, 1999) and soft cohesive soils (b) (Idriss, 1990).*

During a certain number of earthquakes in the last decades, the topography site effects have been also recorded (Silvestri, 1999). The topographic effects (due to, for instance, topographic reliefs and slopes) caused by simple irregularities could be estimated by referring to exact solutions provided for idealized problems, as a wedge-shaped medium subjected to SH-waves

(Sanchez-Sesma, 1990) or cliff-type topographies having different dynamic stabilities and experiencing different levels of seismic shaking (Jibson, 1987).

The observations on the damages localization suggests that, in terms of ground motion amplification, the shallow geometrical features have a larger influence on the upper part of an isolated topographic relief with respect to the base; the following meaningful remarks have been derived from experimental and theoretical studies (Geli et al., 1988; Bard, 1994):

- in the frequency domain, the topographic amplification is maximum in a frequency range corresponding to wavelengths comparable to the width of the topographic relief;
- the topographic amplification on the crest of a topographic relief tends to increase by increasing the relief gradient, i.e. the so called "aspect ratio" H/L, where H is the height of the relief and the L is the half-length measured at the base;
- the surface topography affects the amplitude and frequency content of ground motion also because of the diffraction of body and surface waves which leads to interference patterns between direct and diffracted waves, causing a complex displacement field, amplification and deamplification phenomena, and important differential displacements;
- the topographic amplification is lower for incident P-waves with respect to S-waves and is related to the angles at which the waves approach the relief surface (Altieri, 2012);
- experimental amplification ratios (especially in the frequency domain) are generally greater than those theoretically expected, due to various factors such as the three-dimensional effects, the influence of the adjacent topographic reliefs, the effects of the directivity of the source mechanism.

In particular, Faccioli et al. (2002) have attributed the topographic amplification to two different classes of phenomena: the former is the focusing and defocusing of seismic waves, as shown by geometrical optical methods (Sanchez-Sesma 1990); the latter is the topographic relief resonance that occurs if the wavelength of the seismic action is comparable with the horizontal dimension of the topographic irregularity. The two phenomena have different effects: if the focusing and defocusing of seismic energy leads to an irregular distribution of damage, the resonance phenomenon involves an extended amplification that affects the entire topographic relief (Pagliaroli, 2006).

Bouckovalas and Papadimitriou (2004) have studied the seismic motion of a step-like slope (see Figure 1.8.5), having a linear visco-elastic behaviour and subjected to a harmonic SV wave that propagates vertically. Several factors (i.e. the slope inclination, the material damping, the number of stress cycles and H/L_w, H being the height of the relief and L_w the incident wavelength) have been varied, allowing for a number of meaningful remarks, which are briefly listed in the following:

- the ground motion is generally amplified at the crest and deamplified at the base;
- a purely horizontal action induces a significant vertical motion at the surface too: at the crest, the vertical accelerations can achieve the same order of magnitude of the horizontal acceleration in free-field conditions;
- the effect of the slope topography is to alter (amplify or de-amplify) the peak horizontal seismic ground acceleration close to the crest; it also produces a parasitic vertical acceleration that has to be superimposed to that of the incoming seismic excitation;
- the topographic effects fluctuate intensely with distance away from the slope, because of the multiple reflections of the waves SV on the surface of the slope, the propagation of Rayleigh waves generated at the crest and the possible interaction between these waves (reflected and diffracted) with the incident wave field;
- the topographic effects are linked to the slope inclination and the ratio H/ L_w;
- the soil hysteretic damping ratio ξ has a significant effect only on the distance from the crest of the slope at which the dynamic effects are negligible, while the number of significant cycles N has a relatively minor effect.

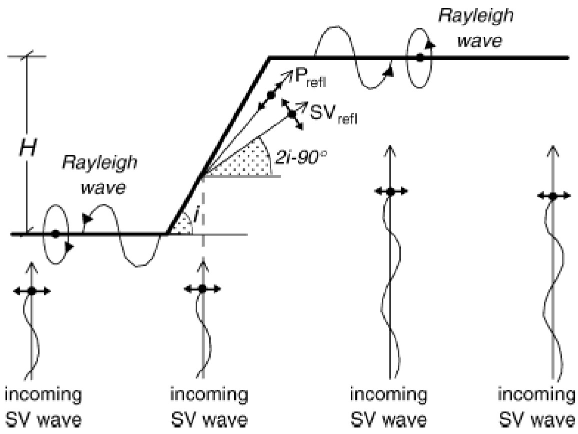

Figure 1.8.5 *Schematic illustration of incoming SV waves and induced P_{refl}, SV_{refl} and Rayleigh in the case of step-like slopes ($i \geq 45°$).*

On the edges of the alluvial valleys, it is possible to observe significant amplification phenomena accompanied by increases in the duration of the seismic motion, much more larger than those predicted by one-dimensional propagation theories based on the vertical propagation of shear waves. In the case of the alluvial valleys or basins, other interaction phenomena due to the 2D or 3D effects, not taken into account by 1D analyses, can be observed, which are:

- the occurrence of seismic waves focusing in areas close to the valley edges, due to the constructive interference between the incident and the diffracted wave fields (Pitarka et al, 1996);
- when the seismic waves touches the non-horizontal rock interfaces at the sides of the valleys, the generation of surface waves with horizontal propagation direction occurs (Aki and Larner, 1970), and, for a large impedance ratio between the soil and the rock outcrop, these waves are entrapped in the inner part of the valley and are subjected to multiple reflection phenomena;
- 2D resonance of the entire valley can occur (Capotorti et al, 1997).

Generally speaking, the seismic response of a sedimentary valley is hardly related to its geometrical features. As far as this aspect in concerned, the so-called “aspect ratio”, defined as the ratio between the maximum depth H of the valley and its half-width L, plays a significant role. When the ratio H/L is lower (approximately <0.2), the valley can be defined “superficial”: in the frequency domain, the 2D and the 1D amplification phenomenon are similar each other. When the ratio H/L is higher, the valley can be defined as “deep”, and its dynamic response significantly differs from the 1D case, because of two-dimensional effects.

1.9. Synthetic parameters used to describe the results.

In this thesis, the dynamic motion has been studied by referring to some of its more significant characteristics, i.e. the amplitude and the frequency content, and to a parameter of efficiency related to the spectral parameters.

The amplitude has been generally referred to the peak values of acceleration, velocity and displacement with time.

In order to describe the variation in the frequency content, amplification ratios and Fourier amplitude spectra are generally reported. The amplification ratio depends on the Fourier amplitude spectrum, because it is the ratio, at a certain frequency, between the Fourier amplitude values calculated at the ground level and at a given position into the soil deposit (usually, at the bedrock level).

The fundamental and the mean periods are also considered to describe the frequency content of the signals.

The fundamental or predominant period T_P is the period that corresponds to the peak Fourier amplitude.

The mean period T_m (Rathje et al., 1998) is the best-simplified parameter for describing the signal frequency content; it is defined as:

$$T_m = \frac{\sum \frac{A_i^2}{f_i}}{\sum A_i^2} \tag{1.9.1}$$

where A_i is the Fourier amplitude at a given frequency, and f_i is the discrete Fourier transform frequency in the range 0.25÷20 Hz.

The response spectra show the response in terms of maximum acceleration, velocity or displacement of a simple oscillator (named: “SDOF”, which meens “Single Degree Of Freedom”), by varying its period, and assuming a damping ratio equal to 5%.

The dynamic motion modifications due to the introduction of a certain treatment deep into a soil deposit could be sharply identified by the S_d-S_a domain (see Figure 1.9.1). In such a representation of the SDOF response, a linear segment coming out from the origin of the axes represents a certain value of the simple oscillator period (see Figure 1.9.1).

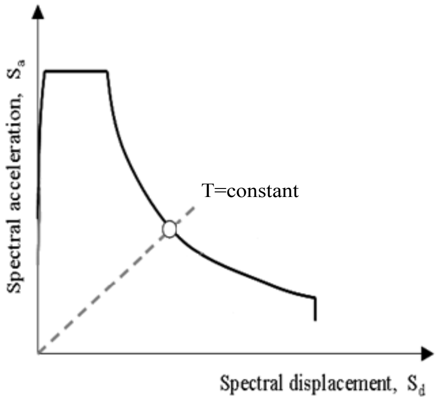

Figure 1.9.1 *Example of* S_d-S_a *curve.*

A synthetic and meaningful parameter is the well-known spectral intensity SI, often called "Housner intensity" (Housner, 1952), which allows to quantify the free-field seismic response. SI is defined as:

$$SI(\xi)=\int_{T_1}^{T_2} S_V(\xi,T)d(T) \tag{1.9.2}$$

where $S_V(\xi,T)$ is the spectral velocity for a given structural damping ratio ξ (5% in this case) and (T_1, T_2) is a reference range of the structural period. The integral quantity SI, which has the dimensions of a displacement, is often adopted as a synthetic ground motion parameter able to capture the combined effect of amplitude and frequency content on seismic response and structural damage (e.g. Bilotta et al., 2011; Lanzo et al., 2011; Puglia et al., 2013).
The integration extremes T_1 and T_2 originally proposed by Housner (1952) were respectively 0.1s and 2.5s, in order to include most of the fundamental periods of civil structures. In this thesis, the integration interval was set to focus the attention on squat masonry structures. Consistently with the indications of National Technical Code (NTC, D.M. 14.I.2008), the natural period T_B[s] of a masonry building of height H_B[m] can be estimated through the simplified formula:

$$T_B = 0.05 \cdot H_B^{3/4} \tag{1.9.3}$$

In this study, buildings with height H_B=3m÷20m are considered of interest; for such H_B values, eq. (1.9.3) yields a fundamental period T_B in the range 0.1s÷0.5 s (corresponding to a range of frequencies 2Hz÷10Hz), thus assumed as integration extremes of the spectral intensity.
The effectiveness of the proposed technique in attenuating the seismic inertial actions can be better inferred by introducing another synthetic parameter, i.e. the isolation efficiency parameter $E_I(T)$, inspired to a similar parameter proposed by d'Onofrio et al (1999).
$E_I(T)$ is defined as:

$$E_I(T)=\frac{S_{a,OFF}(T)-S_{a,ON}(T)}{S_{a,OFF}(T)} \tag{1.9.4}$$

in which $S_{a,OFF}(T)$ and $S_{a,ON}(T)$ are, for any given period T, the amplitudes of the surface acceleration response spectra of the deposit without and with the soft grouted layer, respectively. A perfect isolation will result into the full attenuation of the acceleration at ground surface ($E_I(T)=1$), while negative values will correspond to an amplification of the effects induced by the intervention.

1.10. References

Aki K. (1988). Local site effects on strong ground motion. Earthquake engineering and soil dynamics II: recent advances in ground motion evaluation. *ASCE geotechnical special publication, No.20,* Park City (USA).

Aki K. and Larner K. L. (1970). Surface motion of a layered medium having an irregular interface due to incident plane SH waves. *Journal Geoph. Research., Vol.70.*

Aki K., Richards P. G. (1980). Quantitative Seismology. *W. H. Freeman, San Francisco, California (USA).*

Alterio L. (2012). Seismic vulnerability reduction of monumental building by soils treatment. *Ph.D. Thesis, Università degli Studi di Napoli Federico II (Italia).*

Andersen L., Augustesen A. H. (2009). Mitigation of traffic-induced ground vibration by inclined wave barriers: a three-dimensional numerical analyses. *Proc. 16th International Congress on Sound and Vibration, Krakow (Poland).*

Bard P. Y. (1994) Effects of surface geology on ground motion: recent results and remaining issues. *Proc. 10th European Conference on Earthquake Eingineering, Vienna (Austria), Vol.1.*

Bouckovalas G. D., Papadimitriou A. G. (2004). Numerical evaluation of slope topography effects on seismic ground motion. *Proc. 11th Int. Conf. on Soil Dynamics and Earthquake Engineering and 3th Int. Conf. on Earthquake Geotechnical Engineering, Berkeley, California (USA), Vol.2, pp.329-335.*

Cai Y., Liang X. (2003) Dynamic properties of composite cemented clay Journal of Zhejiang University. *Journal of Zhejiang University SCIENCE, Zhejiang (China).*

Capotorti F., Monachesi G., Mucciarelli M., Sanò T., Trojani L. (1997). Danneggiamenti ed effetti di sito nel terremoto umbro-marchigiano del settembre 1997. *Ingegneria sismica, Vol.14(3).*

Chang S. W., Bray J. D., Seed R. B. (1996). Engineering Implications of Ground Motions from the Northridge Earthquake. *Bull. Seis. Soc. Am, Vol.86(1), Part B Suppl., pp.270-288.*

Chavez-Garcia F.J. (2011). Site effects due to topography and to soft soil layers: progress made and pending issues. A Personal Perspective. *Proc. 5th International Conf. on Earthquake Geotechnical Engineering – State of the art Lectures, Santiago (Chile).*

Chepkoit K. K. , Aggour M.S. 12 (2000) Dynamic properties of untreated and treated cohesive soils. *Proc. 12th World Conference on Earthquake Engineering Auckland (New Zealand).*

Chouw N., Schmid G. (1992). Building isolation using the transmitting behaviour of a soil layer. *Proc. 10th World Conference on Earthquake Engineering, Madrid (Spain), Vol.4, pp.2519-2524.*

Costanzo A., d'Onofrio A., Lanzo G., Pagliaroli A., Penna A., Puglia R., Santucci De Magistris F., Sica S., Silvestri F., Tommasi P. (2007). Seismic response of historical centers in Italy: selected case studies. *Workshop on 'Geotechnical Earthquake Engineering related to Monuments and Historical Centers', 4th ICEGE, Thessaloniki (Greece).*

Dietz M.S., Wood D. M. (2006). Shake table testing of a soft caisson for geotechnical seismic retrofit. *Proc. 4th International Conference on Earthquake Geotechnical Engineering, Thessaloniki (Greece).*

Di Prisco G., Serra M. (1996). Modellazione numerica dell'efficacia di interventi di trattamento del sottosuolo per la riduzione del rischio sismico. *Master Degree Thesis, Università degli Studi di Napoli Federico II, Napoli (Italy).*

D'Onofrio A., Mancuso C., Silvestri F. (1999). Reduction of seismic vulnerability by geomaterial attenuation procedures. *Proc. 2nd International Confererence on Earthquake Geotechnical Engineering, Lisboa (Portugal), pp.725-730.*

Doudomis N., Papadopoulos P. Papaliangas T (2002) Low-cost base isolation system on artificial soil layers with low shearing resistance. *Proc. 12th European Conference on Earthquake Engineering, paper reference 661.*

DM 14/1/2008. Norme Tecniche per le Costruzioni. *S.O. n. 30 - Gazzetta Ufficiale della Repubblica Italiana, No. 20 - 4/2/2008.*

Dolce M., Ponzo F.C., Di Cesare A., Arleo G. (2010) Progetto di edifici con isolamento sismico. *IUSS PRESS, Pavia (Italy), pp.215.*

Evangelista L., d'Onofrio A., Santucci de Magistris F., Silvestri F. (2011). Geotechnical characterization of some site interested by the 2009 L'Aquila earthquake. *Proc. of the 5th Int. Conf. on Earthquake Geotechnical Engineering, Santiago (Chile).*

Faccioli E., Paolucci R. (2005). Elementi di sismologia applicata all'ingegneria. *Pitagora editore, Bologna (Italy), pp.280.*

Gazetas G. (1991). Formulas and charts for impedances and embedded foundations. *Journal of Geotechnical Engineering ASCE, Vol.117(9).*

Giovannardi F., Gulsasola A. (2013) Basic isolation: dalle origini ai giorni nostri. *USGS: http://it.calameo.com/read/001671591369645c5959a.*

Gazetas G., Mylonakis G. (1998). Seismic soil-structure interaction: new evidence and emerging issues. *Proc. 3rd Conf. on Geotechnical Earthquake Engineering and Soil Dynamics, Seattle (USA).*

Geli L., Bard P. Y., Jullien B. (1988). The effect of topography on earthquake ground motion: a review and new results. *Bulletin of the Seismological Society of America, Vol.78, pp.42-63.*

Geli L., Bard P.Y., Jullien B. (1988). The effect of topography on earthquake ground motion: a reviewand new results. *Bull. Seism.Soc. Of America, Vol.78(1).*

Grant F. S., West G. F. (1965). Interpretation Theory in Applied Geophysics. *McGraw-Hill Book Company, New York, New York (USA), pp.583.*

Housner G. W. (1952). Spectrum intensity of strong-motion earthquakes. *Proc. Symp. on Earthquakes and Blast Effects on Structures, EERI, Univ. of California at Los Angeles, Earthquake Engineering Research Institute, Oakland, California (USA), pp.26–36.*

Idriss I.M. (1990). Influence of local site conditions on earthquake ground motions. *Proc. 4th U.S. Nat. Conf. on Earthquake Engineering, Palm Springs, California (USA), Vol.1.*

Islam Saiful A. B. M. , Jameel M. and Jumaat M.Z. (2011). Seismic isolation in buildings to be a practical reality: Behavior of structure and installation technique. *Journal of Engineering and Technology Research, Vol.3(4), pp.99-117.*

Jibson R. (1987). Summary on research on the effects of topographic amplification of earthquake shaking on slope stability. *Open file Report 87-268, U.S. Geological Survey, Menlo Park, California (USA).*

Kellezi L. (2001). Dynamic behavior of a softer layer overlying hard soil / bedrock and vibration reduction. *GEO-Danish Geotechnical Institute, Lyngby (Danmark).*

Kirtas E., Rovithis E., Pitilakis K. (2009). Subsoil Interventions Effect on Structural Seismic Response. Part I: Validation of Numerical Simulations. *Journal of Earthquake Engineering, Vol.13(2), pp.155-169.*

Kirtas E., Pitilakis K. (2009). Subsoil Interventions Effect on Structural Seismic Response. Part II: Parametric Investigation. *Journal of Earthquake Engineering, Vol.13(3), pp.328-344.*

Kramer S.L. (1996). Geotechnical earthquake engineering. *Prentice-Hall, Upeer Saddle River, New Jersey (USA), pp.653.*

Lanzo G., Silvestri F. (1999). Risposta sismica locale. *Hevelius Edizioni, Benevento, pp.159.*

Lanzo G., Silvestri F., Costanzo A., d'Onofrio A., Martelli L., Pagliaroli A., Sica S., Simonelli A. (2011). Site response studies and seismic microzoning in the middle Aterno Valley (L'Aquila, Central Italy). *Bulletin of Earthquake Engineering, Vol.9(5), pp.1417-1442.*

Lirer S., Flora A., Verdolotti L., Lavorgna M., Iannace S. (2006). Permeation grouting of fine grained pyroclastic soils and rocks. *Ground Improvement, Vol.10, pp.135-177, Thomas Telford Ed., London (Great Britain).*

Lombardi D., Flora A., Lirer S. (2012). A new approach for reducing seismic hazard on existing buildings by unusual deep soil grouting. *Int. Conf. on Ground Improvement and Ground Control (ICGI 2012), University of Wollongong, Wollongong (Australia).*

Lombardi D., Flora A., Lirer S., Silvestri F. (2012). Interventi di trattamento profondo dei terreni per la mitigazione del rischio sismico: primi risultati. *Incontro Annuale dei Ricercatori di Geotecnica – IARG 2012, Padova (Italy).*

Lombardi, D., Flora, A., Lirer, S., Silvestri F. (2013). An innovative approach for reducing the seismic risk of existing buildings and historic sites. *2nd Int. Symp. on geotechnical engineering for the preservation of monuments and historic sites, Viggiani C., Bilotta E., Flora A, & Lirer S. Editors, Napoli (Italy).*

Lovisolo F., Vitale S. (2006). Povertà, sviluppo e mobilità rurale in Africa Occidentale. *CCTM-Centro Città del Terzo Mondo, Politecnico di Torino, Torino (Italia).*

Martelli, A., 2009. Proceedings of International Conference Prohitech09.Rome June 2009 Italy.ICOMOS 1964. The Venice Charter (1964) - International charter for the conservation and restoration of monuments and sites. *Proc. 2nd International Congress of Architects and Technicians of Historic Monuments, Venice. ICOMOS, Int. Council on Monuments and Sites. internet: www.icomos.org/charters/venice_e.pdf*

Massarsch K.R. (2004).Mitigation of Traffic-induced Ground Vibrations. *Proc. 11th international conference on earthquake geotechnical engineering, pp.22–31. Berkeley, California (USA).*

Massarsch K.R. (2005).Vibration isolation using gas-filled cushions. *Proc. Sessions of the Geo-Frontiers Congress, Austin, Texas (USA).*

Naderzadeh A. (2009). Historical Aspects of Seismic Base Isolation Application. *Proc. JSSI 15th Anniversary International Symposium on Seismic Response Controlled Buildings for Sustainable Society, 16-18 Sept. 2009, JSSI, Tokyo (Japan).*

Nikolaou S., Mylonakis G., Gazetas G., Tazoh T. (2001). Kinematic pile bending during earthquakes: analyses and field measurements. *Geotechnique 51(5).*

Pagliaroli A. (2006). Studio numerico e sperimentale dei fenomeni di amplificazione sismica locale di rilievi isolati. *Ph.D. thesis, Università degli Studi di Roma La Sapienza, Roma (Italy).*

Pitarka A., Irikura K., Iwata T. (1996). Was the basin edge geometry responsilbe for the ground motion amplification in the disaster belt-like zone during January 17, 1995, Kobe (Hyogo-ken Nambu), Japan earthquake? *Proc. International Workshop on Site Response subjected to Strong Earthquake motions, Yokosuka (Japan).*

Rathje E.M., Abrahamson N. A., Bray, J.D. (1998). Simplified Frequency Content Estimates of Earthquake Ground Motions. *Journal of Geotechnical Engineering, Vol.124(2), pp.150-159.*

Richart F.E, Woods R.D. (1970). Vibrations of soils and foundations *Prentice-Hall, Upeer Saddle River, New Jersey (USA).*

Rogriguez-Marek A., Bray D. J., Abrahamson N. A. (1998) A geotechnical seismic site response evaluation procedure. *Proc. 12th World Conference on Earthquake Engineering (WCEE 2000), Auckland (New Zealand).*

Sanchez-Sesma F.J. (1987). Site effects on strong ground motion. *Soil Dynamics and Earthquale Engineering, Vol.6, pp.124-132.*

Sanchez-Sesma F.J. (1990). Elementary soultions for response of a wedge-shaped medium to incident SH and SV waves. *Bull. Seism.Soc.Of America, Vol.80(3).*

Saxena K. S., Avramidis A. S., Reddy K. R. (1987). Dynamic moduli and damping ratio for cemented sand at low strains. *Can. Geotech.Journ. Vol.25, pp.353-368.*

Seed H.B., Murarka J., Lysmer J., Idriss IM (1976). Relationships between maximum acceleration, maximum velocity, distance from source and local site conditions for moderately strong earthquakes. *Bull. Seism.Soc. of America, Vol.66(4).*

Seed, H. B. and Alonso, J. L. (1974). Soil-structure interaction effects in the Caracas Earthquake of 1967. *Report No. 73023, Earthquake Engineering Research Center, Engineering Department, University of California, Berkeley, California (USA).*

Seed H. B. Romo, M. P. Sun, J. J., Lysmer J. (1987). Relationships Between Soil Conditions and Earthquake Ground Motions in Mexico City in the Earthquake of September 19, 1985. *Report No. UCB/EERC-87/15, Earthquake Eng. Res. Center, College of Eng., University of California, Berkeley, California (USA).*

Silvestri, F. (1991). Analisi del comportamento dei terreni naturali in prove cicliche e dinamiche di taglio torsionale. *Ph.D thesis, consorzio tra le Università di Napoli Federico II, Roma La Sapienza, Bari Politecnico (Italy).*

Spencer L. M. (2010). Evaluation of sand treated with colloidal silica gel. *Phd Thesis Georgia Institute of Technology, Atlanta, Georgia (USA).*

Srbulov M. (2008). Simplified analyses with case studies and examples. *Springer ed., Berlin (Germany), pp.263.*

Taskov L., Antimovki A. and Kokalevki M. (2004). Shaking table test of efficiency of ALSC base-isolation system. *Proc. 13th World Conference on Earthquake Engineering Paper No. 785, Vancouver (Canada).*

Taskov L., Manova K., Krstevska L., Garevski M. (2010). Evaluation of efficiency of ALSC floating-sliding base-isolation system based on shake table test and floor response spectra. *Bull. Earthquake Eng (2010), Vol.(8), pp.995-1018.*

Tsang H.H., Lam N.T.K. Yaghmaei-Sabegh S., Sheikh M.N., Indraratna B. (2010). Geotechnical seismic isolation by scrap tire-soil mixtures. *Proc. the 5th international conference on recent advances in geotechnical earthquake engineering and soil dynamics, San Diego, California (USA).*

Tsang H.H., Lo S.H., Neaz Sheikh M. (2012). Seismic isolation for low-to-medium-rise buildings using granulated. *Earthquake engineering and structural dynamics, John Wiley & Sons, Hoboken, New Jersey (USA), Ltd. rubber–soil mixtures: numerical study.*

Tsang H.H. (2009). Geotechnical seismic isolation. Earthquake Engineering: New Research. *Nova Science Publishers, New York (USA), pp.55-87.*

United States Geological Survey's Largest and Deadliest Earthquakes by Year 1990 - 2011 *USGS: http://earthquake.usgs.gov/earthquakes/eqarchives/year/byyear.php*

Walker B. (1982). Earthquake.Planet Earth. *Time Life Books, pp.153.*

Wood D. M. (2006).Modelling of dynamic soil problems. *Proc. 4th International Conference on Earthquake Geotechnical Engineering – Invited Lectures, Thessaloniki (Greece)*

Wu G., Finn W. (1997). Dynamic Elastic Analyses of pile foundations using finite element method in the frequency domain. *Can. Geotech.Journ., Vol.34(1), pp.34-43.*

Yegian M.K.,Kadakal U. (2004). Foundation isolation for seismic protection using a smooth synthetic liner. *Journal of Geotechnical and geo-environmental Engineering, Vol.130(11).*

Yegian M.K. and Catan M. (2004). Soil Isolation for seismic protection using a smooth synthetic liner. *Journal of Geotechnical and geo-environmental Engineering ASCEE (Nov):1131.*

Zoeppritz K. (1919). Nachrichten von der Königlichen Gesellschaft der Wissenschaften zu Göttingen. *Mathematisch-physikalische Klasse, pp.66-94.*

2. Dynamic Analyses

2.1. Input motions

2.1.1. Natural signals

The performed dynamic analyses have been carried out using real scaled accelerograms and Ricker wavelets. As far as the former are concerned, in Table 2.1.1 the main features of the selected accelerograms are reported. Accelerograms have been recorded on rock outcrops during various earthquake occurrences, and have been chosen in order to obtain a continuous range in terms of their features (Silvestri and Tropeano, 2008). Figures 2.1.1.1÷2.1.1.3 illustrate their most important features, in terms of peak acceleration, main period, duration, time history and Fourier amplitude (see Figure 2.1.1.1 and Table 2.1.1.1). The duration of the seismic motion has been reported (see Table 2.1.1.1) in terms of significant duration, which is calculated as the time interval in which the percentage of the total Arias intensity registered is from 5% to 95% of the total amount. The Arias intensity (I_a) (Arias, 1970) has the dimension of a velocity and is defined as:

$$I_a = \frac{\pi}{2 \cdot g} \cdot \int_0^{\infty} [a(t)]^2 \, dt \tag{2.1.1.1}$$

where a(t) is the accelerogram.

Recording station	earthquake	year	Peak acceleration (g)	Mean period (s)	Predominant period (s)	Significant duration (s)
Sortino	Augusta	1990	0,115	0,464	0,080	8,950
Nocera Umbra - Biscontini	Umbria Marche (aftershock)	1998	0,101	0,111	0,1	3,13
San Rocco	Friuli (aftershock)	1976	0,090	0,293	0,1	5,73
Sturno	Campano Lucano 2	1980	0,078	0,438	0,22	14,12
Torre del Greco	Campano-Lucano 1	1980	0,063	0,589	0,66	30,32
Bagnoli Irpino	Campano-Lucano 1	1980	0,139	0,674	0,18	19,58
Sturno	Campano-Lucano 1	1980	0.358	0.872	0,2	15.48

Table 2.1.1.1 *Main features of the selected accelerograms.*

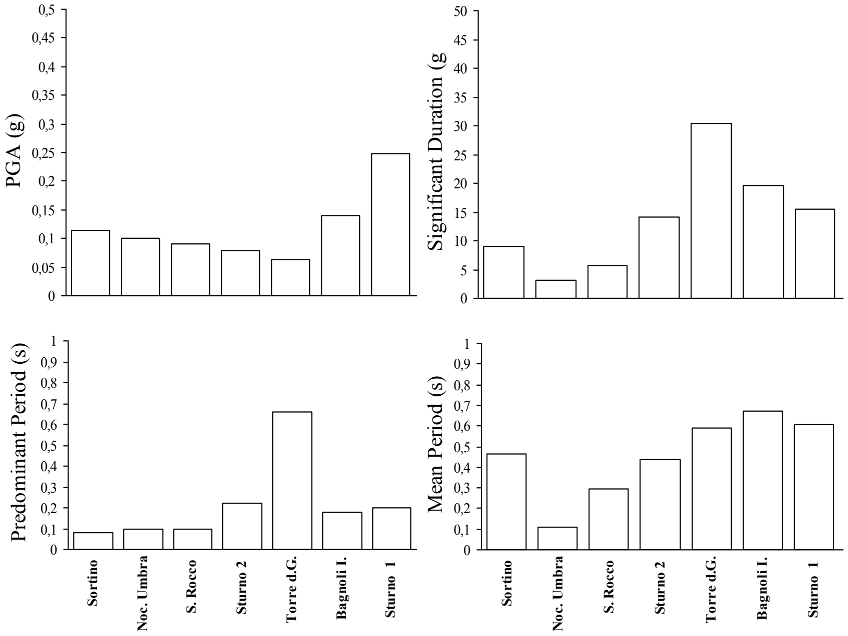

Figure 2.1.1.1 *Main features of the selected accelerograms.*

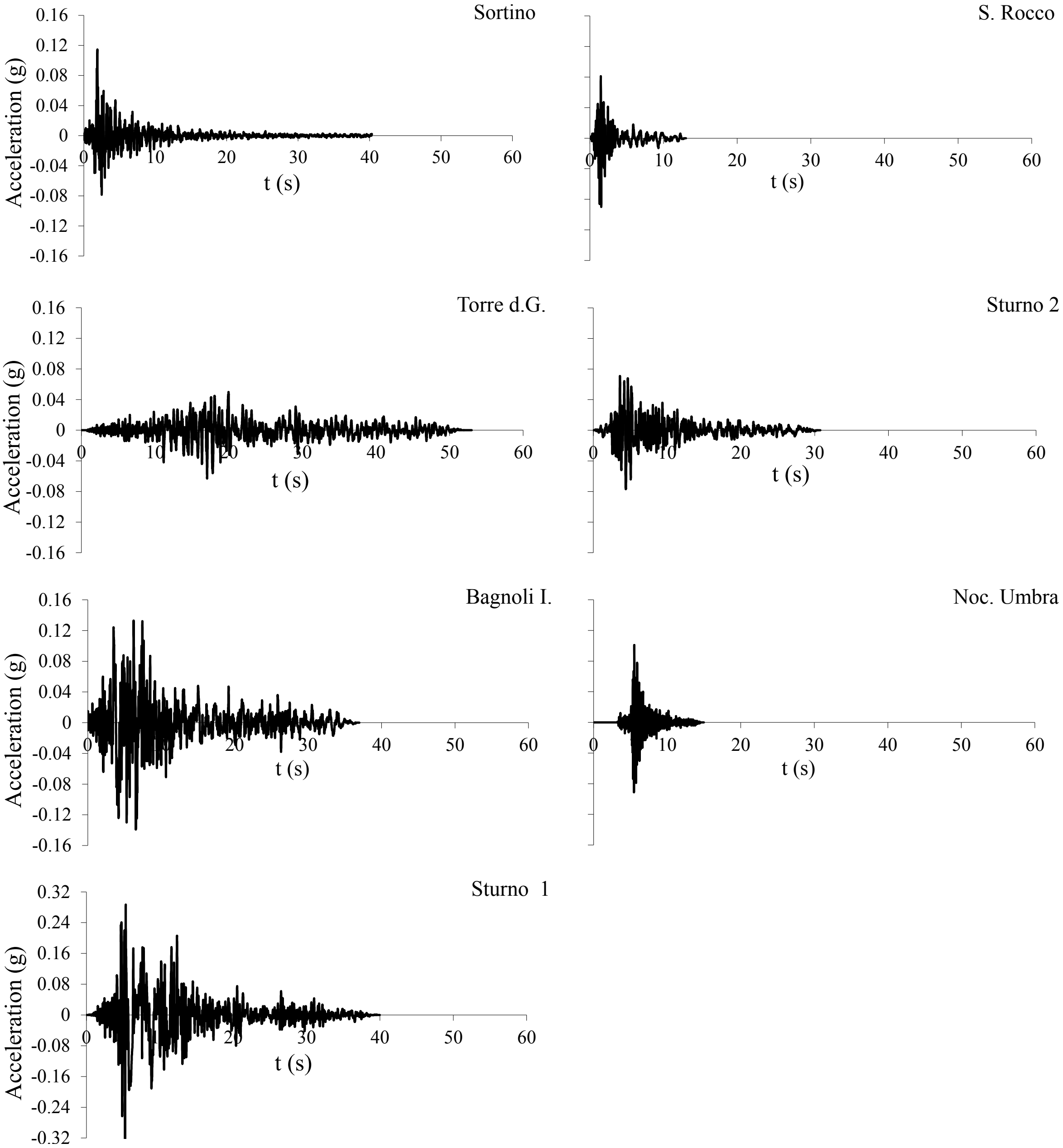

Figure 2.1.1.2 *Time histories of the real accelerograms.*

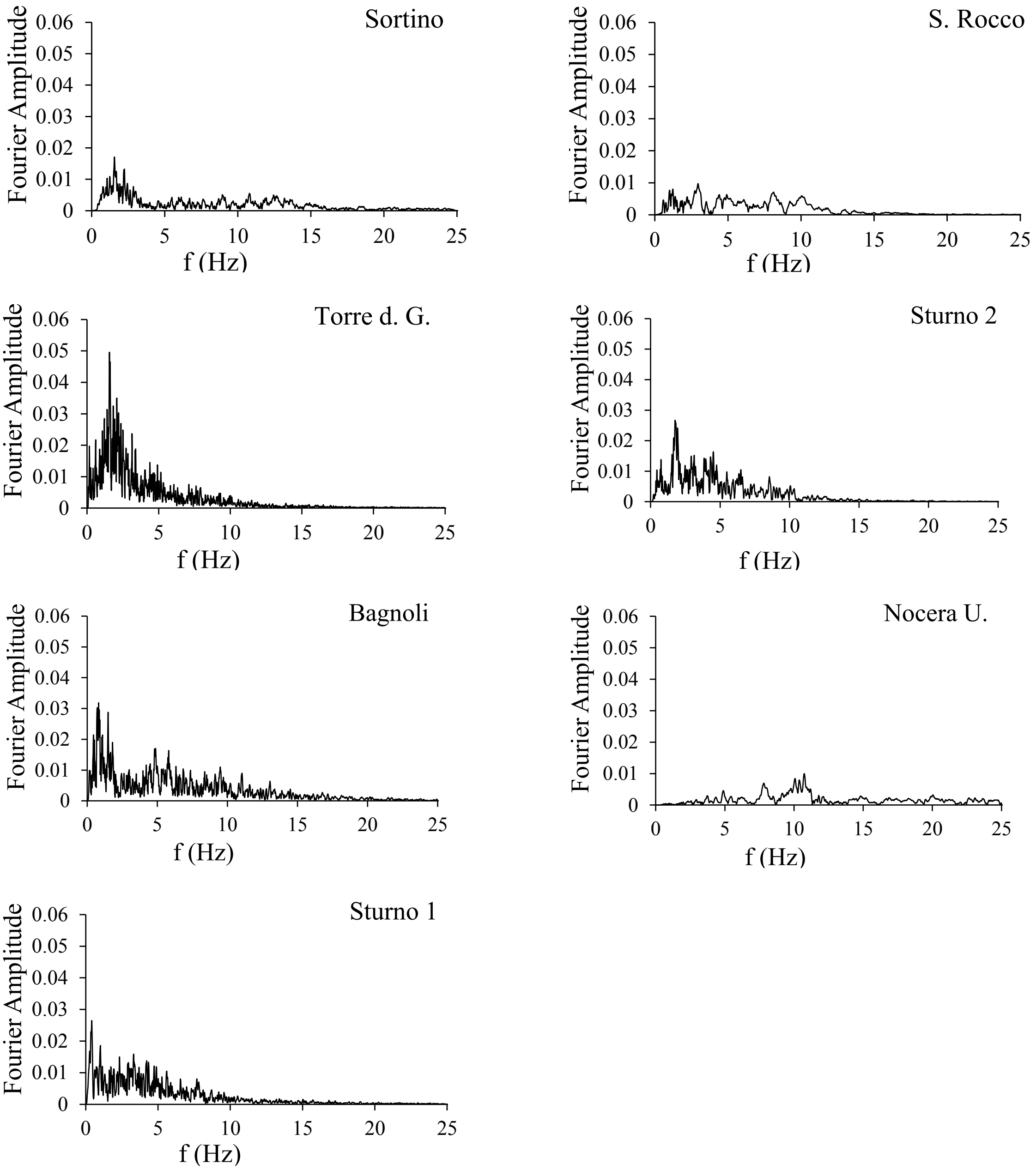

Figure 2.1.1.3 *Scaled Accelerograms Fourier amplitude (with a fixed maximum acceleration of 0,075g).*

2.1.2. Risker Wavelets

In both 1D and 2D analyses, synthetic seismograms, called Ricker wavelets (Ryan, 1994), have been used. These simplified seismograms consist of a zero-phase wavelet with a central peak and two smaller side lobes. The mathematical formula for a Ricker wavelet, in terms of horizontal displacements u(t) imposed to the base of the analysed system, is given by:

$$u(t)=\alpha_m\cdot\left[1-2\cdot\pi^2\cdot f^2\cdot(t-t_c)^2\right]\cdot e^{-\pi^2\cdot f^2\cdot(t-t_c)^2} \tag{2.1.2.1}$$

where α_m is the maximum value of displacement, f is the signal fundamental frequency and t_c is the time instant at which the maximum signal value (u_{ma}) is reached. Actually, both elastic and plastic analyses have been carried out, so the amplitude of the signal is a matter of interest. In eq. (2.2.2.1), t_c is used to move forward or backward in time the signal.
The derivative of the eq. (2.1.2.1) is the related velocity, as reported:

$$\begin{aligned}
\dot{u}(t)=v(t)&=\alpha_m\cdot\left\{\begin{array}{l}\left[-4\cdot\pi^2\cdot f^2\cdot(t-t_c)\right]\cdot e^{-\pi^2\cdot f^2\cdot(t-t_c)^2}+\\ \left[1-2\cdot\pi^2\cdot f^2\cdot(t-t_c)^2\right]\cdot\left(-2\cdot\pi^2\cdot f^2\cdot(t-t_c)^2\right)\cdot e^{-\pi^2\cdot f^2\cdot(t-t_c)^2}\end{array}\right\}=\\
&=\alpha_m\cdot\left\{\begin{array}{l}\left[-4\cdot\pi^2\cdot f^2\cdot(t-t_c)\right]+\\ \left[1-2\cdot\pi^2\cdot f^2\cdot(t-t_c)^2\right]\cdot\left(-2\cdot\pi^2\cdot f^2\cdot(t-t_c)^2\right)\end{array}\right\}\cdot e^{-\pi^2\cdot f^2\cdot(t-t_c)^2}=\\
&=\alpha_m\cdot\left\{-4\cdot\pi^2\cdot f^2\cdot(t-t_c)-(t-t_c)\cdot 2\cdot\pi^2\cdot f^2+4\cdot\pi^4\cdot f^4\cdot(t-t_c)^3\right\}\cdot e^{-\pi^2\cdot f^2\cdot(t-t_c)^2}=\\
&=\alpha_m\cdot\left\{-2\cdot(t-t_c)\cdot\pi^2\cdot f^2\cdot\left[3-2\cdot\pi^2\cdot f^2\cdot(t-t_c)^2\right]\right\}\cdot e^{-\pi^2\cdot f^2\cdot(t-t_c)^2}=\\
&=\alpha_m\cdot\left\{-2\cdot\pi^2\cdot f^2\cdot(t-t_c)\cdot\left[3-2\cdot(\pi\cdot f\cdot(t-t_c))^2\right]\right\}\cdot e^{-\pi^2\cdot f^2\cdot(t-t_c)^2}.
\end{aligned}\tag{2.1.2.2}$$

The corresponding acceleration is obtained as the derivative of eq. (2.1.2.2), as reported in the following:

$$\begin{aligned}
\ddot{u}(t)=a(t)&=\frac{\partial}{\partial t}\left(\alpha_m\cdot\left\{\begin{array}{l}-4\cdot\pi^2\cdot f^2\cdot(t-t_c)-(t-t_c)\cdot 2\cdot\pi^2\cdot f^2+\\ 4\cdot\pi^4\cdot f^4\cdot(t-t_c)^3\end{array}\right\}\cdot e^{-\pi^2\cdot f^2\cdot(t-t_c)^2}\right)=\\
&=\alpha_m\cdot\left\{\begin{array}{l}\left(-4\cdot\pi^2\cdot f^2-2\cdot\pi^2\cdot f^2+12\cdot\pi^4\cdot f^4\cdot(t-t_c)^2\right)+\\ \left(\begin{array}{l}-4\cdot\pi^2\cdot f^2\cdot(t-t_c)-2\cdot\pi^2\cdot f^2\cdot(t-t_c)+\\ +4\cdot\pi^4\cdot f^4\cdot(t-t_c)^3\cdot\left(-2\cdot\pi^2\cdot f^2\cdot(t-t_c)\right)\end{array}\right)\end{array}\right\}\cdot e^{-\pi^2\cdot f^2\cdot(t-t_c)^2}=\\
&=\alpha_m\cdot\left(-6\cdot\pi^2\cdot f^2+24\cdot\pi^4\cdot f^4\cdot(t-t_c)^2-8\cdot\pi^6\cdot f^6\cdot(t-t_c)^4\right)\cdot e^{-\pi^2\cdot f^2\cdot(t-t_c)^2}=\\
&=\alpha_m\cdot 2\cdot\pi^2\cdot f^2\left(-3+12\cdot\pi^2\cdot f^2\cdot(t-t_c)^2-4\cdot\pi^4\cdot f^4\cdot(t-t_c)^4\right)\cdot e^{-\pi^2\cdot f^2\cdot(t-t_c)^2}=\\
&=\alpha_m\cdot\left(-2\cdot\pi^2\cdot f^2\right)\cdot\left(3-12\cdot\pi^2\cdot f^2\cdot(t-t_c)^2+4\cdot\pi^4\cdot f^4\cdot(t-t_c)^4\right)\cdot e^{-\pi^2\cdot f^2\cdot(t-t_c)^2}=
\end{aligned}\tag{2.1.2.3}$$

In Figures 2.1.2.1, the normalized values of acceleration, displacement and velocity (a), and the amplitude Fourier spectrum (b) for a given Ricker wavelet with a peak frequency of 3Hz are reported.

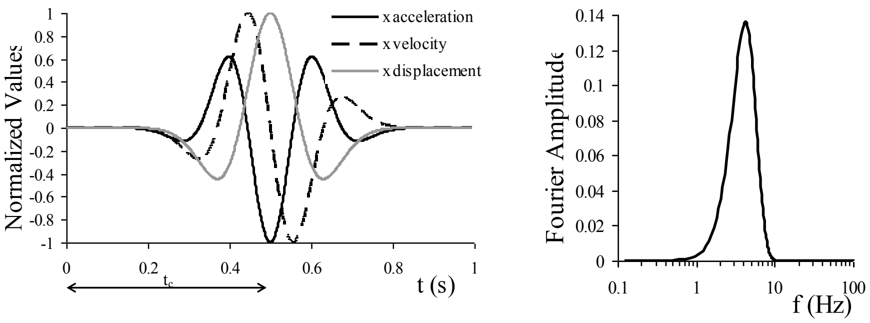

(a) (b)

Figure 2.1.2.1 *Values of acceleration, velocity and displacement for the 3Hz Ricker wavelet normalized to the corresponding maximum values (a); Fourier amplitude of the 3Hz Ricker normalized wavelet (b).*

A Ricker wavelet is specified by using the parameter f. By means of this signal typology, the effects on a given model configuration of signals having an energy amount concentrated in a small frequency range can be analysed. Therefore, it is possible to better understand the link between the propagation of certain signals throughout a soil layer either with or without a particular treatment.

2.2. 1D Analyses

2.2.1. Introduction to 1D Analyses

This paragraph has been added in order to show some concepts on a simple application of mono-dimensional wave propagation (Kramer, 1996). Attention will be given to the principles used to understand more complicated cases starting from simple 1D scheme. It is considered a harmonic stress wave travelling along a constrained rod in the x-direction approaching an interface between two different materials (see Figure 2.1.1.1).

The wave travelling toward the interface could be named “incident wave”; since it is moving through the first material (material 1), its wavelength will be $L_{w\,1}=2\pi/k_{n1}$, where k_{n1} is the wave number of the first material.

The stress induced by the wave may be described by the equation:

$$\sigma_I(x,t)=\sigma_i\cdot e^{i\cdot(\omega\cdot t-k_{n1}\cdot x)} \tag{2.1.1.1}$$

When the incident wave reaches the interface, a certain amount of its energy will be transmitted to the second material (transmitted wave), and another one will be reflected to the first material (reflected wave). These two waves are described by:

$$\begin{aligned}\sigma_T(x,t) &= \sigma_t \cdot e^{i\cdot(\omega\cdot t - k_{n1}\cdot x)} \\ \sigma_R(x,t) &= \sigma_r \cdot e^{i\cdot(\omega\cdot t + k_{n1}\cdot x)}\end{aligned} \tag{2.1.1.2}$$

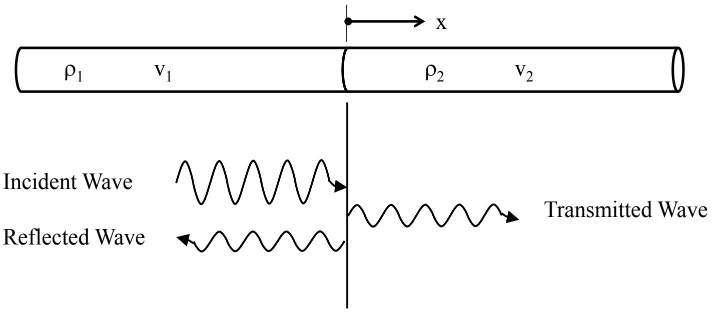

Figure 2.1.1.1 *Reference geometric scheme: propagation of a sinusoidal wave at materials interface.*

Assuming the appropriate boundary conditions, in terms of displacements compatibility and continuity of stresses at the interface, the following values for the amplitudes of the wave can be derived:

$$\sigma_r = \frac{\alpha - 1}{1 + \alpha} \cdot \sigma_i \tag{2.1.1.3}$$

$$\sigma_t = \frac{2 \cdot \alpha}{1 + \alpha} \cdot \sigma_i \tag{2.1.1.4}$$

where α is the dynamic impedance ratio:

$$\alpha = \frac{\rho_2 \cdot V_{S,2}}{\rho_1 \cdot V_{S,1}} = \frac{\mu_2}{\mu_1} \tag{2.1.1.5}$$

where ρ_i is the density of the ith-material, $V_{S,i}$ is the shear wave velocity and μ_i is called dynamic impedance. The impedance ratio has therefore a crucial role in distributing tensions and consequently deformations at the interface between two media.

In table 2.1.1.1, the transmission (σ_r / σ_i) and reflection (σ_t / σ_i) coefficients of a sinusoidal wave approaching the interface between two different materials have been reported, varying the shear stiffness of the second one, using a similar density for the two strata.

ρ (kg/m^3)	$V_{S,2}$ (m/s)	μ_2 (kg/m^2/s)	$V_{S,1}$ (m/s)	μ_1 (kg/m^2/s)	α	σ_r / σ_i	σ_t / σ_i
2040	10	20400	300	612000	30	-0.935	0.065
	20	40800			15	-0.875	0.125
	30	61200			10	-0.818	0.182
	50	102000			6	-0.714	0.286
	100	204000			3	-0.5	0.5
	200	408000			1.5	-0.2	0.8
	300	612000			1	0	1
	500	1020000			0.6	0.25	1.25
	1000	2040000			0.3	0.538	1.538

Table 2.1.1.1 *Transmission coefficient values with respect to the incident wave energy.*

If the value of α is less than 1, i.e. for two materials having the same density, the second layer is softer than the first one, the reflected wave will have an amplitude smaller than the incident one and its sign will be reversed; on the contrary, if $\alpha>1$, the amplitude of the transmitted wave is greater than that of the incident wave, and the stress amplitude of the reflected wave is less than that of the incident wave, but of the same sign.

Let's now consider a slightly more complex 1D scheme (see Figure 2.1.1.2), with a rod made of a certain material (1) interrupted by two interfaces in order to create an inner zone of a different material (2). The waves have to propagate through two close interfaces.

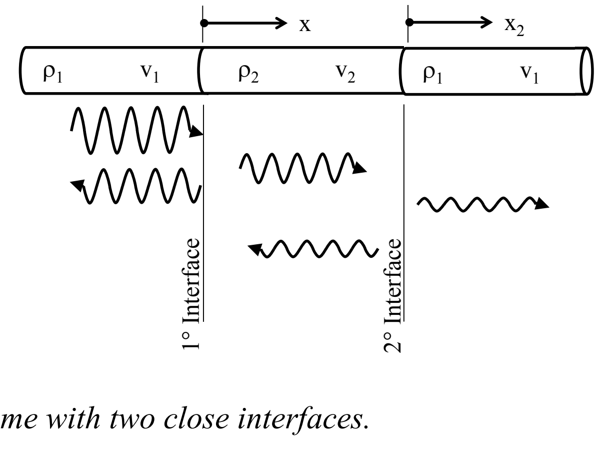

Figure 2.1.1.2 *Scheme with two close interfaces.*

The wave, travelling through the material 1, reaches the 1st interface; depending on the dynamic impedance ratio, touching this 1st interface a certain amount of energy is transmitted to the second layer and another part is reflected to the 1st stratum. The reflected wave moves away from the considered domain, whereas the transmitted wave goes toward the second interface. At this one, the wave undergoes the same mechanism, with a reflected wave travelling back and a transmitted one. By using eq.s (2.1.1.4) and (2.1.1.5) and starting from a wave amplitude equal to 1, the values of σ_i and σ_t at the first incoming through the first (column 1) and second (column 2) interface, could be calculated varying the stiffness of the inner material, and assuming a constant value of V_S for the remaining part of the rod. The values of σ_t pertaining to the second iteration are indicative of the amount of energy transmitted to the third part. If there is no change in shear stiffness among the different parts, the whole energy is transmitted through the rod because of the inexistence of mechanical discontinuities; if the inner part has a different stiffness, a transmission/reflection mechanism will take place at every interface.

All the coefficients are reported in Table 2.1.1.2:

						1			2		
ρ (kg/m^3)	$V_{S,2}$ (m/s)	μ_2 (kg/m^2/s)	$V_{S,1}$ (m/s)	μ_1 (kg/m^2/s)	α	σ_i	σ_r	σ_t	σ_i	σ_r	σ_t
2040	10	20400	300	612000	30	1	-0.935	0.065	0.065	0.06	0.125
	20	40800			15		-0.875	0.125	0.125	0.109	0.234
	30	61200			10		-0.818	0.182	0.182	0.149	0.331
	50	102000			6		-0.714	0.286	0.286	0.204	0.49
	100	204000			3		-0.5	0.5	0.5	0.25	0.75
	200	408000			1.5		-0.2	0.8	0.8	0.16	0.96
	300	612000			1		0	1	1	0	1
	500	1020000			0.6		0.25	1.25	1.25	-0.313	0.938
	1000	2040000			0.3		0.538	1.538	1.538	-0.828	0.71
	2000	4080000			0.15		0.739	1.739	1.739	-1.285	0.454
	3000	6120000			0.1		0.818	1.818	1.818	-1.488	0.331
	4000	8160000			0.075		0.86	1.86	1.86	-1.601	0.26
	5000	10200000			0.06		0.887	1.887	1.887	-1.673	0.214
	10000	20400000			0.03		0.942	1.942	1.942	-1.829	0.113
	20000	40800000			0.015		0.97	1.97	1.97	-1.912	0.058
	50000	1.02E+08			0.006		0.988	1.988	1.988	-1.964	0.024
	100000	2.04E+08			0.003		0.994	1.994	1.994	-1.982	0.012

Table 2.1.1.2 *Values of the transmission coefficients expressed as a percent of the transmitted and reflected waves with respect to the incident energy.*

In order to have a better understanding of the variations of σ_t with V_S of the inner part, in Figure 2.1.1.3 the results have been reported in terms of σ_t with V_S at the second interface.

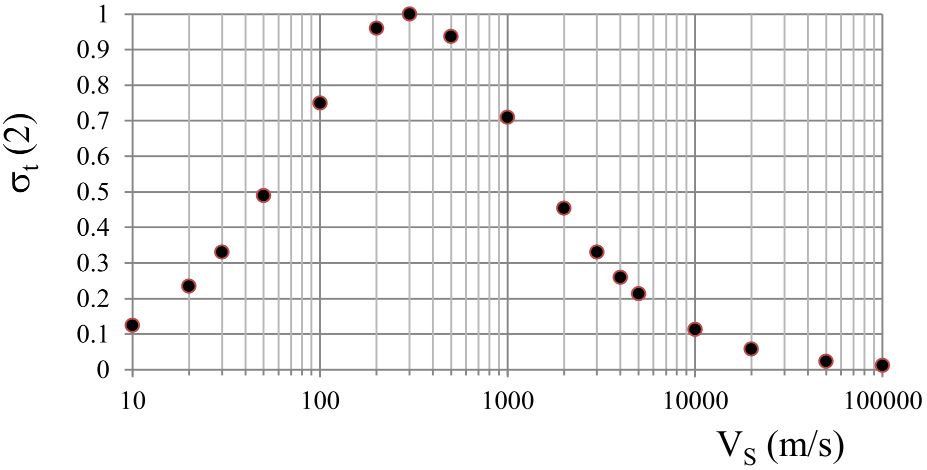

Figure 2.1.1.3 *Values of the transmission coefficients* σ_t *at the second interface.*

To tackle off the energy passing through the second interface into the domain, it seems to be useful softening or stiffening the inner layer; it can be obtained a reduction of the order of the 30 per cent either with an inner V_S equal to 100 or 1000m/s. The former corresponds to the initial shear stiffness of an extremely soft soil whereas the latter is a rock like stiffness. On the stiffening side, in order to obtain larger decreases in the transmission coefficient, extremely high values of V_S of the inner part should be considered. This solution is not realistic, because it would need an enormous increase of the stiffness of the central part of the rod. Table 2.1.1.3 shows how difficult it is to provide such a high value of stiffness: the soil related to the inner part should be substituted with materials like concrete or brass to obtain great decreases of the original shear stiffness.

Inner layer				Real Materials				
ρ (kg/m^3)	$V_{S,2}$ (m/s)	G (GPa)	μ $=\rho \cdot V_{S,2}$ (kg/m^2/s)	Material	G (GPa)	ρ_{min} (kg/m^3)	$V_{S,min}$ (m/s)	μ $=\rho \cdot V_S$ (kg/m^2/s)
2040	10	0.000204	2.04E+04	Concrete C20/25 (DM2008; υ=0.3)	15	2500	2412	6.03E+06
	20	0.000816	4.08E+04	Steel	85	7860	3289	2.58E+07
	30	0.001836	6.12E+04	Aluminium	25	2600	3101	8.06E+06
	50	0.0051	1.02E+05	Iron	80	7880	3186	2.51E+07
	100	0.0204	2.04E+05	Brass	30	8400	1890	1.59E+07
	200	0.0816	4.08E+05	Lead	5	11340	664	7.53E+06
	300	0.1836	6.12E+05	Platinum	60	21400	1674	3.58E+07
	500	0.51	1.02E+06	Copper	40	8890	2121	1.89E+07
	1000	2.04	2.04E+06	Tungsten	140	19250	2697	5.19E+07
	2000	8.16	4.08E+06	Glass	25÷32	2400	3227	7.75E+06
	3000	18.36	6.12E+06					
	4000	32.64	8.16E+06					
	5000	51	1.02E+07					
	10000	204	2.04E+07					
	20000	816	4.08E+07					
	50000	5100	1.02E+08					
	100000	20400	2.04E+08					

Table 2.1.1.3 *Comparison among the stiffness of the inner part of the rod and other real materials.*

Of course, this analysis does not consider the contribution of the remaining part of energy confined inside the insulating layer, the time lag that occurs when the wave has crossed the central layer, the possible effort of energy from the outside and the presence of dissipative phenomena. Considering the energy entrapped in the middle layer (reflected between the two interfaces) and, then, considering, at every interface, the reflected wave to the inner part as the incident wave, it is expected that the continuous changes of sign and the continuous expulsion of energy from the control volume determines a decrease in the contribution of energy into the isolated area; these contribution should be subsequently summed to determine the resulting wave, taking into account the temporal gap of the different contributions (see Table 2.1.1.4).

In Table 2.1.1.4, the transmission coefficients could be seen, in this sense, as single contributions to the wave amplitude, without considering the temporal gaps between two subsequent passages throughout a certain interface.

			1			2			3		
ρ (kg/m^3)	$V_{S,2}$ (m/s)	$V_{S,1}$ (m/s)	σ_i	σ_r	σ_t	σ_i	σ_r	σ_t	σ_i	σ_r	σ_t
2040	10	300	1	-0.935	0.065	0.065	0.060	0.125	0.060	-0.056	0.004
	20			-0.875	0.125	0.125	0.109	0.234	0.109	-0.096	0.014
	30			-0.818	0.182	0.182	0.149	0.331	0.149	-0.122	0.027
	50			-0.714	0.286	0.286	0.204	0.490	0.204	-0.146	0.058
	100			-0.500	0.500	0.500	0.250	0.750	0.250	-0.125	0.125
	200			-0.200	0.800	0.800	0.160	0.960	0.160	-0.032	0.128
	300			0.000	1.000	1.000	0.000	1.000	0.000	0.000	0.000
	500			0.250	1.250	1.250	-0.313	0.938	-0.313	-0.078	-0.391
	1000			0.538	1.538	1.538	-0.828	0.710	-0.828	-0.446	-1.274
	2000			0.739	1.739	1.739	-1.285	0.454	-1.285	-0.950	-2.236
	3000			0.818	1.818	1.818	-1.488	0.331	-1.488	-1.217	-2.705
	4000			0.860	1.860	1.860	-1.601	0.260	-1.601	-1.377	-2.978
	5000			0.887	1.887	1.887	-1.673	0.214	-1.673	-1.484	-3.157
	10000			0.942	1.942	1.942	-1.829	0.113	-1.829	-1.722	-3.551
	20000			0.970	1.970	1.970	-1.912	0.058	-1.912	-1.856	-3.768
	50000			0.988	1.988	1.988	-1.964	0.024	-1.964	-1.941	-3.905
	100000			0.994	1.994	1.994	-1.982	0.012	-1.982	-1.970	-3.952

			4			5			6		
ρ (kg/m^3)	$V_{S,2}$ (m/s)	$V_{S,1}$ (m/s)	σ_i	σ_r	σ_t	σ_i	σ_r	σ_t	σ_i	σ_r	σ_t
2040	10	300	-0.056	-0.053	-0.109	-0.053	0.049	-0.003	0.049	0.046	0.096
	20		-0.096	-0.084	-0.179	-0.084	0.073	-0.010	0.073	0.064	0.137
	30		-0.122	-0.100	-0.221	-0.100	0.081	-0.018	0.081	0.067	0.148
	50		-0.146	-0.104	-0.250	-0.104	0.074	-0.030	0.074	0.053	0.127
	100		-0.125	-0.063	-0.188	-0.063	0.031	-0.031	0.031	0.016	0.047
	200		-0.032	-0.006	-0.038	-0.006	0.001	-0.005	0.001	0.000	0.002
	300		0.000	0.000	0.000	0.000	0.000	0.000	0.000	0.000	0.000
	500		-0.078	0.020	-0.059	0.020	0.005	0.024	0.005	-0.001	0.004
	1000		-0.446	0.240	-0.206	0.240	0.129	0.370	0.129	-0.070	0.060
	2000		-0.950	0.702	-0.248	0.702	0.519	1.221	0.519	-0.384	0.135
	3000		-1.217	0.996	-0.221	0.996	0.815	1.811	0.815	-0.667	0.148
	4000		-1.377	1.185	-0.192	1.185	1.020	2.205	1.020	-0.878	0.142
	5000		-1.484	1.316	-0.168	1.316	1.167	2.483	1.167	-1.035	0.132
	10000		-1.722	1.622	-0.100	1.622	1.527	3.149	1.527	-1.438	0.089
	20000		-1.856	1.801	-0.055	1.801	1.748	3.548	1.748	-1.696	0.052
	50000		-1.941	1.918	-0.023	1.918	1.895	3.813	1.895	-1.872	0.023
	100000		-1.970	1.958	-0.012	1.958	1.947	3.905	1.947	-1.935	0.012

Table 2.1.1.4 *Transmission coefficients due to the propagation of a unitary amplitude wave through a rod divided by two interfaces.*

2.2.2. First 1D analyses on soil column

2.2.2.1 Calculation codes

In the following paragraphs, the reported 1D analyses have been carried out using either the SHAKE ’91 code implemented by EERA or the material model developed by Iwan (1967) and Mroz (1967) implemented by NERA. EERA and NERA are free softwares commonly used to define site response analyses. The hypothesis the codes are based on are that shear waves propagate vertically in a one-dimensional layered system, where soil layers are supposed to be horizontally homogenous, horizontally unlimited, and subjected only to an horizontal excitation from bedrock.

In EERA the soil stress-strain response is based on a Kelvin-Voigt model (see Figure 2.2.2.1.1), where the shear stress τ depends on the shear strain γ and on its rate $\dot{\gamma}$ as follows:

$$\tau = G \cdot \gamma + \eta' \cdot \dot{\gamma} \qquad (2.2.2.1.1)$$

where G is shear modulus and η' the viscosity of the material.

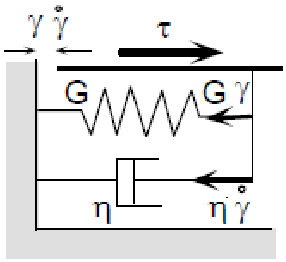

Figure 2.2.2.1.1 *Schematic representation of stress-strain behaviour used in equivalent-linear constitutive model.*

In NERA the non-linear and dissipative soil behaviour is simulated through the kinematic hardening model proposed by Iwan (1967) and Mroz (1967), which yields a hysteretic response under cyclic loads. Therefore, it should be more consistent to the actual behaviour of geomaterials, which can undergo significant sliding deformation, as expected in the problem at issue. In addition, the code uses finite difference integration of the equations of motion in the time and space domains, which should overcome the convergence problems, which can be encountered with the linear equivalent approach adopted by EERA (Bardet et al., 2001).

Iwan (1967) and Mroz (1967) proposed to model nonlinear stress-strain curves using a series of n mechanical elements, having different stiffness k_i and sliding resistance R_i (see Figure 2.2.2.1.2). Sliders have increasing resistance (i.e., $R_1 < R_2 < \ldots < R_n$) because, initially, residual stresses in all sliders are equal to zero, but, during a monotonic loading, the i^{th}-slider yields when the shear stress τ reaches the value R_i and, after having yielded, it retains a positive residual stress equal to R_i.

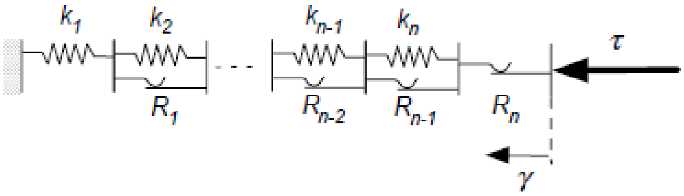

Figure 2.2.2.1.2 *Schematic representation of stress-strain model used by Iwan (1967) and Mroz (1967).*

Using these programmes, the static and kinematical components of one-dimensional site response analyses can be calcuated. Extensive information on EERA and NERA scientific and user features are reported into the EERA manual by Bardet et al. (2000) and NERA one by Bardet and Tobita (2001).

2.2.2.2 1D analyses: propagation of scaled accelerograms

A homogeneous subsoil constituted by a medium plasticity normally consolidated clay (IP=50), has been considered to a depth of 80m, at which the seismic input motion is applied (bedrock). The strain-dependent shear modulus G and the damping ratio D of the natural soil have been assigned considering the typical case of a normally consolidated clay. The small strain modulus, G_0, was set as linearly increasing with depth; being $G_0=\rho\cdot V_{s,s}^2$, the profile of soil shear velocity $V_{s,s}$ results defined by the power function plotted in Figure 2.2.2.2.1b, corresponding to a linear fundamental frequency of the layer equal to 1.20Hz (f_n=1.20Hz), as confirmed by the peak amplitude corresponding to the lower resonance frequency shown in Figure 2.2.2.2.4a. The small strain damping D_0 was set equal to 3% and constant with depth. Both normalized shear modulus G/G_0 and damping ratio D were set as depending on shear strain amplitude γ according to Vucetic and Dobry curves (1991), modified to include D_0 values at small strains (see Figure 2.2.2.2.1c.). In the 1D numerical analyses, the most critical parameters will be the position of the soft layer (H_g) and its thickness (t_g=0.5m) (see Figure 2.2.2.2.1a). The soft layer density has been assumed equal to 1020kg/m^3.

Table 2.2.2.2.1 summarizes the main properties of the natural soil and of the bedrock.

Since V_s and G_0 increase with depth for the natural soil, while for the soft layer their values are ruled by the effect of grouting, it must be expected that the deeper the layer the more effective the reduction in wave propagation towards the ground surface.

material	γ_S (kN/m^3)	ρ (kg/m^3)	V_S (m/s)	D_0 (%)	Material behaviour
Natural soil	20	2040	Hardin, 1978	3	Non linear
Bedrock	20	2040	1000	0	linear

Table 2.2.2.2.1 *Main properties of the materials.*

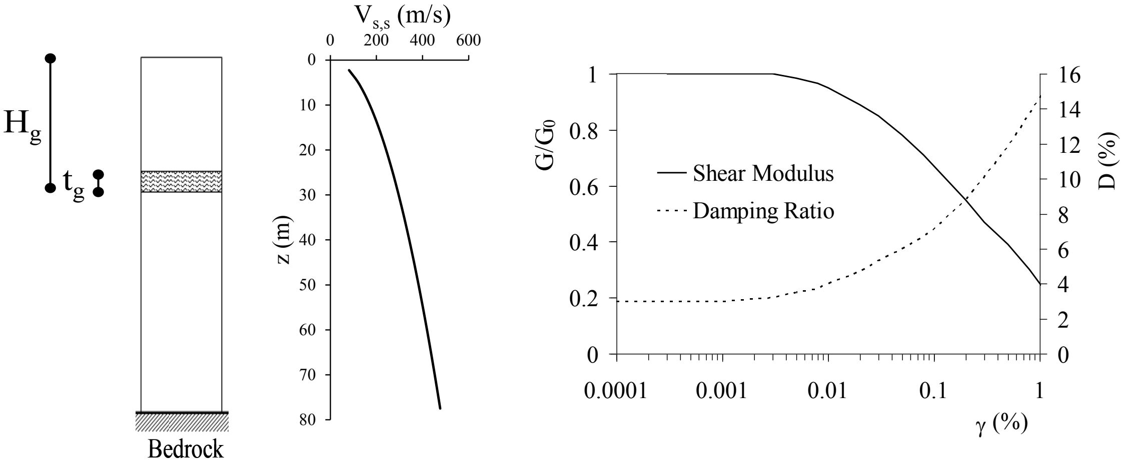

(a) (b) (c)

Figure 2.2.2.2.1 *1D Geometrical scheme adopted (a); Natural soil properties: V_S with depth z (b); $G/G_0(\gamma)$ and $D(\gamma)$ decay curves (c).*

G_0 has been calculated according to the following formulas:

$$\frac{G_0}{p_a} = S \cdot \left(\frac{p'}{p_a}\right)^n \cdot f(e) \cdot OCR^m \qquad \text{(Hardin, 1978)} \qquad (2.2.2.2.1)$$

$$f(e) = \frac{(2.973-e)^2}{1+e} \qquad \text{(Hardin and Black, 1968)} \qquad (2.2.2.2.2)$$

The parameters used in the previous formulations are:

e=0.5

S=110

n=1

The values of these parameters depend on soil typology and decrease by increasing plastic index IP; the values have been chosen to simulate a soft soil with an outstanding site effect. According to the Euro-code and, also to the Italian Technical Code (NTC, 2008), this soil is classified as a D profile (according to Euro-code, V_{S30} = 167,8m/s leads to Deposits of loose-to-medium cohesion-less soil with or without some soft cohesive layers, or of predominantly sot-to-firm cohesive soil; EC8, 2004). Input accelerograms applied to the bedrock (see 2.1.1) have been filtered to 25Hz and scaled to a maximum acceleration value of 0,075g ($a_{max,b}$); in fact most of analyses consider a low value of acceleration to allow the use of equivalent non linear method according to EERA algorithm. The scheme of the analyses, performed by using the software EERA and whose results are reported in this paragraph, is shown in Table 2.2.2.2.1; in this table, $V_{s,g}$ and D_g are respectively the shear wave velocity and the damping ratio of the soft layer. Since no stiffness decay curve is at the moment available for the treated soil, a linear elastic behaviour was considered for it; the hypothesis of null damping is conservative, as it overestimates the transmitted energy.

Accelerograms (Recording station)	$V_{s,g}$ (m/s)	D_g (%)
Sturno	10	0
Nocera Umbra -Biscontini		
San Rocco		
Sturno		
Torre del Greco		
Bagnoli Irpino		
Sortino		
	10/20/30/40/50/100	0
	10	0/1/2/5/10/20/50

Table 2.2.2.2.1 *Analyses scheme.*

Figures from 2.2.2.2.2 to 2.2.2.2.5 report the results deriving by using different depths of intervention, varying the seismic action at the bedrock, for a soft layer with a shear velocity $V_{s,g}$ of 10m/s and no damping. In Figure 2.2.2.2.2, the maximum accelerations a_{max} recorded at ground surface are compared to the continuous lines, which represent the maximum accelerations without any treatment. The vertical profiles of peak acceleration show that the natural soil characteristics are such that, without soft layer, the signal is amplified and a_{max} gets its largest value close to or at ground level, regardless of the seismic input motion. As expected, the vertical profiles of a_{max} show an increasing amplification approaching ground surface. It is in fact well-known from literature analytical studies (Gazetas, 1982) that a subsoil model with an increasing shear stiffness with depth undergoes large amplification in the upper, less stiff part of the soil column. If a soft layer is inserted, the acceleration strongly reduces above it, thus giving a first indication on its effectiveness in mitigating surface inertial actions; note that such a reduction in peak ground acceleration increases with the depth of the soft layer.

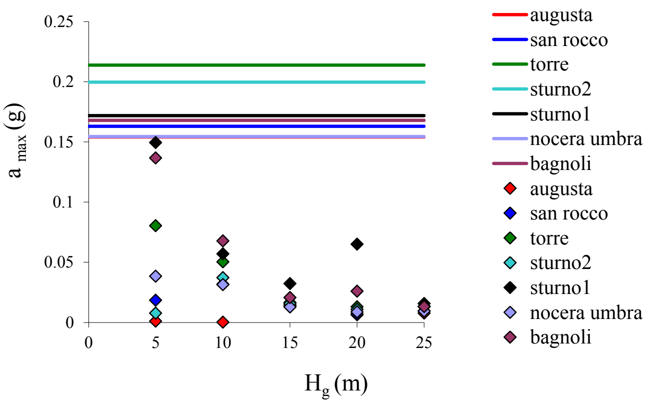

Figure 2.2.2.2.2 *Maximum accelerations at ground surface for different seismic signals and treatment depths; the continuous lines describe the results without treatment.*

Figures 2.2.2.2.3, report the maximum acceleration profiles with depth in absence of any treatment and considering a soft layer with a given treatment depth H_g, which has been varied from 5m to 25m. With respect to the condition of absence of any treatment (see Figure 2.2.2.2.3a), the introduction of the soft layer tends to amplify the maximum accelerations just below the treatment depth. In particular, a concentration of the maximum dynamic effects is observed in the soft layer, but the maximum accelerations have been drastically reduced by the treatment in the zone from the ground surface to the soft layer depth H_g. Generally speaking, the deeper the layer the larger the filtering action. This behaviour has been confirmed by Figures 2.2.2.2.4, where the efficiency E_I profiles are reported by varying the treatment depth. By increasing H_g, the efficiency related to the modifications of the signals calculated at ground surface is amplified, in terms of the efficiency amplitude E_I. Furthermore, the simple oscillator period ranges in which the treatment leads to safer condition is enlarged by increasing H_g. For treatment depth higher than 5m, the simple oscillators with natural periods lower than 1s undergo decrements in their maximum spectral parameters.

As reported in §1.6, the most important parameter in 1D wave propagation is the impedance ratio α; as shown in §2.2.1, when a wave approaches the soft layer, by increasing the value of α, higher reflected wave and lower refracted wave amplitudes occur. If α is increased by substituting deeper soil layers of higher dynamic impedance (for H_g=5m, α=24; for H_g=25m, α=54; see Figure 2.2.2.2.2) or decreasing the soft layer shear velocity (see Figure 2.2.2.2.8), lower dynamic effects are expected at ground surface.

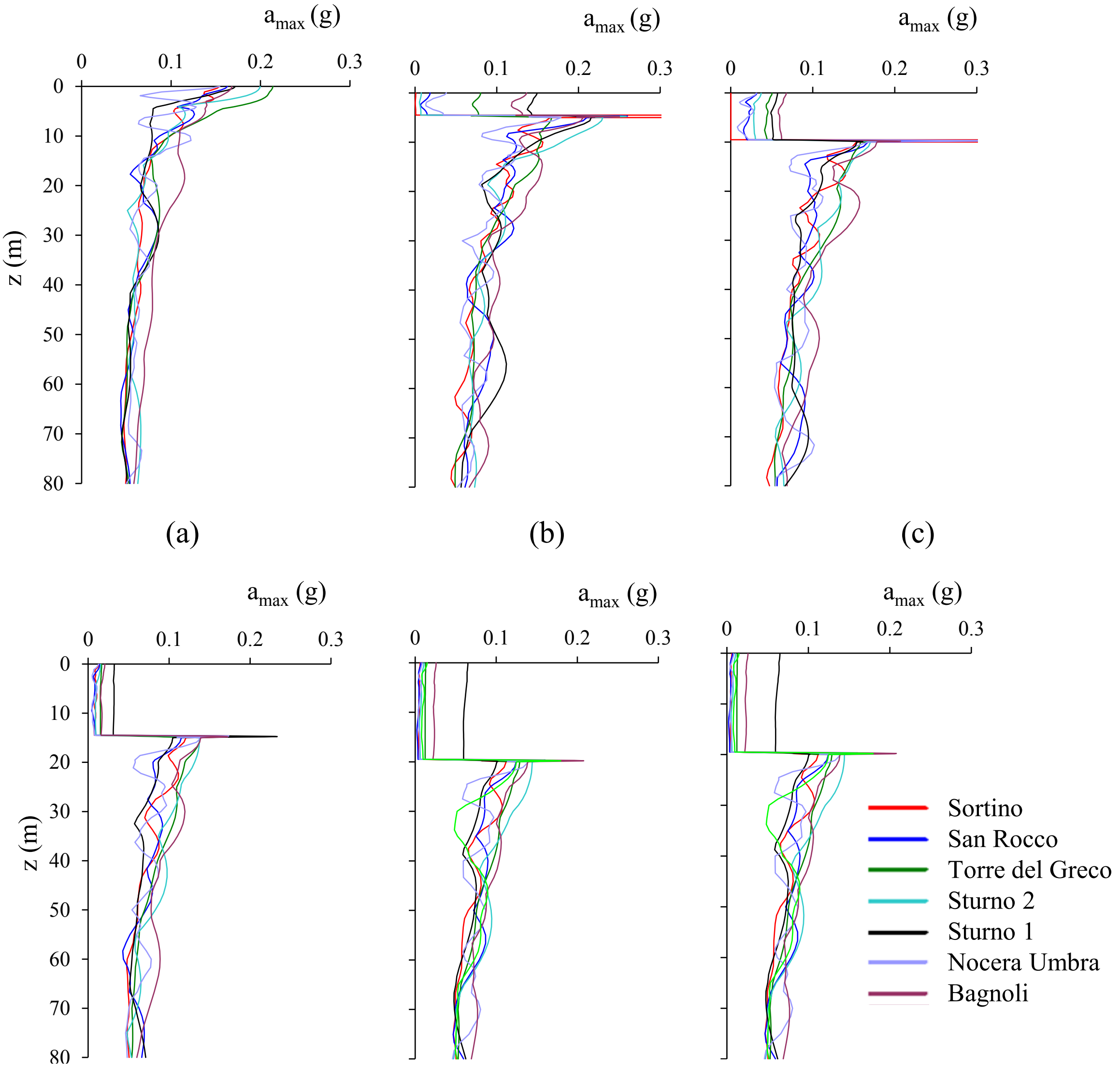

(a) (b) (c)

(d) (e) (f)

Figure 2.2.2.2.3 *Maximum acceleration profiles with depth, varying the seismic signals, in absence of any treatment (a) and considering a soft layer with a given treatment depth H_g, which has been assumed equal to 5m (b), 10m (c), 15m (d), 20m (e) and 25m (f).*

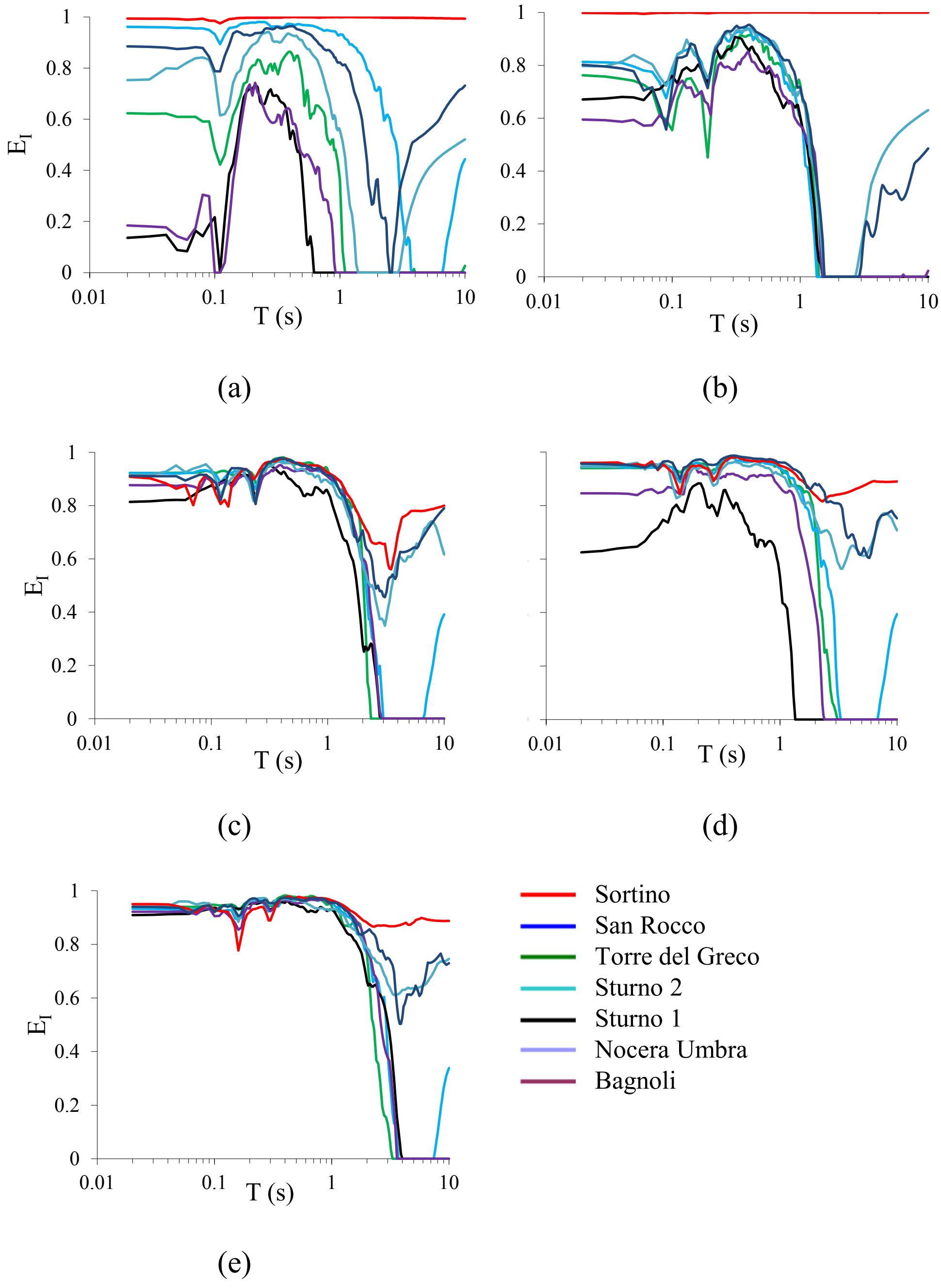

(a) (b)

(c) (d)

(e)

Figure 2.2.2.2.4 *Efficiency E_I profiles, by varying the seismic signals, in absence of any treatment (a) and considering a soft layer with a given treatment depth H_g, which has been assumed equal to 5m (b), 10m (c), 15m (d), 20m (e) and 25m (f).*

Furthermore, if the soft layer is placed at a large depth (see Figure 2.2.2.2.5a), the field of refracted waves will travel through a longer soil column, where it will be reduced by soil damping properties. In a real situation, geometrical damping also decreases the signal amplitude, but, in the mono-dimensional case, its effects are not taken into account. When the signal arrives to touch the ground surface, it will be totally refracted and restart to travel through the soil with ulterior values decreasing; so, when it returns at the disconnecting layer boundary, its amplitude is almost totally erased and eventually reflecting phenomena will take place for a signal with low energy.

If the soft layer is placed at lower depth, there are minor beneficial effects due to the soil damping. The wave passed through the soft layer will be reflected by the surface, but its energy will remain entrapped in the shallowest soil layer. In fact, when this wave, after the reflection at ground surface, touches the upper side of the soft layer, it will be quite totally reflected. Consequently, the signal energy remains in the shallowest layer, with consequent increasing of kinematical effects at the ground surface.

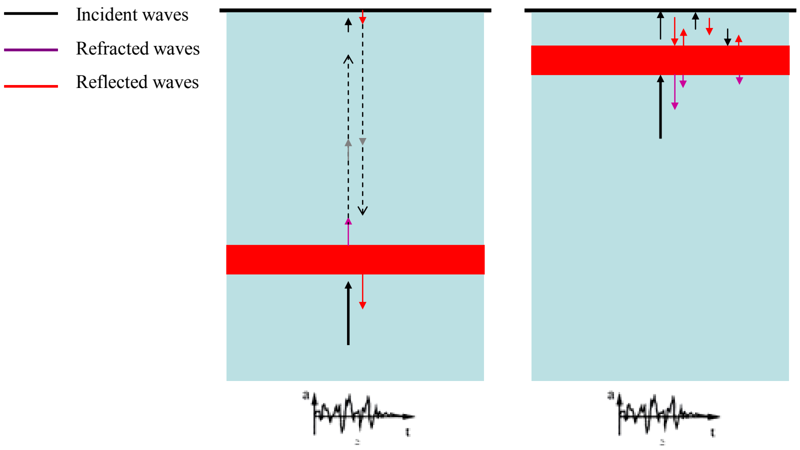

(a) (b)

Figure 2.2.2.2.5 *Simplified schemes describing the wave propagation through the soil column for deeper (a) and shallower (b) treatments.*

Another peculiar effect of the treatment is shown in Figures 2.2.2.2.6 and 2.2.2.2.7.

Figures 2.2.2.2.6 report the amplification ratio profiles, by considering a soft layer with a treatment depth H_g, which varies from 5m to 25m. The reduction experimented in the signals amplitudes at ground surface is evident in the lower amplification ratio values with respect to the scheme without any treatment (see Figure 2.2.2.2.6a).

With the exceptions of some frequencies for H_g=5m and 10m, the amplifications are reduced; peak frequencies can be observed both at higher frequencies (f >2Hz) and at lower ones. In particular, especially for deeper treatments (H_g>15m), the amplifications tend to be concentrated on a continuous frequency range (f < 1Hz).

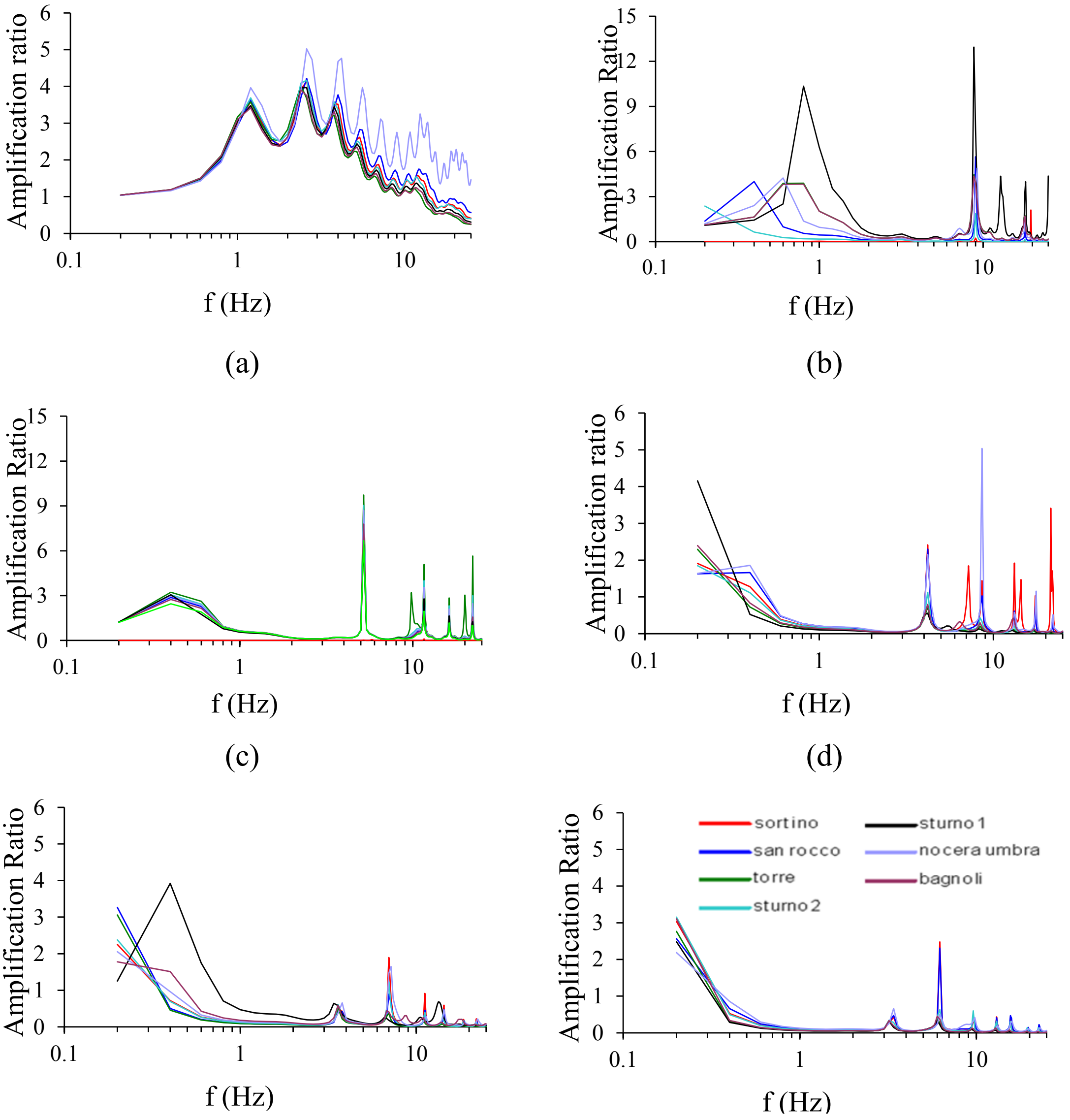

(a) (b)

(c) (d)

(e) (f)

Figure 2.2.2.2.6 *Amplification ratio profiles, by varying the seismic signals, in absence of any treatment (a) and considering a soft layer with a given treatment depth H_g, which has been assumed equal to 5m (b), 10m (c), 15m (d), 20m (e) and 25m (f).*

As far as this concentration of the amplification at lower frequencies is concerned, Figures 2.2.2.2.7 are indicative of the phenomenon. These figures report the effects at ground surface due to the propagation of the Torre del Greco scaled signal, in terms of maximum accelerations, S_d-S_a domain, and response spectra in terms of acceleration, velocity and displacement, by varying the treatment depth H_g from 0m to 25m. The reduction of the maximum acceleration amplitudes could be seen both in terms of a_{max} with depth (se Figure 2.2.2.2.7a) and in terms of spectral accelerations (see Figure 2.2.2.2.7 b and c) of the simple oscillator response. On the other hand, Figure 2.2.2.2.7d reports an increment in terms of maximum displacements, but only for higher periods, depending on the treatment depth: T >1s for $H_g \leq 10$m; T>2s for $H_g \geq 15$m; the response of the column is shifted to higher periods. Figure 2.2.2.2.7b is indicative in this sense: shrinkage of the S_d-S_a domain is observed, which is higher by increasing the depth of the treatment, but also a rotation of the maximum responses in terms of accelerations and displacements to higher periods is clearly shown. It is confirmed that the introduction of a soft layer at a given depth into a soil column leads to a global system response that moves to higher periods.

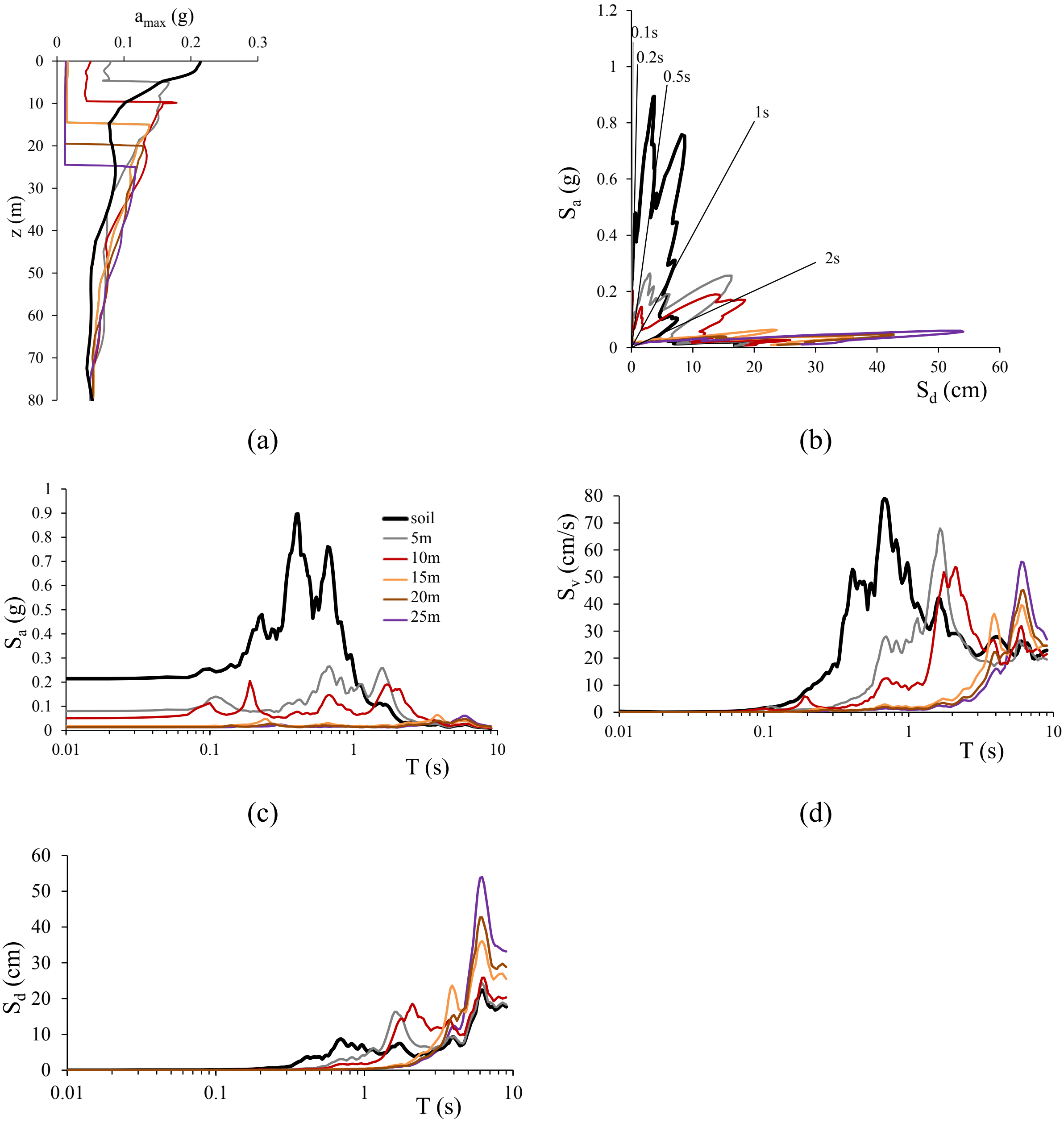

(a) (b)

(c) (d)

(e)

Figure 2.2.2.2.7 *Effects at ground surface of the Torre del Greco scaled accelerogram: maximum accelerations with depth (a), Sd-Sa domain (b), response spectra in terms of acceleration (c), velocity (d) and displacement (e), by varying the treatment depth H_g from 0m to 25m.*

Figures 2.2.2.2.8 report the maximum acceleration profiles with depth considering a treatment depth H_g from 5m to 25m, and the acceleration spectra at ground surface, assuming the propagation of the Sortino accelerogram, and varying the shear velocity $V_{s,g}$ of the soft layer. The shear velocity $V_{s,g}$ of the soft layer has been varied between 10m/s and 100m/s, assuming a damping equal to 0. By varying the shear wave velocity of the soft layer, the impedance ratio assumes the range of values reported in Table 2.2.2.2.1:

$V_{s,g}$ (m/s)	α
100	2÷5
50	5÷10
40	6÷13
30	8÷18
20	12÷27
10	24÷54

Table 2.2.2.2.1 *Impedance ratio related to the variation of shear wave velocity.*

As expected by the relative impedance ratio variation, by increasing the soft layer shear velocity, higher accelerations and spectral accelerations are observed at ground surface, as detected in terms of acceleration spectra too (see Figures 2.2.2.2.9).

By assuming a constant value for $V_{s,g}$ (20m/s), Figures 2.2.2.2.10 and 2.2.2.2.11 report the maximum acceleration profiles with depth and the acceleration spectra at ground surface, considering a treatment depth H_g from 5m to 25m, and the propagation of the Sortino accelerogram in these analyses the damping of the soft layer has been varied from 0 to 50%. The increment in damping determines beneficial effects for shallower treatment depth H_g, with reductions of the maximum accelerations at ground surface. Additionally, a major damping leads to the reduction of the dynamic effects in the soft layers, which are subjected to lower maximum accelerations.

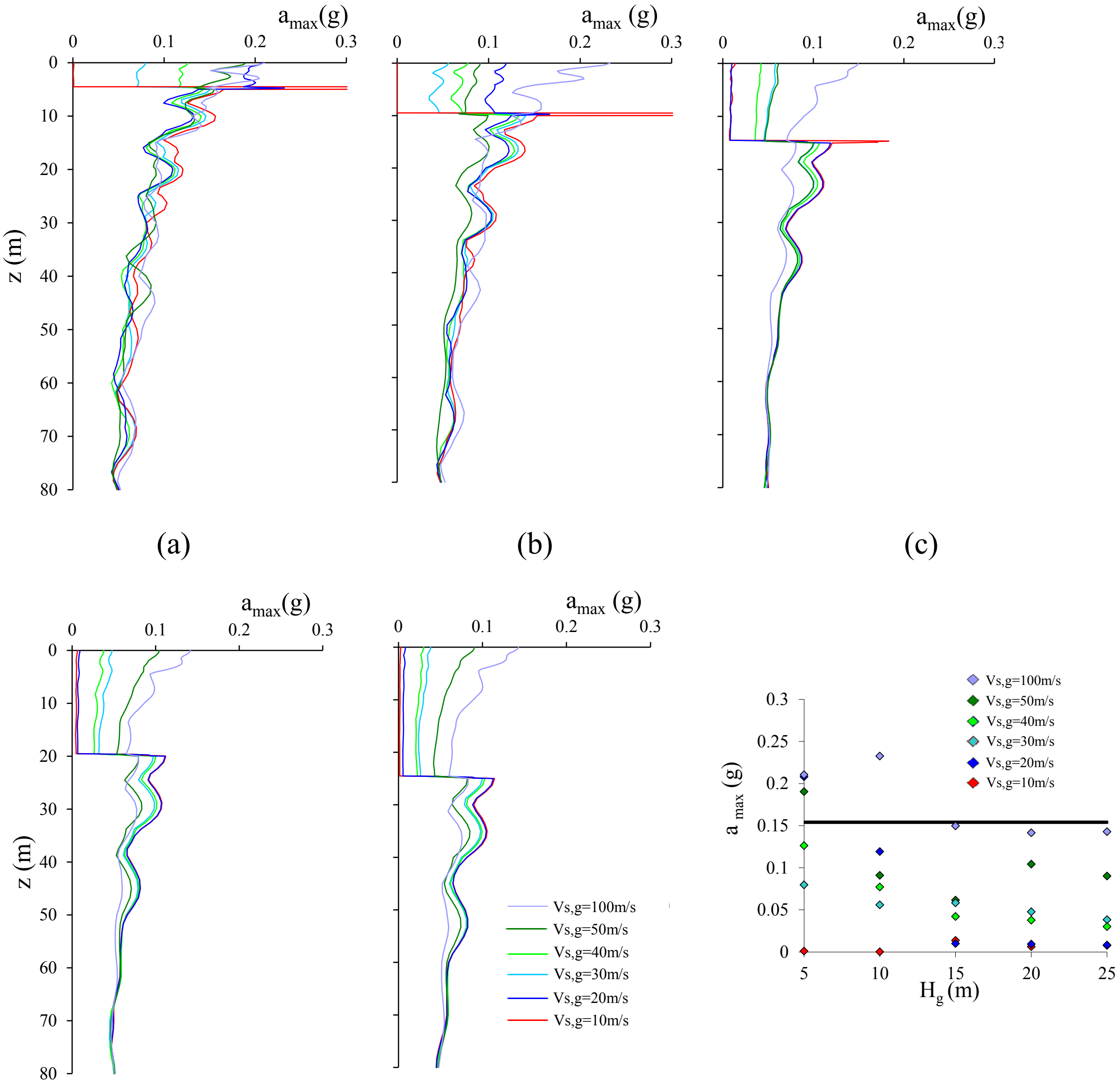

(a) (b) (c)

(d) (e) (f)

Figure 2.2.2.2.8 *Maximum acceleration profiles with depth for treatment depths H_g equal to 5m (a), 10m (b), 15m (c), 20m (d) and 25m (e), assuming the propagation of the Sortino scaled accelerogram, and varying the shear velocity of the soft layer; maximum acceleration at ground surface with H_g (f), where the black line corresponds to the absence of treatment, assuming the propagation of the Sortino accelerogram, and varying the shear velocity of the soft layer (f).*

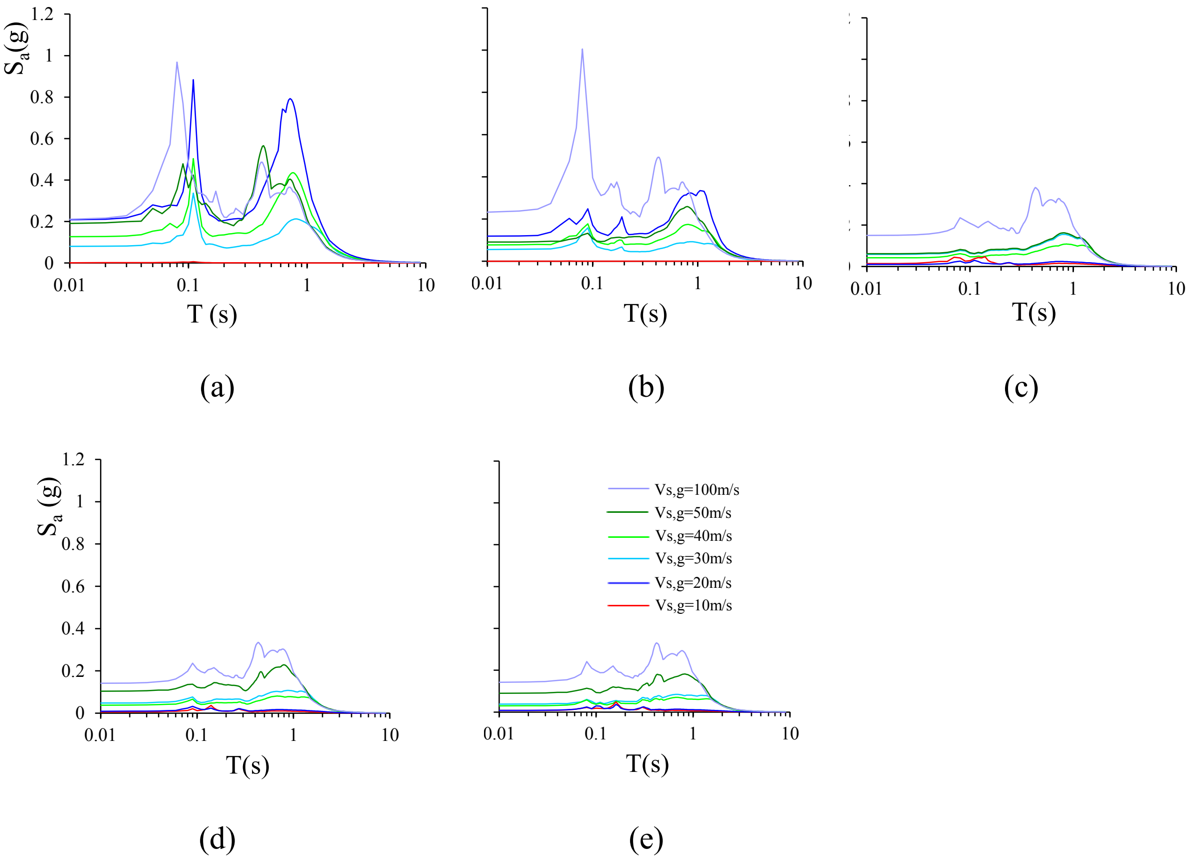

Figure 2.2.2.2.9 *Acceleration spectra considering a treatment depth* H_g *equal to 5m (a), 10m (b), 15m (c), 20m (d) and 25m (e), assuming the propagation of the Sortino scaled accelerogram, and varying the shear velocity of the soft layer.*

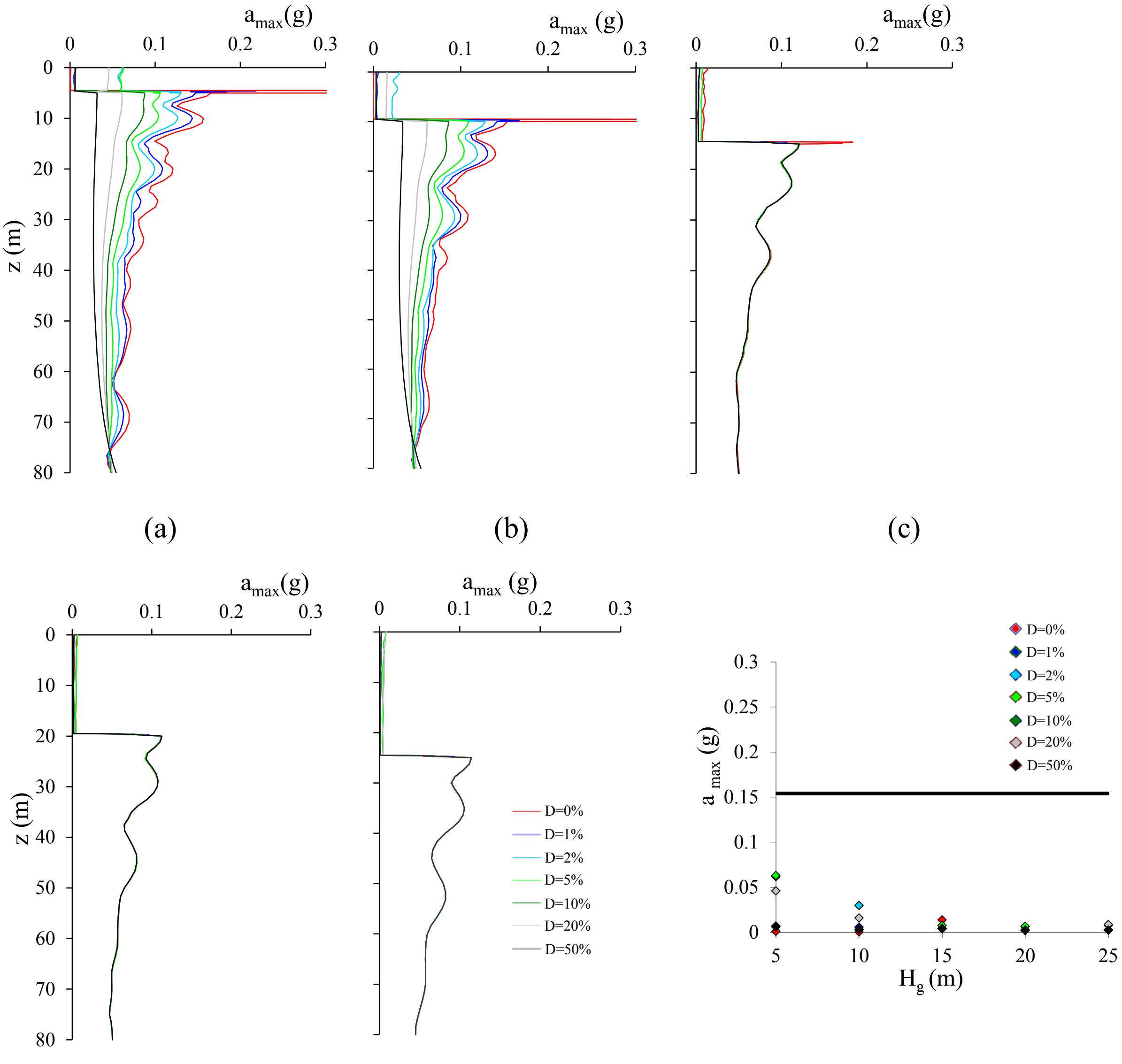

(a) (b) (c)

(d) (e) (f)

Figure 2.2.2.2.10 *Maximum acceleration profiles with depth considering treatment depths* H_g *equal to 5m (a), 10m (b), 15m (c), 20m (d) and 25m (e) assuming the propagation of the Sortino accelerogram, and varying the damping of the soft layer; maximum acceleration at ground surface with* H_g *(f), where the black line corresponds to the absence of treatment, assuming the propagation of the Sortino accelerogram, and varying the damping of the soft layer (f).*

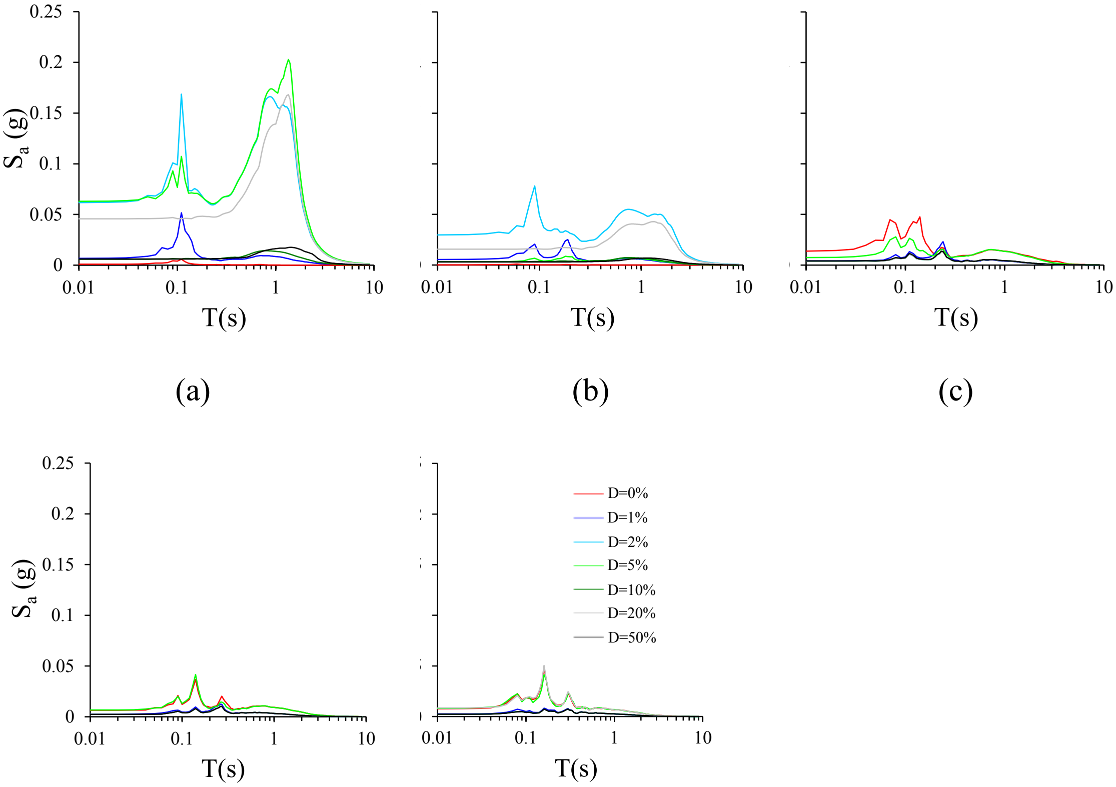

(a) (b) (c)

(d) (e)

Figure 2.2.2.2.11 *Acceleration spectra considering a treatment depth H_g equal to 5m (a), 10m (b), 15m (c), 20m (d) and 25m (e), assuming the propagation of the Sortino accelerogram, and varying the damping of the soft layer.*

2.2.2.3 1D analyses: propagation of Ricker wavelets

In these parametric analyses, a homogeneous fine-grained subsoil has been considered, having the geometrical and mechanical properties reported in §2.2.2.2. At the bottom of the layer, a reference seismic motion with variable frequency content is applied.

A single value of the thickness t_G=0.5m (see Figure 2.2.2.2.1a) and a very low shear wave velocity $V_{s,g}$=20m/s have been considered for the soft grouted layer. The effect of the grouting depth has been analysed by taking into account different values of H_g (10m and 20m). Since the soil shear wave velocity $V_{s,s}$ increases with depth for the natural soil, while for the grouted layer it is considered constant, the impedance ratio α between the soft grouted and the natural soil decreases with depth, as shown in §2.2.2.2 too. Therefore, for a given grout, at least in this simplified 1D scheme it must be expected that the deeper the layer the more effective the screening of wave propagation towards the ground surface.

A set of Ricker wavelets has been applied at the bedrock. For all the signals, the peak acceleration (a_{max}) has been kept constant and equal to 0.4g (see §2.1.2), which is the maximum reference acceleration amplitude expected in Italy for earthquakes with 475 years return period according to the national Seismic Hazard map (INGV, 2006). Five dominant frequencies (f=0.1, 1, 3, 5, 10Hz) are considered for the wavelet in order to highlight the effect of the frequency content of the input motion on the site response. Numerical predictions of 1D non-linear seismic response have been carried out using the code NERA. Table 2.2.2.3.1 summarizes all the analyses carried out combining the variations of the depth H_g and velocity $V_{s,g}$ of the soft layer with the input motions. The behaviour of the natural subsoil without the soft layer has been assumed as the reference case, and has been termed NR. Consistently, the cases with the soft layer has been named SR.

Layering	Case	input motions	H_g (m)	$V_{s,g}$ (m/s)	α	f (Hz)
Natural soil	NR	Ricker wavelet	-	-	-	0.1, 1, 3, 5, 10
With soft layer	SR	Ricker wavelet	10 20	20	0.059 0.042	0.1, 1, 3, 5, 10

Table 2.2.2.3.1 *Summary of the 1D analyses.*

Some of the results of the numerical analyses are plotted in Figure 2.2.2.3.1 in terms of peak acceleration (a_{max}) and peak horizontal displacement (u_{max}) versus depth, as well as in terms of spectral accelerations S_a at the ground level. The figures refer to the case of a soft layer with $V_{s,g}$=20m/s and to the wavelet having dominant frequency f=3Hz, which is taken as a representative example of the site response.

The acceleration profiles show that, due to the downward reflection caused by the soft grouted layer, the peak amplitude below it increases significantly, as observed in §2.2.2.2 too; however, this has no effect on seismic isolation at ground level.

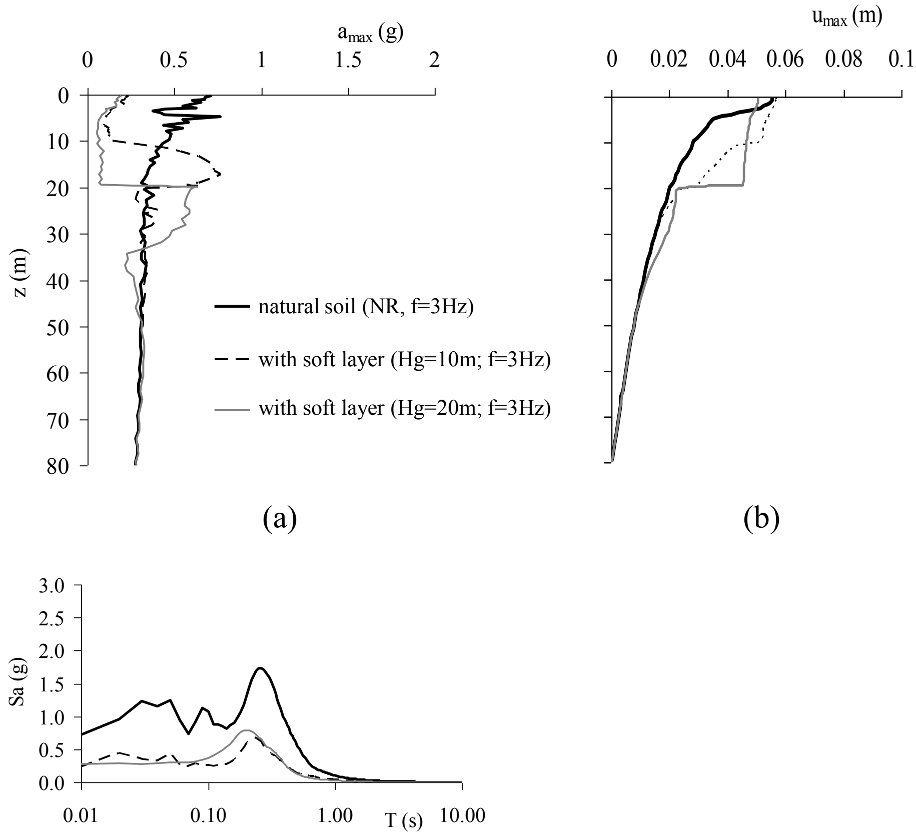

(a) (b)

(c)

Figure 2.2.2.3.1 *Numerical results: vertical profiles of peak acceleration a_{max} (a), maximum displacements u_{max} (b) and acceleration spectra S_a (c) for the Ricker (f=3Hz) signal.*

Figure 2.2.2.3.1b shows that the values of the maximum horizontal displacements $u_{max}(z)$ are significantly increased by the concentration of the shear strain in the grouted layer: above it, horizontal displacements increase, assuming an almost constant value, i.e. the shallow untreated layer slides just like a rigid body. This maximum horizontal displacement u_{max} at a certain depth has been calculated as the sum of the maximum displacements recorded at the different depths below, during the dynamic excitation duration; it is an approach intrinsically over-conservative, because maximum effects are generally out of phase.

The same results are reported in Figure 2.2.2.3.1c in terms of spectral accelerations. The comparison confirms the effectiveness of grouting, highlighting that the reduction in S_a (T) is larger for the deeper than for the shallower treatment. For periods larger than 2 seconds, no significant difference can be observed with or without soft grouting.

The effect of the frequency content of the input motion can be observed looking at Figure 2.2.2.3.2, which summarizes all the results obtained with the Ricker wavelets for $V_{s,g}$ equal to 10m/s and 20m/s. The figure shows that grouting is always effective in scaling down a_{max} for all the investigated frequencies (see Figure 2.2.2.3.2a). The largest values of a_{max} at ground level pertain in all cases to the critical value of f=1Hz, which is close to the fundamental frequency of the natural soil deposit (f_n=1.20Hz).

The grouted layer depth is almost ineffective for the lowest frequency (0.1Hz), while the values of a_{max} at ground level for f ≥3Hz are basically independent of it.

As a result, it is confirmed that the lower the dynamic impedance ratio α the more effective the screening effect of the soft layer on the surface acceleration. Figure 2.2.2.3.2b reports the spectral intensity SI with respect to the predominant frequency of the different wavelets. For the lowest wavelet frequency, f=0.1Hz, SI is even increased by grouting; the reduction of SI is still relatively small, up to f=1Hz, for the layer at H_g=10Hz, while for H_g=20m the SI reduction is already of the order of 50% at f=1Hz. At larger frequencies, SI strongly reduces when the grouted layer is present.

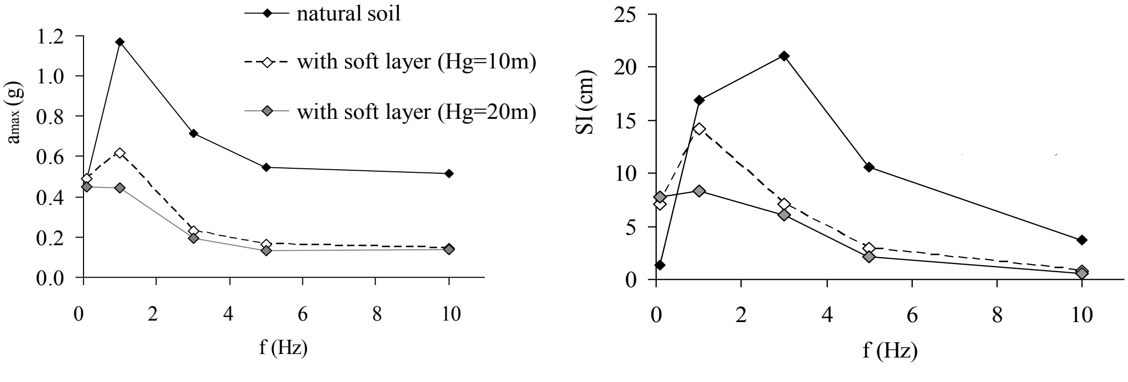

(a) (b)

Figure 2.2.2.3.2 *Peak acceleration a_{max} (a) and spectral intensity SI (b) at the ground level with respect to the dominant input frequency for the Ricker wavelets.*

In terms of system effectiveness E_I, Figure 2.2.2.3.3 summarizes some of the results obtained for the 3Hz wavelet, which leads to larger values of the efficiency E_I, on the average equal to about 0.7 for the shallow treatment, while the deeper grouting proves to be more convenient only for periods between 0.1s and 0.5s.

Figure 2.2.2.3.4 reports the S_d-S_a plot resulting for one of the grouting examples (H_g=20m and α=0.042) compared to that of the natural soil. The extremely large reduction of the demand results, for a given capacity curve of a building, into a much lower intersection point, i.e. a better performance and a higher seismic safety. In the figure, different lines are plotted at constant values of the natural period T of the structure, highlighting that the reduction of the demand can be effective for squat to medium slender masonry buildings.

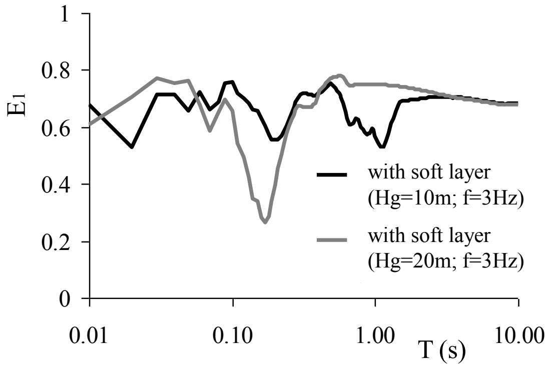

Figure 2.2.2.3.3 *Isolation Effectiveness E_I (T) for the Sturno (a) and for the Ricker signal having a dominant frequency f=3Hz (b).*

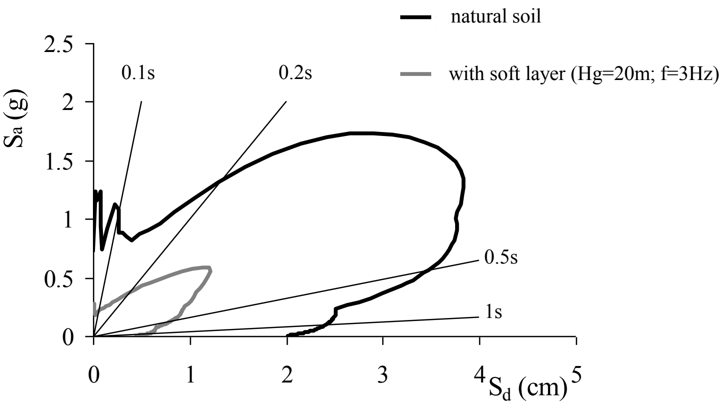

Figure 2.2.2.3.4 *Spectral acceleration (S_a) versus the spectral displacement (S_d) for the case of Ricker wavelet (f=3Hz) and a depth of grouted layer H_g=20m.*

2.2.2.4 1D analyses: effects of the differences between a linear and a non-linear soil stiffeness decay behaviour on dynamic response

In these parametric analysis, a homogeneous fine-grained subsoil has been considered, with a thickness H=60m (Figure 2.2.2.4.1a), a unit weight γ_s=20kN/m^3 and a shear wave velocity $V_{s,s}$=300m/s, corresponding to a medium consistency clay. The natural period T_n of the deposit is therefore T_n=4H/$V_{s,s}$=0.8s. The clay layer overlies a bedrock, with a thickness of 60m, at the bottom of which a reference seismic motion with variable frequency content has been applied. To explore the effects of the possible variability of the reference input motion amplitude, two different hypotheses have been considered for the constitutive model of the clay:

- linear behaviour, characterized by $G=G_0$, where G_0 is calculated as $G_0=\rho\cdot V_{s,s}$;

- non-linear behaviour, with the shear modulus, G, and the damping ratio, D, depending on the shear strain level as shown in Figure 2.2.2.4.1b.

A layer of soft material with thickness t_g=1m is then placed at a depth H_g=20m (Figure 2.2.2.4.1a). The same density as the soil and two extremely different shear wave velocities $V_{s,g}$ are assumed for such layer, in order to simulate either a stiff ($V_{s,g}$=1000m/s) or a very soft grouting ($V_{s,g}$=20m/s). To evaluate the dependency of the results on the grouting stiffness only, in both cases the material is assumed as linear and the damping ratio set to zero.

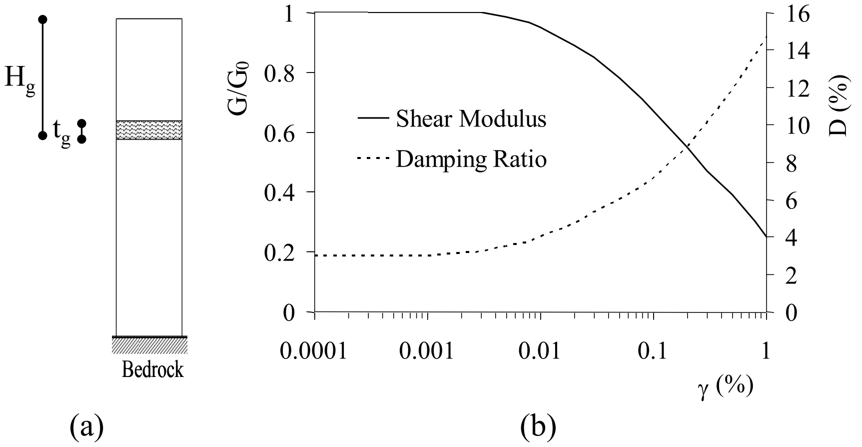

Figure 2.2.2.4.1 *Subsoil model: layering (a), $G(\gamma)/G_0$ and $D(\gamma)$ curves for the natural clay (b).*

Table 2.2.2.4.1 summarizes the main properties of the natural soil, the bedrock and the grouted layer:

material	γ_s (kN/m^3)	ρ (kg/m^3)	V_S (m/s)	D_0 (%)
Natural soil	20	2040	300	3
Soft layer	20	2040	1000	0
			20	
Bedrock	20	2040	1000	0

Table 2.2.2.4.1 *Main properties of the materials.*

The numerical analyses of 1D seismic response have been carried out using the code EERA. Simplified input motions have been applied at the bedrock in terms of acceleration by means of the seismic Ricker wavelet model (see §2.1.2). Three different dominant frequencies (f=1, 3, 5Hz) are considered, while the peak acceleration was kept constant and equal to 0.5g (Lombardi et al, 2013). The seismic response analyses carried out are summarized in Table 2.2.2.4.2. The behaviour of the natural subsoil (without the grouted layer) is assumed as the reference case. The results of the two analyses are plotted in Figures 2.2.2.4.2 (S1, T 20 1) and 2.2.2.4.3 (S3, T20 3) in terms of acceleration and displacement time histories at ground level.

Layering	Case	f (Hz)	V_{sg} (m/s)
natural soil	S1, S1*	1	/
	S3, S3*	3	
	S5, S5*	5	
with soft layer	T 1000 1	1	1000
	T 1000 3	3	
	T 1000 5	5	
	T 20 1, T 20 1*	1	20
	T 20 3, T 20 3*	3	
	T 20 5, T 20 5*	5	

Table 2.2.2.4.2 *Summary of the analyses (*Case with linear soil behaviour).*

As in the examples shown in the figures, in all cases the soft grouted layer increases the duration of the shaking but reducing, even strongly, the peak ground acceleration. On the contrary, the effect is not always the same in terms of maximum surface displacements: in most cases, the introduction of the soft layer does not change significantly the peak value, with the exception of the analysis T 20 1 (see Figure 2.2.2.4.2), for which the dominant frequency of the Ricker wavelet (1Hz) is close to the natural frequency of the deposit (f_n=1.25Hz). In this latter case, even though the peak acceleration is reduced, the peak displacement at ground level is seen to increase.

Table 2.2.2.4.3 summarizes all the results in terms of peak acceleration and displacement at the ground level. The stiff grout layer has no influence on the seismic response: these analyses will not be therefore considered in the following.

The numerical results are also plotted in Figure 2.2.2.4.4, in terms of peak acceleration, a_{max}, and maximum displacement u_{max}, in each layer. For each seismic input considered, the peak acceleration profile strongly decreases across the soft grouted layer, keeping reduced values up to ground surface. At the same time, the peak displacement increments are concentrated within the grouted layer. The effectiveness of the soft grouted layer and the role of soil non-linearity in attenuating the seismic inertial actions can be better inferred by analysing the acceleration response spectra S_a. The spectral accelerations at surface resulting from the non-linear and linear analyses are respectively plotted in Figures 2.2.2.4.5 a and b. For all the input motions, the soft layer significantly modifies the seismic response at surface, reducing the peak values of the spectral acceleration and modifying the corresponding periods. For the range of periods considered as significant in this work (0.1<T<0.5s; see §1.9), both Figures 2.2.2.4.5 a and b indicate that the grouting intervention is effective in reducing the inertial forces on structures.

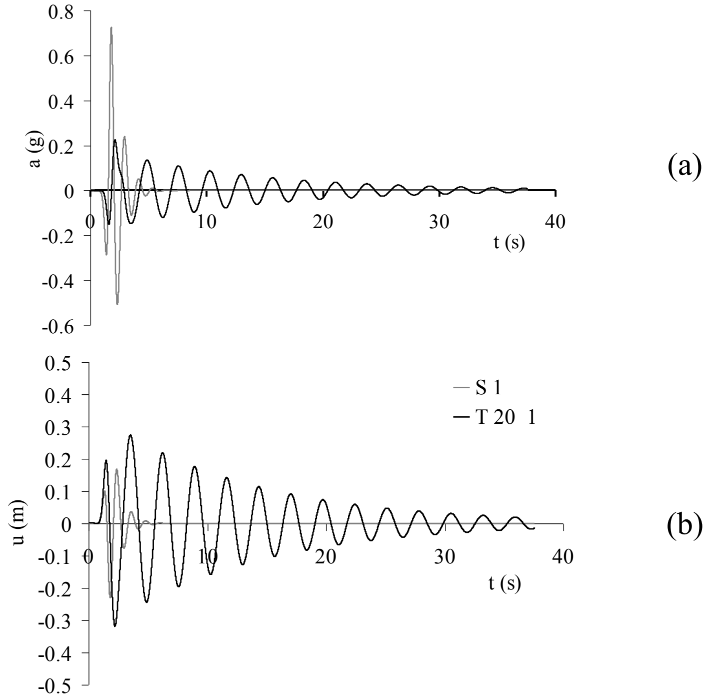

Figure 2.2.2.4.2 *Time histories of acceleration (a) and displacement (b) at the ground surface for natural and treated soil under a 1Hz input motion.*

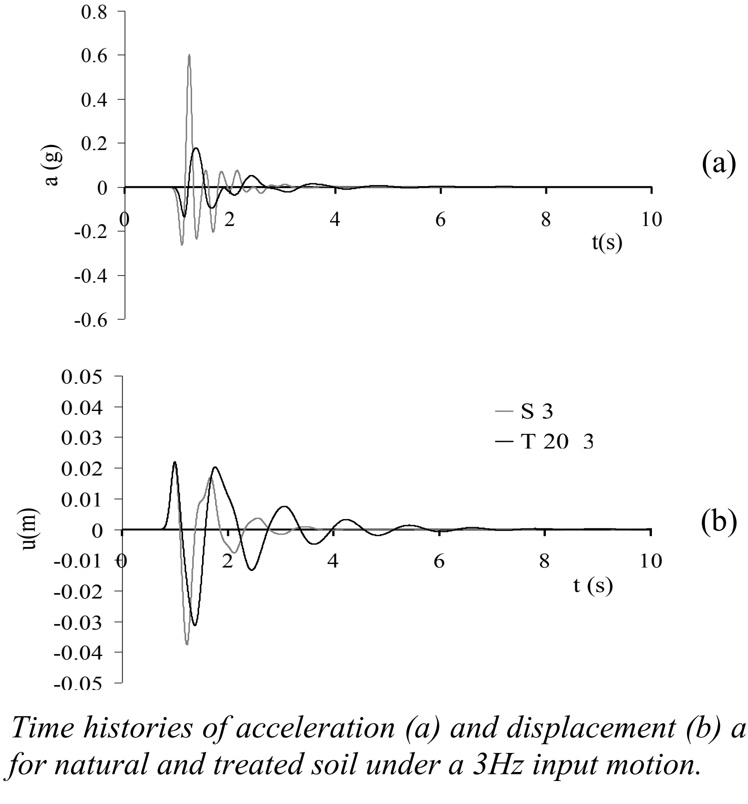

Figure 2.2.2.4.3 *Time histories of acceleration (a) and displacement (b) at the ground level for natural and treated soil under a 3Hz input motion.*

Layering	Case	Peak acceleration a_{max} (g)	Peak displacement u_{max} (m)
Natural soil	S1	0.724	0.230
	S1*	0.911	0.149
	S3	0.602	0.038
	S3*	0.692	0.039
	S5	0.547	0.013
	S5*	0.636	0.013
With soft layer	T 1000 1	0.719	0.228
	T 1000 3	0.602	0.038
	T 1000 5	0.551	0.013
	T 20 1	0.225	0.318
	T 20 1*	0.662	0.339
	T 20 3	0.177	0.031
	T 20 3*	0.097	0.026
	T 20 5	0.070	0.008
	T 20 5*	0.095	0.007

Table 2.2.2.4.3 *Summary of the numerical results (* case with linear soil behaviour).*

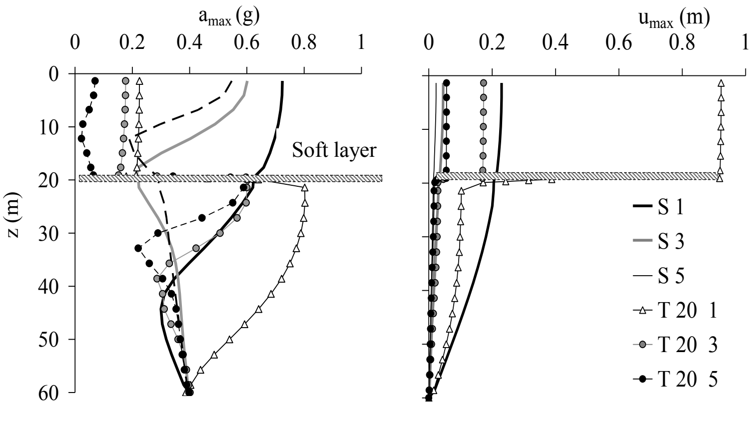

(a) (b)

Figure 2.2.2.4.5 *Vertical profiles of peak horizontal acceleration (a) and peak horizontal displacement relative to the bedrock (b) computed without (S1, S3, S5) and with (T 20 1, T 20 3, T20 5) the grouted soft layer.*

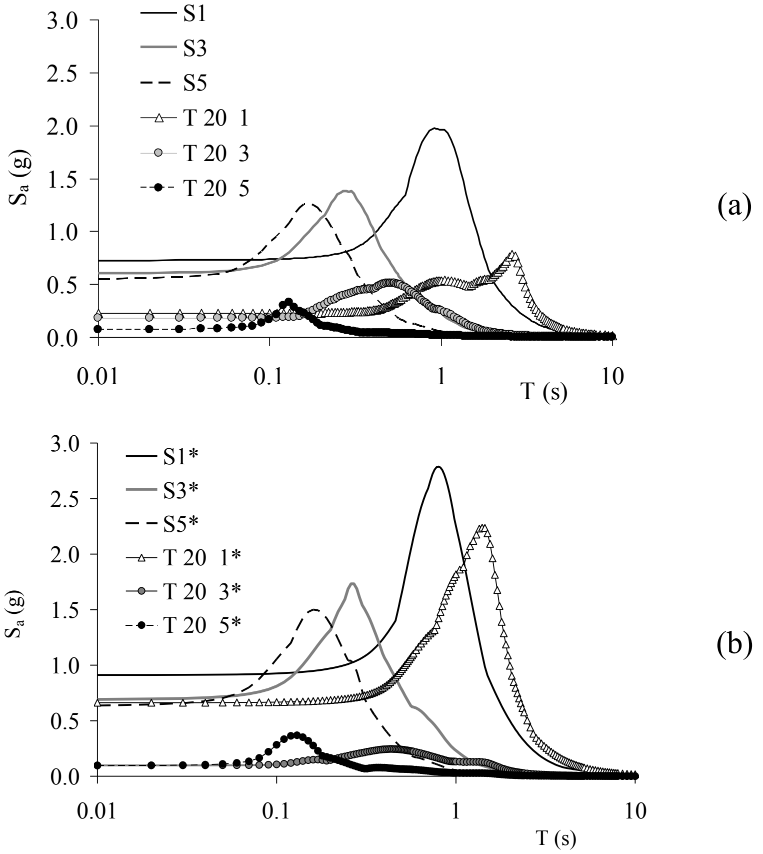

Figure 2.2.2.4.6 *Acceleration response spectra at surface from non-linear (a) and linear (b) analyses without (S1*, S3*, S5*) and with (T 20 1*, T 20 3*, T20 5*) the soft grouted layer.*

In the case of non-linear analysis (2.2.2.4.6a) of untreated soil shaken by the 1Hz Ricker wavelet (S1), the maximum spectral amplification corresponds to the single degree of freedom oscillator with a natural period close to that of the soil deposit (i.e. double resonance mechanism). For such a case, the insertion of the grouted layer (T 20 1) induces a beneficial effect by reducing the maximum acceleration to less than 50%, but on the other hand it increases the corresponding dominant period to more than twice. In this peculiar case, the simple oscillator response with the grouted layer is worse than that of the untreated soil treatment in a range of periods corresponding to structures much slender than those considered in this study. Similar qualitative considerations can also be taken for the spectral accelerations predicted under the hypothesis of linear soil behaviour (Figure 2.2.2.4.6b). The quantitative differences are related to the stiffer response of the clay soil, which in these cases induces larger accelerations. For the cases S1* and T 20 1*, the crossing point of the spectra, individuating the onset of a worse response with the grouted layer, is shifted at a period equal to 1.5s, corresponding to a structure as high as 90m.

The above observations can be further synthesized in terms of spectral intensity SI, plotted in Figure 2.2.2.4.7 with respect to the input frequency, for all the analyses carried out with and without the soft grout layer. For every input dominant frequency adopted (1, 3, 5Hz), the soft grouted layer reduces the effects at ground level in the range of periods T typical for old squat masonry structures. It must be noted that, conversely with respect to what above observed for the spectral acceleration, larger values of SI (up to about 95cm for f=1Hz for the case without the grouted layer) are computed in the analyses in which a non-linear soil behaviour is considered.

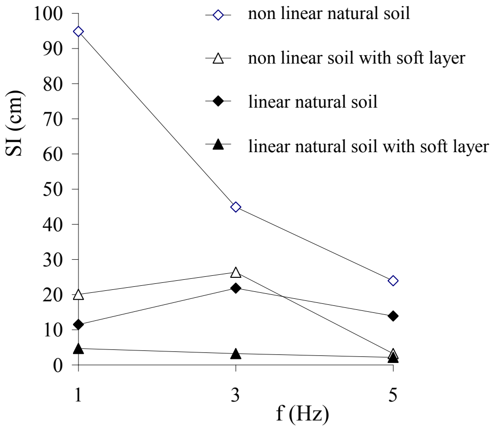

Figure 2.2.2.4.7 *Spectral intensity SI values obtained at surface versus the dominant input frequency.*

2.3. Dynamic 2D analyses

2.3.1. Description of the numerical modelling

2D dynamic analyses have been developed using the software FLAC7 (FLAC7 manual, 2011), an explicit, finite difference program that performs a Lagrangian analysis, in order to solve the full equations of motion, using lumped grid-point masses derived from the real density of the selected mesh zones.

The general calculation sequence embodied in FLAC7 is illustrated in Figure 2.3.1.1. The analyses calculation path is succeeding reported:

1. the procedure first considers the equations of motion to derive new velocities and displacements from stresses and forces;
2. strain rates are derived from velocities;
3. new stresses are calculated from strain rates.

It takes one time step for every cycle around the loop. Each box in Figure 2.3.1.1 updates all of its grid variables from known values that remain fixed while control is within the box. Generally speaking, if for instance a stress changes in a certain zone, it will influence its neighbouring ones with changes in velocities. Consequently, this approach seems to be unreasonable.

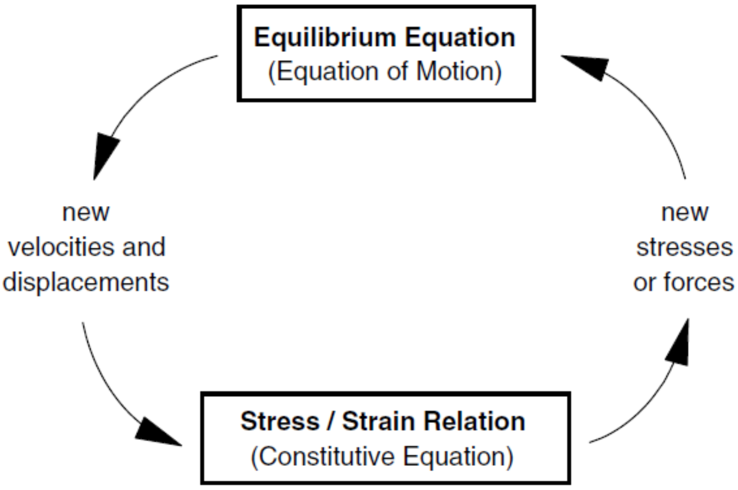

Figure 2.3.1.1 *Basic explicit calculation cycle.*

However, the software chooses a time step so small that information cannot physically pass from one element to another in that interval.

All materials have a maximum speed at which information can propagate, that is the compressive wave velocity V_P, which is expressed as:

$$V_P = \sqrt{\frac{K + 4G/3}{\rho}} \tag{2.3.1.1}$$

After several cycles of the loop, disturbances can propagate across several elements, just as they would propagate physically. Therefore, the calculation wave speed keeps ahead of the physical wave speed, so that the equations always operate on known values that are fixed for the duration of the calculation.

The most important advantage of such an approach is that no iteration process is necessary when computing stresses from strains in an element, even if the constitutive law is wildly nonlinear. The greatest disadvantage of the explicit method seems to be the small time step Δt_d, which means that large numbers of steps must be taken. A general expression of Δt_d is:

$$\Delta t_d = \min\left\{\sqrt{\frac{\sum m}{\sum k}}\right\} \cdot \frac{1}{2} \tag{2.3.1.2}$$

where the min() function is taken over all grid points and structural degrees of freedom, and Σ is a summation over all contributions to the grid point or structural degree-of-freedom. For each triangular subzone in which every rectangular element of the FLAC mesh is divided, k is the stiffness contribution from each of the three grid points of the subzone:

$$k = \left(K + \frac{4}{3}G\right)\left\{\frac{\left(L^{\max}\right)}{6A_\Delta}\right\} \cdot \underline{T} \tag{2.3.1.3}$$

where $L^{\max}$ is the maximum edge-length of the triangle, A_Δ is the area of the triangle and $\underline{T}$ is the out-of-plane dimension, equal to 1.0 for a plane-strain analysis. The stiffness and the mass contributions from all the zones surrounding each grid point are summed, giving a total stiffness term of k and a total mass term of m, respectively.

The stiffness and the zone sizes can widely vary in a model, above all in the assumed models for dynamic analyses of soft caissons, where finely soft zones are connected to natural soil layers.

The differences between the stiff and the small zones may control the time step chosen by FLAC7, due to the min() function and to the stiffness values. So few zones will then determine the critical time step, although the best part of the model should be calculated with a meaningfully larger time step. In order to reduce the computation calculation time, a procedure known as dynamic multi-stepping have been used. In this procedure, the zones and the grid points are ordered into classes of similar maximum time steps and each class is then run at its time step. Information is after transferred between zones at the appropriate time.

However, the performed analyses need large calculation time, because of the important differences in stiffness and mass among the different mesh elements.

The mesh has been calibrated to obtain the smallest model dimension, without sensible variations on motion equation solutions, starting from previously literature considerations (Bouckovalas et al, 2006).

In dynamic analyses, the input at the base of the bedrock has always been applied as a stress history, referring to given velocity histories. Consequently, shear wave signals (τ_{xy}) have been propagated; actually, a velocity can be converted to a stress wave using the formula:

$$\tau_{xy} = \rho \cdot V_{s,b} \cdot v(t) \tag{2.3.1.4}$$

where:

τ_{xy} is the applied shear stress;

ρ is the mass density;

$V_{s,b}$ is the shear wave velocity of the bedrock;

v(t) is the input shear particle velocity.

The modelling of geomechanics problems involves media that should be represented as unbounded; so numerical methods have been defined to describe a suitable discretization of a finite region of space with appropriate condition.

Generally speaking, the dynamic analyses start from the in-situ conditions; so, to describe the initial tensional state of the modelled media, it is necessary a first static calculation stage. In this first stage, the horizontal displacements of the lateral boundaries at the base of the model have been inhibited. In dynamic analyses, however, such boundary conditions may cause a reflection of outward propagating waves back into the model and do not allow the necessary energy radiation. To minimize this problem, a larger model should be used. The material damping will so absorb the major part of the energy of the waves reflected from boundaries; however, this solution leads to a larger computational burden.

Therefore, at the base of the model, quiet boundaries have been placed. These boundaries, which use the viscous boundary theory developed in FLAC7 (Lysmer and Kuhlemeyer, 1969), are made of independent dashpots in the normal and shear directions. The dashpots provide viscous normal and shear tractions.

The boundary conditions at the sides of the models should represent the 1D free-field motion. In order to absorb the outward waves, the lateral vertical boundaries have been forced to free-field motion, by a FLAC7 technique that involves a one-dimensional free-field calculation in parallel with the main-grid analysis. In Figure 2.3.1.2, a scheme of the model used for seismic analyses is reported.

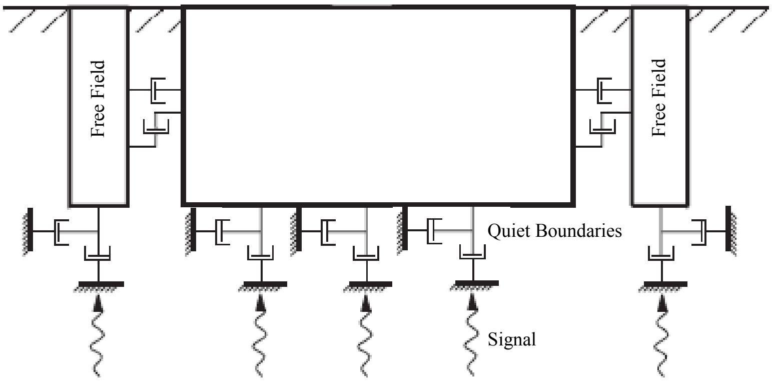

Figure 2.3.1.2 *Model configuration for seismic analyses.*

The natural dynamic systems contain some degree of vibration energy damping (see §1.7); otherwise, the systems would oscillate indefinitely when subjected to dynamic forces.

In order to simulate the loss of energy due to the material damping during oscillation, the analyses have been developed by using a Rayleigh damping (Kelly, 1999). This typology of damping is frequency-dependent, i.e. frequency-independent only on a restricted range of frequencies.

The Rayleigh damping was originally used in the analysis of structures and elastic continua, to damp the natural oscillation modes of the system, to solve the motion equations; these equations can be expressed, in matrix form, as:

$$\hat{M} \cdot \ddot{u} + \hat{C} \cdot \dot{u} + \hat{K} \cdot \dot{u} = \hat{F}(t) \qquad (2.3.1.5)$$

where the reported matrices are, respectively, the mass, the damping and the stiffness ones. $\hat{F}(t)$ is the matrix of the force system applied to the model. This system can be diagonalized if:

$$\hat{C}\cdot\hat{M}^{-1}\cdot\hat{K}=\hat{K}\cdot\hat{C}\cdot\dot{u}+\hat{K}\cdot\hat{M}^{-1}\cdot\hat{C} \tag{2.3.1.6}$$

A typical example, in this sense, is used in performed analyses, because the damping matrix $\hat{C}$ is written as proportional to the mass matrix $\hat{M}$ and to the stiffness $\hat{K}$ one, as reported:

$$\hat{C}=\alpha'\cdot\hat{M}+\beta'\cdot\hat{C} \tag{2.3.1.7}$$

where α' is the mass-proportional damping constant and β' is the stiffness-proportional damping constant (Hashash e Park, 2002).

For a multiple degree-of-freedom system, the critical damping ratio ξ_i at each angular frequencyof the system ω_i can be derived from (Bathe and Wilson, 1976):

$$\xi=\frac{c}{c_c}=\frac{1}{2}\cdot\left(\frac{\alpha'}{\omega_n}+\beta'\cdot\omega_n\right) \tag{2.3.1.8}$$

where the critical damping ratio ξ is the portion of critical damping (c/c_c) with respect to the mode with angular frequency ω. Assigned a value of critical damping and a control frequency f, the two constants can be calculated as:

$$\begin{aligned}\alpha'&=\xi\cdot 2\cdot\pi\cdot f\\ \beta'&=\frac{\xi}{2\cdot\pi\cdot f}\end{aligned} \tag{2.3.1.9}$$

FLAC7 has a mono-frequency approach, which considers only one control frequency; at this frequency, the system exhibits the assumed damping value ξ. On the other frequencies, the system is over-damped (Figure 2.3.1.3).

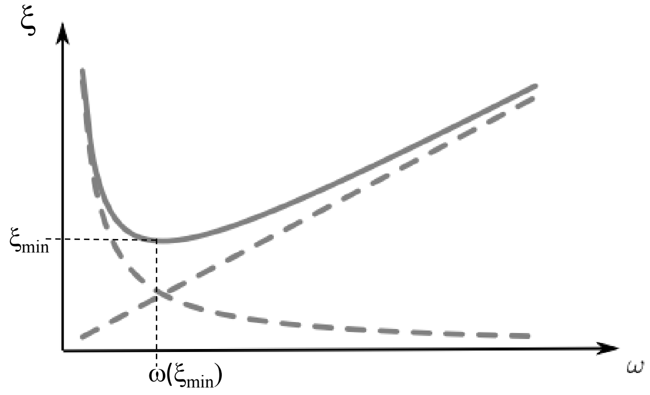

Figure 2.3.1.3 *Damping ratio ξ as a function of angular frequency ω in the mono-frequency approach.*

To tackle out this inconvenient, two equivalent values of damping and control frequency have been previously calculated. By modifying the mono-frequency approach, a damping similar to the chosen one can be imposed to a frequency range including the frequencies of interest i.e. the natural frequency of the untreated layer and the peak signal frequency.

In a double frequency approach, two different angular frequencies ω_1 and ω_2 are defined; the constants previously described can be derived from:

$$\alpha' = 2 \cdot \xi \cdot \frac{\omega_1 \cdot \omega_2}{\omega_1 + \omega_2}$$
$$\beta' = \frac{2 \cdot \xi}{\omega_1 + \omega_2} \tag{2.3.1.10}$$

In this approach, the value of ξ is obtained for two different frequencies. Between these two values, the system is slightly under-damped; outside it is over-damped (see Figure 2.3.1.4).

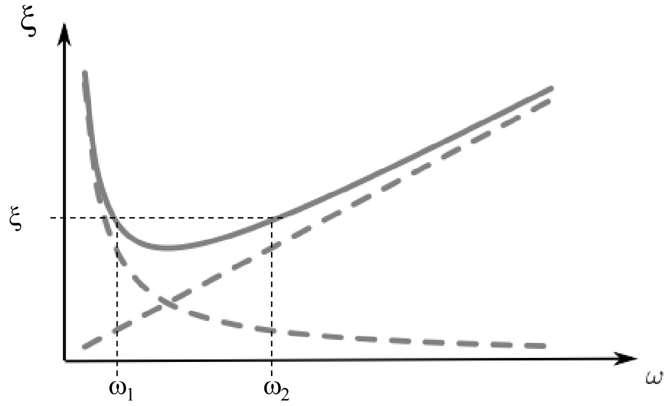

Figure 2.3.1.4 *Damping ratio ξ as a function of the angular frequency ω in the double-frequency approach.*

An equivalence between the mono and double frequency approaches can be obtained by the superposition of the curves of Figures 2.3.1.3 and 2.3.1.4. For a mono-frequency approach, an equivalent angular frequency and an equivalent damping ratio can be derived as:

$$\begin{aligned} \omega_P &= \frac{2 \cdot \omega_1 \cdot \omega_2}{\sqrt{4 \cdot \omega_1 \cdot \omega_2}} \\ \xi_P &= \frac{\xi}{\omega_1 \cdot \omega_2 \cdot \sqrt{4 \cdot \omega_1 \cdot \omega_2}} \end{aligned} \tag{2.3.1.11}$$

Consequently, two modified values of frequency and damping ratio are used to consider a double frequency approach into the FLAC7 numerical solution, where only a one-control frequency approach is implemented.

As far as the depth of the single element of the mesh is concerned, both the frequency content of the input wave and the wave-speed characteristics of the system may affect the numerical accuracy of the wave transmission, with numerical distortions of the propagating wave.

In order to take into account such an effect, Kuhlemeyer and Lysmer (1973) indicate a spatial element size Δl. This spatial element should be smaller than, approximately, one-tenth to one-eighth of the wavelength associated with the highest frequency component of the input wave:

$$\Delta l \le \frac{L_w}{8 \div 10} \tag{2.3.1.12}$$

where L_w is the wavelength associated with the highest frequency component that contains appreciable energy. In the definition of the mesh used into dynamic analyses, these ranges of element size have been used to define the geometrical configurations. Similar dimension constraints, used to describe the soft grouts, correspond to very small mesh elements sizes, with important analyses time increments.

Assuming the previously reported criteria, 2D dynamic analyses have been performed. Initially some preliminary schemes with vertical and horizontal soft layers have been studied. Then, some schemes with a more complex treatment system consisting of a “soft caisson” with a rectangular section or made of inclined injections have been analysed.

2.3.2. Preliminary 2D analyses with vertical and horizontal diaphragms

2.3.2.1 Generalities

As already discussed in §1.2, trenches and screens are used to tackle out vibration isolation. Semblat and Pecker (2009) have presented different theoretical schemes where vibration isolation has been studied by trenches embedded in the soil crossed by harmonic plane waves. Actually, they have considered an infinite layer of constant thickness (i.e. a discontinuity simulating an infinite screen) inserted in an infinite homogeneous isotropic medium, crossed by a harmonic SV-wave with an angular frequency equal to ω. Soil and screen are characterized by physical and mechanical properties as shown in Figure 2.3.2.1.1. In this case, the SV-wave, i.e. polarized in the vertical plane, impacts the intrados of the diaphragm, generating at its extrados both SV-waves that P-waves, depending on the incident angle θ.

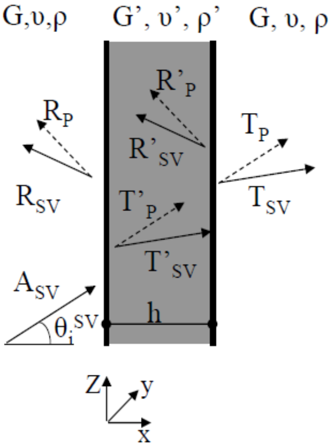

Figure 2.3.2.1.1 *Propagation of a plane SV-wave impacting on an infinite vertical layer.*

In Figure 2.3.2.1.1, A_{SV} is the maximum amplitude of the incident SV-wave; R_{SV} and R_P are respectively the maximum amplitudes of the reflected SV and P-waves. T_{SV} and T_P are respectively the maximum amplitudes of the refracted SV and P-waves. The amplitudes of the waves generated at extrados depend on two transmission coefficients called Γ_{VS} e Γ_P, which depend, themselves, on the velocity ratio χ_S i.e. the ratio between the S-wave propagation velocity of the screen and the S-wave of the surrounding medium, as reported:

$$\chi_S = \frac{V'_S}{V_S} \cong \sqrt{\frac{G' \cdot \rho'}{G \cdot \rho}}$$

$$\Gamma_{SV} = \frac{T_{SV}}{A_{SV}} e^{\frac{i \cdot \omega}{V_S} \cdot h} = f(\chi_S) \qquad (2.3.2.1.1)$$

$$\Gamma_P = \frac{T_P}{A_{SV}} e^{\frac{i \cdot \omega}{V_S} \cdot h} = g(\chi_S)$$

As shown by the graphs in Figures 2.3.2.1.2, modal conversion occurs only for values of the angle of incidence (θ) greater than zero, as confirmed by analyses that have been developed and will be described in the following. The waves having an angle of incidence at the interface with the diaphragm equal to zero do not generate any P-wave.

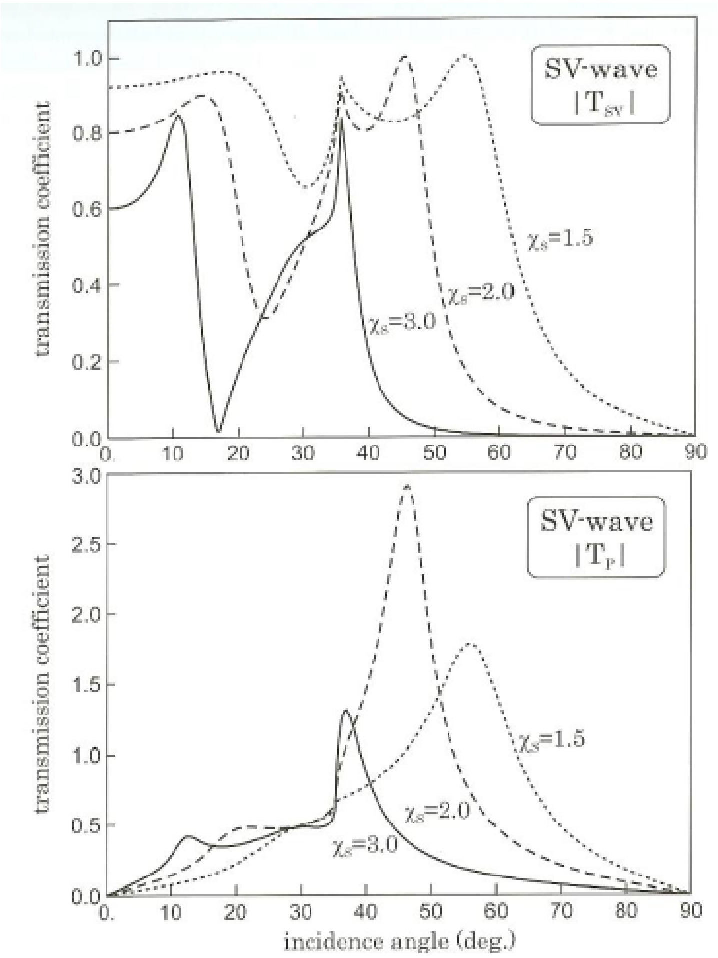

Figure 2.3.2.1.2 *Transmission coefficients Γ_{VS} andΓ_P as functions of the incident angle for different velocity ratios χ_S.*

2.3.2.2 Infinite vertical layers

In the case studied by Semblat and Pecker (2009), the attention is put on screens stiffer then the surrounding medium.

In spite of this, the analyses reported in this chapter study the effects of softer screens on the wave propagation. All analyses consider a linear elastic behaviour for the involved materials, assuming a certain value of stiffness and damping ratio constant with tensional state and shear deformations (ξ_s=3%). The first scheme that has been considered is similar to the Pecker and Semblat model; it consists of a soil medium with a density ρ_s of 2040kN/m^3 and a shear velocity $V_{s,s}$ equal to 300m/s.

The mesh used for these analyses has a dimension of 120m in the x-axis and 60m in the y-direction. In Figures 2.3.2.2.1, the geometrical configuration and some indications on vertical denominations are reported. At the middle in the x-dimension a vertical screen is placed, whose thickness is taken constant and equal to 1m; its density ρ_g is equal to 1020kN/m^3. The choice of such a value for the density has been made to prevent numerical analyses problems using the software FLAC7 due to the necessity to obtain extremely low values of impedance.

The choice of this value for density is due to different observations: the resolving time depends on the stiffness differences between close materials and the motion solution is hardly dependent on impedance ratio.

By using a low-density value, larger shear velocities can be assumed with low impedances. Furthermore, the materials that have been tested exhibit very low density values. The material called SAP (see §4.2.2), which seems to be potentially suitable to be formed as a soft layer, has a unit weight close to 10kN/m^3.

A series of analyses without considering any sort of treatment has been previously performed for the soil, so defining a reference scheme. The signals, which are Ricker wavelets transmitted as SV waves, have been propagated starting from the base of the right side of the model (from the point called RSV to RBV; see Figure 2.3.2.2.1b). The left side of the model is thought as the part to protect from the dynamic input.

In Figures 2.3.2.2.2, the results in terms of the ratio between the maximum acceleration with ($a_{max,g}$) and without screen ($a_{max,s}$) are reported; these results refer to two different series of analyses where the Poisson Ratio ν of materials is assumed equal to 0.3 both in soil and screen: in the former, assuming a certain value for the fundamental frequency of the Ricker wavelet propagated trough the layer, it is observed an important decrease in horizontal acceleration (see Figure 2.3.2.2.2 a); in the latter, considering a certain value of shear velocity for the vertical screen ($V_{s,s}$=20m/s), the fundamental frequency of the signal is varied.

At a frequency equal to 1Hz, the high values of acceleration are due to the closeness of the fundamental frequency of the signal to the natural frequency of the soil deposit without any treatment (assuming H=60m, $f_n=V_S/(4H)=1.25$Hz).

In Figures 2.3.2.2.3, the maximum acceleration ratios $a_{max,g}$ / $a_{max,s}$ along the verticals pertaining to the sections called LV and RV (se Figure 2.3.2.2.1b) are reported. By varying the fundamental frequency of the signals, and assuming a shear wave velocity of the protecting screen equal to 20m/s, a great decrease in a_{max} is observed. A soft screen is so useful in reducing the maximum effects due to the propagation.

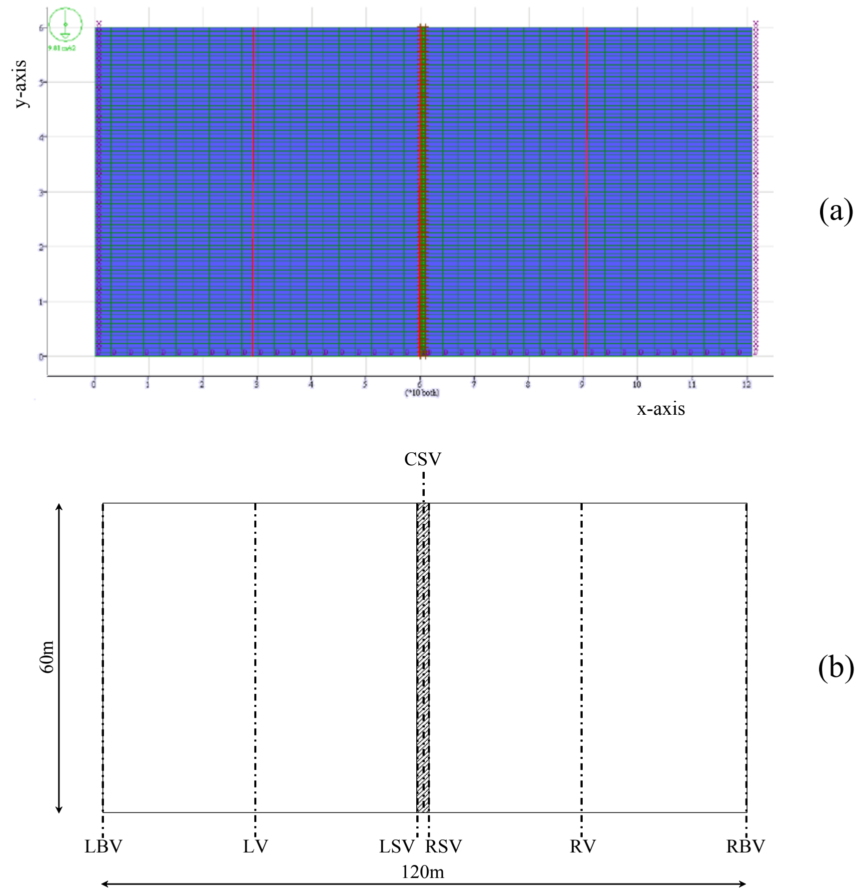

Figure 2.3.2.2.1 *Geometrical model for the vertical screen analyses: mesh used for analyses (a); geometrical dimensions and indications of the vertical axis (b).*

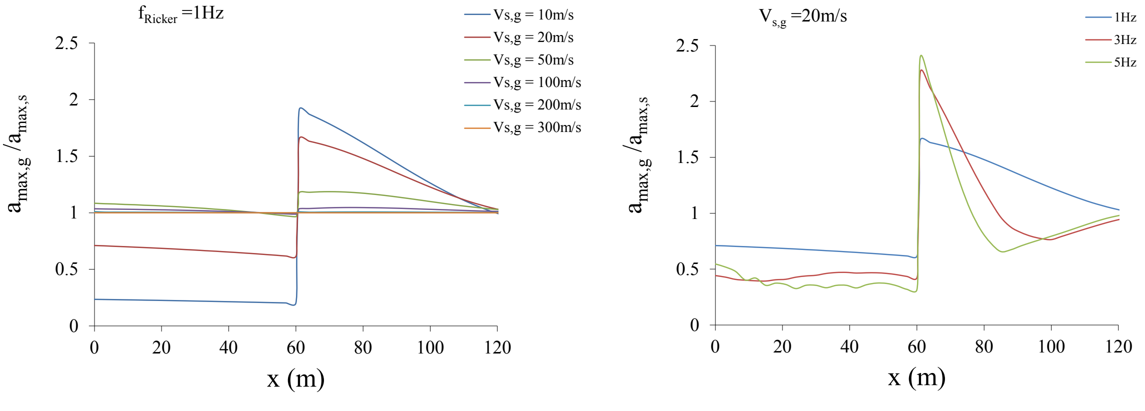

(a) (b)

Figure 2.3.2.2.2 *Maximum accelerations at ground surface for f=1Hz by varying* $V_{s,g}$ *(a); maximum acceleration at ground surface by varying the Ricker fundamental frequency and assuming* $V_{s,g}$ *equal to 20m/s (b).*

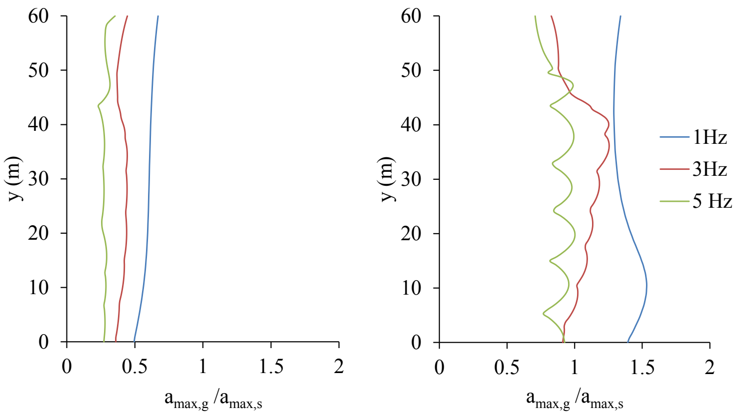

(a) (b)

Figure 2.3.2.2.3 *Maximum acceleration ratios* $a_{max,g}$ */* $a_{max,s}$ *along the verticals pertaining to the sections LV and RV.*

If attention is focused on the maximum displacement observed, it can be understood that a decrease in shear stiffness may cause an increase in horizontal displacements; in the following figures (Figures 2.3.2.2.4), the maximum x-displacements at ground surface by varying the stiffness of the screen (Figure 2.3.2.2.4 a) and along two verticals in the right and left side of the model (Figure 2.3.2.2.4 b) are reported assuming a screen $V_{s,g}$ equal to 20m/s. In such figures, the worst possible case is assumed, by propagating a Ricker wavelet with a fundamental frequency equal to 1Hz. Only assuming a screen $V_{s,g}$ equal to 10m/s (extremely low, difficult to obtain in real cases), it is observed a decrease in x-displacements in the right side of the model; if a larger $V_{s,g}$ is assumed, values of $u_{max,s}/u_{max,g}$ larger than 1 are observed along RV.

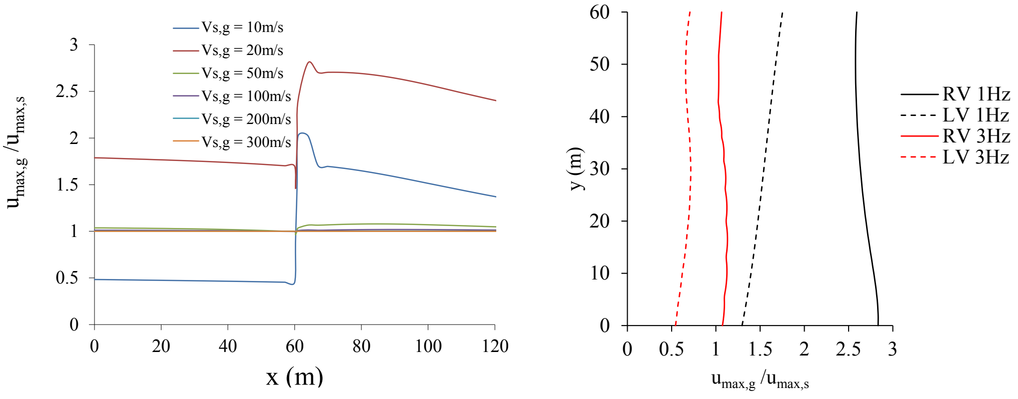

(a) (b)

Figure 2.3.2.2.4 *Maximum displacements at ground surface for f=1Hz, by varying* $V_{s,g}$ *(a); maximum displacements along two different verticals (LV, RV), by varying the Ricker wavelet fundamental frequency and assuming* $V_{s,g} = 20m/s$ *(b).*

Figures 2.3.2.2.5 illustrate the ratio $a_{max,g}/a_{max,s}$ obtained by varying the Ricker fundamental frequency and assuming a screen $V_{s,g}$ equal to 27 m/s i.e. the minimum value of shear wave velocity recorded in laboratory tests (see §4.2.2.6) As previously shown, by increasing the frequency of the signal, the acceleration ratio in the left side decreases.

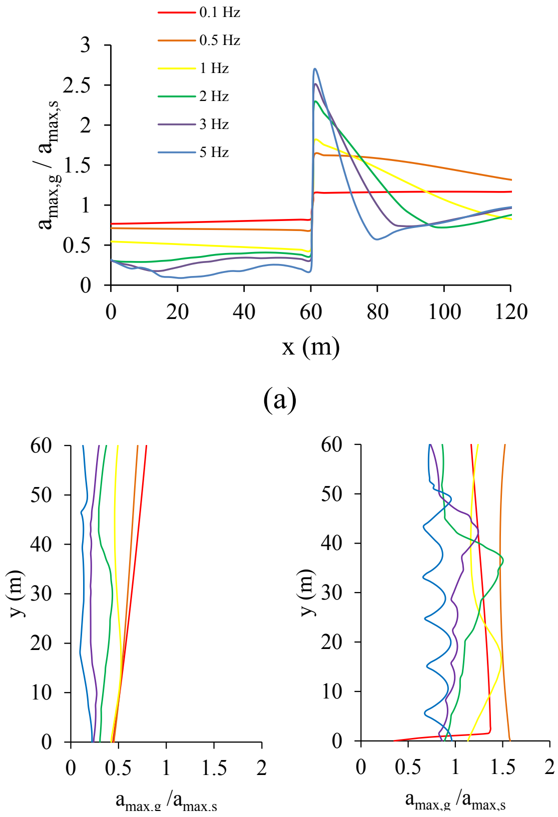

(b) (c)

Figure 2.3.2.2.5 *Maximum accelerations for different Ricker wavelets by assuming* $V_{s,g}$*=27m/s at ground surface (a), along LV (b) and RV (c) (see Figure 2.3.2.2.1b).*

The general increase in signal effect on the right side of the model is due to the reflection of energy caused by the installation of the screen, which is more important at larger frequencies. In the mechanism observed by this first typology of isolating scheme, it is observed that the shear deformability of the screen plays a fundamental role in signal propagation, as reported in literature studies. When the frequency is similar to the natural frequency of the soil layer, a worst behaviour is detected; above all, low frequencies are harder to isolate, because the signal is so low that the deformation of the screen tends to be similar to the surrounding soil one. Physically the entire model moves together at lower frequencies.

By assuming the mechanical and geometrical properties of the model previously considered (see Figures 2.3.2.2.1), the value of the Poisson ratio ν of the soft screen has been varied, to study the effect of the volumetric stiffness in the system response. Precisely, two further values of screen volumetric stiffness K have been considered, as reported in Table 2.3.2.2.1:

Scheme	V_S (m/s)	G (Pa)	ν	K (Pa)
K	20	$4.079\cdot10^5$	0.300	$8.838\cdot10^5$
0.5K	20	$4.079\cdot10^5$	0.147	$4.419\cdot10^5$
10K	20	$4.079\cdot10^5$	0.477	$88.38\cdot10^5$

Table 2.3.2.2.1 *Values of screen stiffness assumed for analyses.*

Observing Figures 2.3.2.2.6, it is clear that the value of the assumed Poisson ratio is fundamental in the wave propagation. The 10K schemes seem to be unhelpful in isolating wave propagation in comparison to the reference scheme (see Figures 2.3.2.2.6 d, e and f). The shear waves, impacting the diaphragm on the lateral side, generate a volumetric compression of the screen; if this compression is enabled by volumetric incompressibility, the wave is transmitted in the protected side without important reduction in amplitude, and without modal conversions.

In Figures 2.3.2.2.7, the accelerograms calculated at a depth of 30m from the ground surface along the verticals called LSV, CSV and RSV (see Figures 2.3.2.2.1b) are reported by varying the volumetric stiffness of the screen. For the 10K scheme (see Figure 2.3.2.2.7b), only a small variation in amplitude of the wave takes place by passing through the screen; this behaviour confirms the inefficiency of a volumetric stiffer vertical layer in reducing the wave amplitude.

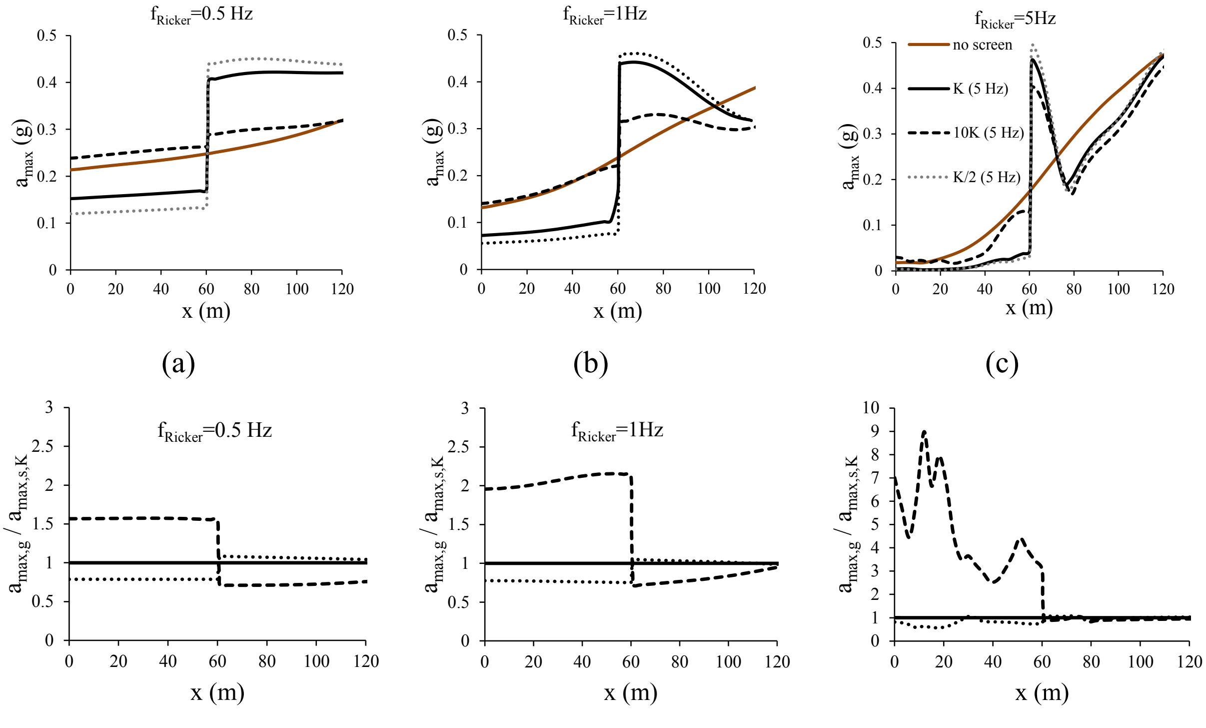

(a) (b) (c)

(d) (e) (f)

Figure 2.3.2.2.6 *Maximum acceleration at ground surface without any screen and by varying the volumetric stiffness K for a Ricker wavelet with a fundamental frequency of 0.5Hz (a), 1Hz (b) and 5Hz (c); maximum acceleration at ground surface with respect to the maximum accelerations of the K scheme, assumed as reference model ($a_{max,g,K}$), for a Ricker wavelet with a fundamental frequency of 0.5Hz (d), 1Hz (e) and 5Hz (f).*

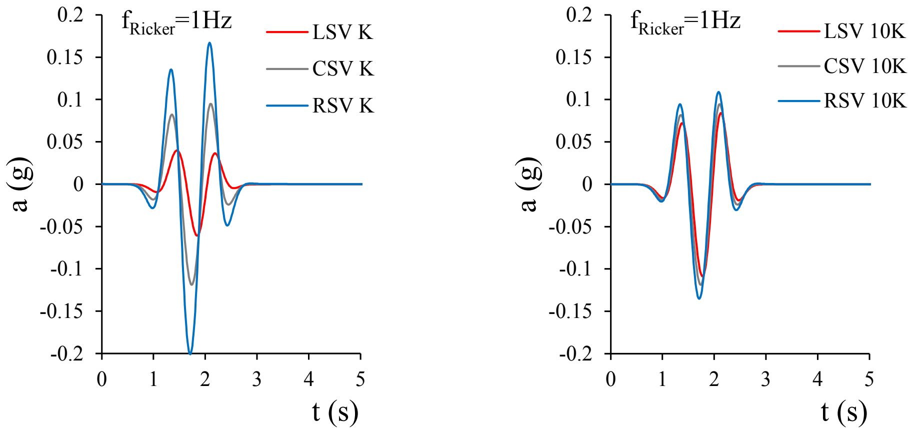

(a) (b)

Figure 2.3.2.2.7 *Accelerograms in the central part of the diaphragms by varying the volumetric stiffness of the screen, for K schemes (a) and 10K schemes (b).*

2.3.2.3 Infinite horizontal layer

A different scheme can be considered with a screen totally enclosed into the soil layer, assuming a shear stiffness equal to which assumed for the previous scheme (see Table 2.3.2.2.1). In Figure 2.3.2.3.1, the scheme adopted for analyses is reported:

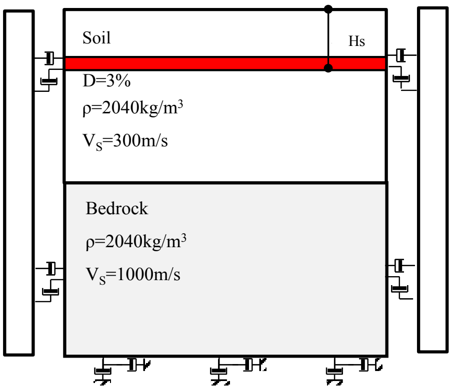

Figure 2.3.2.3.1 *Model adopted for the signal propagation through horizontal layer.*

In this scheme, always assuming the hypothesis of linear elasticity, it is assumed a different geometrical configuration, where the signal is previously propagated trough a stiffer layer, called bedrock ($V_{s,b}$=1000m/s; ρ_b=2040kg/m^3; damping ratio D_b=0). This typology of schematization will be used in the more complex schemes analysed (see §2.3.3 and 2.3.4).

Ricker wavelets of different fundamental frequencies with a maximum amplitude of 0.5g are propagated from the base of the bedrock to the ground level, by varying the volumetric stiffness of an horizontal screen. This 1m thick screen is placed at a depth of 10m from the ground surface and assuming a $V_{s,g}$ equal to 20m/s and 3 values of Poisson ratio, respectively equal to 0.147 (scheme 0.5K), 0.3 (scheme K) and 0.477 (scheme 10K); by varying Poisson ratios, it is not observed any sort of differences in terms both of maximum acceleration along the depth (see Figure 2.3.2.3.1a) and Fourier amplitude of the signals at ground surface (see Figure 2.3.2.3.1b), confirming what has been observed by Pecker (2009) in the propagation of sinusoidal waves into an infinite medium. The K soft layer value is ineffective in wave propagation.

The model with a horizontal layer simulates a 1D propagations scheme, which is, in a certain approximated way, similar to the Pecker scheme (see Figure 2.3.2.1.1). On the upper part of the soft layer, in fact, the transmitted wave will propagate through the soil above and impact the surface, being totally reflected; however, in the Pecker scheme, the transmitted wave will be propagated into a semi-infinite medium.

The schemes previously examined suggest that the volumetric stiffness could be important also for more complicated treatments with more realistic geometric configurations. In the case of horizontal layers, a larger volumetric stiffness could be more important on the static side of the problem, because it is expected a larger static displacements where the volumetric stiffness is lower.

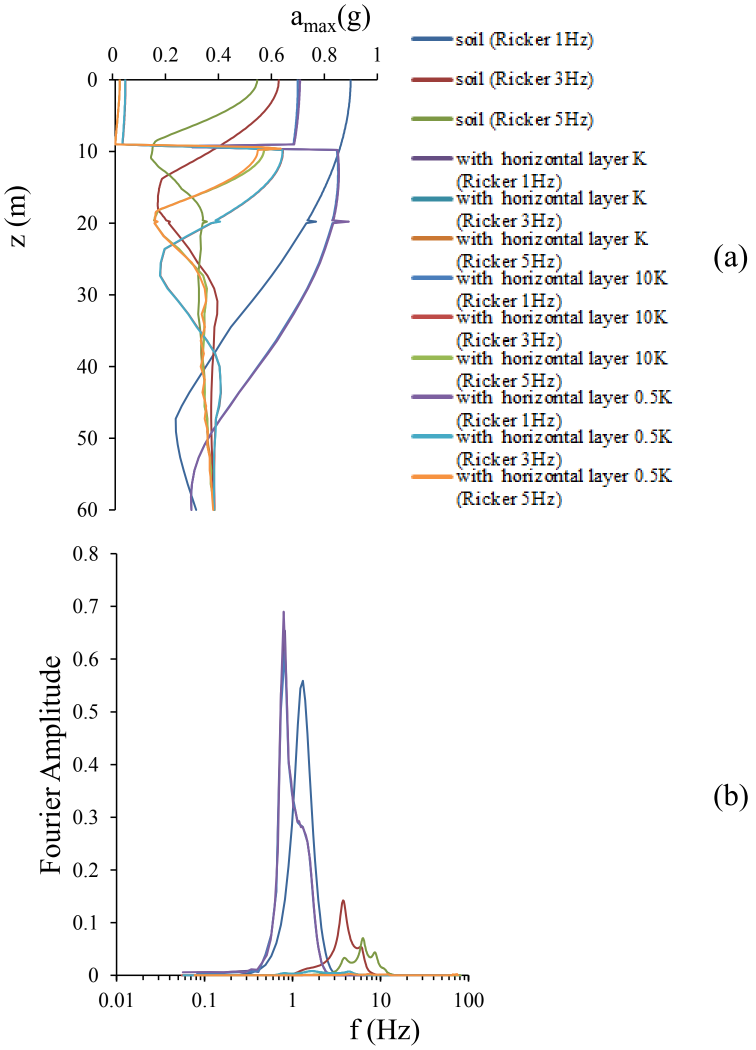

Figure 2.3.2.3.2 *Maximum accelerations with depth (a) and Fourier amplitude of the signal at ground surface (b) by varying the volumetric stiffness of the horizontal screen.*

2.3.2.4 Finite length horizontal layer

A geometrical configuration with a horizontal screen has been studied in order to understand if an isolated horizontal soft layer may be useful in reducing the effect of the propagation of a signal to ground level. Important geometrical properties in similar schemes are the depth of the treatment H_g and the horizontal length of the screen L_g, assuming a constant value for the screen thickness equal to 1m. Preliminary investigations (Kirtas, 2009) revealed that large intervention lengths, much longer than the width of the foundation of the structure to be protected at ground surface, are required in order to achieve a considerable modification of the structural response, leading to non-realistic mitigation solutions since the layer should expand below neighbouring buildings. An entirely different response would be expected if the soft layer is placed exactly below the foundation and not at the depth assumed during the current investigation, but this solution resembles more a seismic isolation approach, varying from the propagation wave filtering. This approach has also been studied, and is described in §2.3.3.3.

The model assumed for the first analyses with a finite length horizontal layer is reported in Figure 2.3.2.4.1; the soil layer and the bedrock have an equal thickness (H=60m). The mesh is 120m wide. In this first scheme, it has been assumed a length for the screen equal to 40m at a depth H_g of 10 or 20m. The screen has a shear velocity equal to 20m/s and a damping ratio equal to 0. The dynamic properties of the soil are reported in Figure 2.3.2.12; the analyses are made by assuming a linear elastic behaviour for the involved materials.

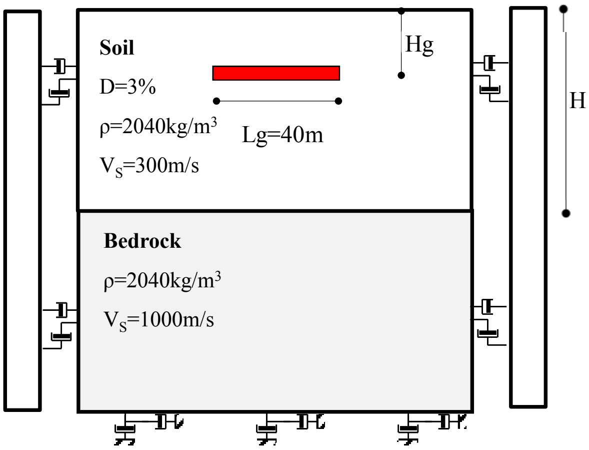

Figure 2.3.2.4.1 *Geometry and materials properties.*

By observing the results reported in Figures 2.3.2.4.2, it is clear that such a large soft horizontal layer can’t preserve the ground level from dynamic shaking caused by the propagation of Ricker wavelets with a maximum acceleration amplitude at the base of the bedrock equal to 0.5g and fundamental frequencies equal to 1Hz, 3Hz and 5Hz. This treatment generally determines worst security conditions, because a decrease in maximum effect at ground surface is not granted. In Figure 2.3.2.4.2a the maximum horizontal acceleration with depth is reported by varying the fundamental frequency of the signal; in Figure 2.3.2.4.2b the maximum horizontal accelerations are reported with respect to one side of the mesh. Actually, one-half of the horizontal layer is placed into the soil from 40 m to 60 m in the x-axis reported.

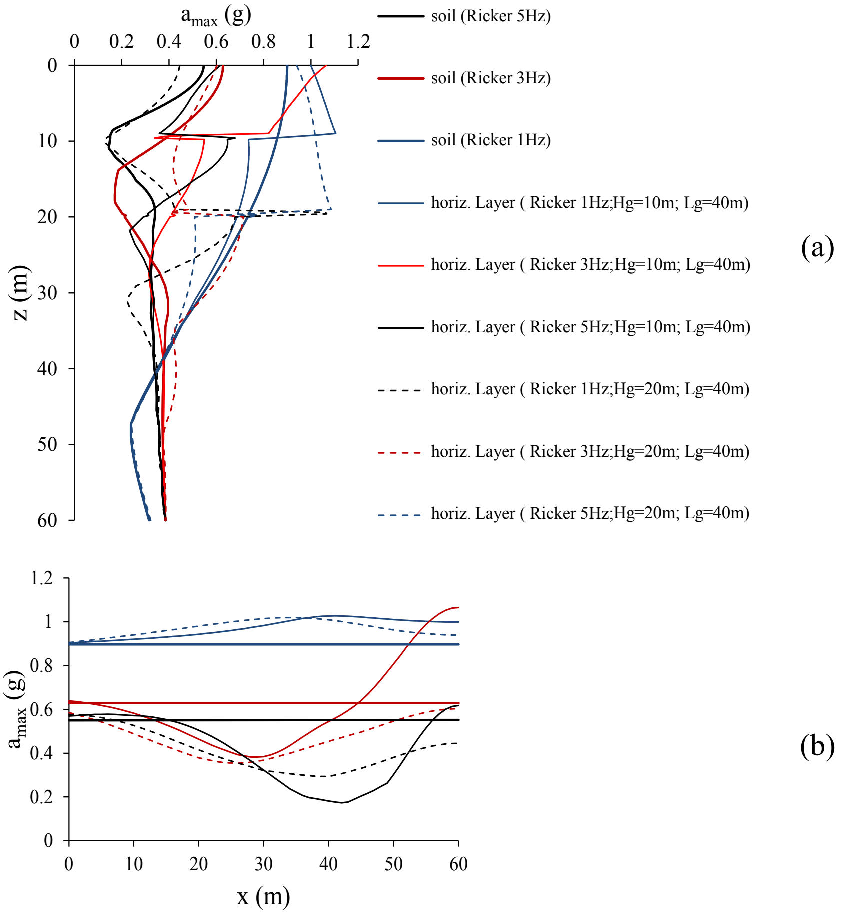

Figure 2.3.2.4.2 *Maximum accelerations along the vertical (a) and at ground surface (b) by varying the fundamental frequency of the signal and the depth of the horizontal screen.*

By assuming a unique value of H_g equal to 20m (see Figure 2.3.2.4.3 a) and by varying the length of the horizontal screen, no important decrease in acceleration amplitude can be observed, unless the entire length of the mesh is involved (see Figure 2.3.2.4.3c). These analyses are partially simplified, because, extending the length of the screen close to the width of the mesh, boundary numerical effects play a role in the results. This is not the case if the screen is sufficiently far from the boundaries of the mesh or if a 1D propagation scheme is modelled by totally extending the screen in the horizontal direction. If the screen reproduces a 1D wave propagation, it is observed, from all the scheme reported, a decrease in horizontal acceleration at ground surface, but the reproduction of a similar treatment in the engineering field is not a matter of interest, confirming the observations by Kirtas (2009).

The efficiency of a similar scheme in reducing the dynamic effects at ground level depends on the ratio H_g/L_g. The lower the ratio H_g/L_g the higher the efficiency.

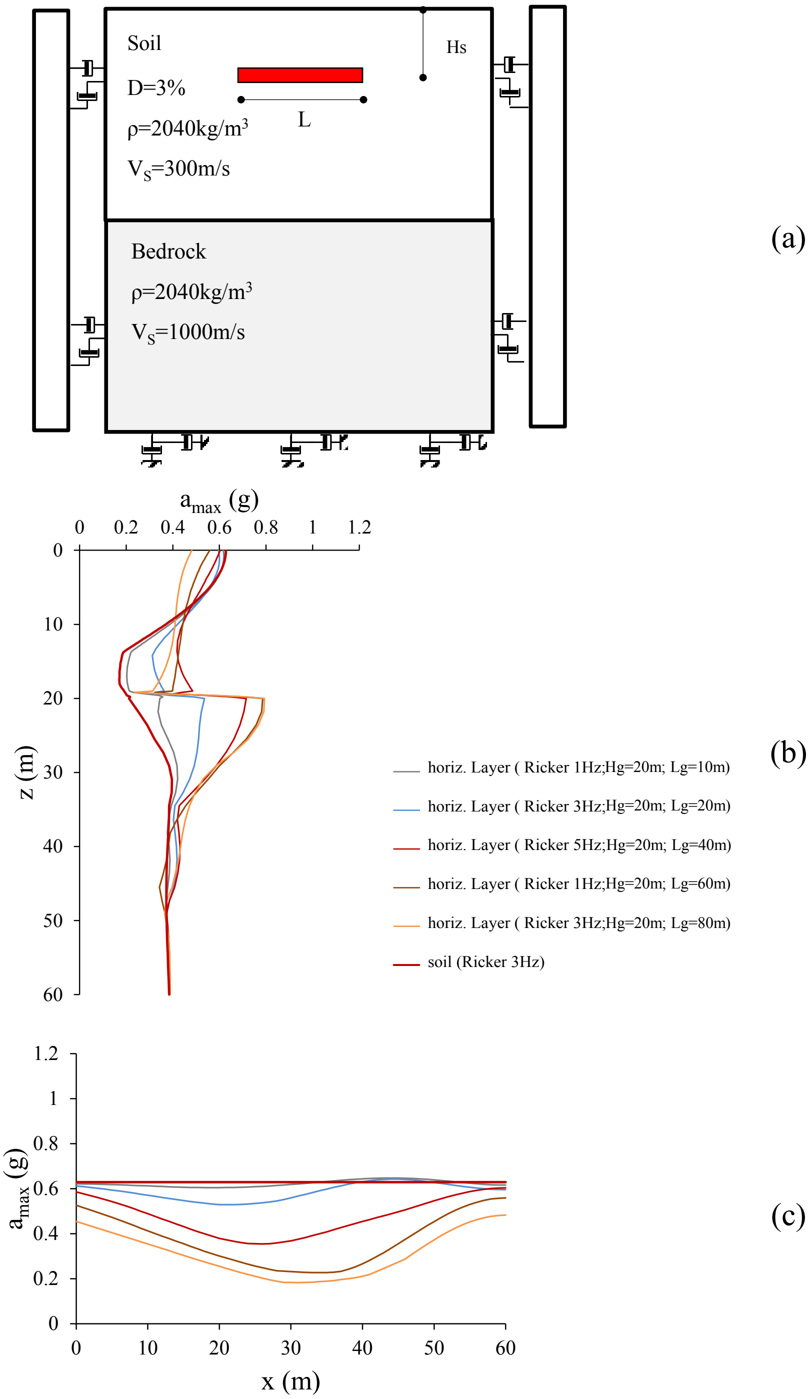

Figure 2.3.2.4.3 *Geometrical features of the model used for the progressive enlargement of the horizontal layer (a); maximum horizontal accelerations with depth (b) and at ground surface (c).*

2.3.2.5 Finite length double vertical layers

Another possible scheme to isolate seismic signals may be the installation of vertical and soft diaphragms next to the foundation of the building to be protected, in order to aim at isolating a soil mass underneath the foundation and the superstructure, and reduce the induced ground shaking and allow independent oscillation from the surrounding soil (Kirtas, 2009).

The seismic response of the system is determined by the dynamic characteristics of the isolated soil mass. The most efficient isolated soil depth (D_d), after preliminary investigation of several configurations, was selected by Kirtas (2009) equal to $D_d = 5B_d/3$, where $2B_d$ is the distance between the two vertical soft layers which define the lateral boundaries of the isolated soil. The elastic modulus of the diaphragms material plays an important role on the seismic response, controlling the compliance of the vertical sides during oscillation.

Figures 2.3.2.5.1 report one of the results from Kirtas (2009) which focuses his attention on a simple oscillator at ground surface simulating the presence of a structure with a rigid foundation. The superstructure acceleration ratio (i.e. the ratio of the Fourier transform of the response time-histories of the simple oscillator at ground surface in the modified system to the corresponding response of the initial unmodified system), in the case of the soft diaphragms, presents a wide range of values lower than unity near the fundamental effective period of the structure, indicating an efficient mitigation of the seismic response (Figures 2.3.2.5.1). The efficiency of the intervention increases by increasing the structural mass in both time and frequency domains. Because of the high flexibility of the implemented intervention compared to the initial foundation subsoil conditions, it is reasonable to expect an increase of the seismic displacements of the system; Kirtas (2009) indicates the possibility of either increased or reduced displacements, depending on the frequency content of the imposed seismic motion.

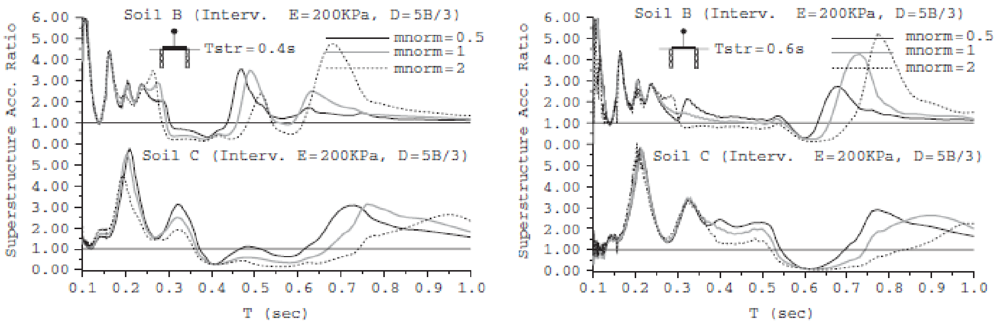

(a) (b)

Figure 2.3.2.5.1 *Soft diaphragms: superstructure acceleration ratios for T_{str}=0.4s (a) and T_{str}=0.6s (b).*

Figures 2.3.2.5.2 show a scheme where attention is focused on defending the ground surface from shaking due to the propagation of Ricker wavelets with an initial amplitude of 0.5g. The area to be protected is 40m large; diaphragms are made of a soft material ($V_{s,g}$=20m/s; ν_g=0.3; ρ_g=2040kg/m^3) and are 20m long. Results shown in Figures 2.3.2.5.2 demonstrate that the presence of two vertical soft layers could not be effective in any case, as reported in Kirtas (2009).

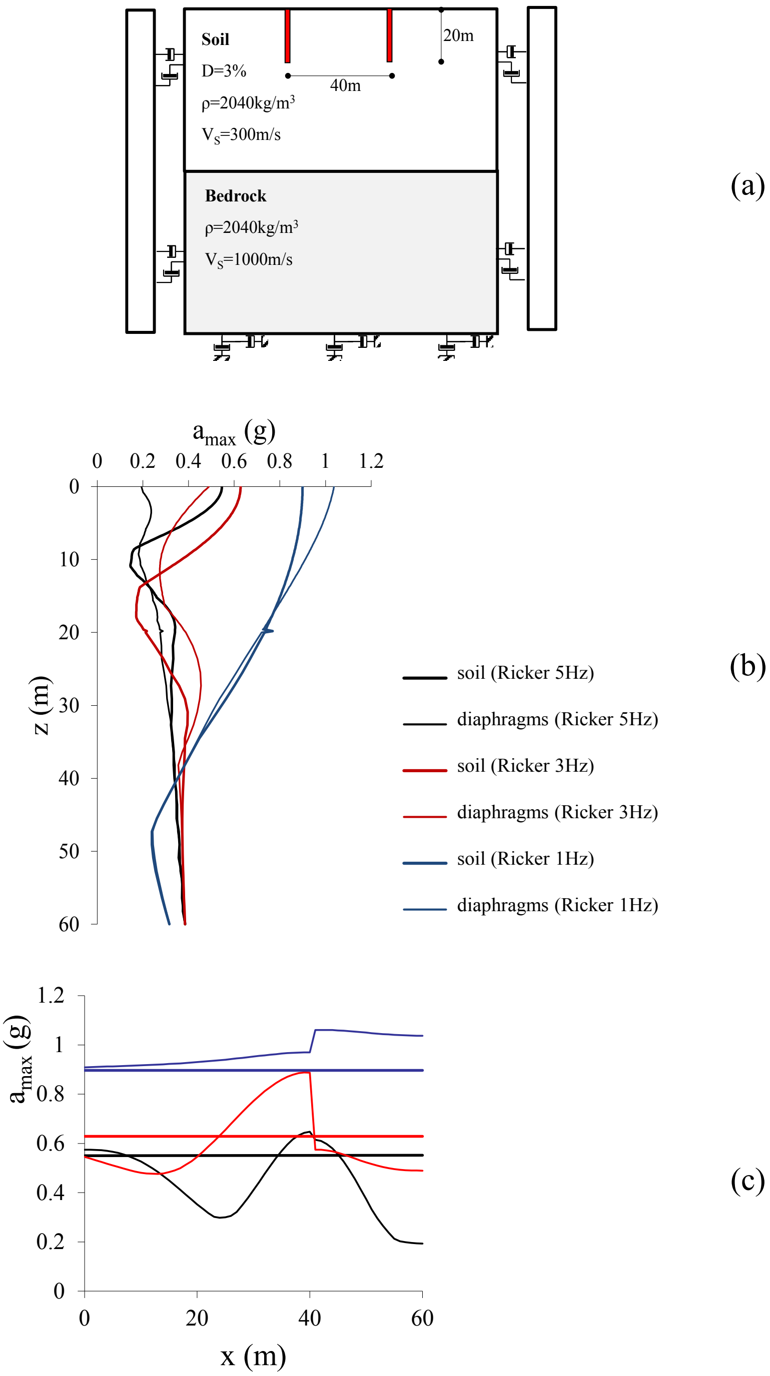

Figure 2.3.2.5.2 *Geometrical configuration for the diaphragms model (a); maximum accelerations with depth (b) and at ground surface from the right side of the geometry to the symmetry axis at the middle of the mesh (c), by varying the frequency of the signal.*

The analyses reported in this and the other paragraphs seem to indicate that vertical diaphragms and horizontal layers, if correctly assembled from a geometrical and mechanical point of view, may be able to tackle out the energy transmitted to the ground surface by the propagation of a dynamic signal. Therefore, in the following paragraphs different schemes will be introduced, where an entire soil area underneath the structure to protect is enclosed by systems made of horizontal and vertical soft layers and inclined injections.

2.3.3. Soft Caisson: rectangular section

The combination of the two lateral soft vertical diaphragms with a horizontal soft layer can form a complete seismic isolation configuration around the zone at ground surface to be protected. Figures 3.3.1 describe the geometrical configuration adopted for examining this typology of treatment scheme: the soft caisson is made of two vertical layers and a horizontal one embedded into soil to form a soft caisson. The soil layer and the bedrock on which soil is placed have the same size, in terms of thickness and width in the plane, and in the following reported analyses both cases with possible slippages at the boundary between soft layers and soil and case where analyses are exclusively linear elastic have been considered.

Results are generally reported referring to:

- a point at ground surface at the centre of the soft caisson (CP) (see Figure 2.3.3.1b)
- a section called "central vertical" (see Figure 2.3.3.2)
- a reference system whose axes are shown in Figure 2.3.3.2.

In this chapter, observations are reported by taking in account different configurations of the soft caisson, considering:

1. the effects of the variation of the dynamic impedance ratio by varying the shear wave velocity of the soft layers;
2. the effects of the variation of the dynamic impedance ratio on the soft caisson performance;
3. the effects of the variation of the soil deposit depth;
4. the effects of the variation of the lateral soft layers length;
5. the effects of the variation of a load on ground surface;
6. the effects of the variation of the dimension of the soft caisson;
7. the effects of the variation of the soft layers thickness;
8. the effects of the variation of the soft layers damping ratio;
9. the effects of the variation of the soft layers volumetric stiffness;
10. the effects of the constitutive model on the efficiency of the isolating box.

The following subparagraphs report the results, following the above reported order. In these sections, the thickness of the soft layers has been assumed equal to 1m, with the exception of the 7th subparagraph where the effects of the soft layer thickness is studied. In the performed analyses, the material behaviour is generally assumed as linear-elastic, with the exception of the 10th subparagraph, where the failure condition effects are considered.

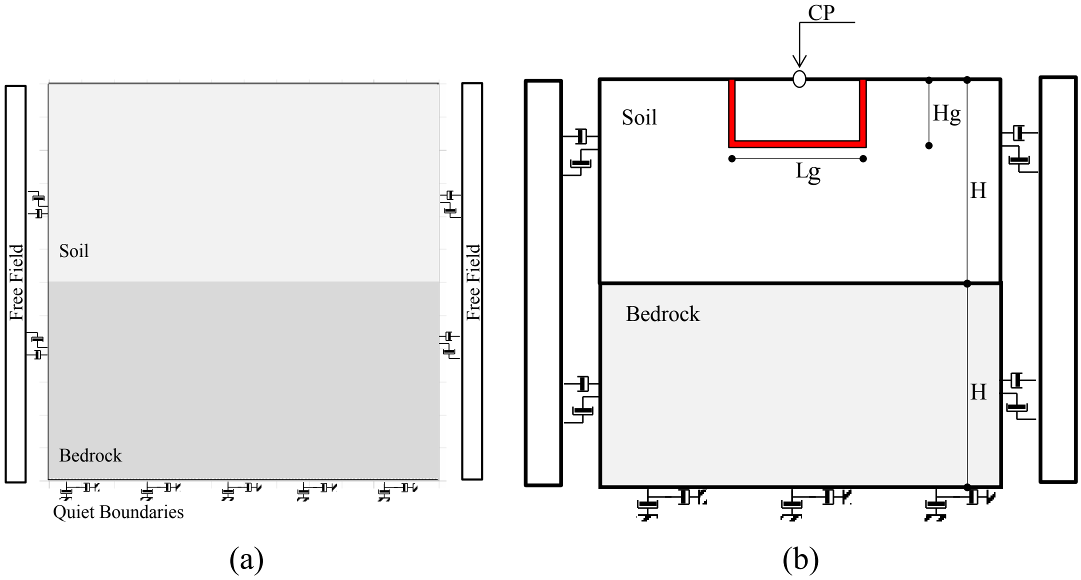

Figure 2.3.3.1 *Geometrical configuration and model for the 2D analyses on soft caisson: an example of mesh used for analyses (a); indications on the boundary conditions and on the position of the Control Point, CP (b).*

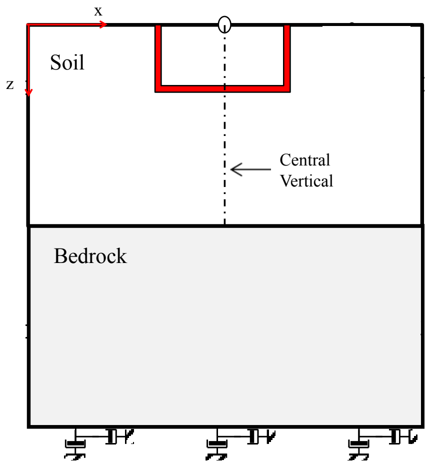

Figure 2.3.3.2 *Indications on the reference system and the central vertical position.*

2.3.3.1 Effects of the variation of the dynamic impedance ratio by varying shear wave velocity of the soft layers

The first scheme has been examined in order to understand the importance of the variation of the dynamic impedance ratio α on the propagation of waves. In these analyses, different Ricker wavelets with maximum amplitude of 0.5g and a fundamental frequency from 0.1Hz to 5 Hz have been propagated upward as shear waves SV, starting from the lower boundary of the bedrock to the ground surface. It has been assumed a model where (see Figure 2.3.3.1)

H_g=20m, L_g=40m, the width of the entire mesh, equal to the depth both H of the soil layer and the bedrock, is 120m, the shear wave velocity of the soil layer and of the bedrock is assumed respectively equal to $V_{s,s}$=300m/s and $V_{s,b}$=1000m/s, with a density ρ_s of 2040kg/m^3.

In this first kind of model configuration, the shear wave velocity of the layers composing the soft caisson has been varied from 10 to 20 and 30m/s, assuming a density ρ_g of 1020kg/m^3. Consequently, the dynamic impedance ratio α assumes values 60, 30 and 20 (see Table 2.3.3.1.1).

Natural Soil		Grouted System		
$V_{s,s}$ (m/s)	ρ_s (kg/m^3)	$V_{s,g}$ (m/s)	ρ_g (kg/m^3)	α
300	2040	10	1020	60
		20		30
		30		20

Table 2.3.3.1.1 *Values of the dynamic impedance ratio.*

Figures 3.1.1.1 report the maximum horizontal accelerations a_{max} (see Figure 2.3.1.1.1 a) and the values of spectral intensity SI (see Figure 2.3.1.1.1 b) in the control point by varying the fundamental frequency of the signal. In these figures, the black thicker line refers to the case of no treatment (only soil); so, it is the reference result, to which it is necessary to compare the other one to check if the soft caisson has a beneficial effect (reduction of a_{max} and SI) or not. The finer lines results refer to the different soft caissons. An important reduction in signal effects is observed in CP when the frequency of the signal is larger than 2Hz; for such cases, all treatments are useful in reducing maximum accelerations and SI values. For lower frequencies, a worse response is observed, with the exception of the model with $V_{s,g}$=10m/s, for which treatment is beneficial also for f=1Hz. The propagation of the signal characterized by the lowest frequency (f=0.1Hz) does not seem to be influenced by the introduction of the grouts. This is probably due to the extreme slowness of the propagated wave; so the mesh has been deformed for all his extension with the same amplitude, without an important contribution on the deformability of the soft layers.

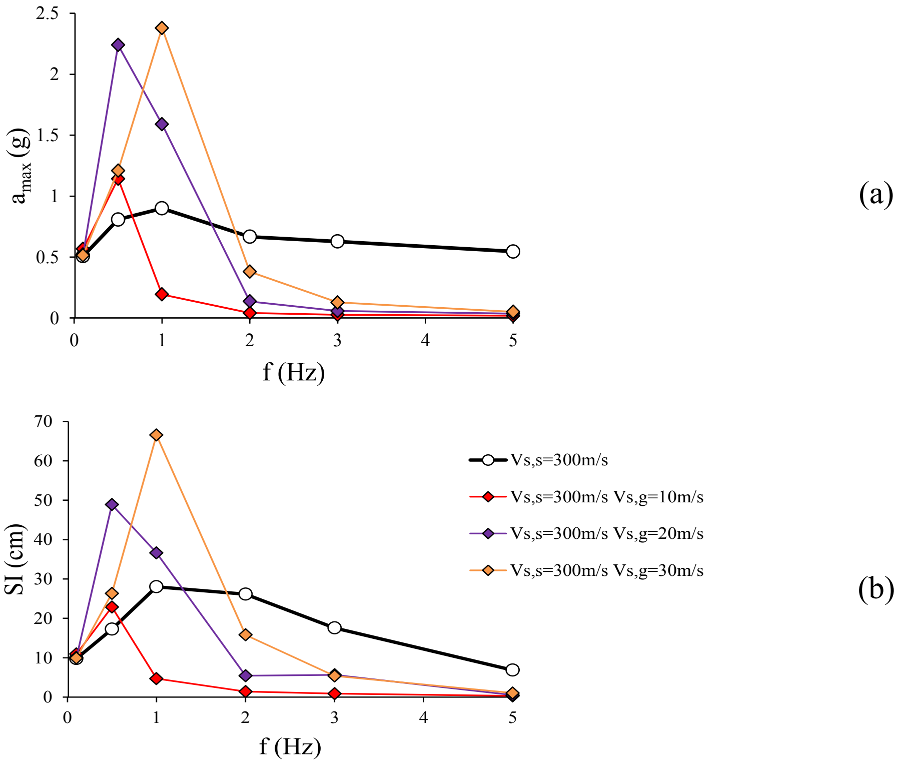

Figure 2.3.3.1.1 *Maximum horizontal acceleration* a_{max} *(a) and spectral intensity SI (b) by varying the fundamental frequency of the Ricker wavelets and assuming different values of the soft layers* $V_{s,g}$.

In Figure 2.3.3.1.2a, the amplification ratio is reported. In this case, this function quantifies the variation in Fourier amplitude from the ground level to the base of the soil layer. The ticker line indicates the amplification ratio in the natural soil; it is totally coherent with literature indications (Kramer, 1996), where the natural frequencies of a soil deposit with a certain shear stiffness, placed on a bedrock either deformable or indeformable, comes from the following expression:

$$f_n = \frac{(2 \cdot n - 1) \cdot V_S}{4 \cdot H} \qquad n = 1, \ldots, \infty \tag{2.3.3.1}$$

Consequently, the first natural frequency of the soil deposit is 1.25Hz.

If the red line, showing results of $V_{s,g}$=20m/s, is considered, it is clear that the amplifications are expected in a range of frequencies close to 0.5Hz and 1Hz. Actually, looking at the results in terms of maximum acceleration and spectral intensity (see Figure 2.3.3.1.1), amplifications are clearly observed at the same frequencies, i.e. the deposit has resonance phenomena when a signal with such frequencies are propagated through layers.

Similar observations can be made also for $V_{s,g}$=10m/s or 30m/s; when resonance phenomena between the natural frequencies of the modified soil layer deposit and the signal occur, amplification is observed.

In Figure 2.3.3.1.2a, the amplification ratio is reported as a synthetic parameter describing the effect variations between the ground surface and the deposit base; in Figures 2.3.3.1.2 from b to d, comparisons between the amplification ratios, by varying the soft layers shear wave velocity $V_{s,g,}$ are reported, by referring the calculated function to different depths into soil.

In fact, this function has been also calculated between the ground level in the control point and the upper side of the horizontal soft layer, A(0-19m).

The two different methods to describe the variations in energy distribution of the signal define a similar behaviour of the system when subjected to a wave propagation.

The function A(0-19) seems to be more effective in identifying the resonance frequencies (for $V_{s,g}$=20m/s, for instance, the resonance phenomenon is distinctly defined for slower signal frequencies; see Figure 2.3.3.1.2c).

The soft caisson has the effect of reducing the natural frequencies of the soil included in it. Therefore, lower frequencies are amplified and larger ones reduced. Based on these first results, it is obvious that the soft caisson must be designed taking into account also the natural frequency of the structure to be protected.

The observations on amplification ratios are totally confirmed by Figures 2.3.3.1.3 and 2.3.3.1.4, in which the maximum accelerations and displacements along the vertical symmetry axis and at ground surface from the left boundary to the centre of the mesh are reported. As far as accelerations are concerned, the maximum observed values are consistent with the peaks of the amplification ratio (see Figure 2.3.3.1.2). Observing results in terms of acceleration at ground surface, when the soft caisson (see Figure 2.3.3.1.3 f - h) produces a reduction in the effects (see Figure 2.3.3.1.3e), a reduction inside the area to be protected (from 40m to 60m on the x-axis) is observed along with an increase in effects outside the isolating box. This is due to the reflecting effect of the waves impacting the lateral soft screen, which are reflected back. When this kind of mitigation system does not reduce the effects in the zone to be protected, on the contrary, no significant increase of the accelerations outside the caisson are observed. About displacements, it is not generally observed an increase in horizontal displacements with respect to the condition of absence of any treatment (see Figures 2.3.3.1.3 e-h and Figures 2.3.3.1.4 e-h). It is also interesting to observe that the beneficial screening effect in terms of acceleration, in the case where it takes place, does not necessarily correspond to an increase in displacements in the soil within the soft caisson.

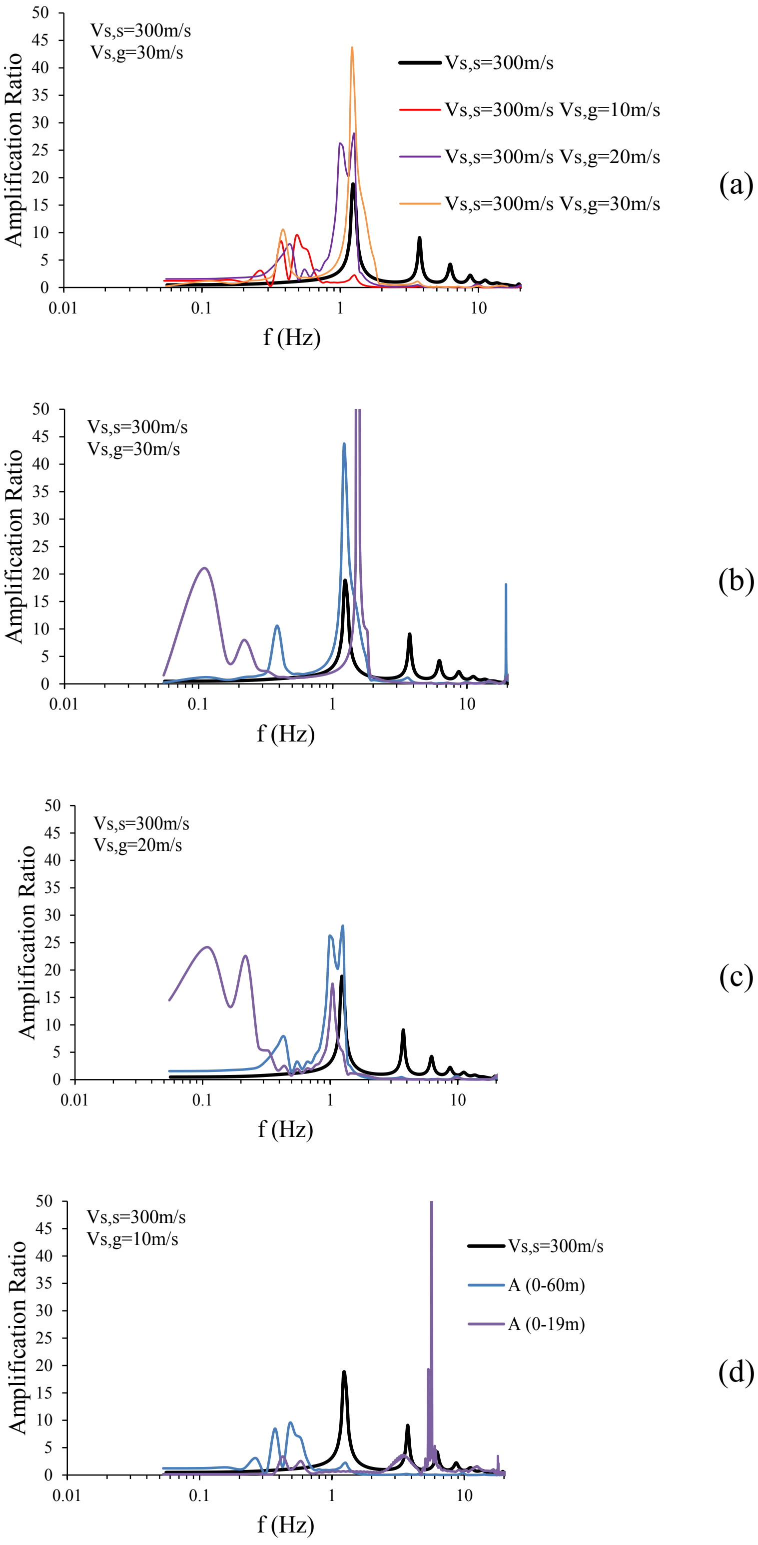

Figure 2.3.3.1.2 *Amplification ratios by varying* $V_{s,g}$ *between the ground surface and the deposit base (a); comparisons between the amplification ratios A(0-60m) and A(0-19m) by varying* $V_{s,g}$ *(b, c, d).*

This depends on both the fundamental frequency of the propagated signal and the shear stiffness of the soft layers, especially when the treatment works well. For the lowest value of $V_{s,g}$, actually, both accelerations and displacements are reduced within the soft caisson.

In order to visually explain the amplitude and duration changes of a signal transmitted from the base of the deposit to the surface, in Figures 2.3.3.1.5, signals at different depths from the ground level, along the vertical at the centre of the mesh, are depicted, by propagating a Ricker wavelet through a model both without any treatment (a) and with a soft caisson having $V_{s,g}$=10m/s (b), for two different frequencies (1Hz, a and b; 3Hz, c and d). Signals are clearly and sharply modified in amplitude by impacting the softer layer. In the case of a Ricker fundamental frequency equal to 1Hz, it is observed an increase in the duration of the signal at ground surface (see Figure 2.3.3.1.5 b), amplified with respect to the reference condition (see Figure 2.3.3.1.5 a).

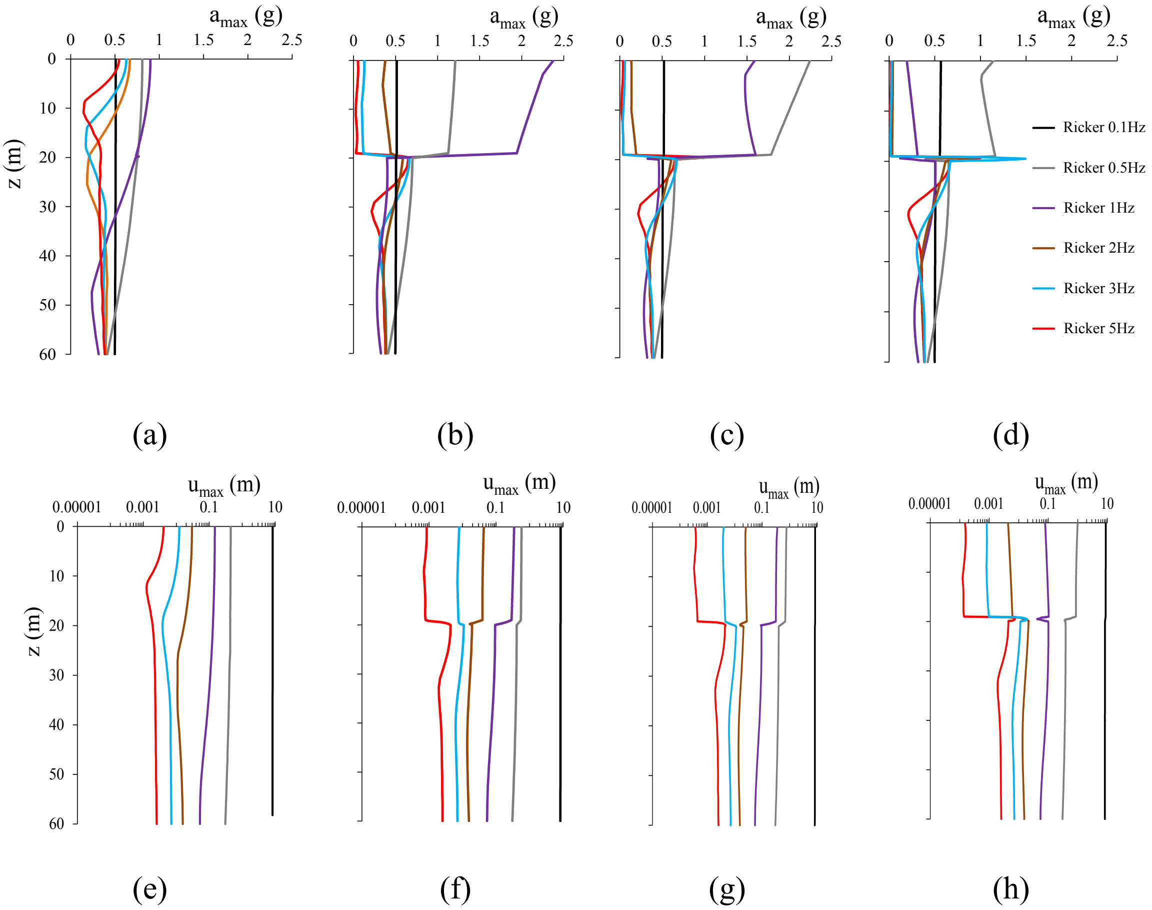

Figure 2.3.3.1.3 *Maximum horizontal accelerations with depth by varying the fundamental frequency of the Ricker wavelets in the case of no treatment (a) and for soft layers having $V_{s,g}$ equal to 30m/s (b), 20m/s (c) and 30m/s (d); maximum horizontal displacements with depth by varying the fundamental frequency of the Ricker wavelets in the case of no treatment (e) and for soft layers having $V_{s,g}$ equal to 30m/s (f), 20m/s (g) and 30m/s (h).*

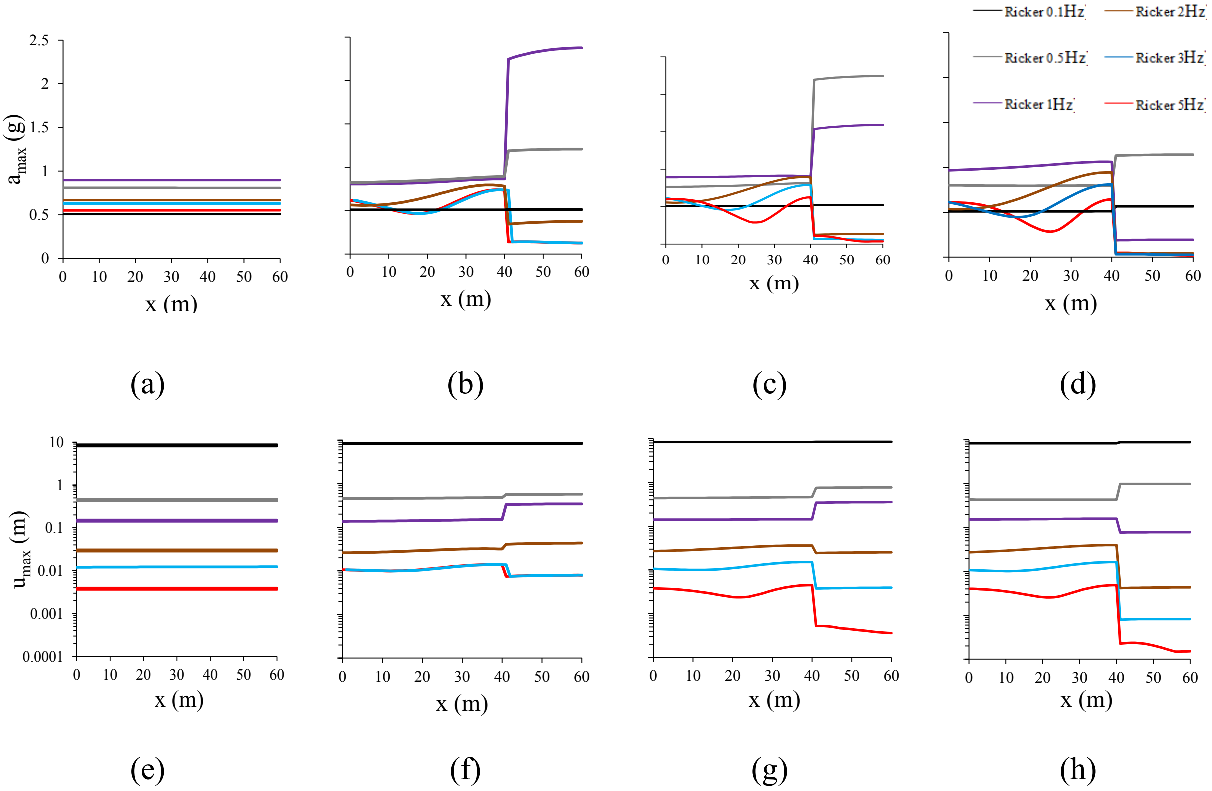

Figure 2.3.3.1.4 *Maximum horizontal accelerations at ground surface from the left boundary to the centre of the geometrical configuration by varying the fundamental frequency of the Ricker wavelets in the case of no treatment (a) and for soft layers having* $V_{s,g}$ *equal to 30m/s (b), 20m/s (c) and 30m/s (d); maximum horizontal displacements at ground surface from the left boundary to the centre of the geometrical configuration by varying the fundamental frequency of the Ricker wavelets in the case of no treatment (e) and for soft layer having* $V_{s,g}$ *equal to 30m/s (f), 20m/s (g) and 30m/s (h).*

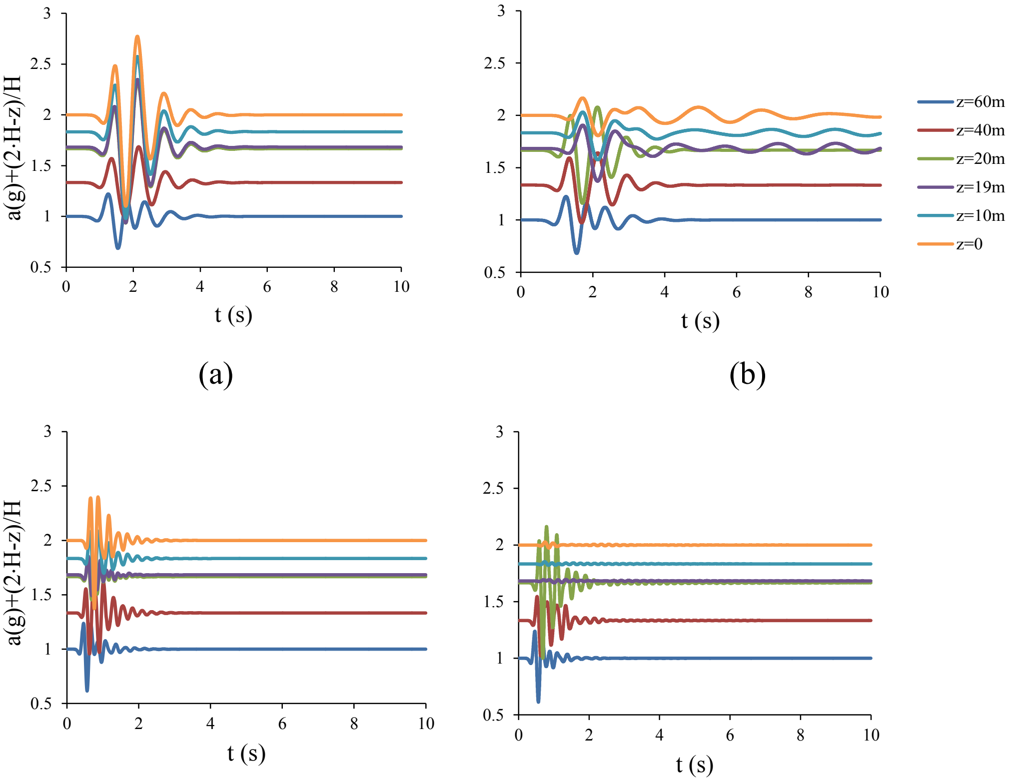

(a) (b)

(c) (d)

Figure 2.3.3.1.5 *Signals at different depths along the central vertical of the model starting from free surface: by propagating a 1Hz Ricker wavelet through a model without (a) and with a soft caisson having $V_{s,g}$=10m/s (b); by propagating a 3Hz Ricker wavelet through a model without (c) and with a soft caisson having $V_{s,g}$=10m/s (d).*

In Figures 3.3.1.6, the effects of the propagation of a 1Hz Ricker wavelet are reported in terms of the Fourier amplitude of the signals calculated at different depths along the central vertical axis of the model, for a soil deposit without and with a soft caisson having $V_{s,g}$=10m/s. The peaks of the signal over the soft layer decrease in amplitude and are shifted to lower frequencies. It is then confirmed that the maximum detrimental effects will be for structures to be protected having higher natural periods. This is confirmed by looking at Figures 3.3.1.6, in which acceleration spectra for signals at different depths for soil without and with soft layers ($V_{s,g}$ =10m/s) are reported. With respect to the reference condition (see Figure 2.3.3.1.6c), the maximum acceleration of the simple oscillator is reduced by including the soft layers. The spectra also point out that the peaks are not only reduced, but also shifted towards higher periods. Again, the soft caisson seems better suited for squat buildings, having lower natural frequencies.

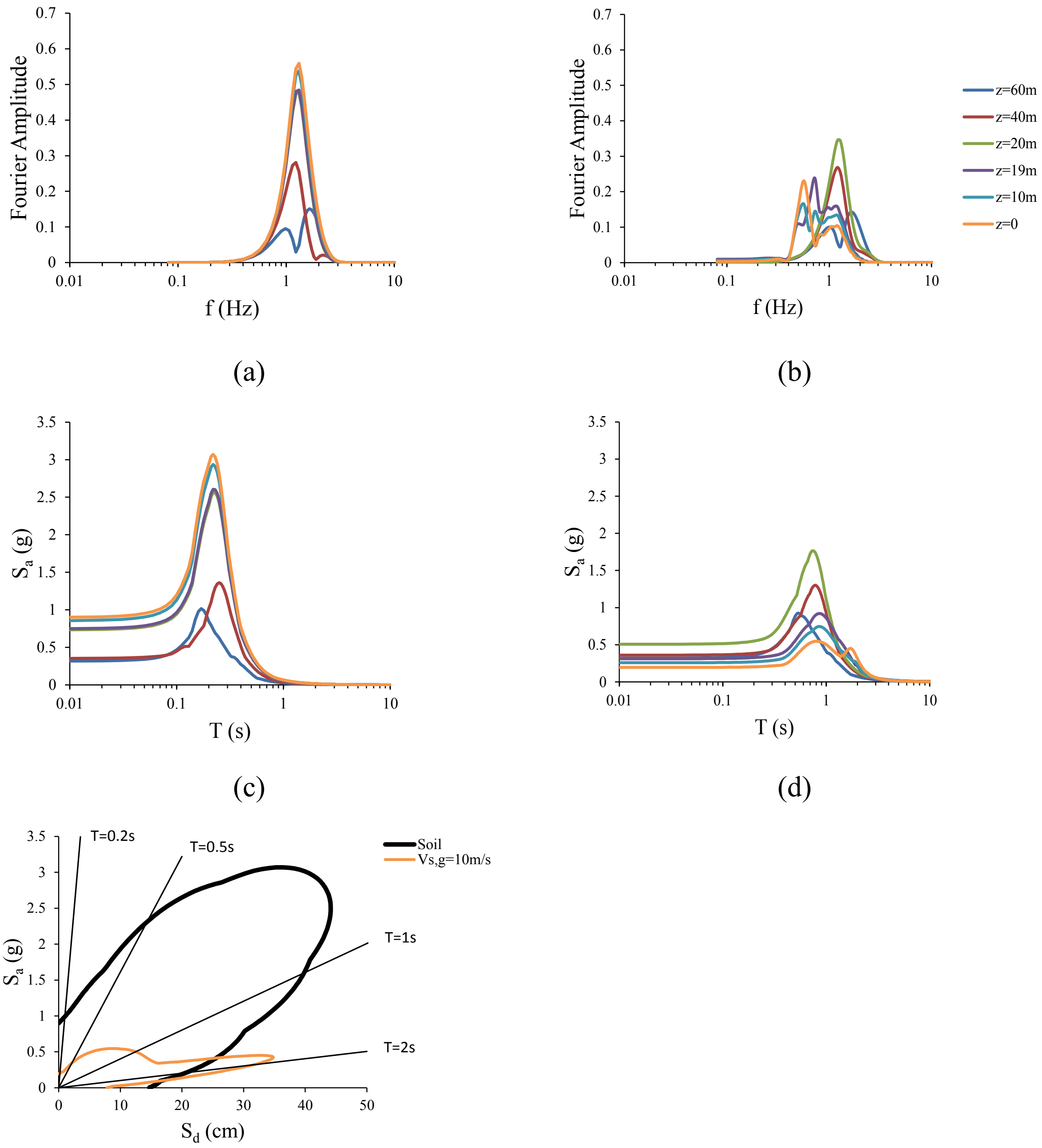

(a) (b)

(c) (d)

(e)

Figure 2.3.3.1.6 *Effects of the propagation of a 1Hz Ricker wavelet: Fourier amplitude for signals at different depths along the central vertical axis for soil without (a) and with a soft caisson having $V_{s,g}$=10m/s (b); acceleration spectrum for signals at different depths for soil without (c) and with a soft caisson having $V_{s,g}$=10m/s (d); variation of the acceleration and of the displacement spectra in the control point due to a soft caisson having $V_{s,g}$=10m/s.*

Figure 2.3.3.1.6e reports the effects of the soft caisson in terms of S_d-S_a domain; a large reduction is clearly observed in terms of both spectral acceleration and displacement, with a rotation of the response domain to higher periods. This domain is shrunken for lower SDOF periods and lengthened for higher ones.

From this first example, it is clear that the isolating box is able to cut off energy from the system when it modifies the entire way in which signals are propagated, avoiding phenomena of resonance. For soft layers with $V_{s,g}$ equal both to 20m/s and 30m/s, a signal with a fundamental frequency of 1Hz, for example, determines a resonance phenomenon (see Figure 2.3.3.1.2), whereas for $V_{s,g}$=10m/s this occurrence is avoided. It is possible to have a view of this topic by observing either Figure 2.3.3.1.7 or 2.3.3.1.8. In figures 2.3.3.1.7, signals at different position at ground level are reported. These signals have been calculated by propagating a 1Hz Ricker wavelet through a model with a soft caisson with $V_{s,g}$ = 30m/s (b), $V_{s,g}$ = 20m/s (b) and $V_{s,g}$ = 10m/s (c). Differences in terms of effects of the soft layers on the signal approaching the boundary of the soft caisson are clearly observed. Only for the lower impedance ratio, a decrease in acceleration with time is observed.

For $V_{s,g}$=30m/s and 20m/s, increases in the maximum amplitude of the signal and in the time duration are observed; these phenomena are probably due to the multiple reflection of the signal reflected from the surface on the lateral and the inferior boundaries of the caisson and are amplified by the important amount of energy transmitted to the ground level. In these cases, the soft caisson has a negative, amplifying effect.

Similar oservations can be done by observing the efficiency curves too (see Figures 2.3.3.1.8); actually values of the efficiency E_l by varying the soft layers shear wave velocity are effective in showing the changes with respect to the variation of the period of the simple oscillator. For $V_{s,g}$=10m/s, with the exception of the signals having lower frequencies, E_l is higher than 0.5 for all periods. Generally speaking, structures with a natural period lower than 0.2s take advantage of the soft caisson for all the geometrical and mechanical properties investigated in these first analyses. It is expected that other treatment geometrical configurations may have different effects.

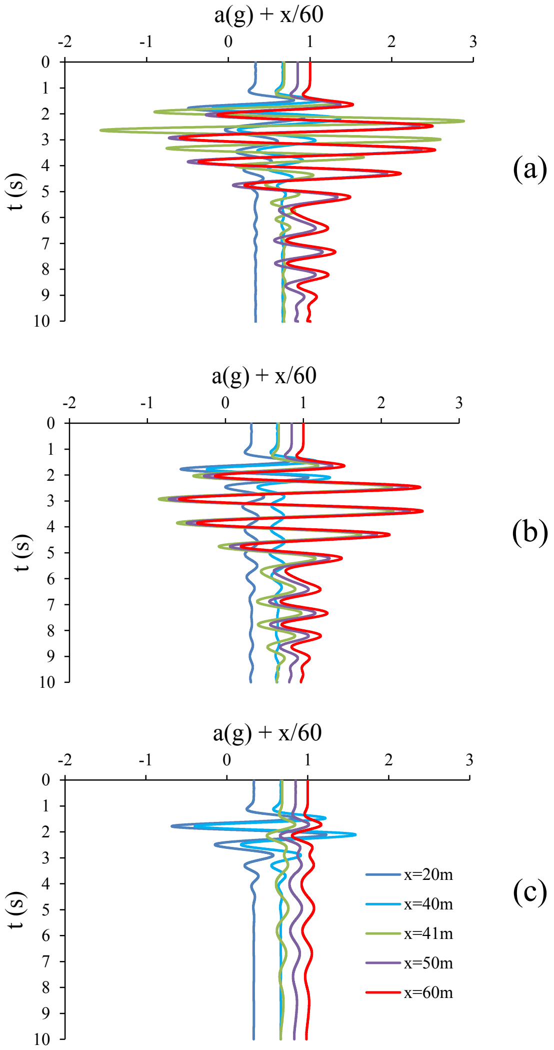

Figure 2.3.3.1.7 *Signals at different position at ground level by propagating a 1Hz Ricker wavelet through a model with a soft caisson having* $V_{s,g}$ *= 30m/s (b),* $V_{s,g}$ *= 20m/s (b) and* $V_{s,g}$*=10m/s (c).*

Figures 2.3.3.1.9 report the ratios between the values of the predominant periods, $T_{p,g}$ and $T_{p,s}$, as well as the ratios between the mean periods, $T_{m,g}$ and $T_{m,s}$. As usual in this thesis, the pedex “s” indicates the soil deposit with no treatment, and the pedex “g” indicates the case with treatment. Figure 2.3.3.1.9b clearly shows that, when grouts are able to positively modify the signal effects in the control point, the main period is shifted to higher values with respect to the previous ones. This seems to confirm 1D analyses.

The shift towards higher periods, when the treatment seem to be helpful in reducing dynamic effects at ground surface, is evident also in Figure 3.3.1.10 c and d, where acceleration spectra for $V_{s,g}$ equal to 20m/s and $V_{s,s}$=300m/s are reported and compared to the case of no treatment, for the case of a frequency of 5Hz. When the soft caisson is not effective, for instance for 1Hz, there is also no shift in periods (see Figures 2.3.3.1.10 a and b).

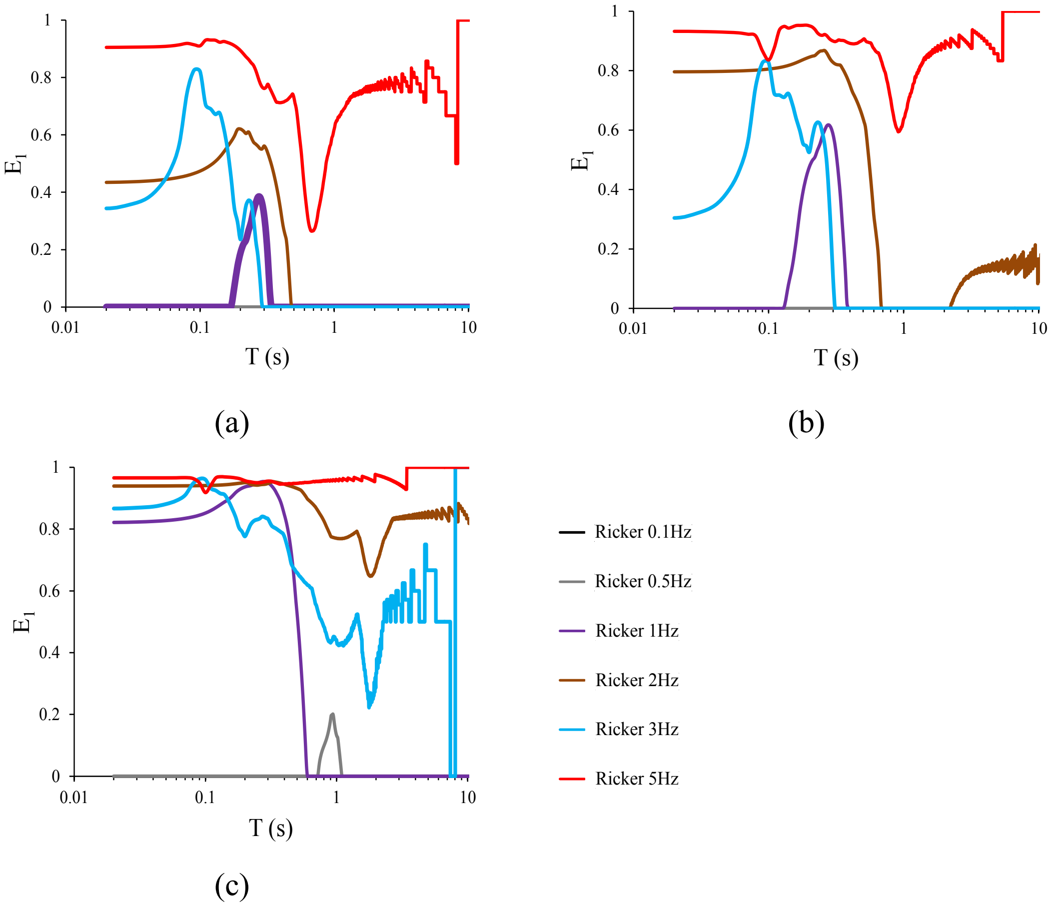

(a) (b)

(c)

Figure 2.3.3.1.8 *Values of the efficiency E_1 by varying the soft layers velocity, equal, respectively, to 30m/s (a), 20m/s (b) and 10m/s (c).*

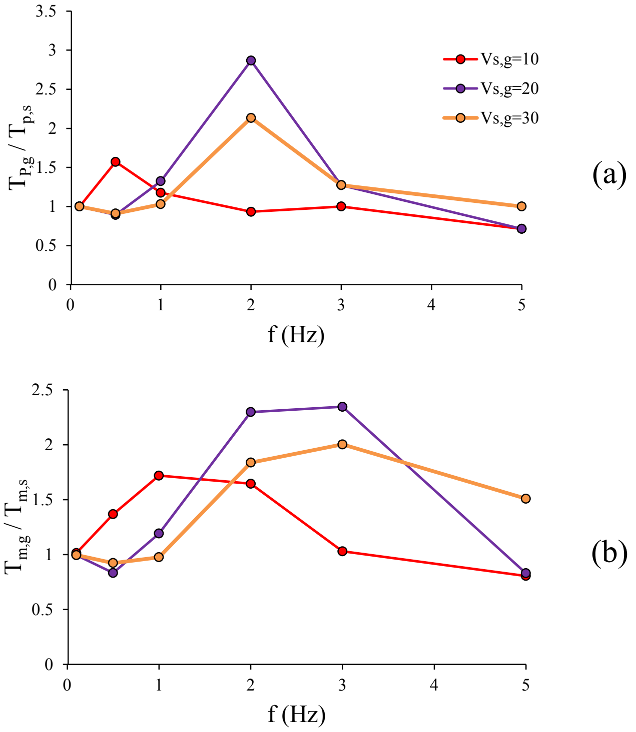

Figure 2.3.3.1.9 *Values of the ratios in terms of predominant periods, $T_{p,g}/T_{p,s}$ (a) and mean periods, $T_{m,g}/T_{m,s}$ (b) in the control point.*

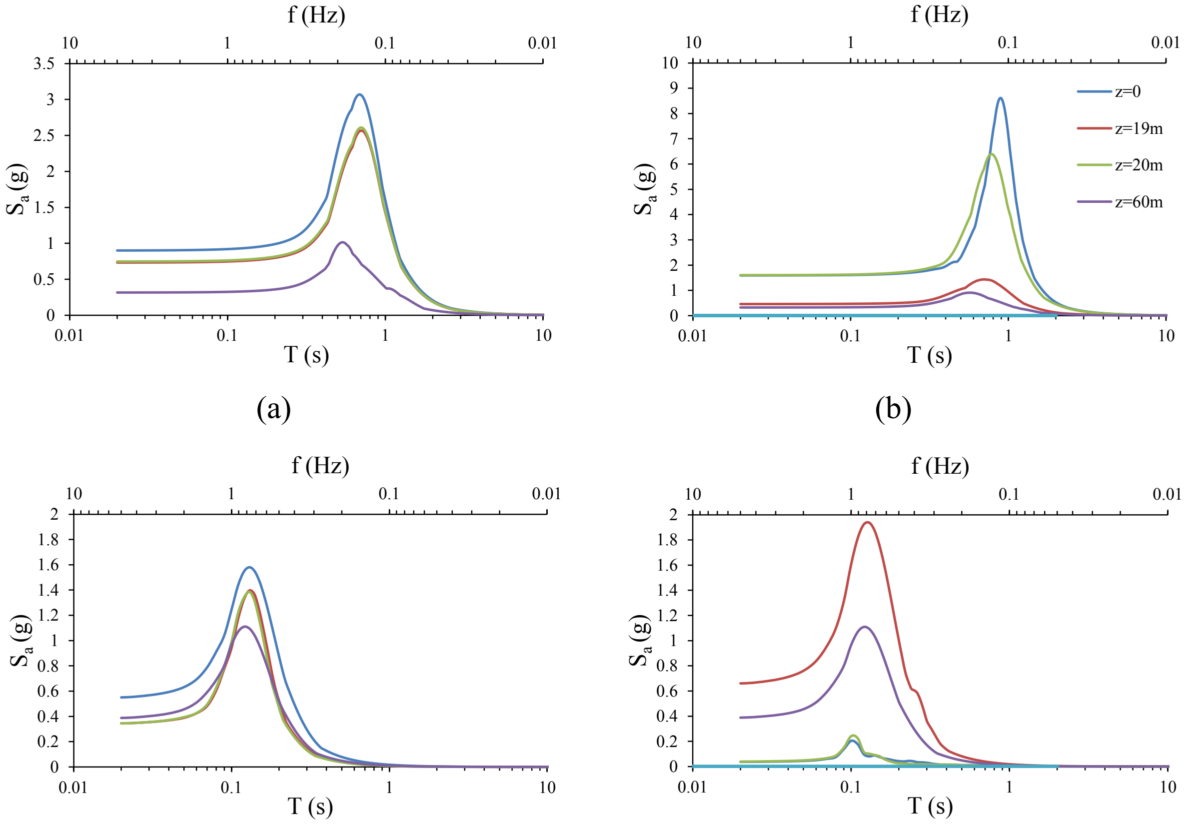

(a) (b) (c) (d)

Figure 2.3.3.1.10 *Acceleration spectra at different depths along the central vertical axis in the case of no treatment and f=1Hz (a) or 5Hz (c), and in the case of soft caisson with* $V_{s,g}$*=20m/s and f=1Hz (b) or 5Hz (d).*

In the previous plots, the horizontal effects in terms of accelerations and displacements have been considered, but the proposed seismic mitigation system may induce further effects in the vertical direction, which are not present in a scheme where the deposit has not been treated. The interaction of the wavefront with the boundaries of the soft caisson could be significant in generating secondary wavefronts whose effects on ground surface, for instance, could be unexpected. The interference takes place because there is an extremely complex interaction among the waves coming from the boundaries of the soft layers, the base of the model and the inside of the soft caisson. These interactions are governed by the principle of superposition, i.e. when waves interact, the resulting wave function is the sum of the individual wave functions (Born and Wolf, 1959). In Figures 2.3.3.1.11 and 2.3.3.1.12, the effects at ground surface in terms of horizontal and vertical accelerations for a model in which the soft isolating box has a shear wave velocity of the layers equal to 20m/s are reported for different Ricker wavelets. The figures clearly show that the soft caisson has the negative effect of causing vertical accelerations at ground level, obviously not observed in the case with no treatment.

When the frequency is equal to 1Hz, which implies a resonance phenomenon in the deposit, the generation, inside the caisson, of vertical accelerations of the same order of magnitude of the horizontal ones is expected. Outside the box, vertical accelerations rapidly decrease (see Figure 2.3.3.1.11).

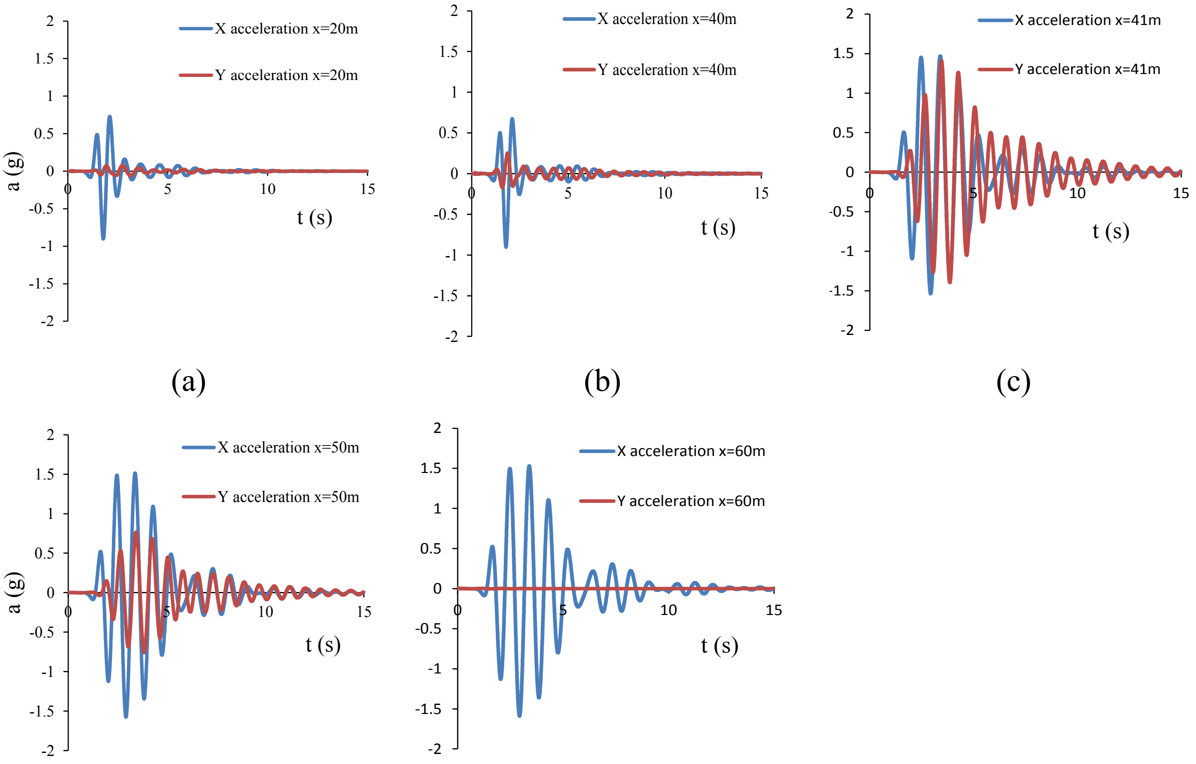

(a) (b) (c)

(d) (e)

Figure 2.3.3.1.11 *Accelerations for different positions (a - e), from the left boundary of the model, at ground surface, by propagating a Ricker wavelet with a fundamental frequency* $f = 1Hz$*, for a soft layer shear velocity* $V_{s,g} = 20m/s$.

When the propagated signal does not induce resonance of the whole system, such as for f=3Hz, significant values of vertical accelerations are relegated to the outside of the caisson (see Figure 2.3.3.1.12); in the inner part, accelerations in the two directions are extremely low, of the same order of magnitude. The system seems therefore to be able to isolate the interior part from effects in terms of accelerations both in the vertical and horizontal directions. It must be pointed out, however, that the soft barrier may increase the seismic effects immediately outside, and thus possible negative effects on buildings adjacent to the one to protect have to be considered.

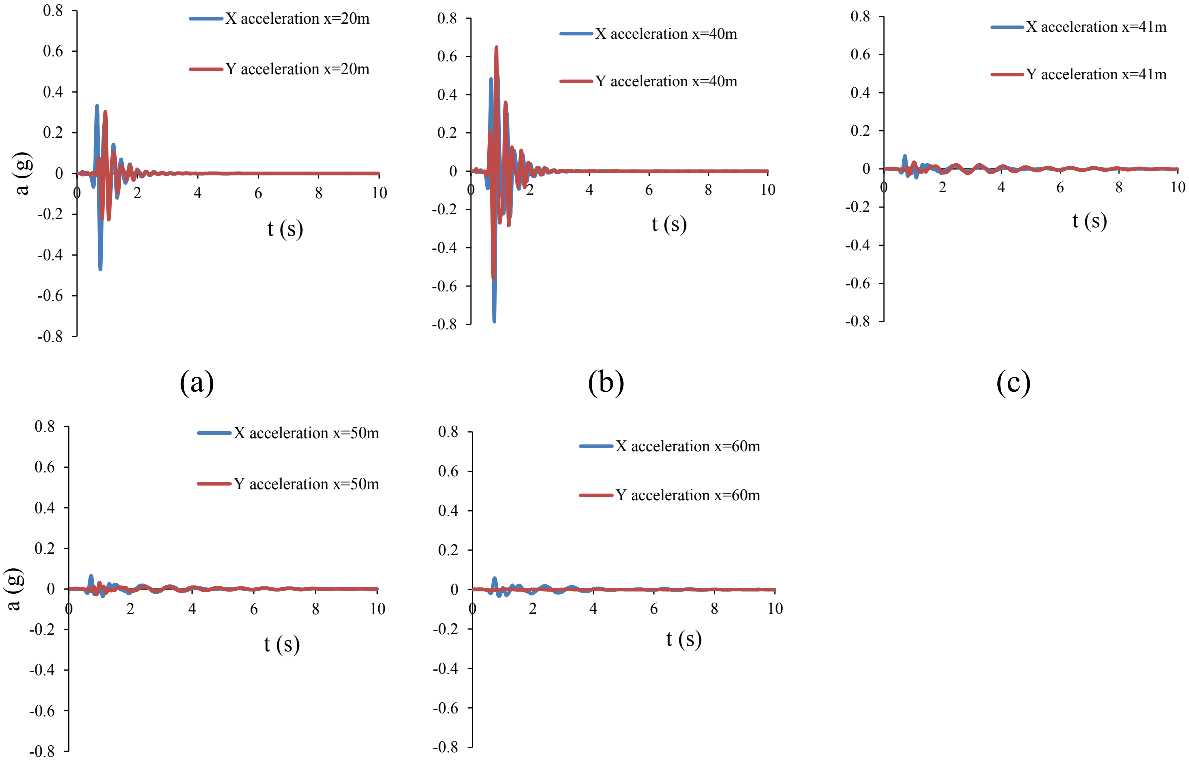

(a) (b) (c)

(d) (e)

Figure 2.3.3.1.12 *Accelerations for different positions (a - e) from the left boundary of the model at ground surface by propagating a Ricker wavelet with a fundamental frequency of 3Hz, for a soft layer shear velocity* $V_{s,g}$*= 20m/s.*

The vertical accelerations could be partially related to the calculation limits of the adopted model: when a dynamic simulation is performed with FLAC, a rotation of the model base may take place (Flac7 Manual, 2011).

Generally speaking, this rotation may happen when a dynamic loading is applied to the base of the model, when quiet boundaries or free-field conditions are imposed along the lateral boundaries.

In the performed analyses, the previously reported conditions, which may determine model base rotation, are contemporary in the model. The wave transmission through the model can produce a variation in the distribution in stresses that becomes locked-in, above all if material failure occurs. Consequently, the reaction forces along the side boundaries, calculated when the free-field boundaries were assigned at the initial equilibrium state of the model, may no longer satisfy equilibrium for the redistributed stress state in the model and so the base of the model can then start to rotate.

To prevent rotation, the depth of the model may be increased. This solution does not produce significant improvements to the quality of the numerical solutions, increasing, at the same time, the calculation duration; low vertical acceleration values are then observed at the ground level of a soil deposit with no treatment subjected to a shear wave. These accelerations are then subjected to minor errors, which do not seem depend on the propagated signals (see Figures 2.3.3.1.13).

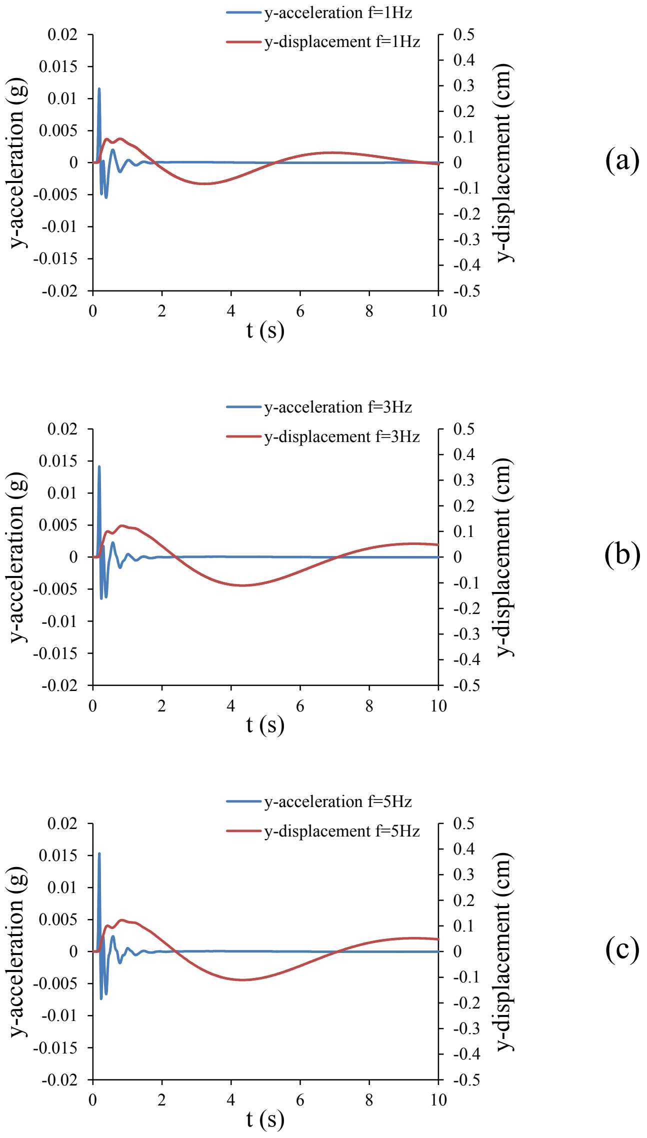

Figure 2.3.3.1.13 *Accelerations and displacements at ground surface with time due to the propagation of Ricker wavelets with fundamental frequencies of 1Hz (a) and 5Hz (b).*

2.3.3.2 Effects of the variation of the dynamic impedance ratio on the soft caisson performance

Having assumed constant values for the height of the deposit, it is interesting to see the relevance of a change in the dynamic impedance ratio caused, for example, by an increase in soil stiffness, by assuming a given geometrical configuration (see §2.3.3.1) and dynamic impedance for treated layers. In Table 2.3.3.2.1 the values of natural periods and frequencies in the hypothesis of elastic behaviour for the soil deposit without treatment has been considered (see §2.3.3):

$$T_n = \frac{4 \cdot H}{V_{s,s}} \tag{2.3.3.2.1}$$

H (m)	$V_{s,s}$ (m/s)	T_n (s)	f_n (Hz)	$V_{s,g}$ (m/s)	α
60	200	1.2	0.83	20	20
	300	0.8	1.25		30
	500	0.48	2.08		50

Table 2.3.3.2.1 *Values of the natural periods and frequencies for the soil deposit without any treatment, and impedance ratios due to the introduction of the soft layers.*

Ax expected, the natural periods T_n decreases for increasing values of soil stiffness.

If a soft caisson of $V_{s,g}$=20m/s is inserted into the soil deposit (i.e. α=30), the effects in the control point will be calculated in terms of mean periods, spectral intensities and maximum accelerations (see Figure 2.3.3.2.1), amplification ratios (see Figures 2.3.3.2.2) and compared to the case of no treatment.

First of all, the effects in terms of maximum accelerations and spectral intensities in the control point by considering the different impedance ratios are similar, with some little differences for the system responces for f=0.5Hz, 1Hz and 3Hz (see Figures 2.3.3.2.1).

The system seems to be slightly influenced by the dynamic impedance ratio between the soil and the soft grout. In terms of accelerations and spectral intensities, the "$V_{s,s}$=500m/s $V_{s,g}$=20m/s" model, which is characterized by the higher impedance ratio value, is the best in reducing the effects in the control point for f > 0.5Hz. Unexpectedly, even in this frequency range, the system behaviour does not seem to be influenced only by the variation of the impedance ratio, because the "$V_{s,s}$=200m/s $V_{s,g}$=20m/s" model, which is characterized by the lower impedance ratio value, is not the less effective in reducing the dynamic effects. This can be seen by a comparison between the effects in terms of accelerations or spectral intensities of the "$V_{s,s}$=200m/s $V_{s,g}$=20m/s" model and the "$V_{s,s}$=300m/s $V_{s,g}$=30m/s" one for f=1Hz and 3Hz: the "$V_{s,s}$=300m/s $V_{s,g}$=30m/s" model is the most ineffective.

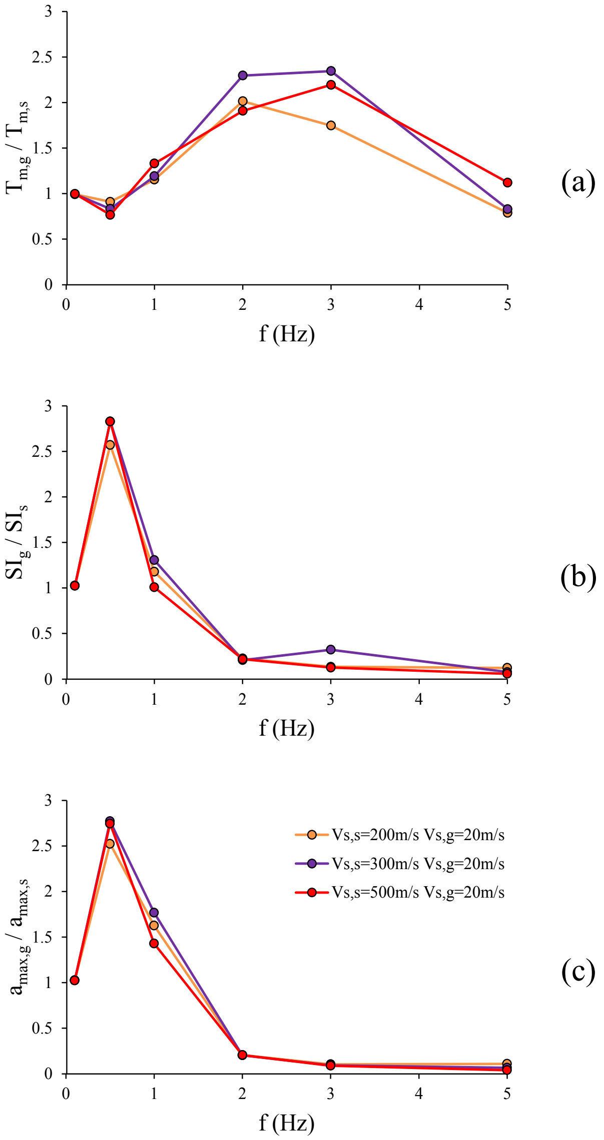

Figure 2.3.3.2.1 *Values of $T_{m,g}$ / $T_{m,s}$ (a), SI_g / SI_s(b) and $a_{max,g}$ / $a_{max,s}$(c) by varying the fundamental frequency of the Ricker wavelet and assuming $V_{s,g}$=20m/s and a soil deposit with $V_{s,s}$=300m/s.*

Figures 2.3.3.2.2 report the amplification ratios referred both to the base of the soil deposit (A(0-60m)) and to a depth equal to 19m (A(0-19m)), i.e. the upper side of the horizontal soft layer. For all the three analysed cases, the A(0-60m) profiles indicate that the introduction of different soft caissons with $V_{s,g}$=20m/s modifies the resonance frequency range, shifting the maximum response of the deposit close to f = 1Hz.

The resonance frequency of the soft caisson can be shown in the A(0-19) trend (see Figures 2.3.3.2.2). The A(0-19m) function plays a relevant role in propagating some frequencies to the ground level, because it considers the amplification phenomena due to the mechanical and geometrical properties of a given soft caisson, without taking directly into account the effects of the lateral soft layers in filtering the signals. In fact, Figures 2.3.3.2.2 show different A(0-19m) profiles for the three cases, due to the dissimilar soil and soft layer stiffnesses.

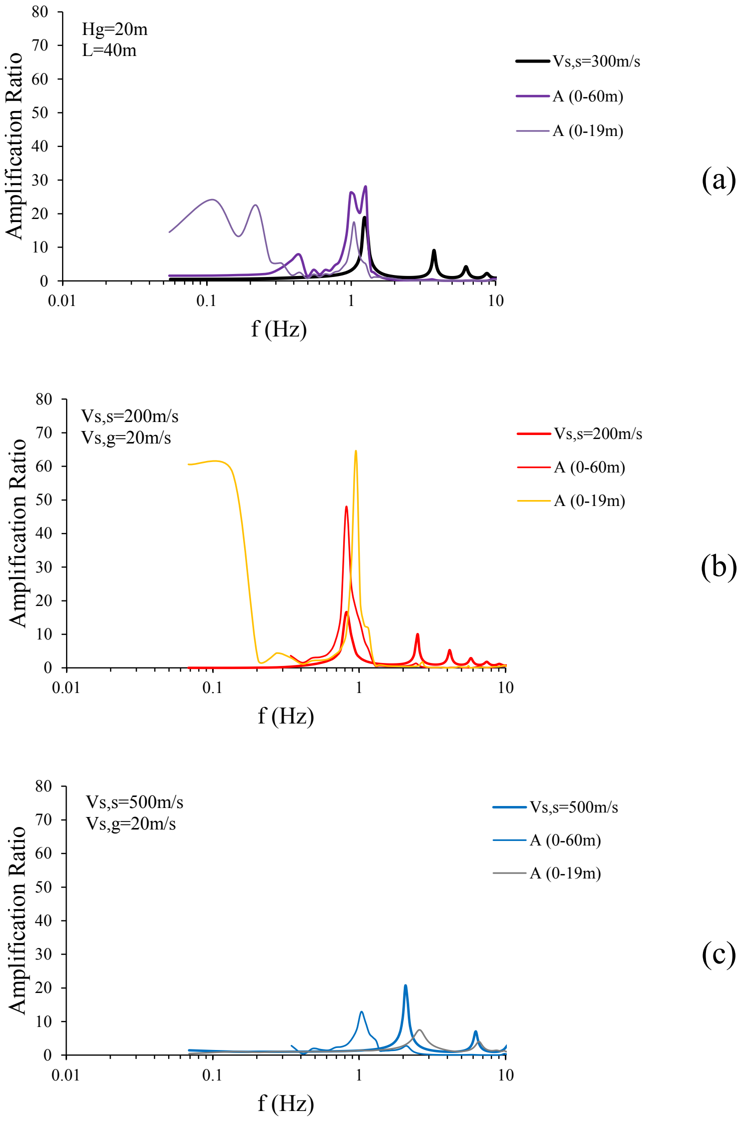

Figure 2.3.3.2.2 *Amplification ratios A(0-60m) and A(0-19m) by assuming* $V_{s,g}$*=20m/s and* $V_{s,s}$*=300m/s (a), 200m/s (b) and 500m/s (c).*

If the response of the three studied systems (see Table 2.3.3.2.1) is not largely influenced by the impedance ratio and, at the same time, resonance frequencies close to 1Hz are observed, it is expected that the absolute shear wave velocity of the soft layers plays a relevant role on the soft caisson behaviour.

Thereafter, a geometrical configuration similar to the one previously assumed (see Table 2.3.3.2.1) has been considered. By referring to a geometrical scheme having H_g=20m, L=40m, H=60m, and assuming ρ_s=2040kg/m^3, ξ_s=3%, ρ_g=1020kg/m^3, some considerations on the importance of the impedance ratio on the soft caisson behaviour can be made; in particular, three different schemes with the same impedance ratio (α=20) between soil and soft layers, have been analysed, as reported in Table 2.3.3.2.2.

Scheme	$V_{s,s}$ (m/s)	T_n (s)	f_n (Hz)	$V_{s,g}$ (m/s)	α
$V_{s,s}$=200m/s $V_{s,g}$=20m/s	200	1.2	0.83	20	20
$V_{s,s}$=300m/s $V_{s,g}$=30m/s	300	0.8	1.25	30	
$V_{s,s}$=500m/s $V_{s,g}$=50m/s	500	0.48	2.08	50	

Table 2.3.3.2.2 *Schemes adopted for analyses.*

The responses of the three schemes differ each others, as reported both in Figures 2.3.3.2.3 and 2.3.3.2.4, where the maximum accelerations are shown for two different signals (f=1Hz and 5Hz). Table 2.3.3.2.3 reports the spectral intensities in the control point for two different signals (f=1Hz and 5Hz) referred to the three schemes: it seems to show that, by assuming a certain constant impedance ratio, the response of the model is sensible to the differences between the dynamic impedances of the soils and the soft layers, in the sense that lower stiffness values correspond to lower SI values.

The efficiency of the system improves by decreasing the stiffness both of the soil and the soft layers; as reported in Figure 2.3.3.2.5, the efficiency trends are similar among the different schemes, but lower stiffness values show higher efficiencies on larger structural periods.

These effects depend on the interaction between the soil layers, the deposit and the propagated signals. Figures 2.3.3.2.3 report the amplification ratios for the three schemes. The aim is to identify some connection between a given value of the impedance ratio and the response of the deposit. However, as expected by looking at the previous results in terms of spectral intensities and accelerations (see Figure from 2.3.3.2.3 to 2.3.3.2.5), the less the stiffness values the more the maximum amplifications A(0-60m) on lower frequencies. Due to the different mechanical properties of the soils inside caisson, the amplification ratios between the ground level and the upper part of the horizontal soft layer A(0-19m) differ each others (see Figures 2.3.3.2.3). Generally speaking, it seems that both the shear wave velocity of the soft layers and the impedance ratio are relevant parameters in the propagation of the signal through the insulating box, but the former plays a more significant role. To mitigate the seismic risk, it is more convenient the injection of soft layers with very low shear wave velocity, also when the soil deposit has a high shear stiffness value.

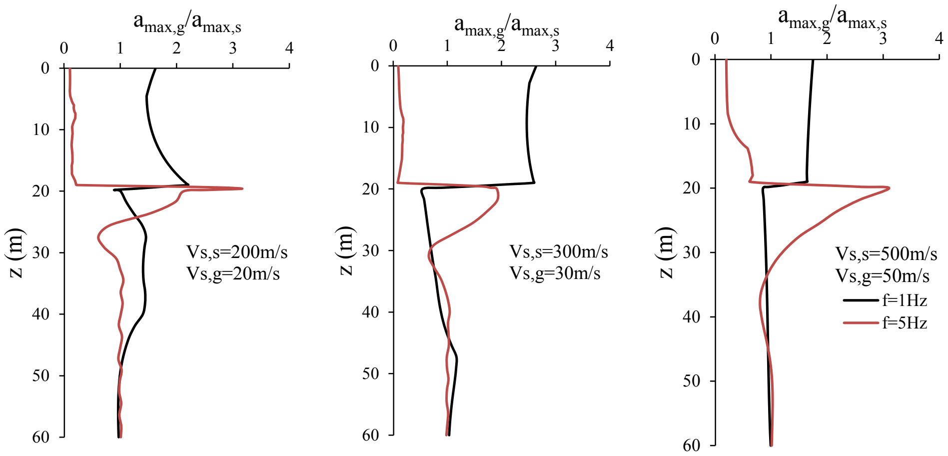

(a) (b) (c)

Figure 2.3.3.2.3 *Maximum accelerations with depth along the central vertical axis for two different signals (f=1Hz and 5Hz).*

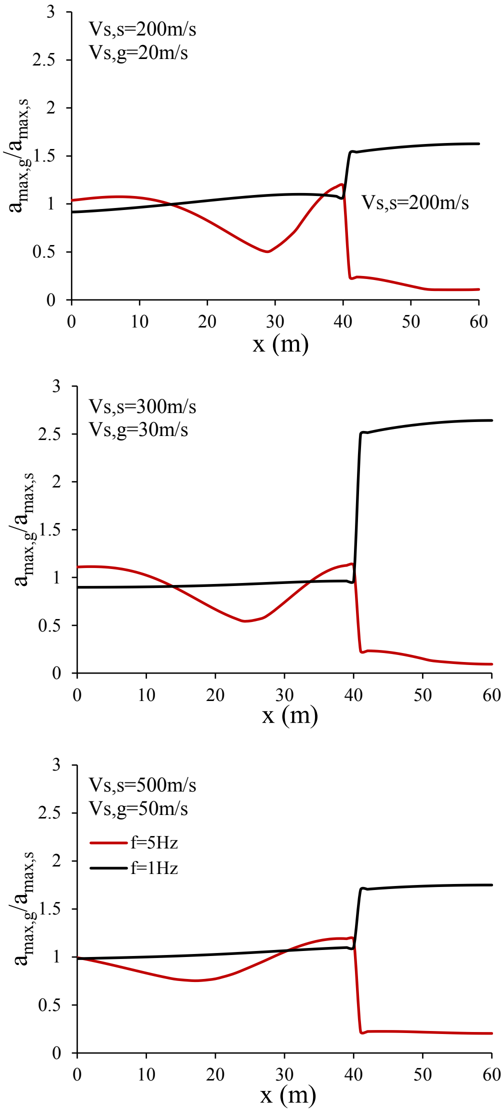

(a)

(b)

(c)

Figure 2.3.3.2.4 *Maximum accelerations at ground surface on the left side with respect to the central vertical axis for two different signals (f=1Hz and 5Hz).*

	SI_g/SI_s [0.1÷0.5]		
f (Hz)	$V_{s,s}$=200m/s $V_{s,g}$=20m/s	$V_{s,s}$=300m/s $V_{s,g}$=30m/s	$V_{s,s}$=500m/s $V_{s,g}$=50m/s
1	1.18	2.37	2.09
5	0.12	0.15	0.65

Table 2.3.3.2.3 *Spectral intensities in the control point for two different signals (f=1Hz and 5Hz).*

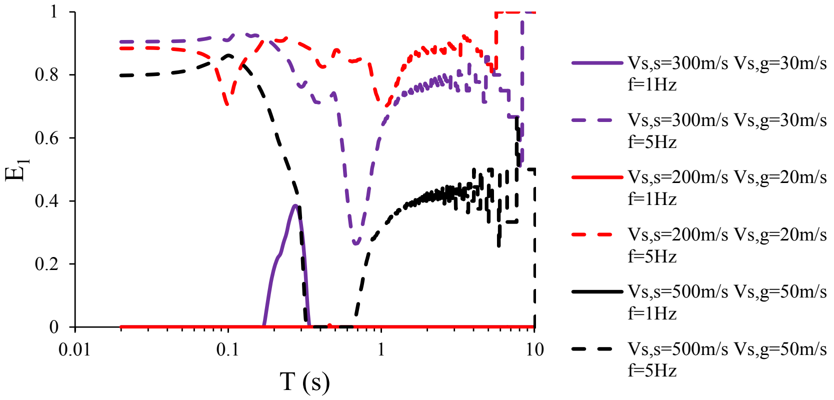

Figure 2.3.3.2.5 *Efficiency E_I in the control point for two different signals (f=1Hz and 5Hz).*

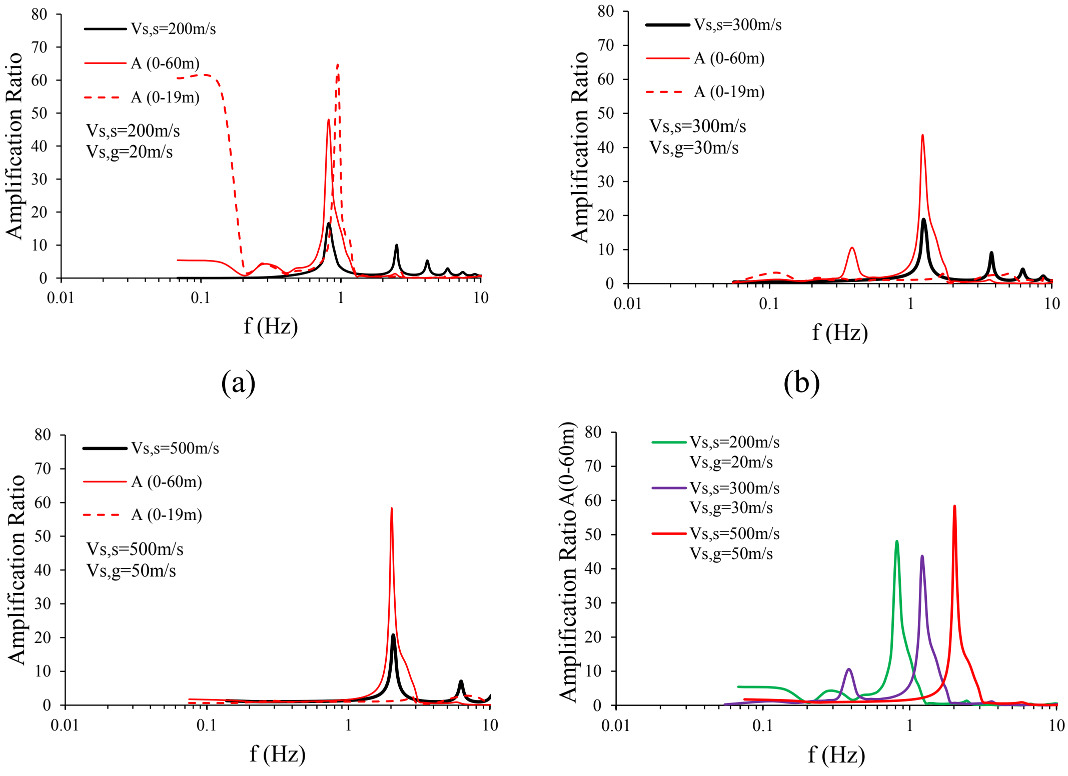

(a) (b)

(c) (d)

Figure 2.3.3.2.5 *Amplifications ratios for the different schemes.*

2.3.3.3 Effects of the variation of the soil deposit depth

Having assumed constant values for the dynamic impedance of the isolating box, in this series of analyses the depth of the soil deposit H has been varied, and assumed equal to 60m, 40m and 80m. The schemes assume $V_{s,s}$=300m/s and $V_{s,g}$=20m/s (i.e. α=30).

In Table 2.3.3.3.1, the values of natural periods and frequencies, in the elastic field, for the soil deposit with no treatment are reported (see §2.3.3.1):

H (m)	$V_{s,s}$ (m/s)	T_n (s)	f_n (Hz)	$V_{s,g}$ (m/s)	α
40	300	0.53	1.88	20	20
60		0.8	1.25		
80		1.07	0.94		

Table 2.3.3.3.1 *Values of the natural periods and frequencies for the soil deposit without any treatment.*

Figures 2.3.3.3.1 report the variations in response among the different schemes, which are justified by the amplification ratio profiles shown in Figures 2.3.3.3.2. For H equal to 80m, the natural frequency of the soil layer without treatment is close to 1Hz, which is close to one of the frequencies amplified by the insertion of the isolating box (i.e. $V_{s,g}$=20m/s with the geometrical configuration depicted in §2.3.3.1), as reported in §2.3.3.2. Therefore, the response of the model is amplified for a Ricker wavelet having a fundamental frequency of 1Hz. Figure 2.3.3.3.2b shows that, in the case of H=40m, the insertion of the soft caisson amplifies the response of the system for f=1Hz, as in the case of H=80m, but the maximum amplification is close to 0.3Hz. The first resonance frequency of the soil deposit with no treatment, for H=40m, is 1.88Hz (see Table 2.3.3.3.1); therefore, the treatment leads to a shift of the response of the soil deposit to higher periods.

This observation can be extended to the case of H=60m and 80m, because the higher amplifications are focused on frequencies lower than the ones of resonance of the soil deposits (see Figures 2.3.3.3.2).

The observations contained in this paragraph and in §2.3.3.2 suggest that the geometrical features and the mechanical properties of the soft caisson should be conceived referring to the specific requirements of the soil deposit which it is working on, in the sense that, by using this treatment system, it is possible to change the most amplified frequencies passing through the grouted layers.

Therefore, the soft box can be designed to de-amplify the frequencies most critical for the building to be protected.

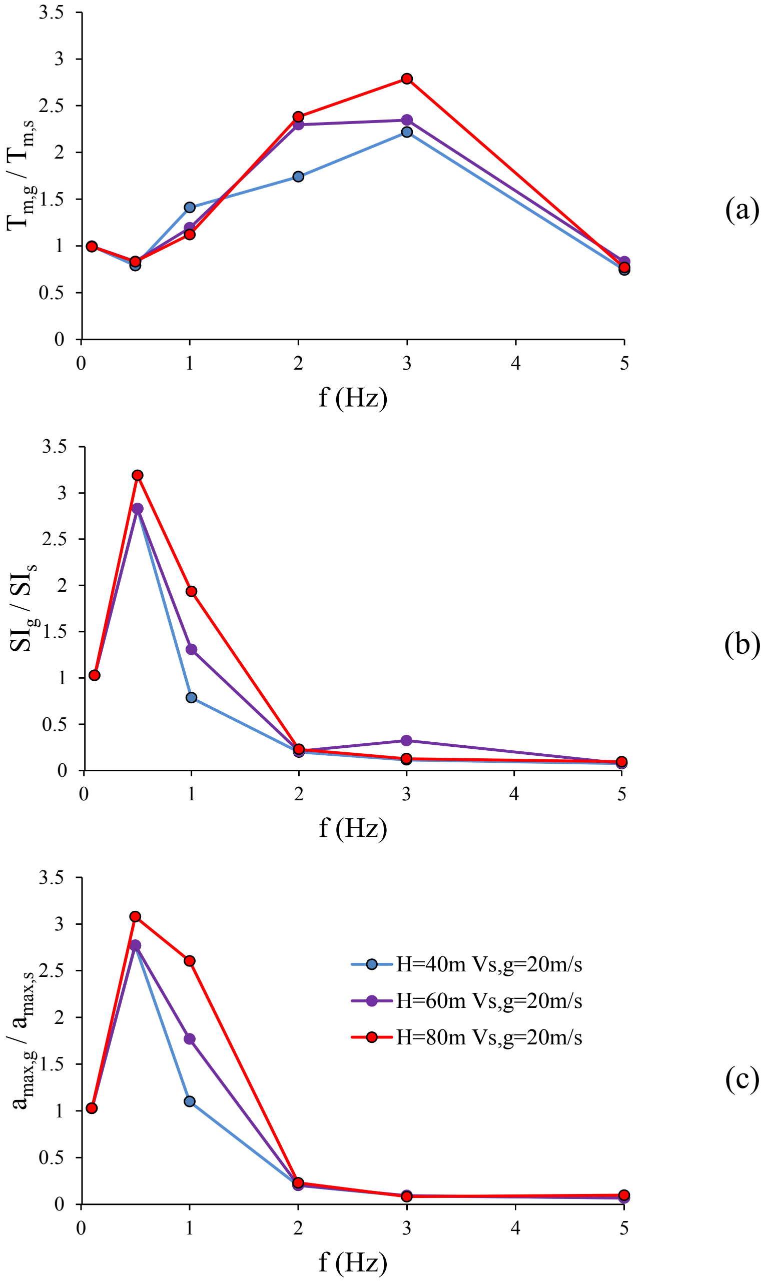

Figure 2.3.3.3.1 *Variations of the mean period* $T_{m,g}$*(a), the spectral intensities* SI_g *(b) and the maximum accelerations* $a_{max,g}$ *(c), by varying the deposit depth H and the propagated signal.*

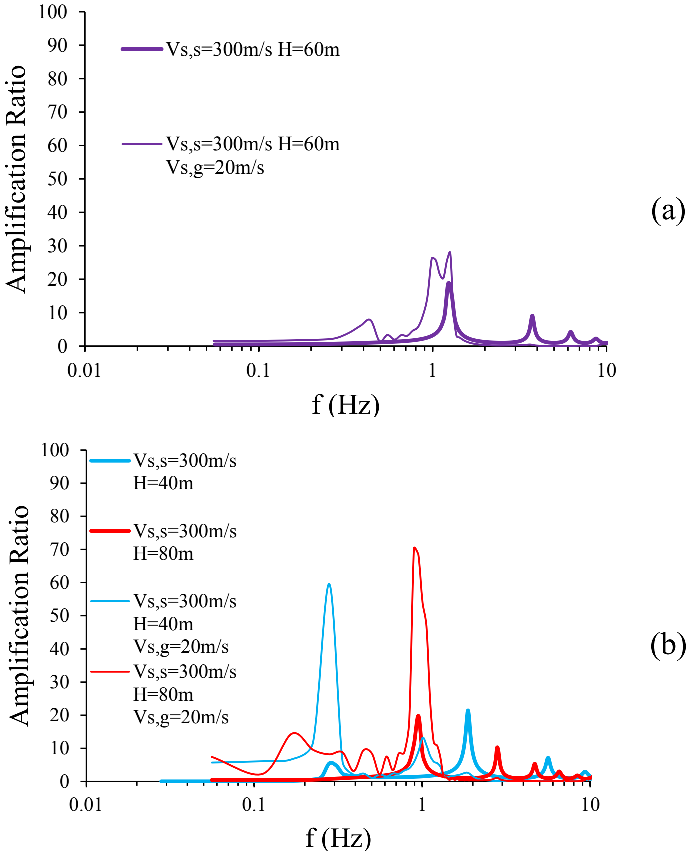

Figure 2.3.3.3.2 *Amplification ratios of the model configurations with $V_{s,s}$=300m/s and $V_{s,g}$=20m/s , by assuming deposit depths H equal respectevely to 60m (a), 40m and 80m (b), by varying the fundamental frequencies of the propagated signals.*

2.3.3.4 Effects of the variation of the lateral soft layers length

Other schemes have been tested by starting from the geometrical configuration adopted in §2.3.3.2, with an isolating box 20m depth and 40m long, with soft layers having $V_{s,g}$ equal to 20m/s, and changing the length of the lateral vertical soft layers. Two kinds of modifications of the reference geometrical configuration have been made: the former consists in gradually reducing the vertical layers length from ground level going downwards to the lower part of the diaphragms (schemes named S; see Figure 2.3.3.4.1 a); the latter consists in reducing length by cutting upwards, from the deepest part to ground level (schemes named S*; see Figure 2.3.3.4 b). Both schemes result into a soft caisson which is not continuous; the goal of these analyses it to see if the same isolating results can be obtained reducing grouting.

In Figures 2.3.3.4.2, the values of the ratios $a_{max,g}/a_{max,s}$ and SI_g/SI_s for the schemes S (a) are reported along the ones of the reference case (continuous soft caisson). The non-continuous schemes give rise to values of $a_{max,g}/a_{max,s}$ and SI_g/SI_s close to 1 for most frequencies, thus indicating that they are not as effective as the closed caisson. Only the scheme S1* may help, but only for the higher frequencies. To be really effective, therefore, the isolating box has to be closed (reference scheme).

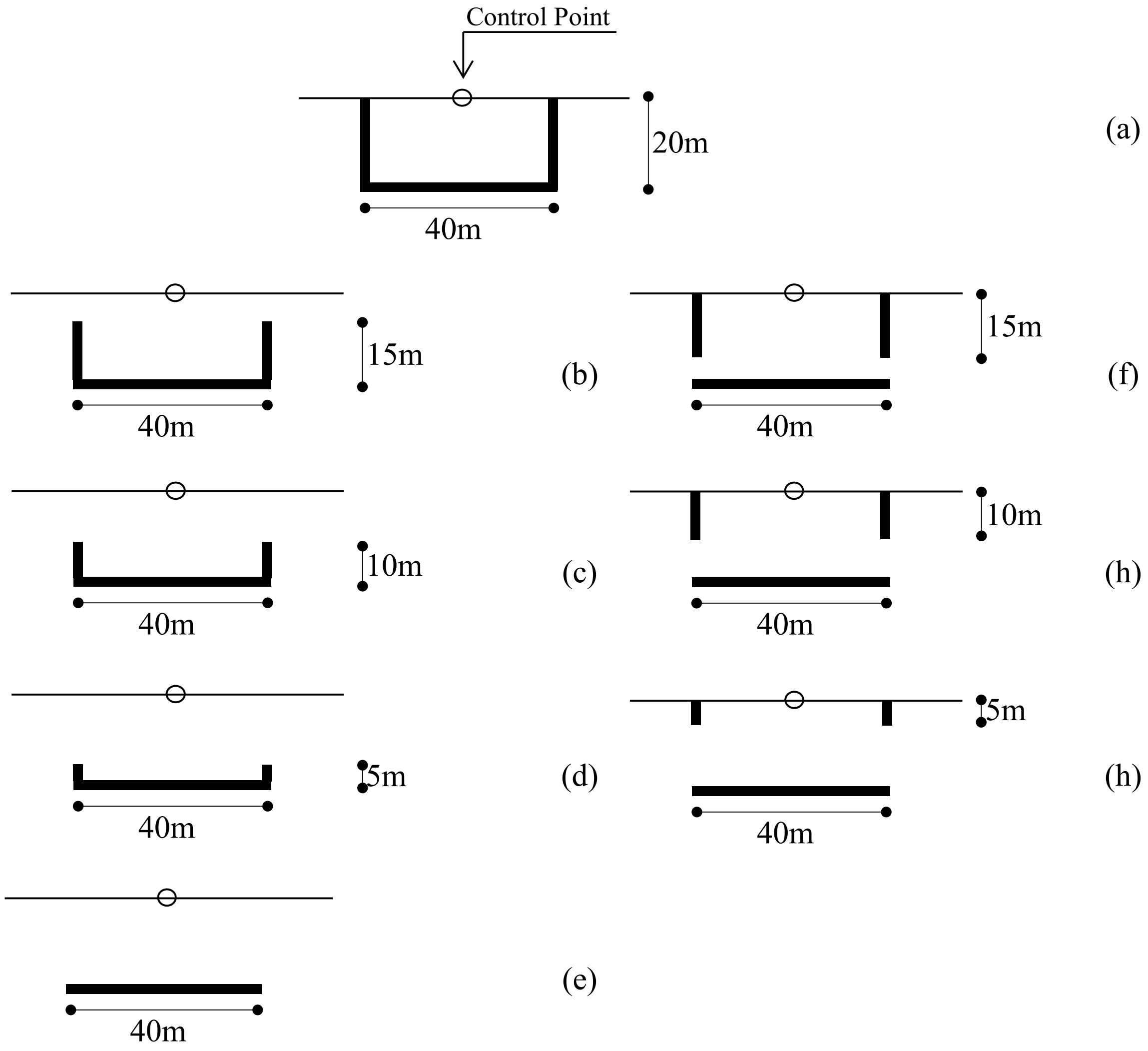

Figure 2.3.3.4.1 *Reference scheme with* $V_{s,s}$*=300m/s and* $V_{s,g}$*=20m/s (a); S1 (b); S2 (c); S3 (d); S4 (e); S1* (f); S2* (g); S3* (h).*

Similar observations can be made also with reference to the amplification ratios reported in Figure 2.3.3.4.3 for the schemes S (a) and S* (b). Schemes S* tend to amplify both the frequencies amplified by the reference scheme and the ones amplified in absence of any treatment.

In Figure 2.3.3.4.4, the S_a-S_d domains referred to the control point obtained by propagating a Ricker wavelet with a fundamental frequency of 5Hz, for different model configurations, are reported. S2 and S2* schemes show a shrinkage of the envelope essentially, because of a reduction of the maximum values of S_a, but no rotation towards larger periods. In other words, these incomplete schemes may have the only effect of slightly reducing the maximum accelerations hitting the structure to be protected. The form of the domains shows that these schemes are able to reduce the effects only at higher periods. The reference scheme shows the best performance.

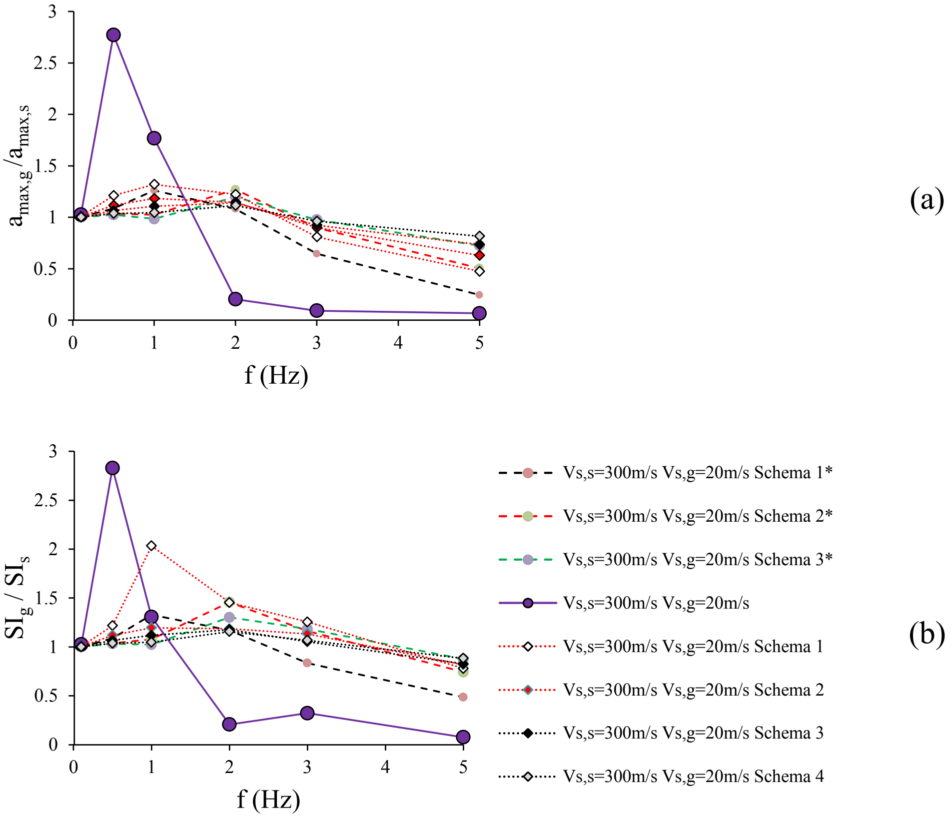

Figure 2.3.3.4.2 *Values of the ratios $a_{max,g}/a_{max,s}$ and SI_g/SI_s for schemes S (a) and S*(b) with comparisons to the amplification ratio of the reference scheme with a closed isolating box.*

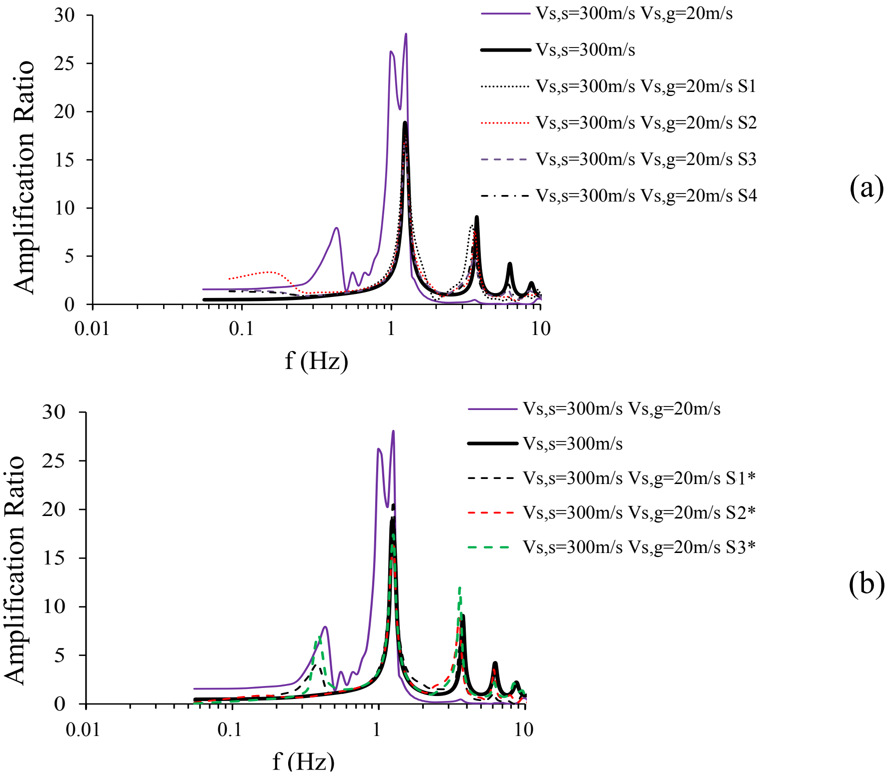

Figure 2.3.3.4.3 *Amplification ratios for the schemes S (a) and S* (b) with comparisons to the amplification ratio in the case of no treatment (black thick line) and in the reference scheme with a closed soft caisson.*

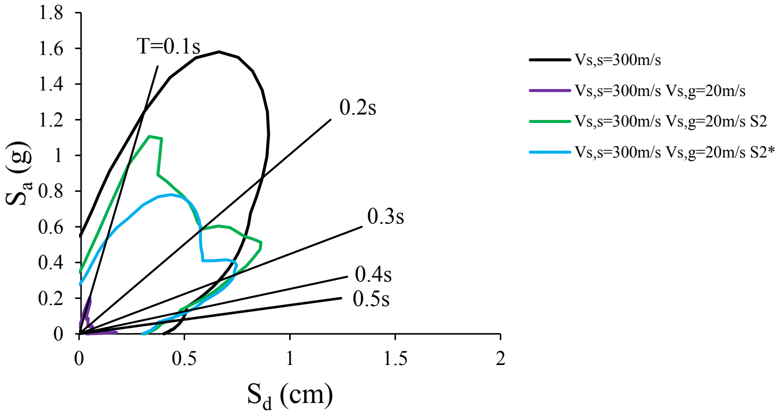

Figure 2.3.3.4.4 *S_a-S_d domains in the control point by propagating a Ricker wavelet with a fundamental frequency of 5Hz, for different geometrical configurations.*

2.3.3.5 Effects of the variation of a load on ground surface

The existence of a structure at ground level has not been considered in terms of dynamic interaction between the soil and the structure behaviour in this work, even though, it is expected to play a relevant role. By considering a given structure only as a supplementary weight, analyses have confirmed that such a weight does not play a relevant role. Tables from 2.3.3.5.1 to 2.3.3.5.3 show these results in terms of maximum accelerations, spectral intensities and predominant periods of the signals calculated in the control point of a scheme with $V_{s,s}$=300m/s, $V_{s,g}$=20m/s, H=60m, L=40m and H_g=20m, by applying a distributed load (q_w equal to 0, 50kPa and 100kPa) on a length equal to 20m at ground surface, at the centre of the isolating box (see Figure 2.3.3.5.1).

A distributed load at ground level does not play a relevant role because it does not constitute a participant mass to the motion of the system; however, the presence of a structure at ground level plays a noteworthy role, because of the mutual interaction with the soil (Venditozzi, 2013).

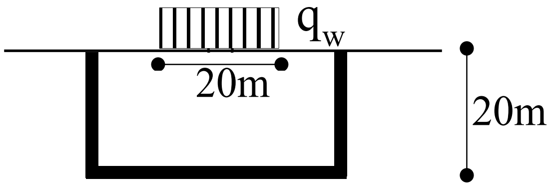

Figure 2.3.3.5.1 *Geometrical configuration, with the indication on the position of the load distribution.*

f (hz)	Soil q_w=0kPa			$V_{s,s}$=300m/s $V_{s,g}$=20m/s q_w=0kPa				
	a_{max} (g)	SI (cm)	T_p (s)	a_{max} (g)	SI (cm)	T_p (s)	$a_{max,g}$ / $a_{max,s}$	$SI_{max,g}$ / $SI_{max,s}$
0.1	0.508	9.791	3.480	0.521	10.050	3.480	1.026	1.026
0.5	0.808	17.276	1.120	2.240	48.880	1.000	2.772	2.829
1	0.900	28.040	0.680	1.590	36.620	0.900	1.767	1.306
2	0.667	26.138	0.300	0.136	5.430	0.860	0.204	0.208
3	0.628	17.569	0.220	0.058	5.670	0.280	0.092	0.323
5	0.546	6.870	0.140	0.037	0.528	0.100	0.067	0.077

Table 2.3.3.5.1 *Effects in the control point for different signals and a distributed load q_w equal to 0kPa.*

f (hz)	Soil q_w=50kPa			$V_{s,s}$=300m/s $V_{s,g}$=20m/s q_w=50kPa				
	a_{max} (g)	SI (cm)	T_p (s)	a_{max} (g)	SI (cm)	T_p (s)	$a_{max,g}$ / $a_{max,s}$	$SI_{max,g}$ / $SI_{max,s}$
0.1	0.508	9.791	3.480	0.522	10.052	3.480	1.026	1.027
0.5	0.808	17.276	1.120	2.244	48.879	1.000	2.776	2.829
1	0.900	28.038	0.680	1.591	36.617	0.900	1.768	1.306
2	0.667	26.139	0.645	0.136	5.670	0.860	0.204	0.217
3	0.628	17.546	0.220	0.058	2.057	0.280	0.093	0.117
5	0.550	6.89	0.140	0.037	0.528	0.100	0.066	0.077

Table 2.3.3.5.1 *Effects in the control point for different signals and a distributed load q_w equal to 50kPa.*

f (hz)	Soil q_w=100kPa			$V_{s,s}$=300m/s $V_{s,g}$=20m/s q_w=100kPa				
	a_{max} (g)	SI (cm)	T_p (s)	a_{max} (g)	SI (cm)	T_p (s)	$a_{max,g}$ / $a_{max,s}$	$SI_{max,g}$ / $SI_{max,s}$
0.1	0.508	9.791	3.480	0.522	10.052	3.480	1.026	1.027
0.5	0.808	17.276	1.120	2.244	48.879	1.000	2.776	2.829
1	0.900	28.038	0.680	1.591	36.617	0.900	1.768	1.306
2	0.667	26.139	0.300	0.136	5.670	0.860	0.204	0.217
3	0.628	17.546	0.220	0.058	2.057	0.280	0.093	0.117
5	0.549	6.898	0.120	0.036	0.528	0.100	0.066	0.077

Table 2.3.3.5.1 *Effects in the control point for different signals and a distributed load q_w equal to 100kPa.*

2.3.3.6 Effects of the variation of the dimension of the soft caisson

In order to check the influence of the dimensions of the isolating box, the analyses summarized in Table 2.3.3.6.1 have been carried out. In all of them, the soil deposit is 60m thick, its shear wave velocity $V_{s,s}$ is of 300m/s with a damping ratio of 3%, and the shear wave velocity of the soft layers $V_{s,g}$ is equal to 20m/s.

Scheme	H_g (m)	L_g (m)
H_g=0m L=40m	1	40
H_g=10m L=40m	10	40
H_g=20m L=40m	20	40
H_g=10m L=30m	10	30
H_g=20m L=30m	20	30
H_g=10m L=20m	10	20
H_g=20m L=20m	20	20

Table 2.3.3.6.1 *Different scheme configurations by varying H_g and L_g of the soft caisson.*

Also a scheme with H_g=1m (soft layer at ground surface), which is more similar to a building base isolation system, has been considered. However, since in this case the soft layer does not have the possibility to freely slide in the horizontal direction (because of the lateral soil constraint), it may be expected to be not as effective as a base isolator. The effect of soil lateral constraint is reported in Figures 2.3.3.6.1, where the variations in the response of the system in the control point in terms of predominant period, mean period, spectral intensity and maximum acceleration are reported, for different values of the soil caisson depth H_g, assuming a constant length L_g of the horizontal layer (L_g = 40m).

The green line reported in Figures 2.3.3.6.1 shows the response of the system for H_g=1m; as previously anticipated, this case is not effective, as all the ratios in the Figures 2.3.3.6.1 keep a constant value of 1. The purple and dark red lines in Figure 2.3.3.6.1a represent the variations in predominant periods in the signal calculated in the control point. The trend is similar, but larger values are observed for H_g=20m.

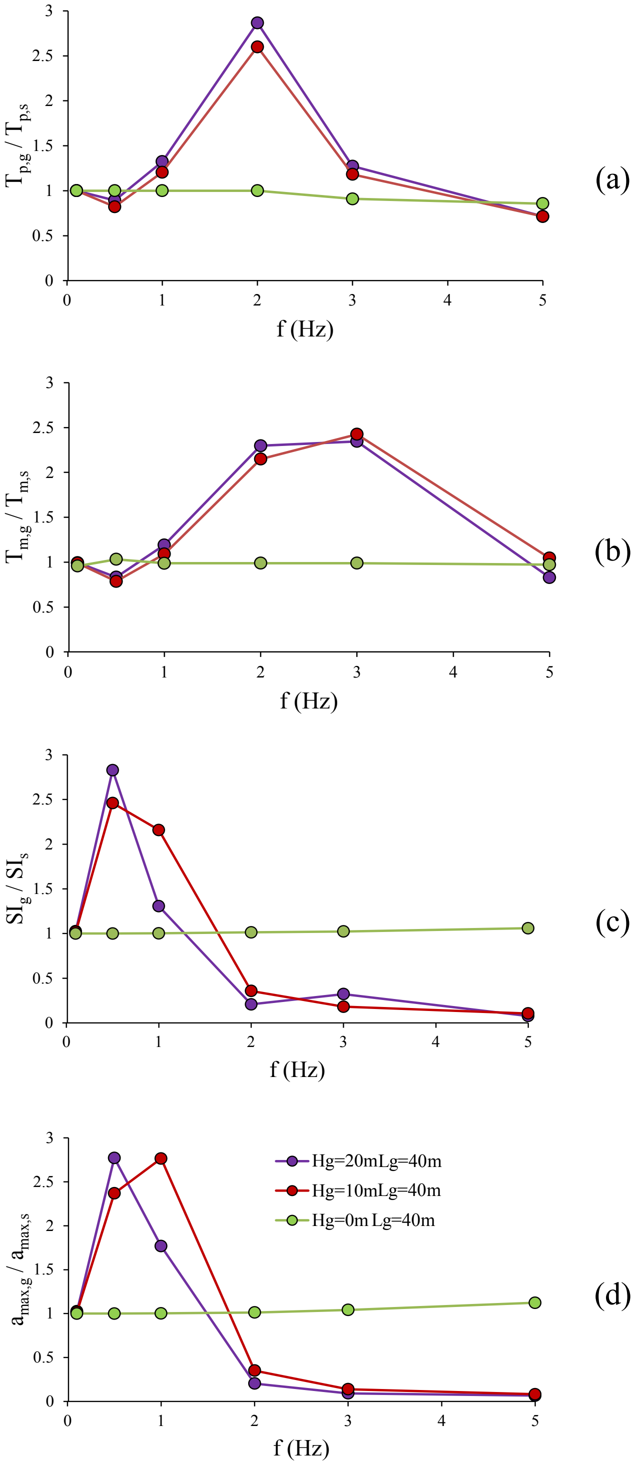

Figure 2.3.3.6.1 *Variations in the response of the system in the control point in terms of predominant period, mean period, spectral intensity and maximum acceleration for different* H_g*, assuming a constant* $L_g = 40m$*.*

In order to explain these results, it is convenient to consider a simple analogical model (see Figure 2.3.3.6.2) in which the soil on the sides of the isolating box is replaced by an equivalent elastic spring with a stiffness k*, and the mass involved by the motion is m*.

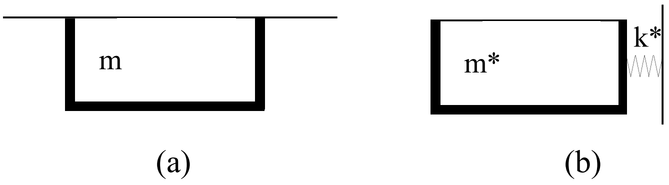

Figure 2.3.3.6.2 *Schematization of the system (a) in an equivalent SDOF (b).*

Since such a system could be studied as a simple oscillator, its fundamental period is:

$$T^* = 2 \cdot \pi \cdot \sqrt{\frac{m^*}{k^*}} \qquad (2.3.3.6.1)$$

The period may increase by increasing the mass m* or decreasing the stiffness k*. In these cases, the periods seem to slightly increase by varying the depth of the soft caisson, with a significant effect of the mass m* variations in determining the response of the caisson. However, for f=0.1Hz and 5Hz no differences in terms of predominant periods are observed.

As previously observed in the 1D analyses too (see §2.2.2.2), the treatment effectiveness increases increasing the depth H_g (see Figure 2.3.3.6.1 c and d).

This can be appreciated by observing the amplification ratios of the system in the control point (see Figures 2.3.3.6.3) by varying the depth of the treatment H_g (0m (a), 10m (b) and 20m (c)) for L_g = 40m. Amplification ratios are reported both in terms of differences in response between the ground level and the soil layer base and in terms of differences in response between the ground level and the upper side of the soft horizontal layer.

Amplification ratios confirm results in terms of spectral intensities and maximum accelerations (see Figures 2.3.3.6.1 c and d); the scheme with H_g=10m tends to amplify the effects in correspondence of some frequencies more than the scheme with H_g=20m, especially for f=1Hz. By observing results in terms of efficiencies (see Figures 2.3.3.6.4), a wider range of periods in which the treatment is able in reducing dynamic effects is observed by increasing soft horizontal layer depth. Again, this result is consistent with 1D analyses results, and is due both to frequencies amplification distribution and material damping which is more impacting by considering a deeper soft caisson.

In Figure 2.3.3.6.5 the maximum accelerations at ground surface for $V_{s,g}$ = 20m/s, and varying the different values of L_g are reported. Three different fundamental frequencies of the Ricker wavelet are shown; by varying the size of the soft caisson, the maximum accelerations inside assume different values.

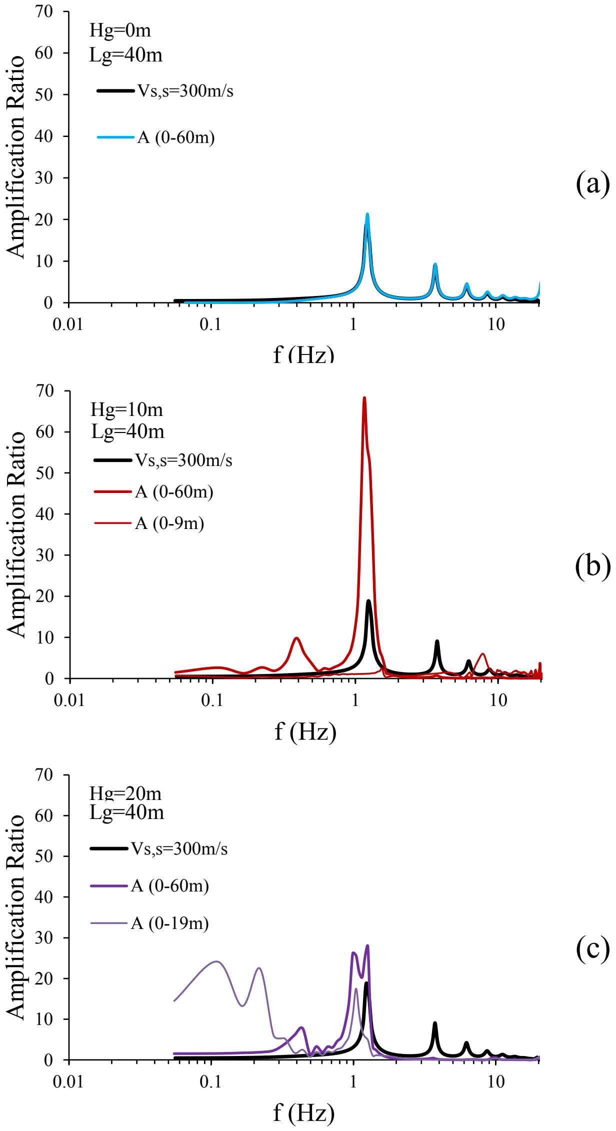

Figure 2.3.3.6.3 *Amplification ratios of the system in the control point by varying the depth of the treatment H_g (0m (a), 10m (b) and 20m (c)) for L_g = 40m.*

A comparison among different geometrical configurations by varying both the length and the depth of the soft caisson for different input wavelets is reported in Figures 2.3.3.6.6. Comparisons have been made in terms of predominant, mean periods, spectral intensities and maximum accelerations in the control point for different depths of the horizontal layer (10m or 20m). By shrinking the soft caisson, it seems that the fundamental period increases on a larger range of signal frequencies. This is less evident with reference to the mean period. For Ricker fundamental frequencies larger than 0.5Hz, an enlargement of the soft caisson leads to lower maximum accelerations and spectral intensities values (see Figures 2.3.3.6.6 from e to h). This may be explained by looking at amplification ratios (see Figures 2.3.3.6.7).

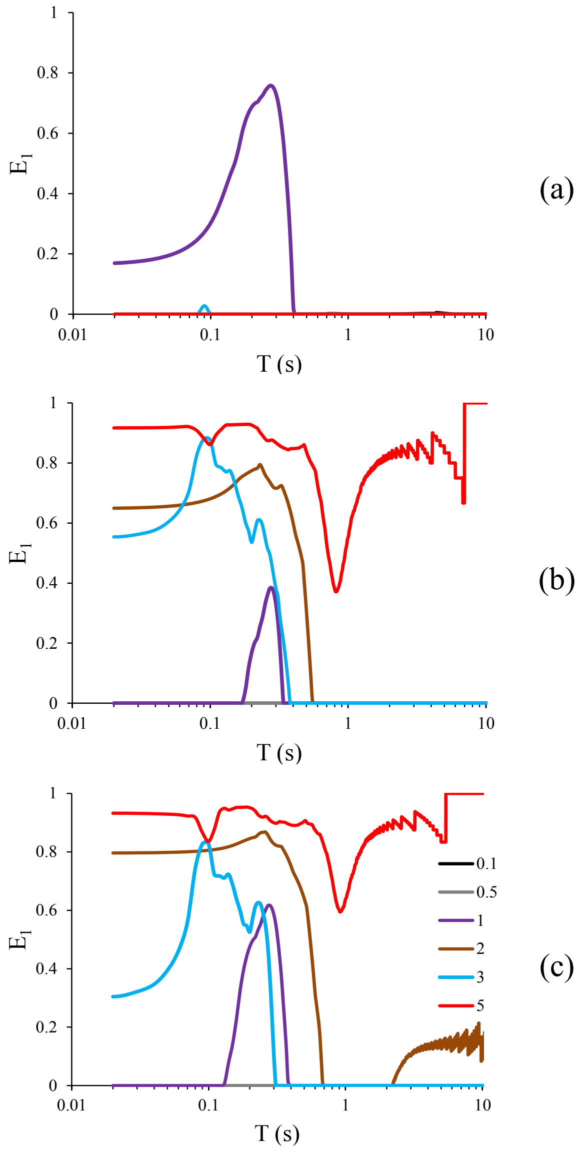

Figure 2.3.3.6.4 *Efficiencies for different geometrical configurations of the isolating box, by assuming* $V_{s,g}$*=20m/s,* L_g*=40m and* H_g*=0m (a), 10m (b) and 20m (c).*

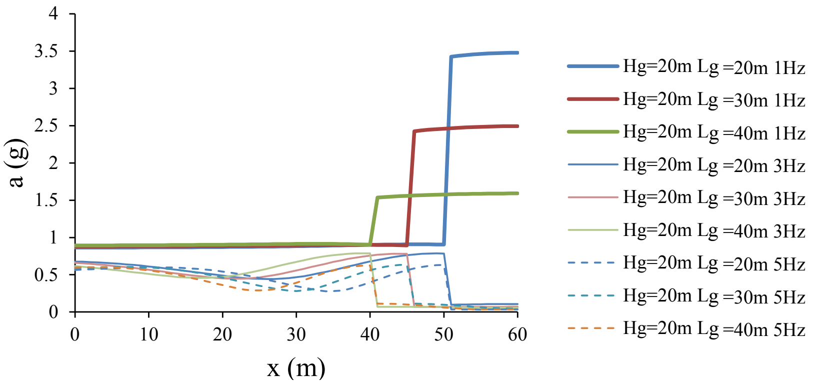

Figure 2.3.3.6.5 *Maximum accelerations at ground surface, by assuming* $V_{s,g}$*=20m/s, and varying the length* L_g *of the soft caisson.*

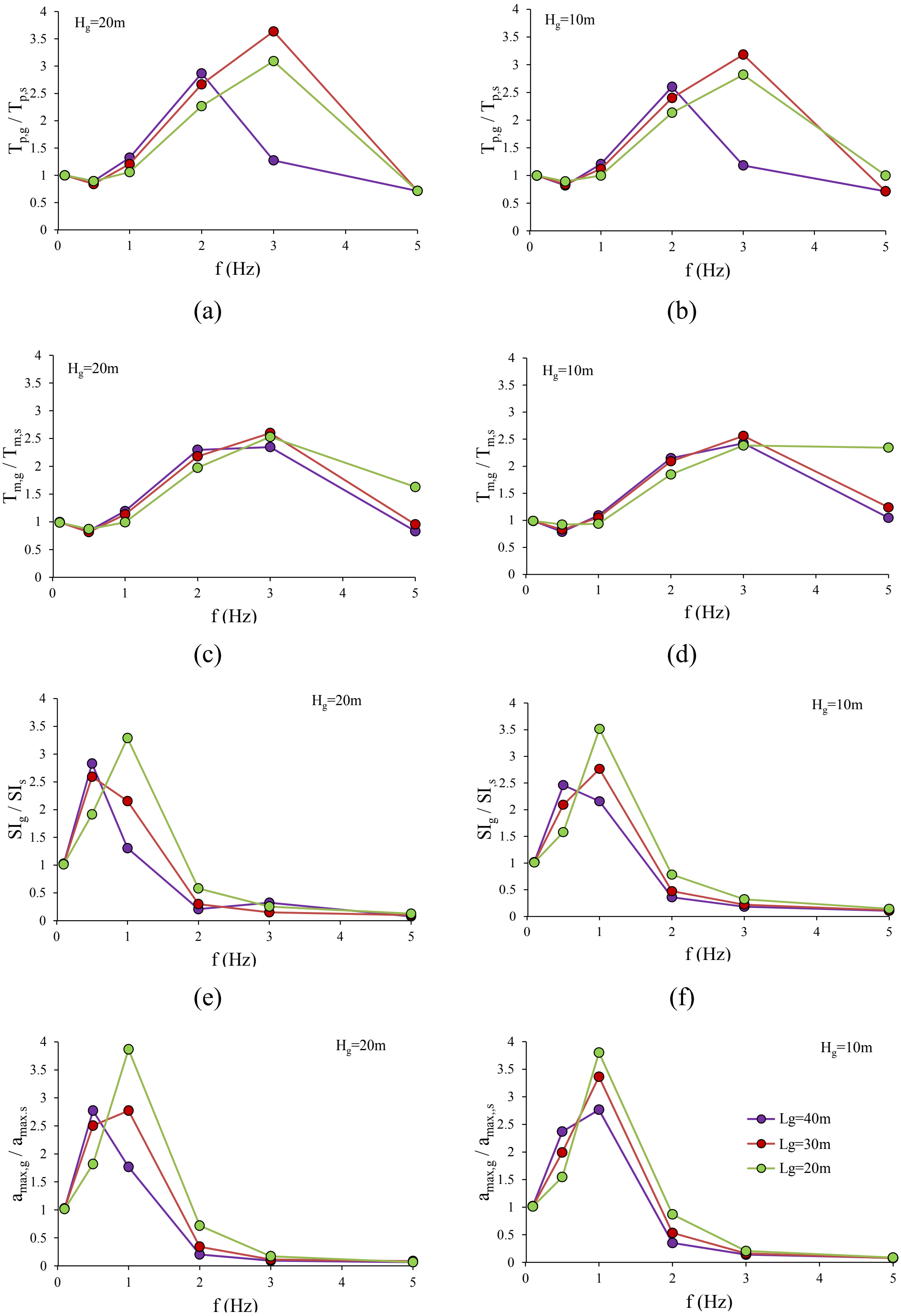

(a) (b)

(c) (d)

(e) (f)

(g) (h)

Figure 2.3.3.6.6 *Effects, in the control point, in terms of predominant (a and b) and mean periods (c and d), spectral intensities (e and f) and maximum accelerations (g and h) for different depths of the horizontal layer (10 or 20m).*

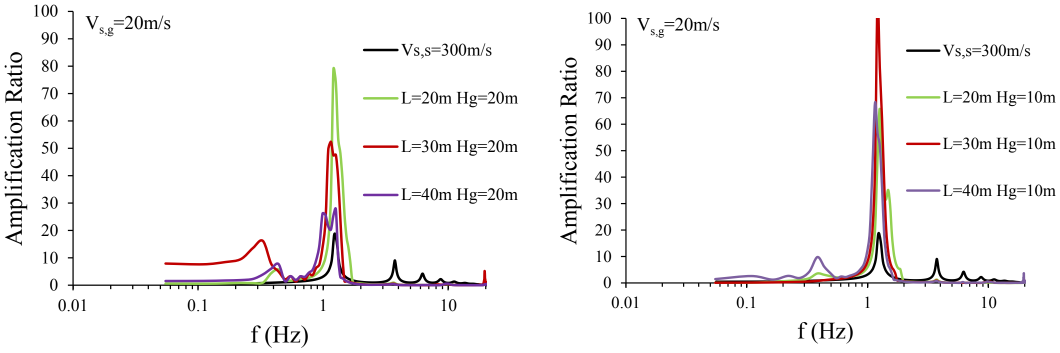

(a) (b)

Figure 2.3.3.6.7 *Amplification ratios for H_g equal to 10m (a) and 20m (b).*

2.3.3.7 Effects of the variations of the soft layers thickness

In the analyses reported in the previous sections, a constant value of the thickness of the soft layers has been considered, equal to 1m. In order to understand if a larger thickness may determine important differences in response at ground surface, two other values have been taken into account, i.e. 2m and 3m, by considering a soil deposit of 60m, $V_{s,s}$=300m/s, and a soft caisson with $V_{s,g}$=20m/s, L_g=40m, H_g=20m.

By assuming a larger thickness, effects are really impacting on system. In terms of fundamental and mean periods of the signal in the control point, by enlarging the thickness of the soft layers periods tend to decrease. This is clearly testified in terms of mean period (see Figure 2.3.3.7.1 b) whose value decreases by increasing soft layer thickness.

Above all, increasing soft layer thickness is determinant in reducing spectral intensity and maximum acceleration values (see Figure 2.3.3.7.1 c and d) in correspondence to the frequencies of 0.5Hz and 1Hz, whose effects have not been cut down by inserting 1m thick layers. By increasing thickness, a reduction of the effects in the control point is possible, as also reported in Figures 2.3.3.7.2.

Such figures describe the effects along the central vertical axis in terms of horizontal maximum accelerations and the effects at ground surface at the left side with respect to the symmetry vertical axes in terms of horizontal maximum accelerations.

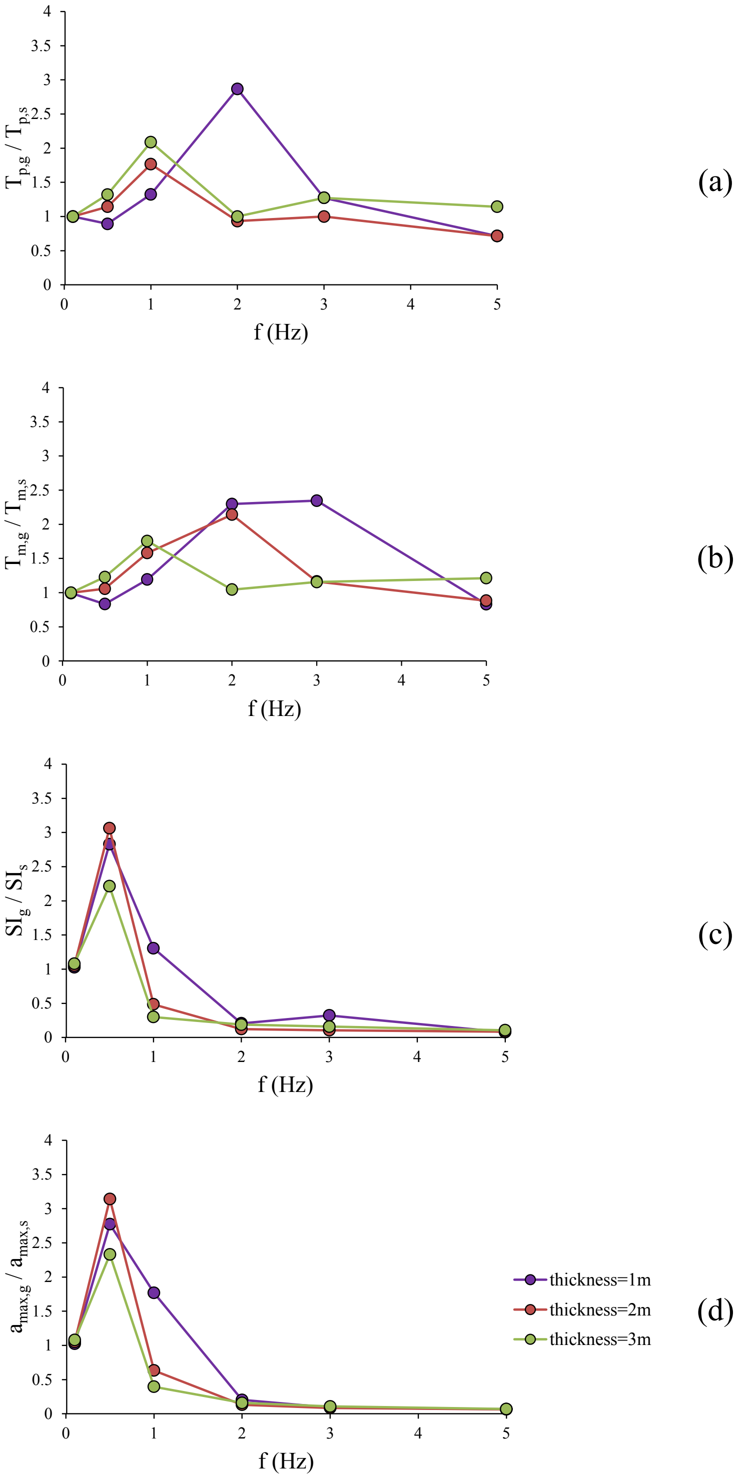

Figure 2.3.3.7.1 *Effects, in the control point, in terms of predominant (a) and mean periods (b), spectral intensities (c) and maximum accelerations (d) for different thicknesses of the soft layers, assuming* $V_{s,g}$*=20m/s,* H_g*=20m,* L_g*=40m,* $V_{s,s}$*=300m/s.*

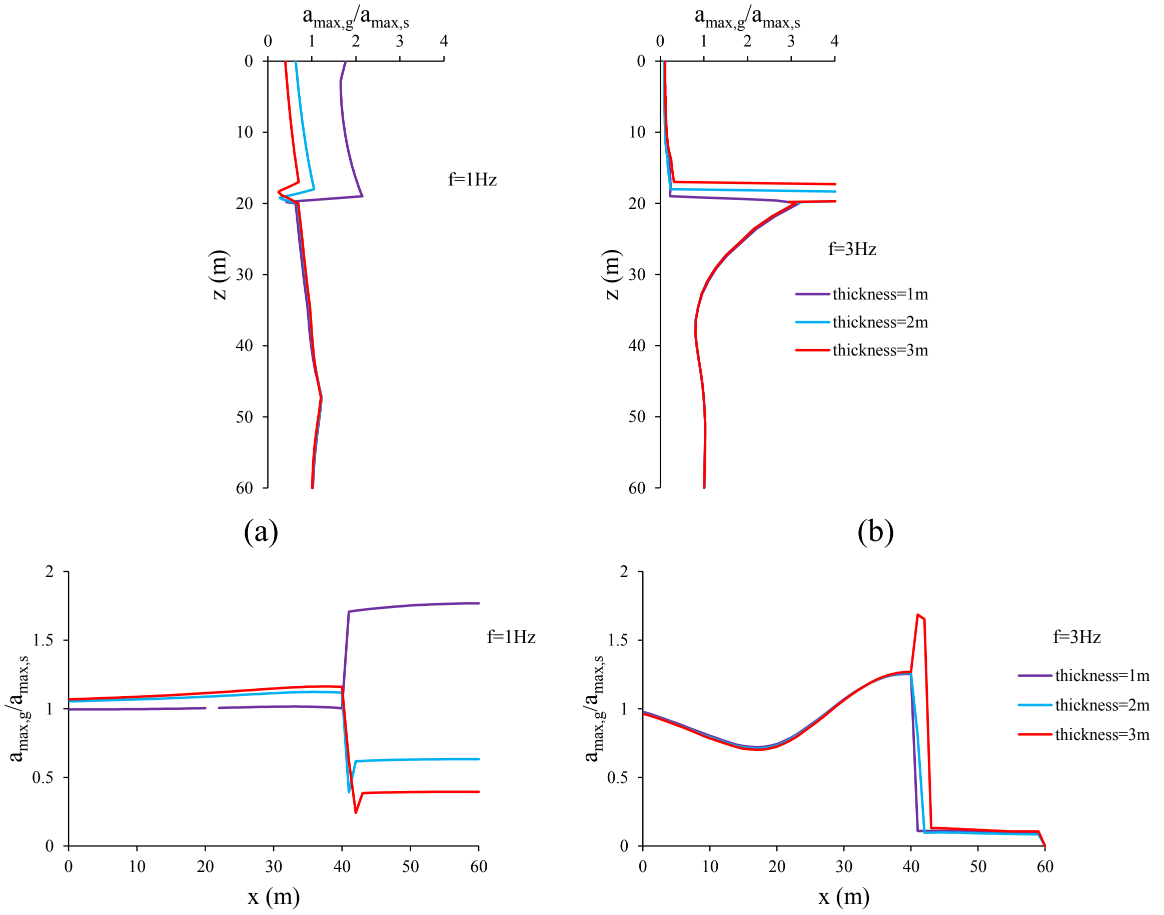

(a) (b)

(c) (d)

Figure 2.3.3.7.2 *Effects along the central vertical axis in terms of horizontal maximum accelerations by varying the thicknesses of the soft layers for a Ricker wavelet fundamental frequency of 1Hz (a) and 3Hz (b); effects at ground surface on the left side of the symmetry vertical axes, in terms of horizontal maximum accelerations by varying the thicknesses of the soft layers for a Ricker wavelet fundamental frequency of 1Hz (c) and 3Hz (d).*

Amplification ratios (see Figures 2.3.3.7.3a) confirm that by increasing the thickness of the treated layers lower frequencies are the most amplified ones, but the ratio amplitude in correspondence of the frequency of 1Hz drastically reduces; furthermore, the soft caisson tends to amplify higher frequencies (see Figures 2.3.3.7.3b).

A similar effect can be seen by looking at efficiency E_I (see Figures 2.3.3.7.4) for different thicknesses of the soft layers. By increasing the thickness, the system has E_I larger than 0 for higher SDOF period ranges; in this sense, the increase of thickness of the soft layers seems to correspond to better safety conditions for a structure placed at ground surface.

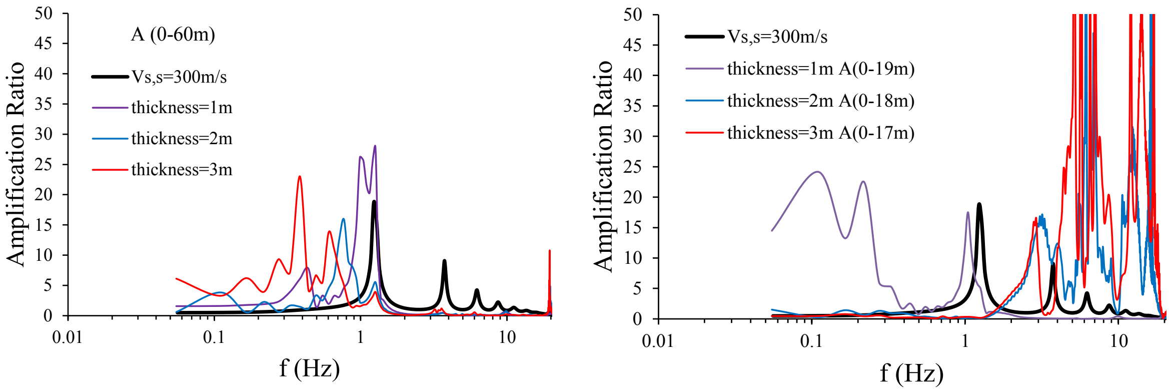

(a) (b)

Figure 2.3.3.7.3 *Amplification ratios between the ground level and the base of the soil deposit (a) and between the ground level and the upper part of the layer (b) for different thicknesses of the soft layers.*

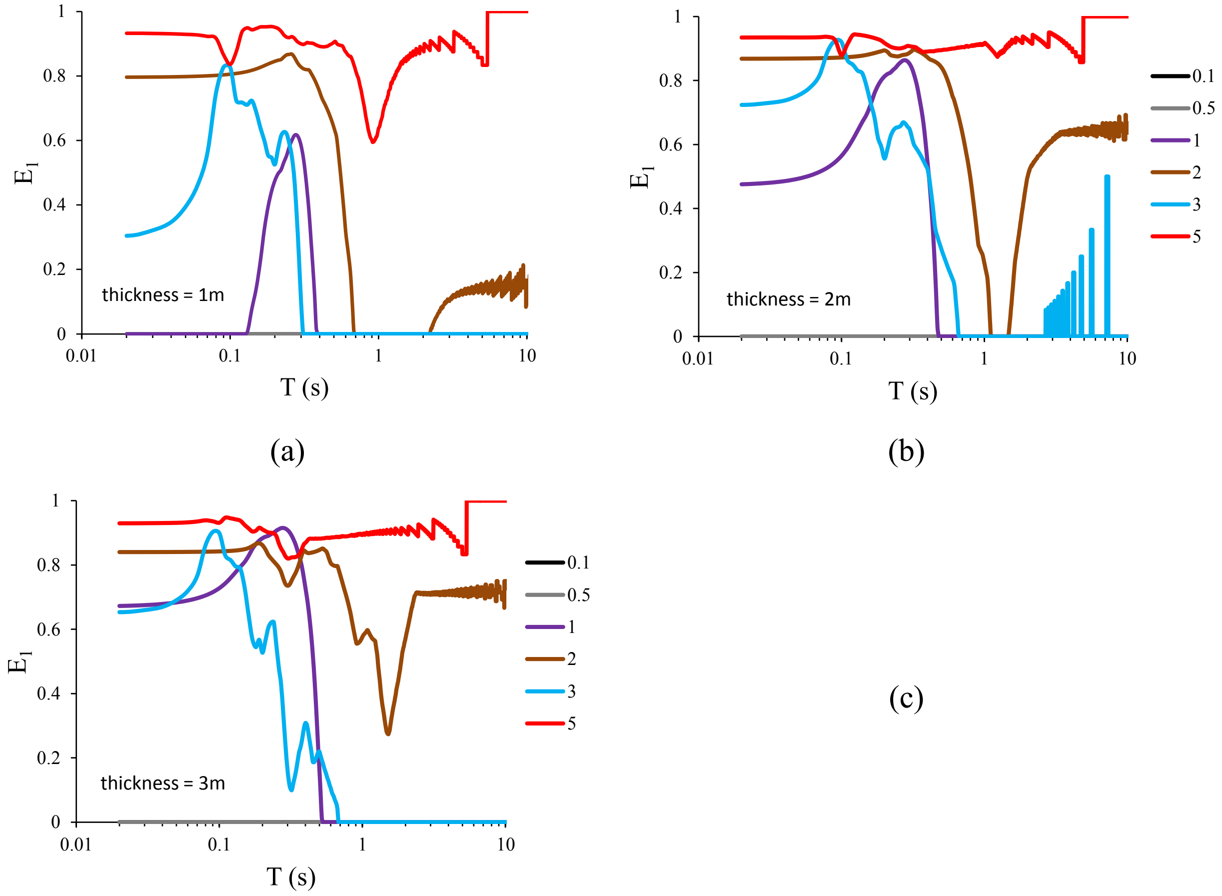

(a) (b) (c)

Figure 2.3.3.7.4 *Efficiencies for different thicknesses of the soft layers, equal respectively to 1m (a), 2m (b) and 3m (c).*

2.3.3.8 Effects of the variation of the soft layers damping ratio

By taking into account a soil deposit 60m deep with $V_{s,s}$=300m/s, an isolating box having H_g=20m, L_g=40m and $V_{s,g}$=20m/s, different values of the damping ratio for the soft layers have been considered. Three damping ratio values have been used, i.e. 0, 3% and 10%. Even though the three values largely differ each other, they have no effect at all on the results. Spectral intensity values in the control point are reported in Table 2.3.3.8.1: only extremely low dissimilarities are seen. This observation may be expressed by looking at Figure 2.3.3.8.1 too, where the maximum accelerations along the central vertical axis are reported, considering different values of damping ratios for the case f=5Hz. By changing the damping ratio of the soft layers, only a tiny variation in the distribution of results is observed. This result is physically consistent, as the small thickness of the soft layer reduces the possibility to dissipate energy within it, regardless of this value of the damping ratio.

SI (cm)				
f (Hz)	No Treatment	D0 (ξ_g=0)	D3 (ξ_g=0.03)	D10 (ξ_g=0.1)
0.1	9.791	10.050	10.052	10.052
0.5	17.276	48.880	48.879	48.879
1	28.040	36.620	36.617	36.617
2	26.138	5.430	5.670	5.670
3	17.569	5.670	2.057	2.057
5	6.870	0.528	0.528	0.528

Table 2.3.3.8.1 *Values of SI in the control point due to the different values of damping ratio.*

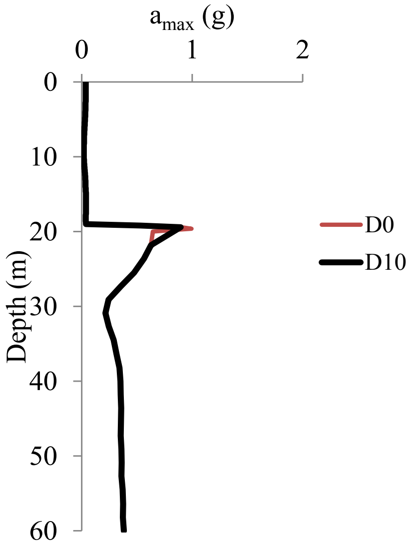

Figure 2.3.3.8.1 *Maximum accelerations along the central vertical axis for f=5Hz, by considering two different values of damping ratio.*

2.3.3.9 Effects of the variation of the soft layers volumetric stiffness

As done for simpler schemes, in these 2D analyses the variation in volumetric stiffness of the soft layers forming the isolating box (characterized by $V_{s,s}$=300m/s; H=60m; $V_{s,g}$=20m/s; L_g=40m; H_g=20m) has been considered. Four different typologies of analyses have been performed, by varying not only the volumetric stiffness K of all the soft layers, but also considering a different distribution of the parameter K across the thin treated layers.

In this sense, a scheme named Kv (see Table 2.3.3.9.1) has been considered, where, assuming a given value of the shear stiffness G, the lateral soft layers keep a stiffness linked to a Possion ratio ν=0.3, and the horizontal one assumes a stiffness K derived by ν=0.147.

This scheme is interesting because a higher volumetric stiffness of the horizontal soft layer may determine lower static settlements (see §3.1.4.2).

			Horizontal soft layer			Lateral soft layers		
Scheme	$V_{s,g}$ (m/s)	G (Pa)	ν	K (Pa)	G/K	ν	K (Pa)	G/K
K	20	$4.079 \cdot 10^5$	0.300	$8.838 \cdot 10^5$	0.46	0.300	$8.838 \cdot 10^5$	0.46
0.5K	20	$4.079 \cdot 10^5$	0.147	$4.419 \cdot 10^5$	0.92	0.147	$4.419 \cdot 10^5$	0.92
10K	20	$4.079 \cdot 10^5$	0.477	$88.38 \cdot 10^5$	0.05	0.477	$88.38 \cdot 10^5$	0.05
Kv	20	$4.079 \cdot 10^5$	0.477	$88.38 \cdot 10^5$	0.05	0.300	$8.838 \cdot 10^5$	0.46

Table 2.3.3.9.1 *Schemes adopted to study the influence of the volumetric stiffness on the soft layers efficiency.*

In terms of periods (see Figures 2.3.3.9.1 a and b), two different behaviours are observed: on one hand the schemes 0.5K and K; on the other hand the scheme 10K. Kv scheme is intermediate between the two conditions, with a mean period trend with no large variations and the fundamental period values, which are more closely linked to the signal frequencies.

By observing Figures 2.3.3.9.1, a lower volumetric stiffness reduces the maximum accelerations and spectral intensities in the control point, with the exception of f=0.5Hz (see azure lines of Figures 2.3.3.9.1 c and d). The worst scheme seems to be the 10K one, which amplifies dynamic actions with the exception of f=0.5Hz. The Kv scheme is intermediate between these two conditions, but with a remarkable tendency to attenuate the effects of the signal propagations. In this sense, its results are more similar to K and 0.5K schemes. These behaviours are detected by observing the amplification ratio values for the different schemes (see Figures 2.3.3.9.1) both between the ground level and the base of the soil deposit A(0-60m) (a) and between the ground level and the upper part of the horizontal soft layer A(0-19m) (b).

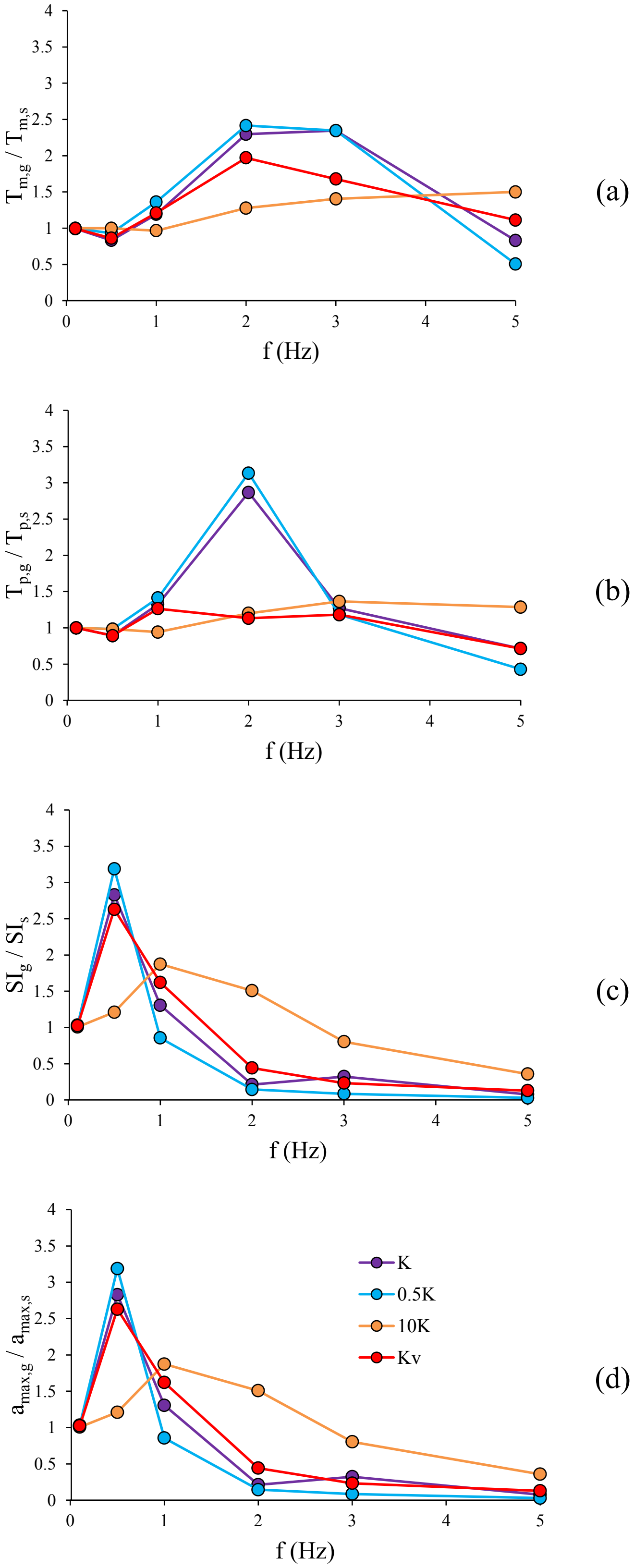

Figure 2.3.3.9.1 *Effects in the control point in terms of predominant (a) and mean periods (b), spectral intensities (c) and maximum accelerations (d) for K of the soft layers, for* $V_{s,g}$*=20m/s,* H_g*=20m, L=40m,* $V_{s,s}$*=300m/s.*

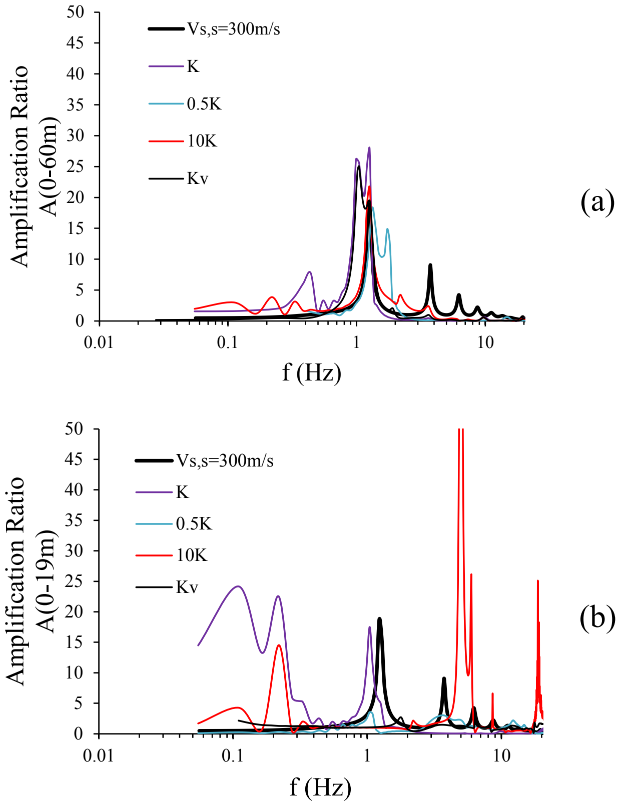

Figure 2.3.3.9.1 *Amplification ratio A(0-60m) (a)and A(0-19m)(b) by varying the volumetric stiffness K of the soft layers.*

In the time domain, the horizontal accelerations for different positions x from the left boundary of the model at ground surface by propagating a Ricker wavelet with a fundamental frequency of 2Hz (see Figures 2.3.3.9.10) show differences in the response of the system by varying the volumetric stiffness of the soft layer.

By comparing the K scheme (see Figure 2.3.3.9.10 a), for example, with the 10K one (see Figure 2.3.3.9.10 b), differences are evident in amplitude variations and signal duration inside caisson and at its lateral boundary.

In terms of vertical accelerations (see Figures 2.3.3.9.11), differences can be seen above all for signal durations, which are more sensible to the variation of scheme.

By increasing the volumetric stiffness, the soft caisson is less effective, due especially to the low compressibility of the lateral soft layers (as detected from the behaviour of the Kv scheme, similar to the K and 0.5K ones) which are subjected to compression because of vertical shear wave propagation. The higher the compressibility of the lateral layers the larger the decrease in horizontal dynamic actions in the soft caisson.

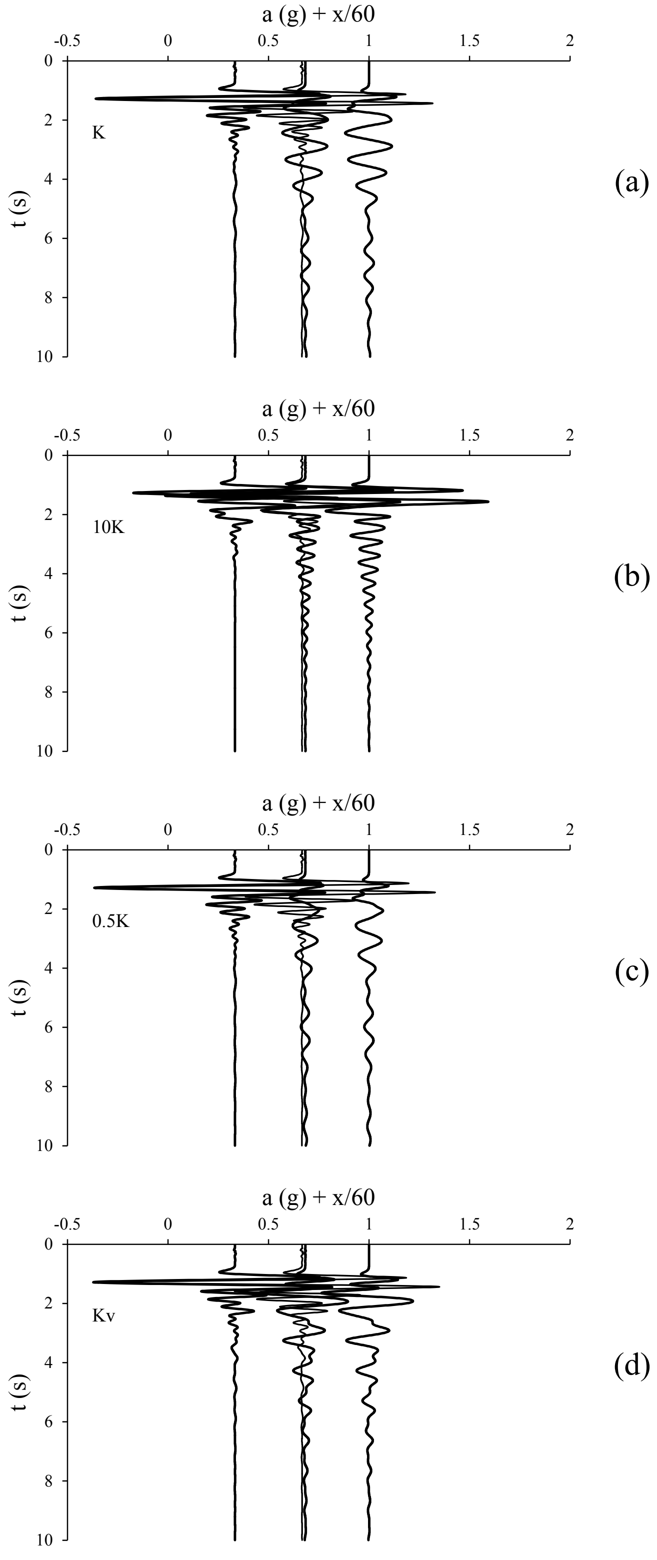

Figure 2.3.3.9.10 *Horizontal accelerations for different positions x at ground surface by propagating a Ricker wavelet with a fundamental frequency of 2Hz, for* $V_{s,g}$*= 20m/s and varying the volumetric stiffness K of the soft layers.*

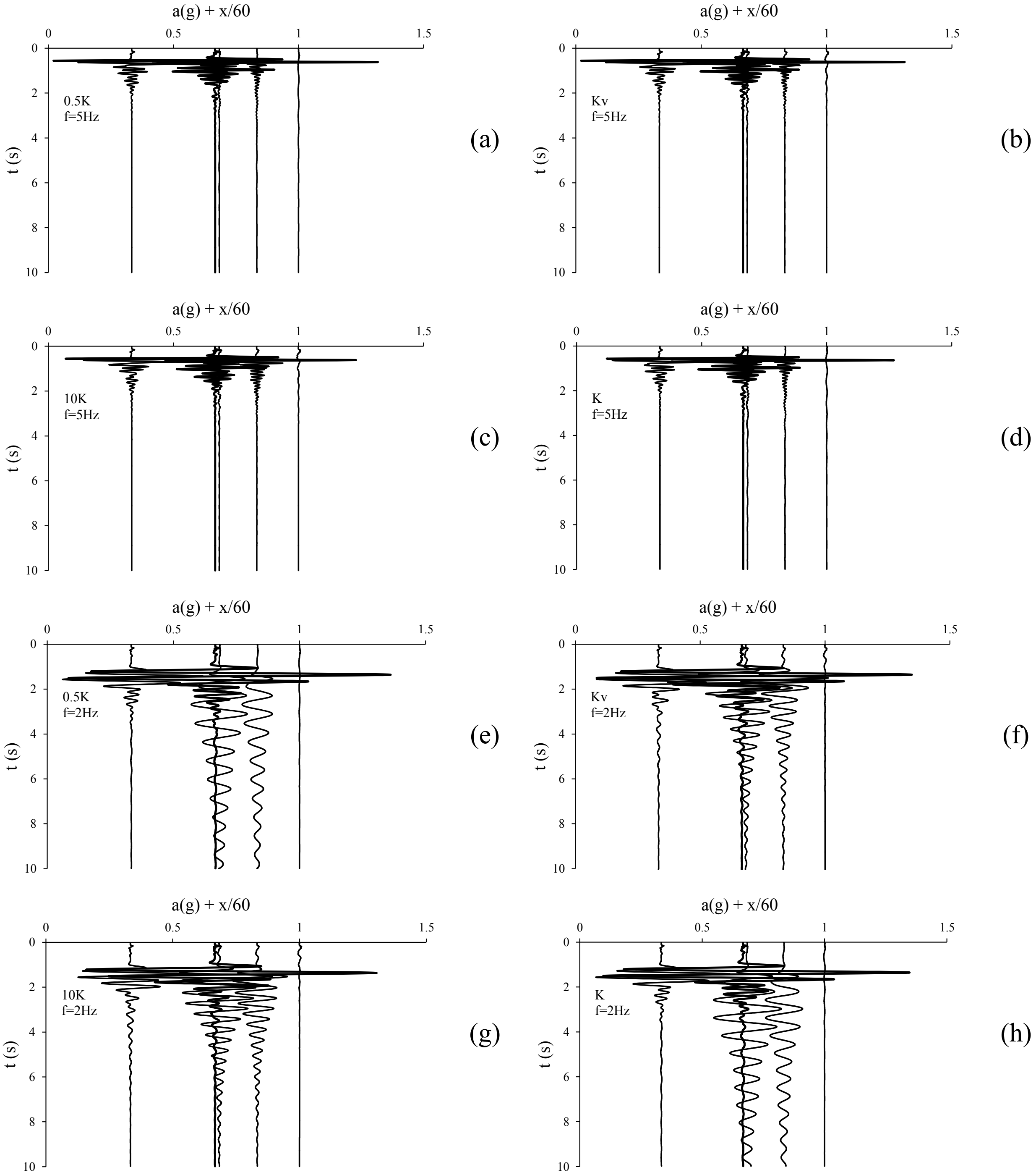

Figure 2.3.3.9.11 *Vertical accelerations for different positions x at ground surface by propagating a Ricker wavelet with a fundamental frequency of 5Hz (from a to d) and 2Hz (from e to h), for* $V_{s,g}$ *= 20m/s and varying the volumetric stiffness K of the soft layers.*

2.3.3.10 Effects of the constitutive model on the efficiency of the isolating box

The analyses reported in the previous pages have all been carried out considering the natural and grouted soils as linearly elastic materials. As a consequence, the results obtained were not affected by the amplitude of the dynamic excitation, in the sense that such an amplitude affected the absolute values of accelerations and displacements, but not the mechanical behaviour of the soft caisson, i.e. its effectiveness. In the case of elastic behaviour, the amplification ratio functions depend only on the geometrical configurations and mechanical properties of the layers which signals have been propagated through. However, such elastic analyses may be representative of the true behaviour of the system only for small amplitude seismic excitations. If amplitudes get larger, the true elasto-plastic behaviour of soils plays a role, and therefore has to be considered. In this case, the model introduced to this aim is a linear elastic-perfectly plastic model, with a Mohr-Coulomb failure criterion. As usual, the elastic part of the behaviour needs two parameters to be defined (for instance E and ν, or G and K), while the plastic one needs three more parameters: two (the cohesion c' and the shear strength angle φ') needed to define the position of the yield envelope (which coincides with the failure envelope in this case), and one (the dilatancy angle ψ) needed to define the flow rule, and therefore the direction of the plastic strain increment vector. The parameters adopted in the analyses described in this paragraph are reported in Tables 2.3.3.10.1 and 2.3.3.10.2. Two maximum amplitudes (0.05g and 0.5g) were then considered for every wavelet input frequency, in order to check the influence of the plastic behaviour of the natural and treated soil on the effectiveness of the soft caisson in filtering and reducing the dynamic effects in the protected soil mass and, specifically, in the considered control point CP.

Scheme	Model	Maximum Ricker wavelet Amplitude (g)
S	Linear Elastic	0.5
E		0.5
S*		0.05
E*		0.05
SP	Elasto Plastic	0.5
SP*		0.05
EP D5		0.5
EP D15		0.5
EP D5*		0.05
EP D15*		0.05

Table 2.3.3.10.1 *Scheme of the performed analyses.*

Material	V_S (m/s)	ν	G (MPa)	K (MPa)	φ' (°)
Soil	300	0.3	183.6	397.7	30
Soft layer	20	0.3	0.407	0.884	5/15

Table 2.3.3.10.2 *Materials mechanical properties.*

The acronyms “E” and “S” (see Table 2.3.3.10.1) indicate analyses in which the materials have an elastic behaviour; EP and SP are elasto-plastic analyses; starred acronyms define the analyses in which signals have a maximum amplitude equal to 0.05g. D15 and D5 indicate the analyses in which soft layers have been characterized with shear strength angles φ'_g equal to 15 and 5 degrees respectively. These values have been chosen on the basis of the results of the preliminary laboratory tests on some possible grouts to be used.

Figures 2.3.3.10.1 report the effects in the control point in terms of predominant (a) and mean periods (b), spectral intensities (c) and maximum accelerations (d) for the different schemes considered. In terms of predominant period and mean period, the behaviour seems to be similar in the elastic and elasto-plastic analyses, with the exception of the case f=0.1Hz for which the signals in the control point after treatment show lower periods for the elasto-plastic analyses.

In terms of accelerations, it is very interesting to notice that the more realistic elasto-plastic model leads to a better behaviour for the most critical frequencies ($f \leq 1$). In particular, even though the signal is not largely reduced, at least it is not as amplified as in the linear elastic analyses.

In this sense, the failure conditions act as a “safety valve” (Anastasopoulos, 2010). Also for starred analyses, the development of plastic points around the caisson reduces the maximum accelerations, because of the plasticization of the soft layers also in the case of φ'_g=15°.

In Figure 2.3.3.10.2 the amplification ratios for soil (a), and schemes with soft caisson for f=1Hz (b and d) and f=5Hz (c and e) are reported. As expected, amplification ratios depend on the characteristics of the propagated signal. This observation is extremely clear by looking at the Figures 2.3.3.10.2 b and c where amplification ratio for f=1Hz and 5Hz are reported. The former amplifies the frequencies higher than 1Hz; vice versa the latter amplifies the frequencies lower than 1Hz, as also shown in Figures 2.3.3.10.2 d and e, where amplification ratios are considered between the ground level and the upper part of the horizontal soft layer.

Differences can be found for soil schemes too (Figure 2.3.3.10.2 a); generally speaking, starred schemes amplify frequencies which are not amplified by linear elastic schemes, but tend to energize the elastic resonance frequencies.

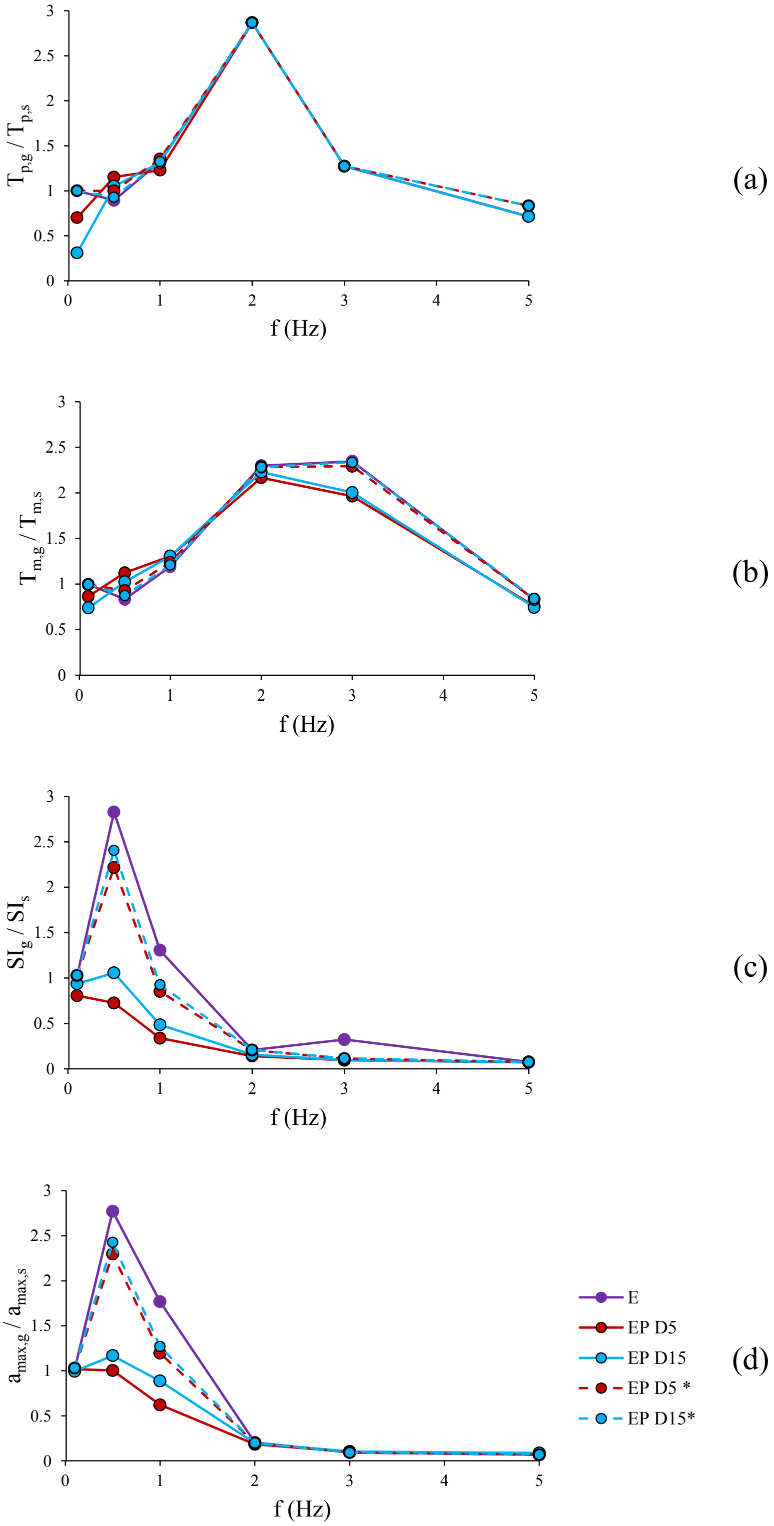

Figure 2.3.3.10.1 *Effects, in the control point, in terms of predominant (a) and mean periods (b), spectral intensities (c) and maximum accelerations (d by varying the shear resistance of the soft layers.*

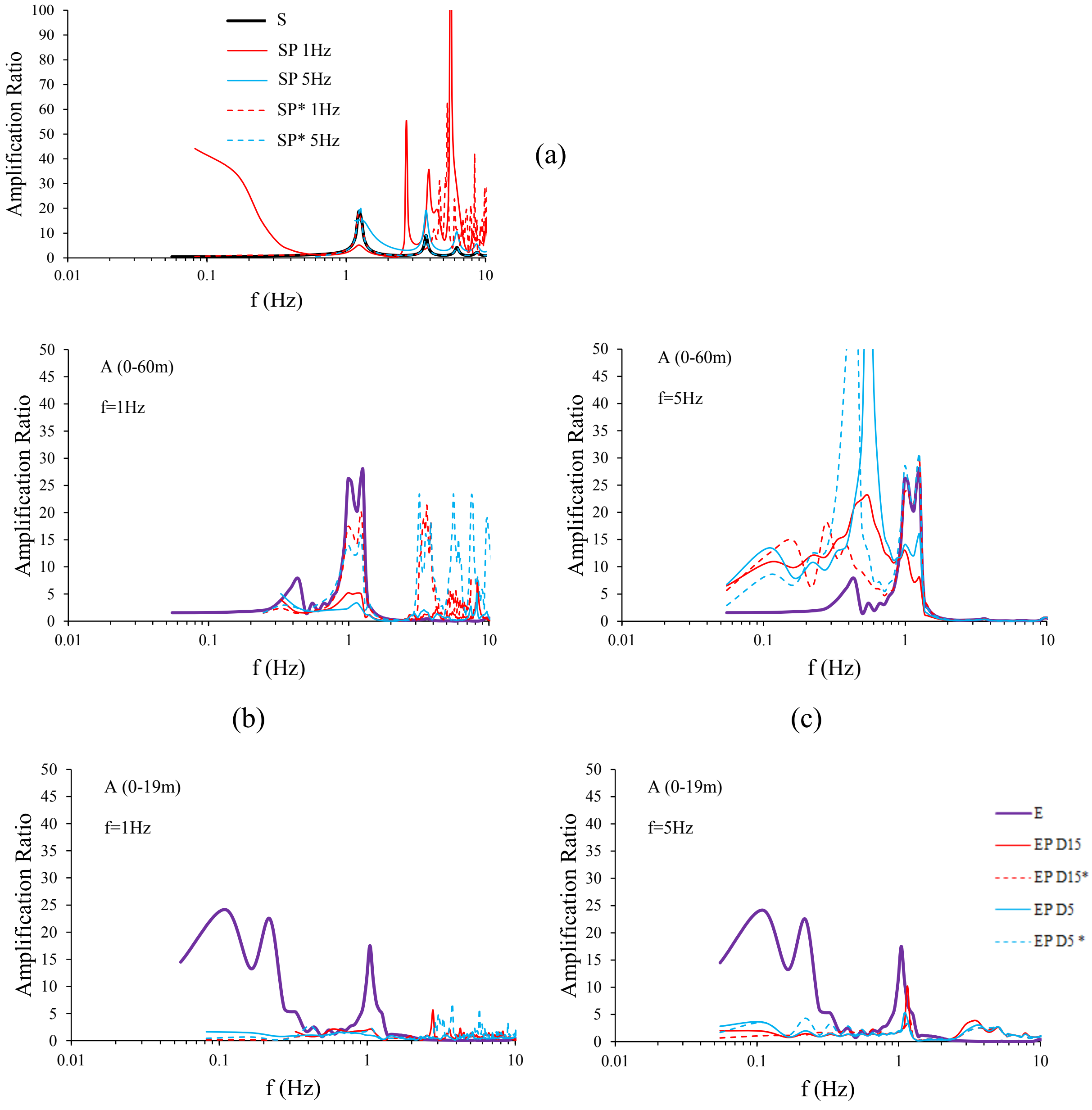

(d) (e)

Figure 2.3.3.10.2 *Amplification ratios for the soil deposit (a), and for the soft caisson schemes, for f=1Hz (b and d) and f=5Hz (c and e).*

The positive effect of the elasto-plastic behaviour of materials is confirmed in terms of maximum horizontal both accelerations and displacements. Figures 2.3.3.10.3 show the maximum effects along the central vertical by introducing the soft caisson, i.e. the maximum accelerations (a) and displacements (b) for f=1Hz and the maximum accelerations (a) and displacements (b) for f=5Hz.

For f=1Hz, the reductions in terms of maximum effects of the elasto-plastic models with respect to the linear elastic one are extremely significant. For f=5Hz, as reported in Figures 2.3.3.10.1 too, the differences are limited along the central vertical axis, but are significant on the area of intersection between the vertical diaphragms of the soft caisson and the ground level (named “edges” in the following) in terms of displacements (see Figures 2.3.3.10.4d).

At the ground level and for f=1Hz, the failures limit the horizontal displacements and acceleration to ratios close to 1.

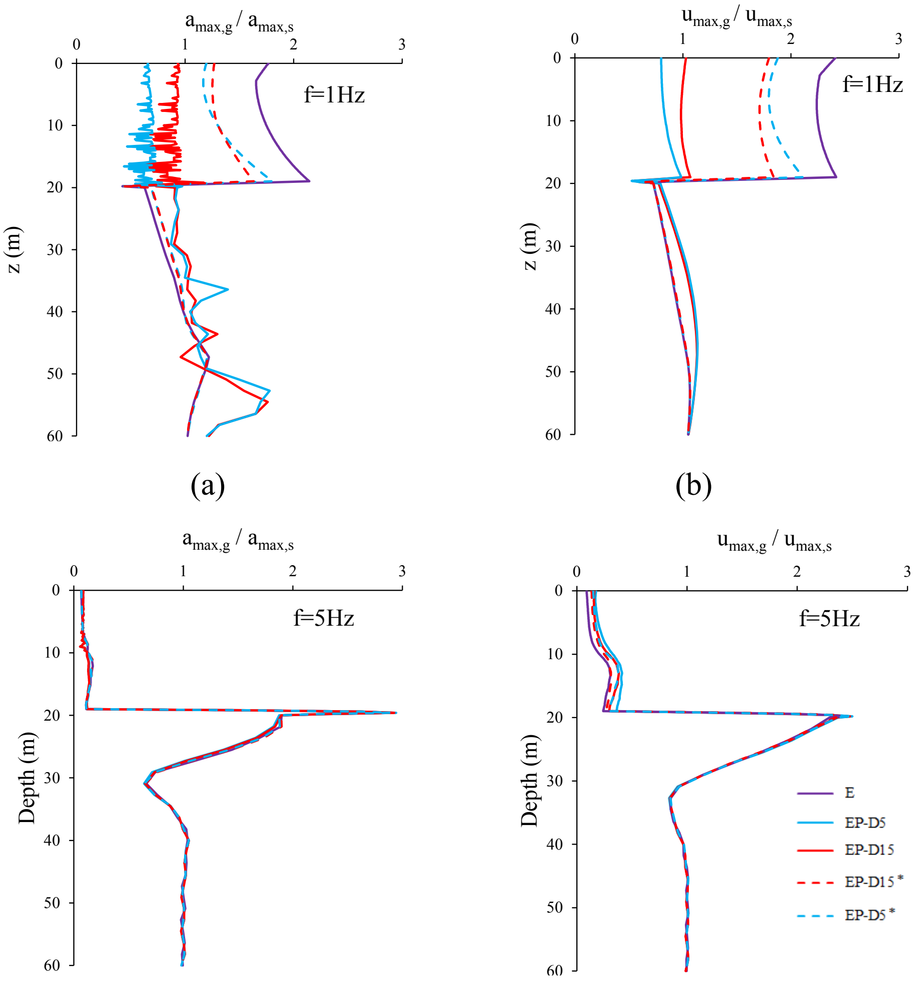

(a) (b)

(c) (d)

Figure 2.3.3.10.3 *Maximum effects along the central vertical axis by introducing the soft caisson: maximum accelerations (a) and displacements (b) for f=1Hz; maximum accelerations (c) and displacements (d) for f=5Hz.*

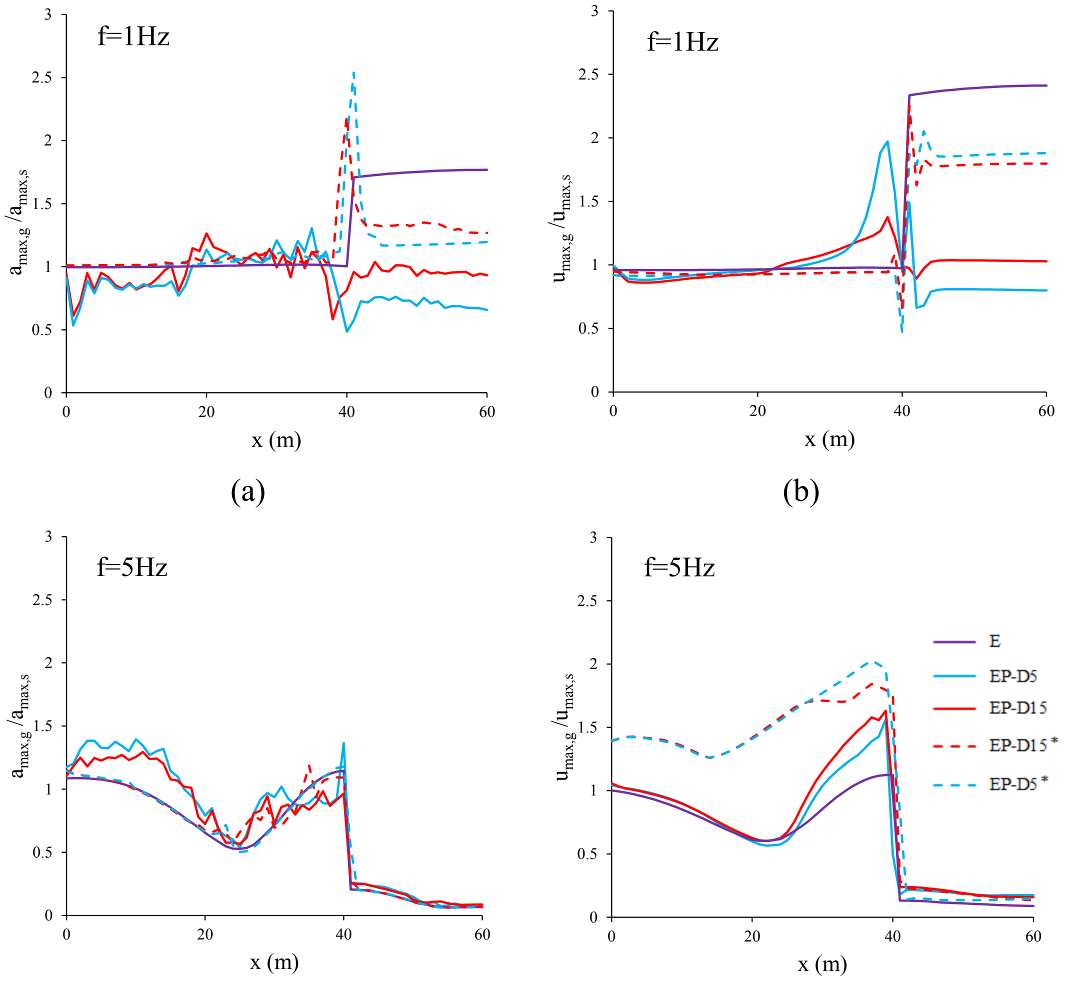

(a) (b)

(c) (d)

Figure 2.3.3.10.4 *Maximum effects at ground surface at the left side of the central vertical by introducing the soft caisson: maximum accelerations (a) and displacements (b) for f=1Hz; maximum accelerations (a) and displacements (b) for f=5Hz.*

A better behaviour for f=1Hz is observed in terms of E_I too (see Figure 2.3.3.10.5): EP schemes amplify the ranges of efficiency of the treatment, whereas EP* schemes seem to de-amplify the periods which are protected and tend to improve security on higher periods. For f=5Hz, no sensible differences are observed both for EP and EP* schemes.

The consideration of the elasto-plastic behaviour of soils causes the development of both horizontal and vertical residual displacements, which are displacements whose values differ from zero after the ending of the dynamic excitation.

The calculated signals may suffer problems due to unrealistic high frequencies contents or they may show incongruent displacements behaviour trends, which could be incompatible with the ending of the signal, i.e. the displacements may show drifts with respect to the final values even if the dynamic excitation is ended.

Signals have been therefore filtered by using a 15Hz low-pass Butterworth filter (Butterworth, 1930), a type of signal processing filter designed to have as flat a frequency response as possible in the range of frequencies that can pass through a filter without being attenuated.

Figures from 2.3.3.10.6 to 2.3.3.10.9 report the accelerations and the displacements calculated in the control point for the schemes called S, EP D5 and EP D15 by varying the frequency of the signal propagated (1, 3 and 5Hz). When the oscillations end, residual displacements can be observed, especially for horizontal ones. By observing Figures 2.3.3.10.7, it is clear that residual displacements, after the introduction of the soft caisson, are of the same order of magnitude of the S schemes. The major displacements can be observed for f=1Hz in terms of vertical displacements too.

The reported schemes may be subjected to numerical errors because the trend of the residual displacements is not always constant, as reported in Figures 2.3.3.10.9, where graphs relative to f=1Hz for EP D5 (b) and EP D15 (c) show some discrepancies. Generally speaking, an increase in signal time duration from the starting of the dynamic action to the ending of oscillation may be observed when soft caisson induces resonant phenomena with the propagated signal (f=1Hz). Schemes called EP D5 seem to be more efficient in decreasing maximum accelerations and displacements with time with respect to EP D15 schemes.

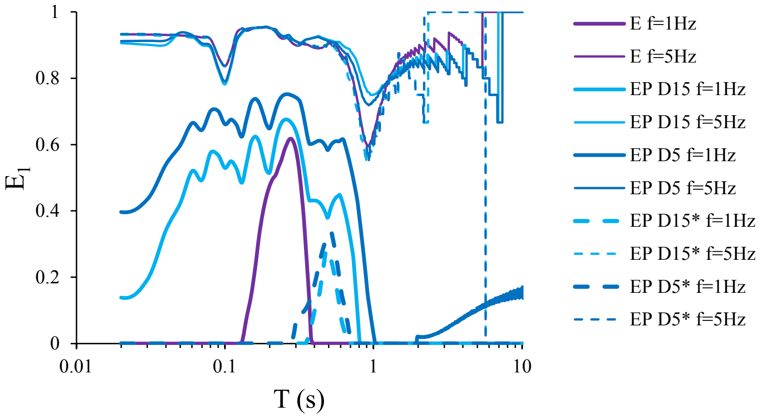

Figure 2.3.3.10.5 *Efficiency parameter* E_I *for different analyses schemes.*

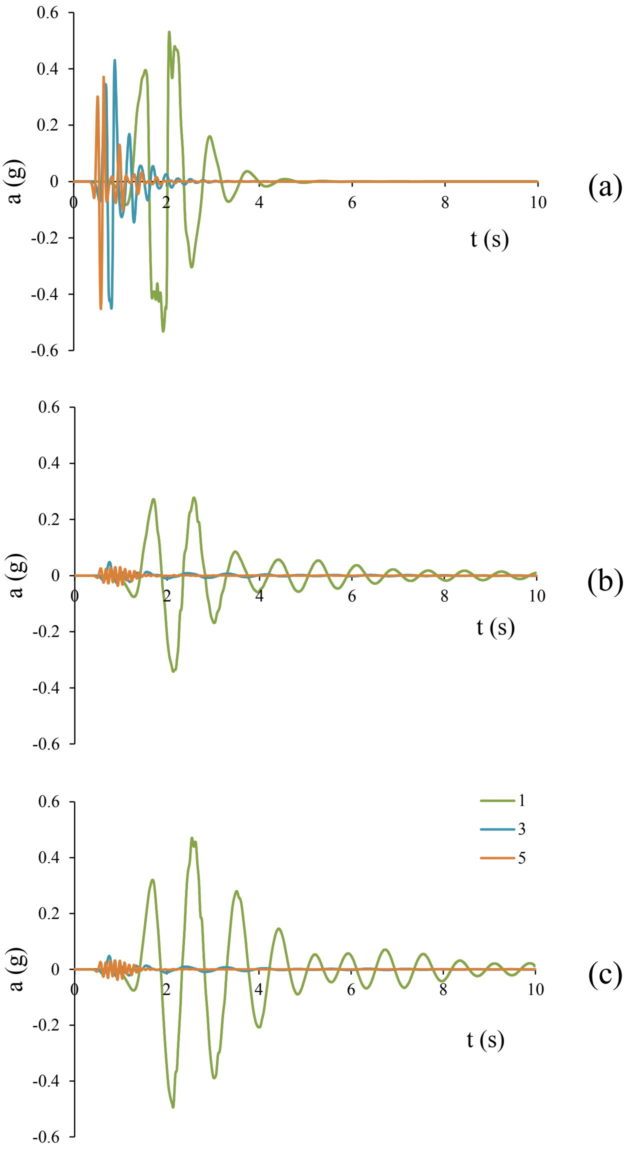

Figure 2.3.3.10.6 *Horizontal accelerograms calculated in the control point by varying the frequency of the signal propagated (f = 1, 3 and 5Hz), adopting an elasto-plastic model for schemes S (a), EP D5 (b) and EP D15 (c).*

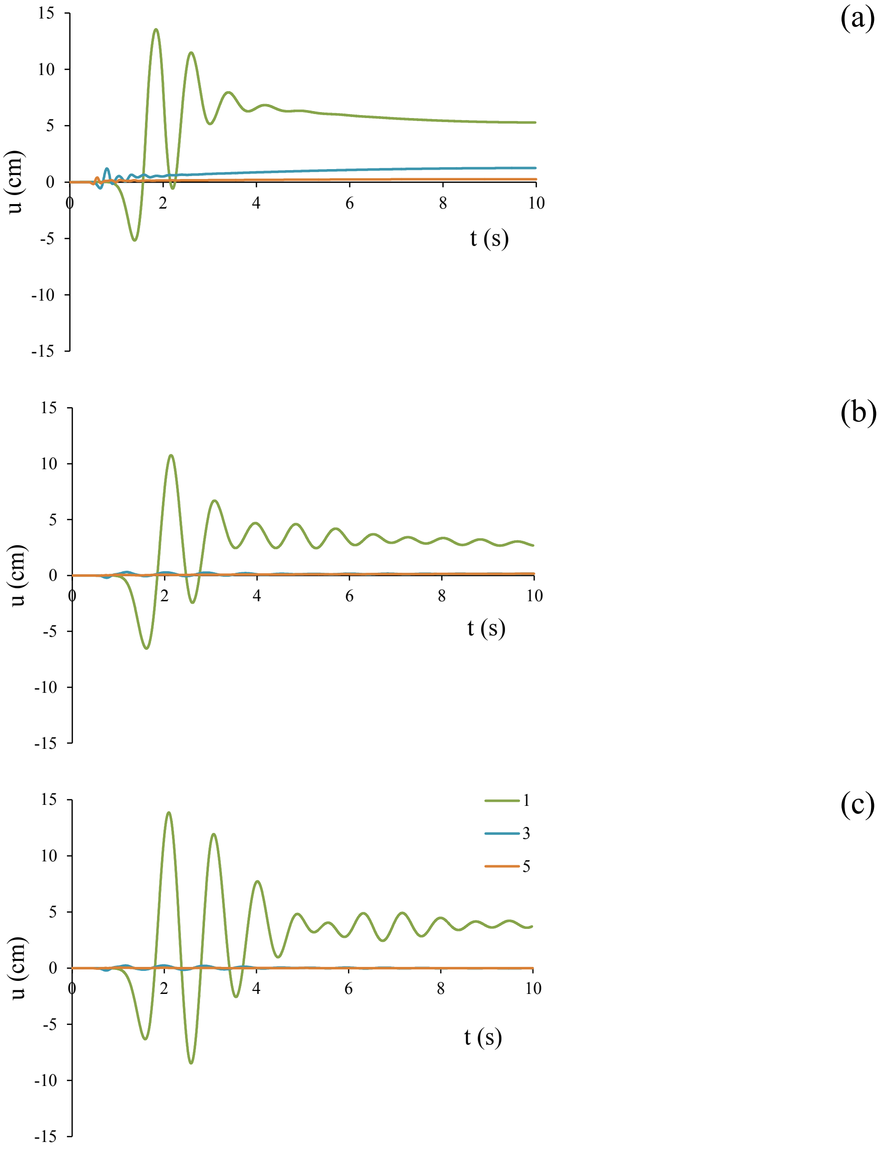

Figure 2.3.3.10.7 *Horizontal displacements calculated in the control point by varying the frequency of the signal propagated (f =1, 3 and 5Hz), adopting an elasto-plastic model for schemes S (a), EP D5 (b) and EP D15 (c).*

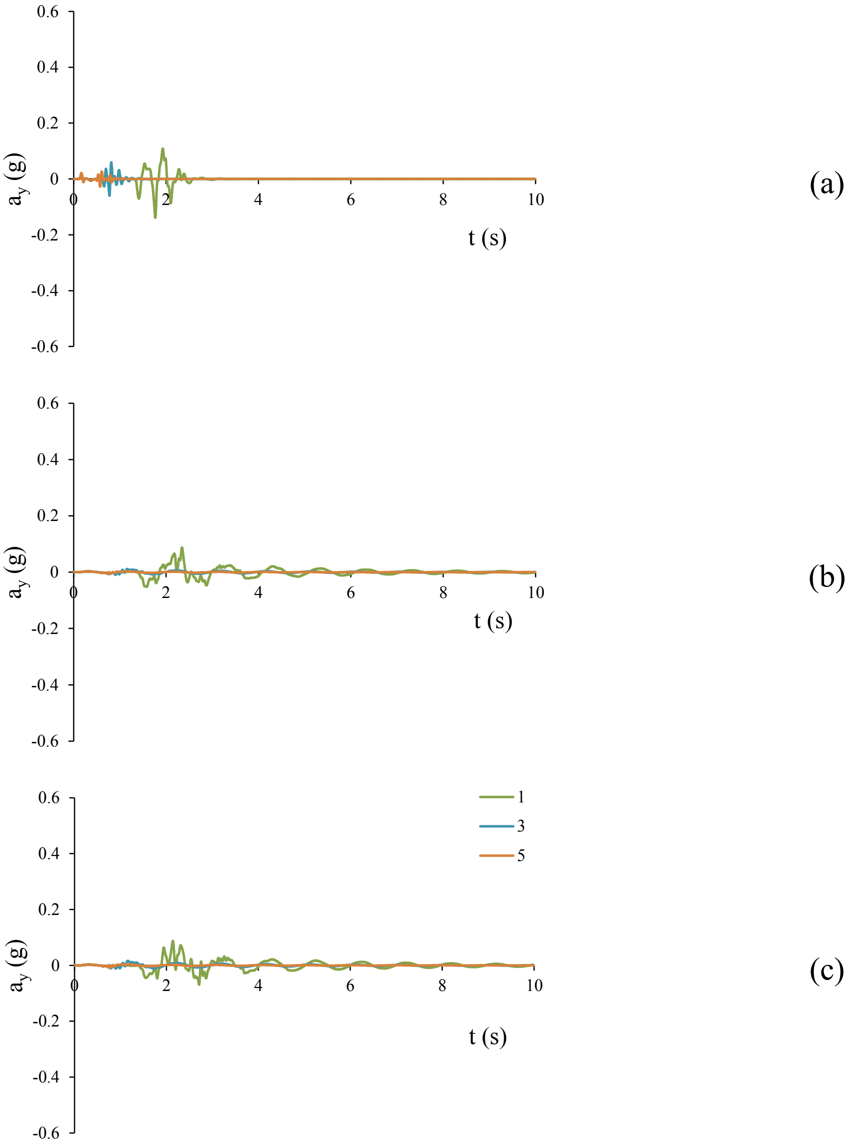

Figure 2.3.3.10.8 *Vertical accelerations calculated in the control point by varying the frequency of the signal propagated (f = 1, 3 and 5Hz), adopting an elasto-plastic model for schemes S (a), EP D5 (b) and EP D15 (c).*

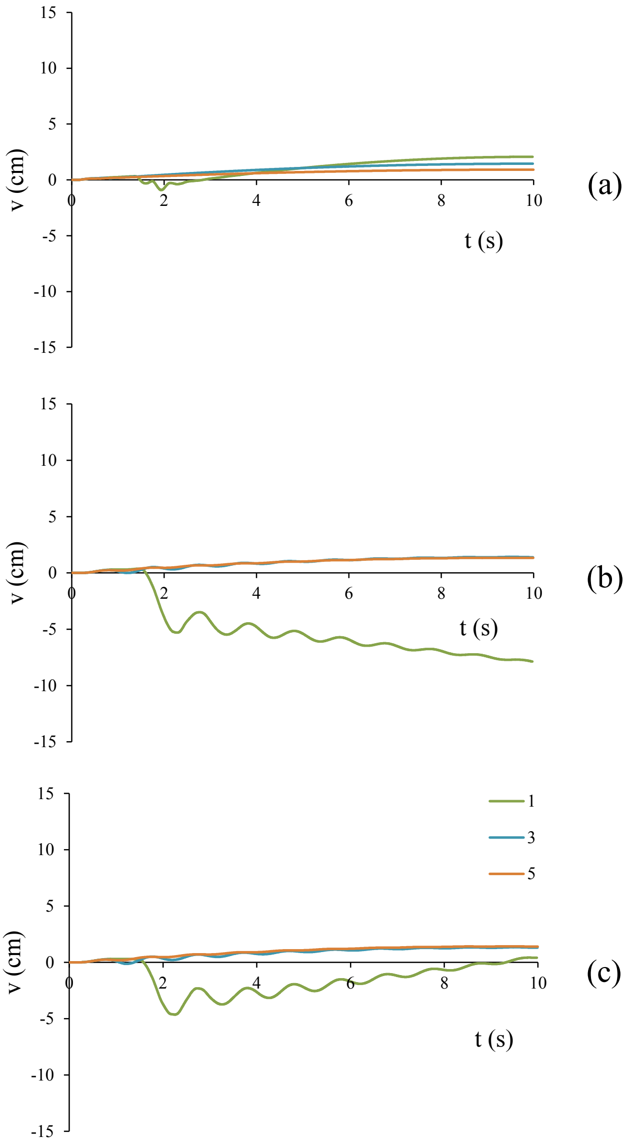

Figure 2.3.3.10.9 *Vertical displacements calculated in the control point by varying the frequency of the signal propagated (f = 1, 3 and 5Hz), adopting an elasto-plastic model for schemes S (a), EP D5 (b) and EP D15 (c).*

Figures from 2.3.3.10.10 to 2.3.3.10.17 report the accelerations and the displacements with time referred to different positions at ground surface, for f=1Hz and f=5Hz. In terms of horizontal (x) accelerations, for f=1Hz, i.e. resonance conditions, out of the soft caisson (x=20m), accelerations with time are similar between S scheme and EP ones. On the edges of the soft layer (x=40m and 41m), EP accelerations show a behaviour more complex than the S one, probably due to the various reflection effects of the waves propagating from and to the isolating box. Inside the caisson (x=50m and 60m), the amplitudes are similar but EP accelerations have a duration larger than the S one. This result is encouraging because in resonance conditions too the proposed treatment has not detrimental effects. For f=5Hz, which is a condition far from resonance, for x=20m and 40m, the accelerations in the S and EP schemes are similar. For x=41m, accelerations are still lower than S one. Signals have oscillations around very low values and rapidly tend to zero. In terms of horizontal displacements, for x=20m and f=1Hz, EP schemes show larger residual displacements but maximum ones similar to the ones pertaining to the S scheme. For x=40m and 41m, EP schemes tend to increase displacements, whereas for x=50m and 60m dynamic actions are reduced. For f=5Hz residual displacements seem to be larger outside and on the edges of the soft caisson, but they drastically reduce inside.

As far as the vertical (y) direction is concerned, for f=1Hz the EP schemes show higher values in terms of accelerations and displacements outside and on the sides of the caisson, with extremely high increments on the zone just around the boundary of the caisson. For x=50m, the effects are still higher and similar to the S scheme. For x=60m, vertical acceleration and vertical displacement amplitudes for the S and EP schemes are similar; EP schemes show a higher time duration for the signals. For f=5Hz, for x=20m and 40m EP schemes record slightly higher vertical acceleration and vertical displacement values, whereas for x=41m they show amplitudes similar to the condition of no treatment. For x=50, the signals have a similar amplitude, but EP schemes show higher time durations.

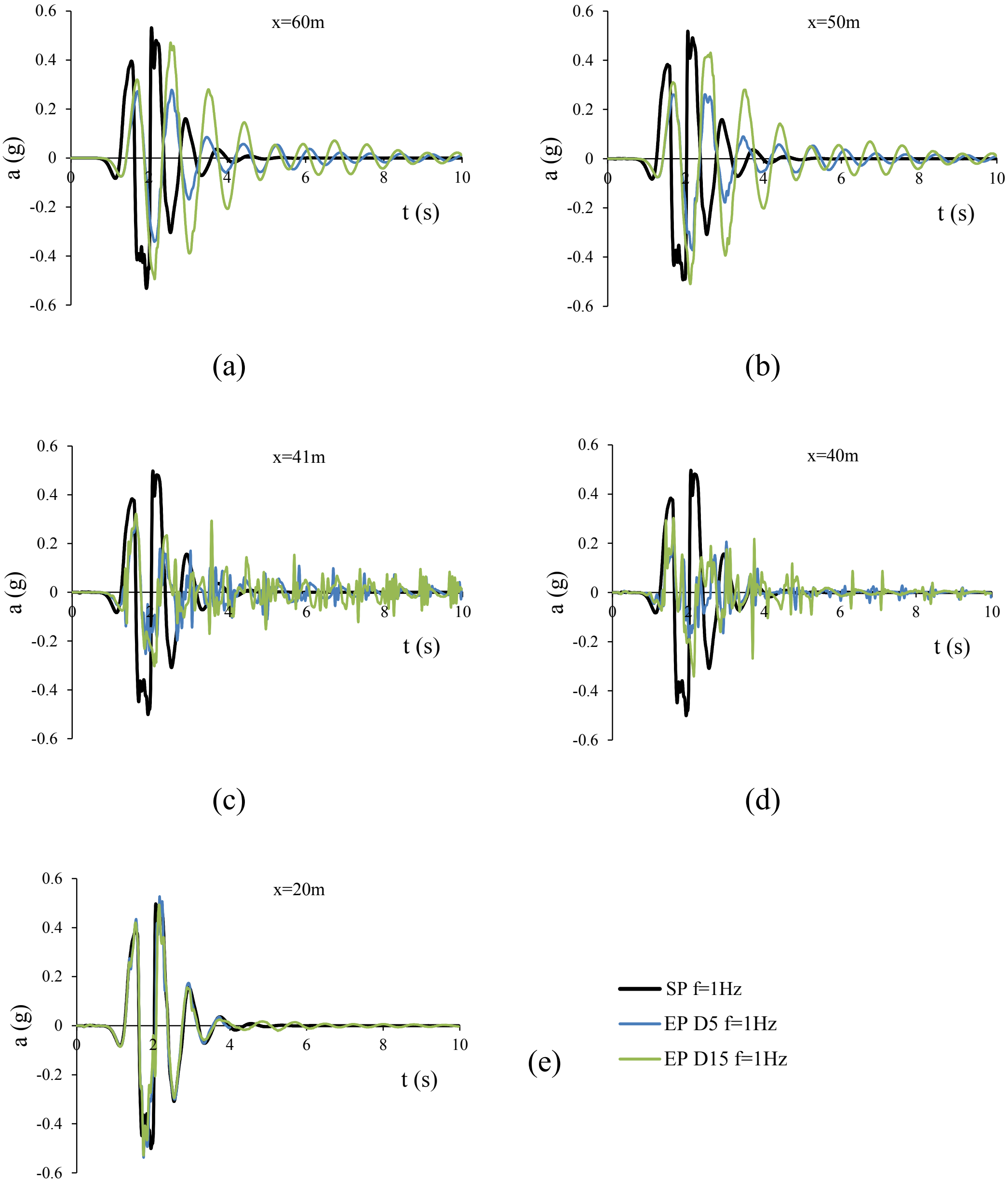

(a)

(b)

(c)

(d)

(e)

Figure 2.3.3.10.10 *Horizontal accelerations in different points at ground level for f=1Hz, adopting an elasto-plastic model for schemes SP (a), EP D5 (b) and EP D15 (c).*

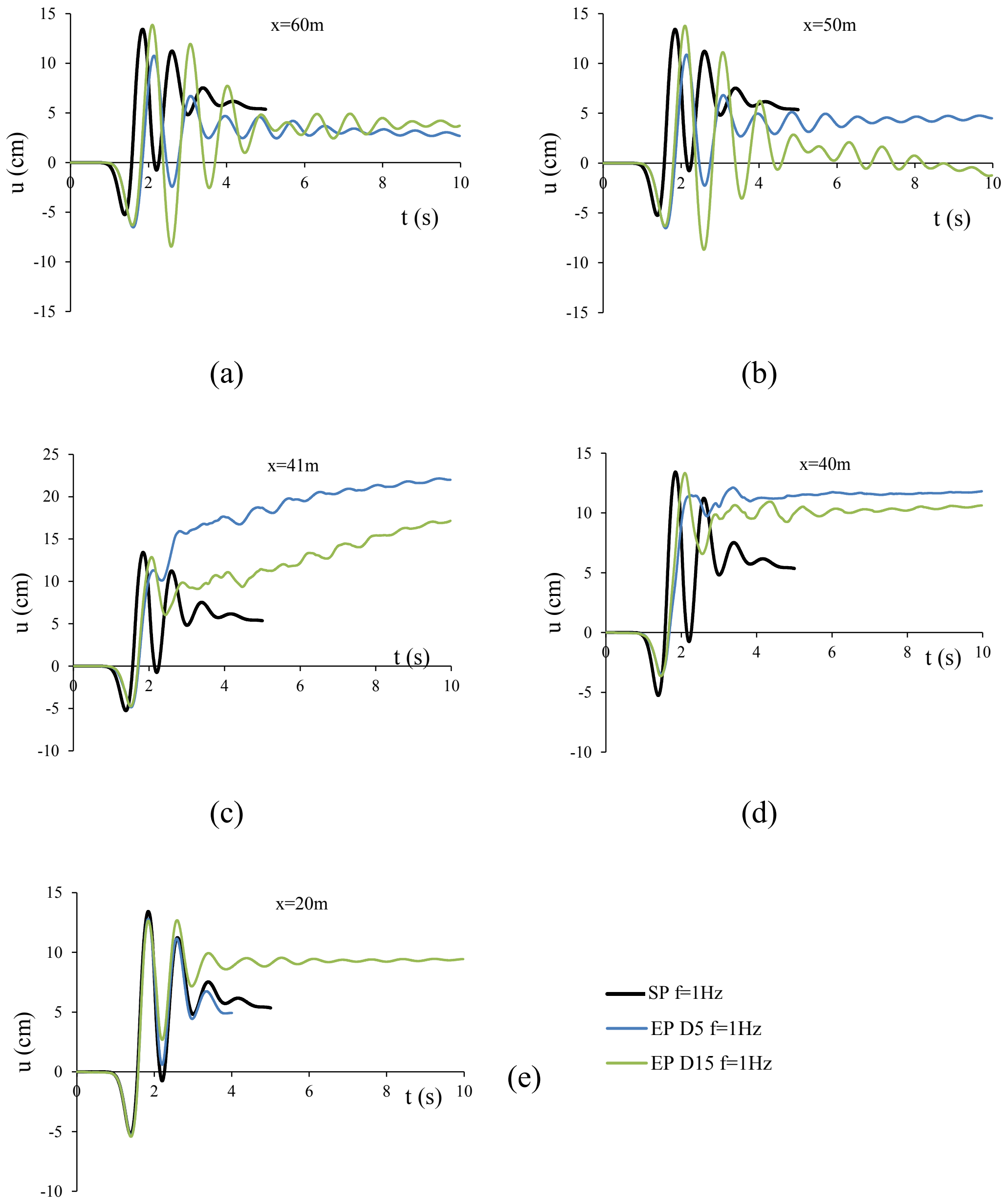

(a)

(b)

(c)

(d)

(e)

Figure 2.3.3.10.11 *Horizontal displacements calculated in different points at ground level for f=1Hz, adopting an elasto-plastic model for schemes SP (a), EP D5 (b) and EP D15 (c).*

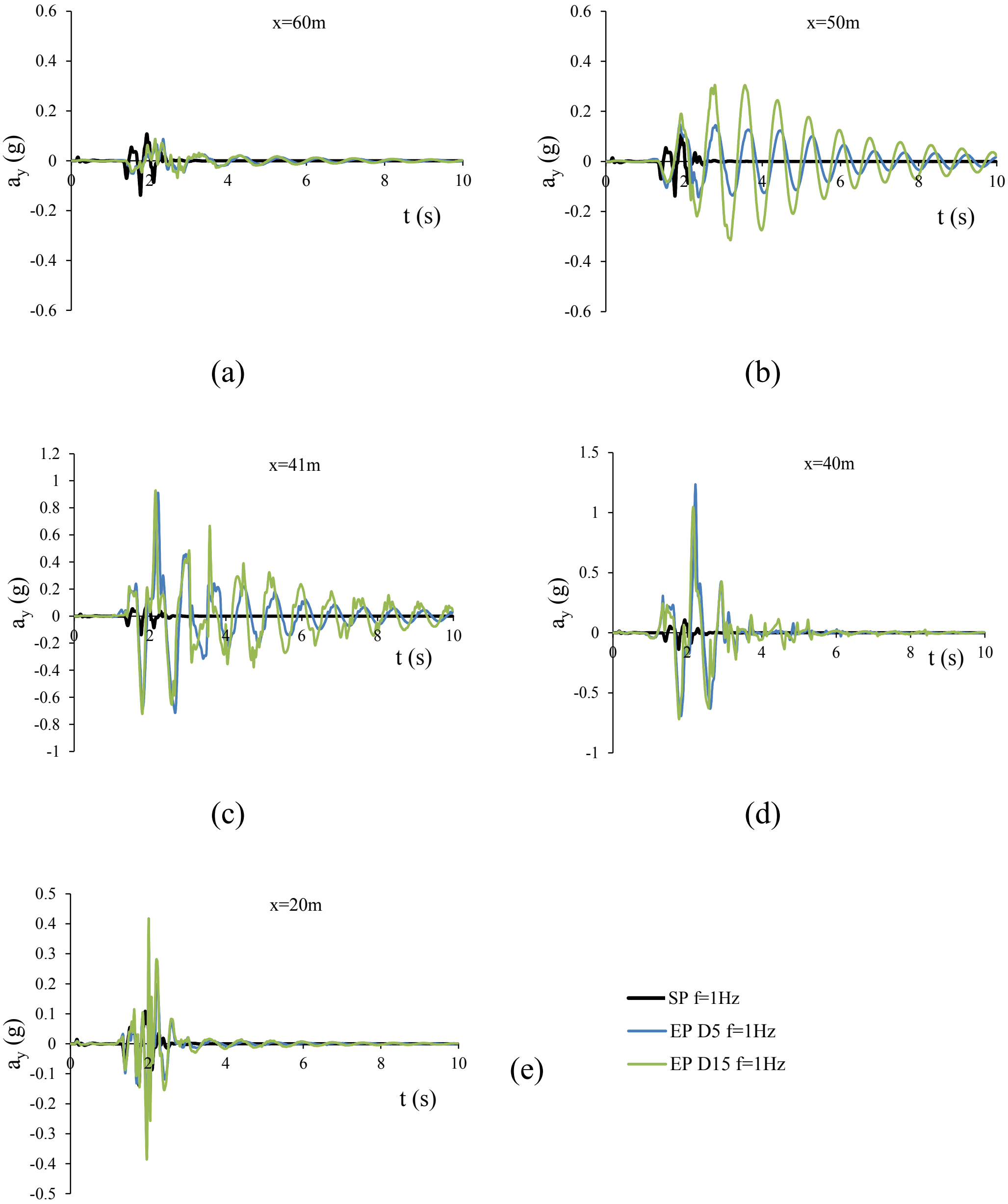

(a) (b)

(c) (d)

(e)

Figure 2.3.3.10.12 *Vertical accelerations calculated in different points at ground level for f=1Hz, adopting an elasto-plastic model for schemes SP (a), EP D5 (b) and EP D15 (c).*

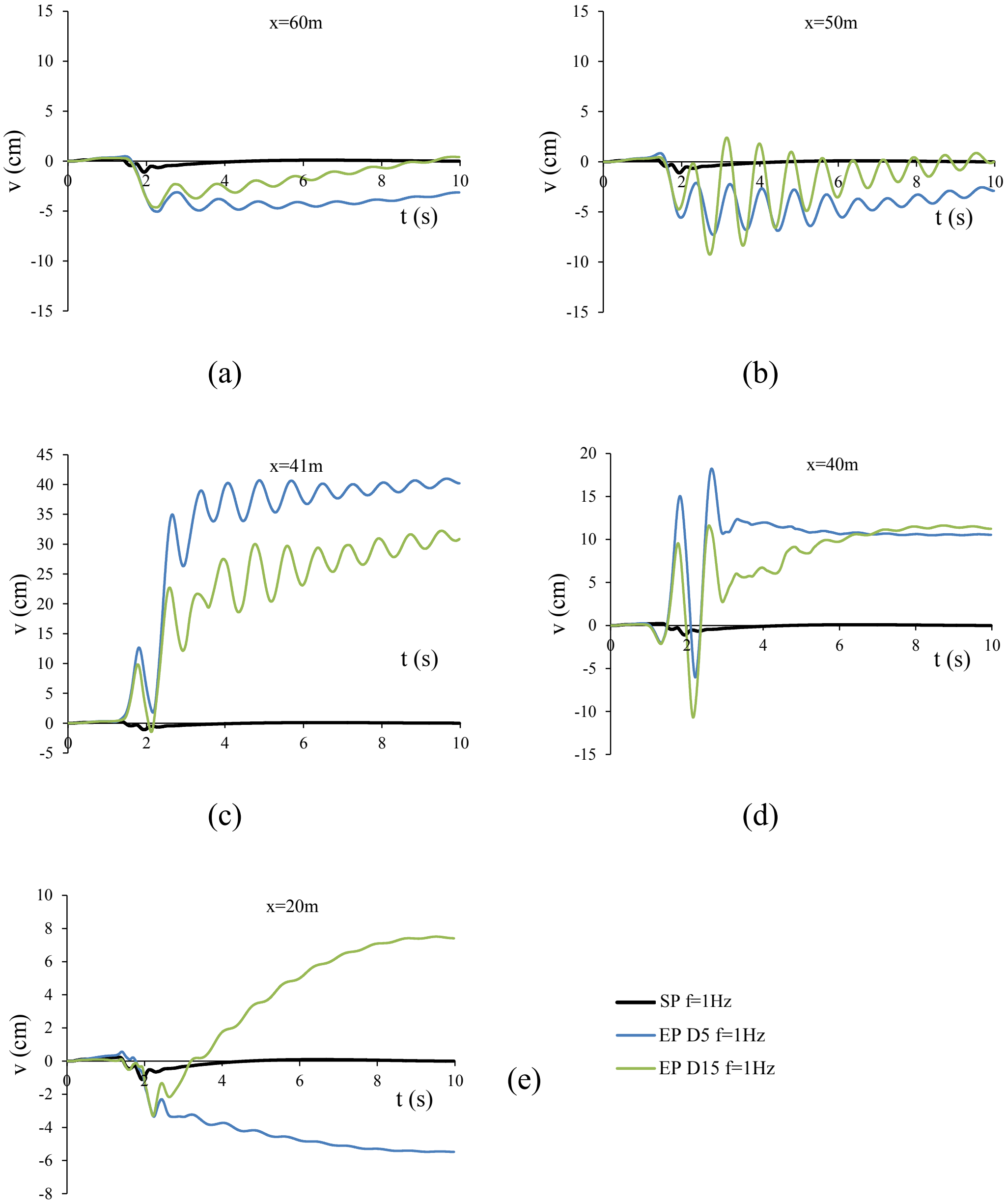

(a) (b)

(c) (d)

(e)

Figure 2.3.3.10.13 *Vertical displacements calculated in different points at ground surface for f=1Hz, adopting an elasto-plastic model for schemes SP (a), EP D5 (b) and EP D15 (c).*

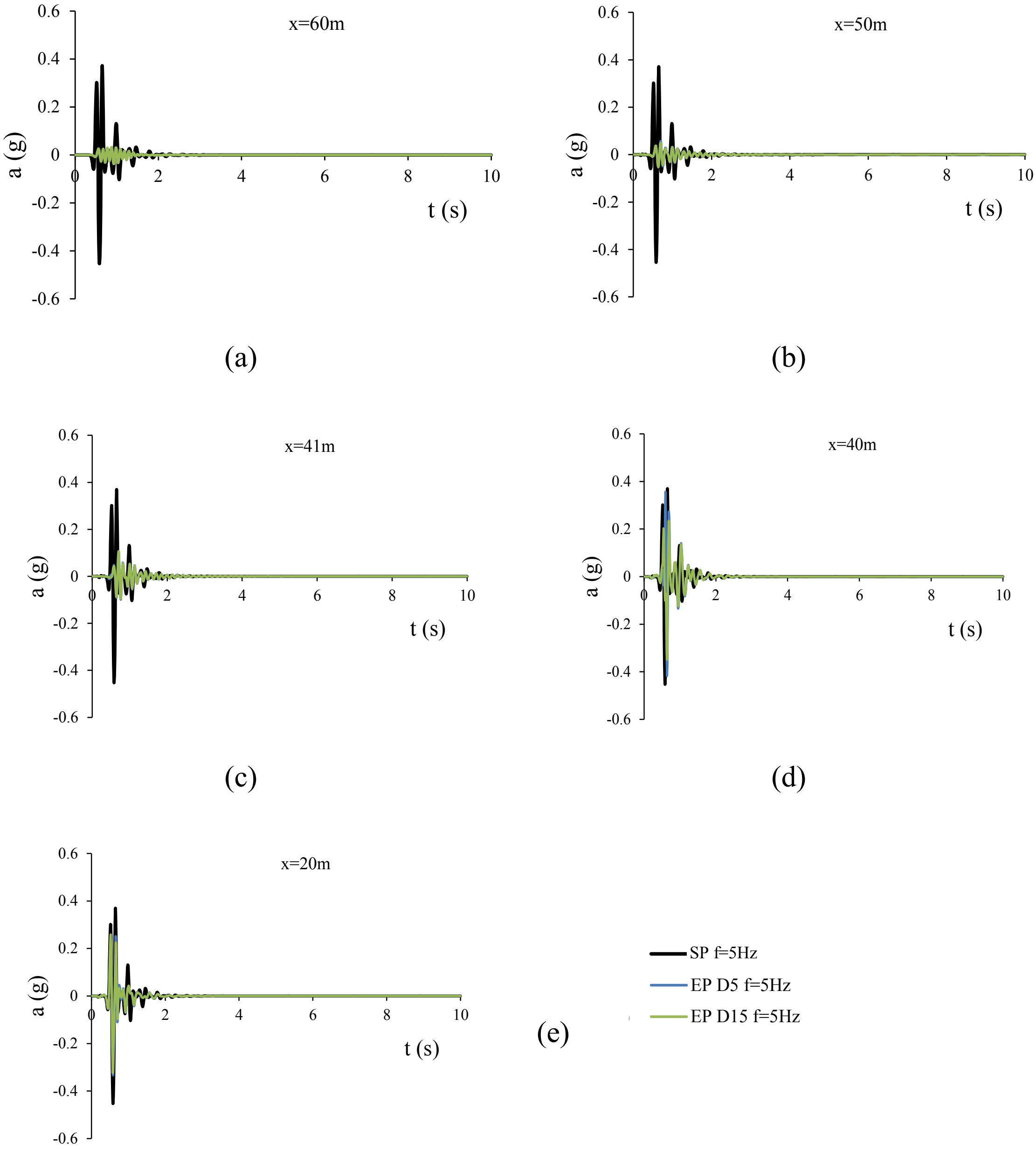

(a) (b) (c) (d) (e)

Figure 2.3.3.10.14 *Horizontal accelerations calculated in different points at ground surface fo f=5Hz, adopting an elasto-plastic model for schemes SP (a), EP D5 (b) and EP D15 (c).*

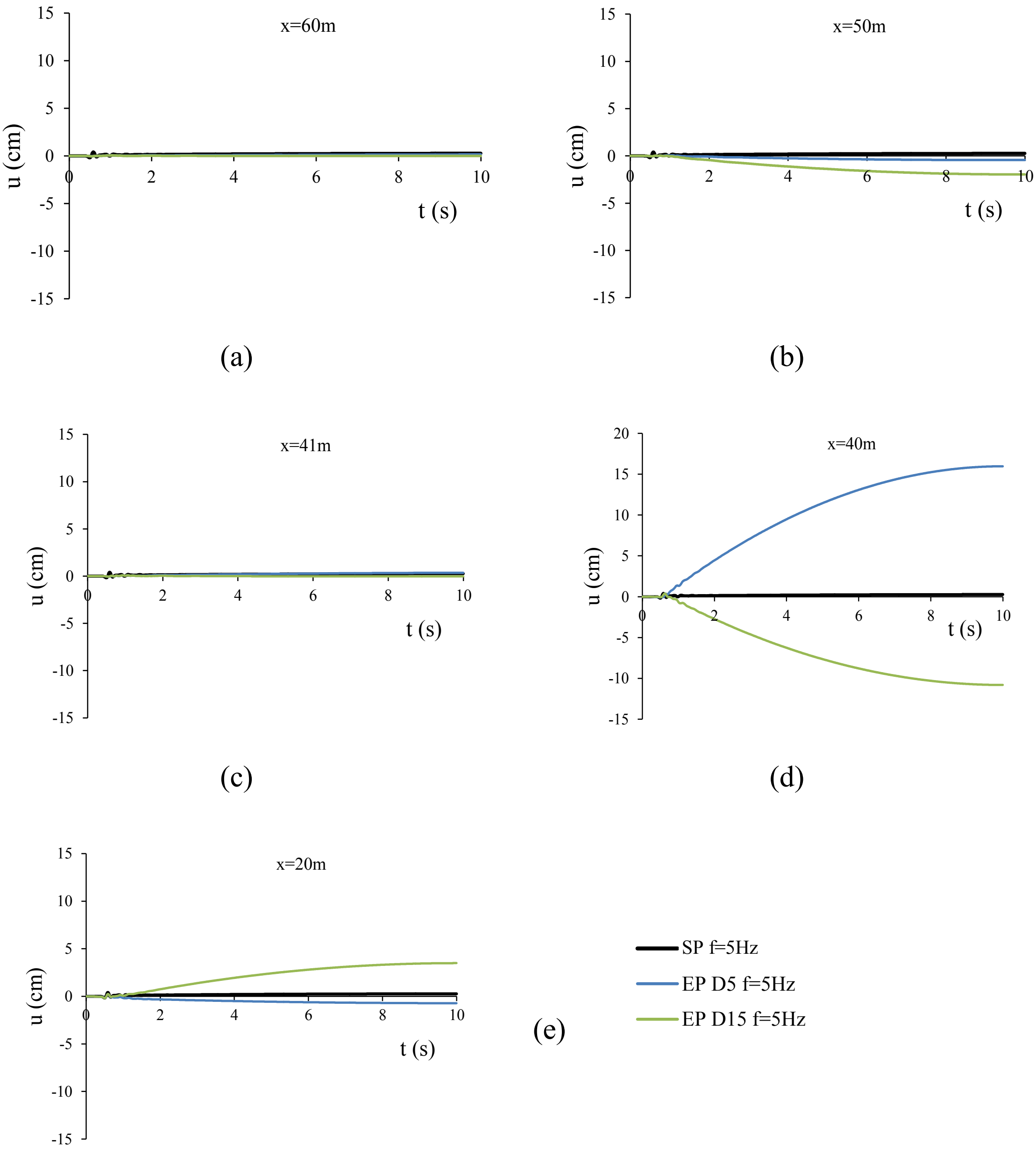

(a) (b) (c) (d) (e)

Figure 2.3.3.10.15 *Horizontal displacements calculated in different points at ground surface for f=5Hz, adopting an elasto-plastic model for schemes SP (a), EP D5 (b) and EP D15 (c).*

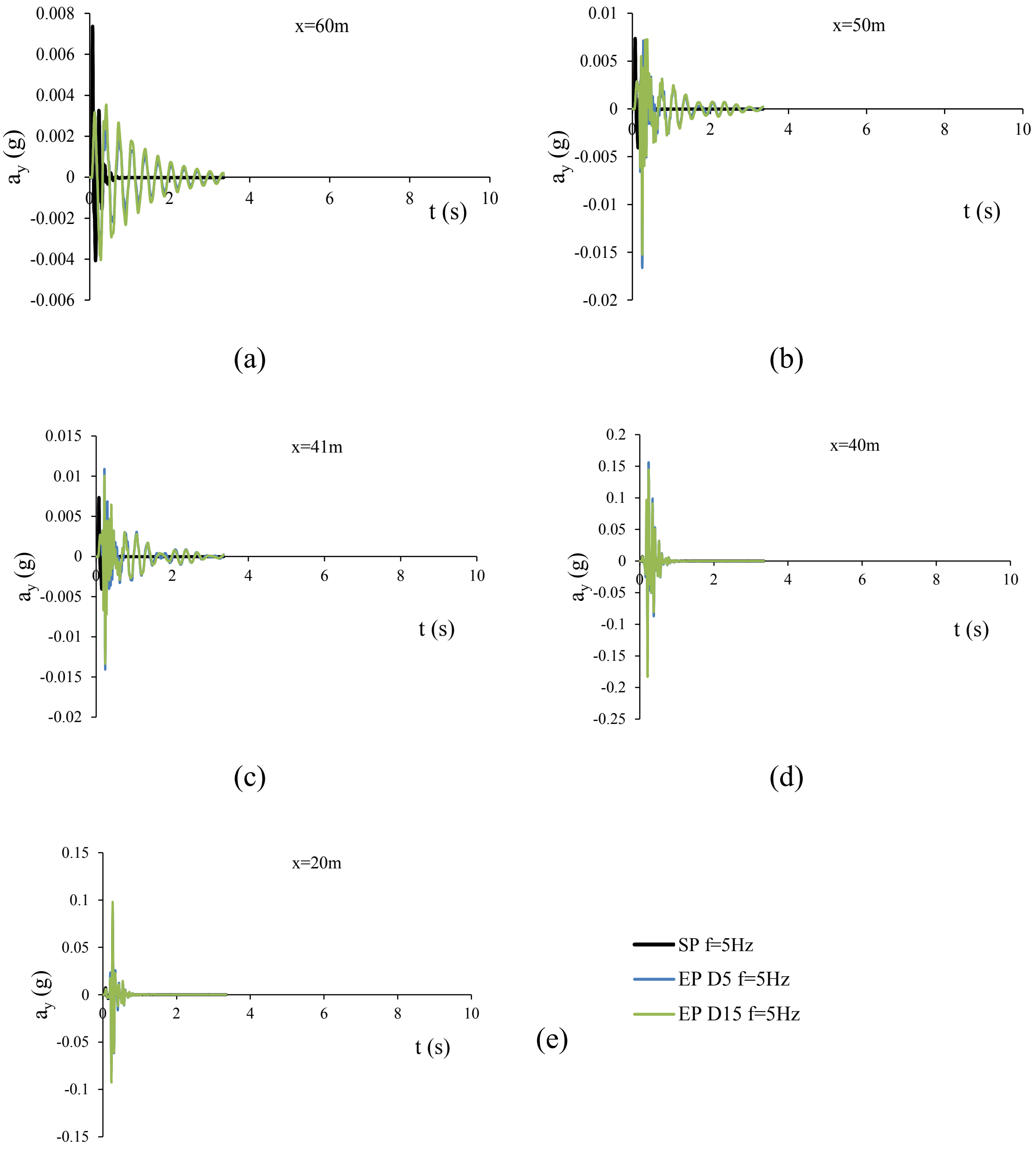

Figure 2.3.3.10.16 *Vertical accelerations calculated in different points at ground surface for f=5Hz, adopting an elasto-plastic model for schemes SP (a), EP D5 (b) and EP D15 (c).*

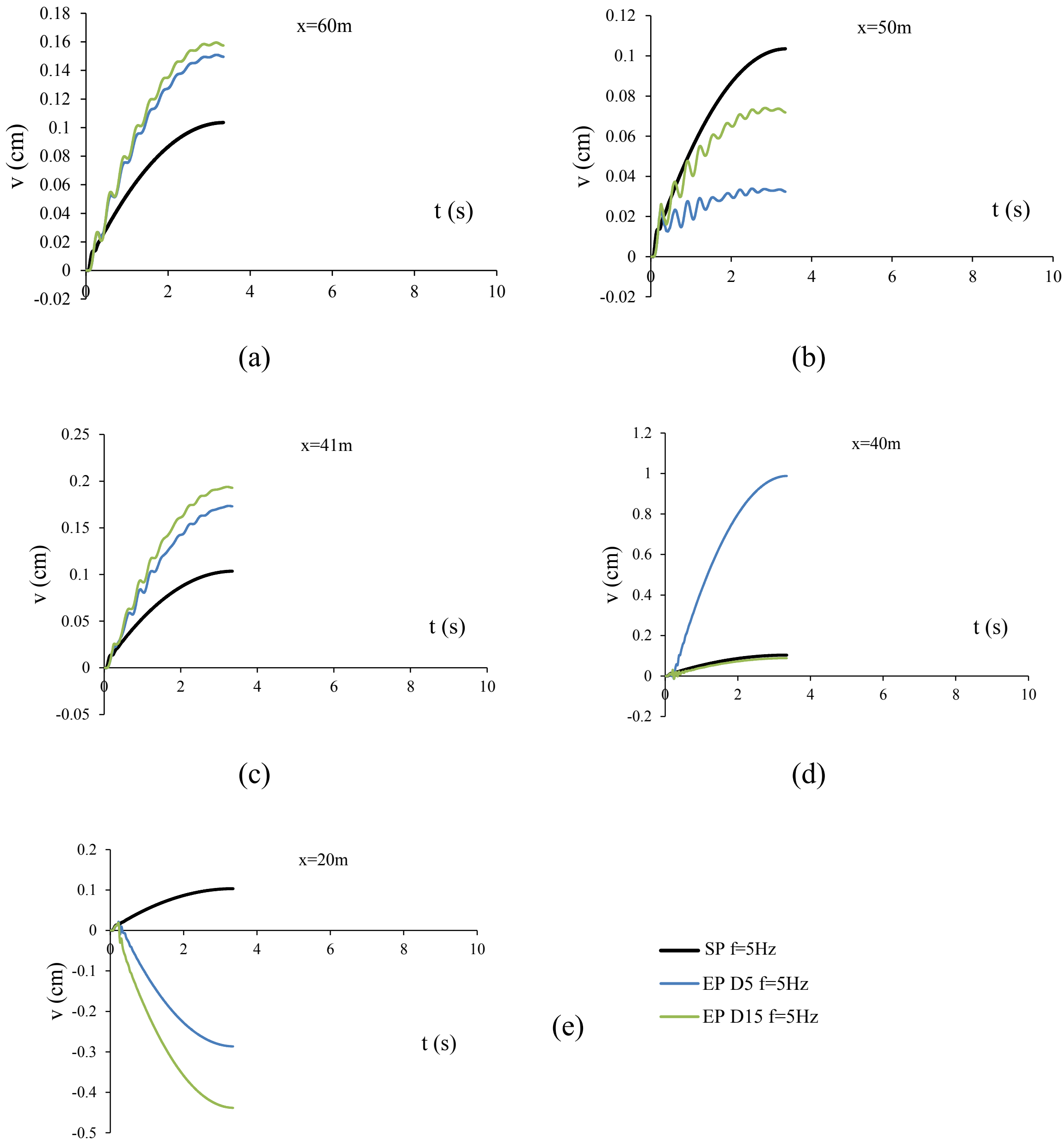

Figure 2.3.3.10.17 *Vertical displacements calculated in different points at ground surface for f=5Hz, adopting an elasto-plastic model for schemes SP (a), EP D5 (b) and EP D15 (c).*

2.3.4. Soft Caisson: inclined injections

The second geometrical configuration taken into account is reported in Figures 2.3.4.1: two inclined injections are enclosed into the soil layer to form a V-shaped soft caisson. This scheme is certainly more feasible than the rectangular caisson from a technical point of view, and it is therefore of extreme practical interest. In all the analyses, the soft layers have been assumed with a constant value of thickness (1m). The analyses involve a large computational effort, because of the reduced dimensions of the mesh elements necessary to properly define the geometry (as reported, for example, in Figure 2.3.4.1a), with the constraints posed by the discretization rules (see §2.3.1).

The indications provided by the analyses carried out on rectangular soft caissons have been considered to finalize the analyses.

The parameters, which characterize this treatment scheme, are the maximum depth H_g and the inclination ι (see Figure 2.3.4.1b). The analyses have been carried out to study the effects of:

1. the variations of the treatment depth by assuming a given inclination;
2. the variations of the geometrical configuration of the treatment in terms of depth and inclination;
3. the variations of the soft layers volumetric stiffness;
4. the constitutive model on the efficiency of the isolating box.

The signal used for these dynamic analyses is the Ricker wavelet, with a constant amplitude equal to 0.5g and a fundamental frequency in the range 0.1Hz÷5Hz.

The analyses have been performed by considering a linear-elastic behaviour for the materials, with the exception of the ones reported in §2.3.4.4.

The results generally refer to the control point (CP) at ground level, to the central vertical section and to the ground surface (see Figure 2.3.4.2). The mesh assumed for the analyses has an x-total length equal to 200m and a height H of 60m (see Figure 2.3.4.1 b); soil and soft layers have been assumed with the characteristics reported in Table 2.3.4.1.

Layer	V_S (m/s)	ξ (%)	ρ (kg/m^3)
Soil	300	3	2040
Soft layer	20	0	1020

Table 2.3.4.1 *Parameters adopted for analyses.*

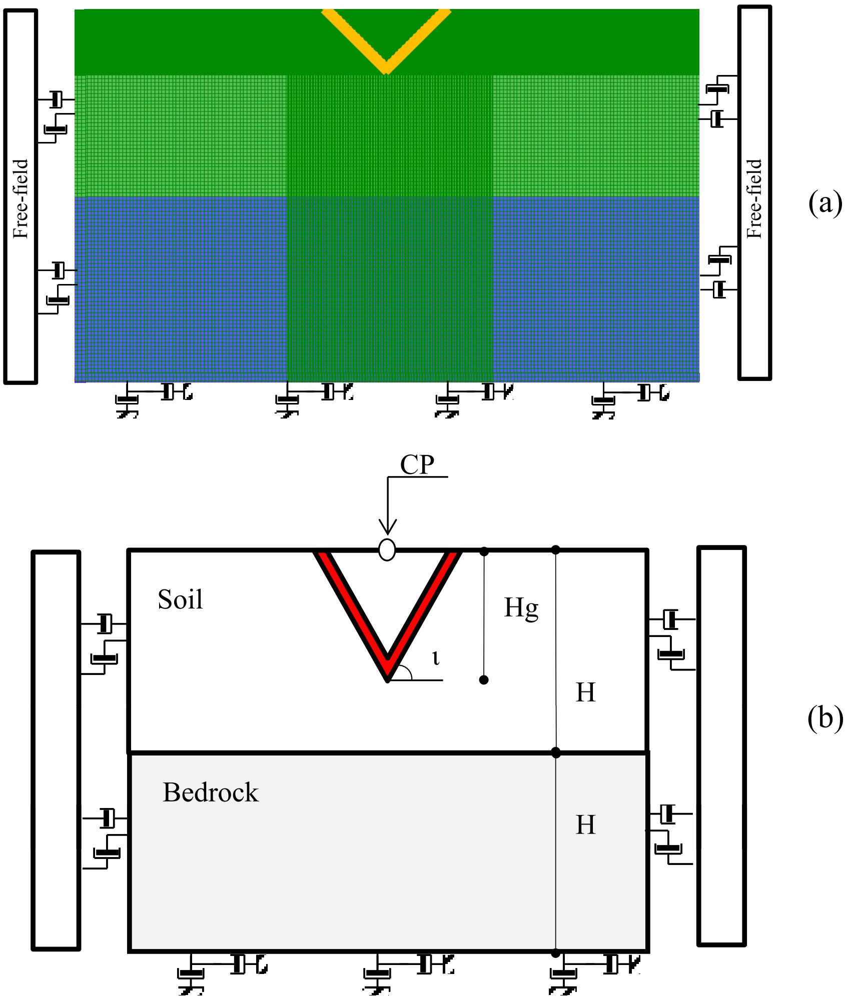

Figure 2.3.4.1 *Mesh and geometrical configuration for 2D analyses with inclined injections: example of mesh (a); indications on the boundary conditions and the control point CP at ground surface (b).*

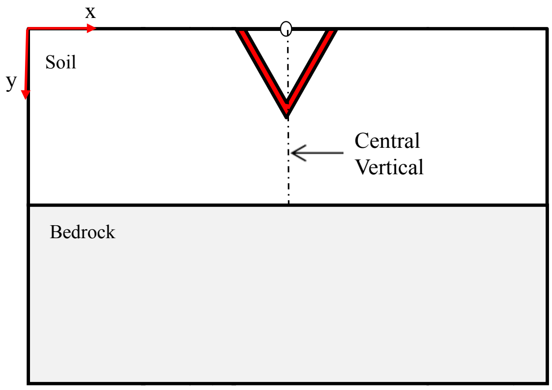

Figure 2.3.4.2 *Indications on the reference system and the central vertical position.*

2.3.4.1 Effects of the variations of the treatment depth (for ι=45°)

A model configuration with a soft layer inclination ι equal to 45° and two different maximum treatment depths H_g, equal respectively to 10m and 20m, has been considered to check the effect of H_g.

Figures 2.3.4.3 report the effects calculated in the control point, in terms of maximum accelerations, spectral intensities, predominant and mean periods by varying the fundamental frequencies of the propagated Ricker wavelet. The results clearly indicate that H_g plays a relevant role, and it is convenient to use the largest possible values.

For H_g=20m, the effects are attenuated for $f > 1$Hz, whereas for H_g=10m the attenuation is attained only $f > 3$. A larger treatment depth is therefore more effective to tackle off the dynamic effects in the control point, like for the rectangular caisson.

For $f \geq 1$Hz, the configurations tend to assure longer periods (see Figures 2.3.4.3 c and d), as clearly shown in terms of mean periods (see Figure 2.3.4.3 d), where, for H_g equal to 10m, the period variation trend is substantially linear with the signal frequency.

In terms of amplitude ratio (see Figure 2.3.4.4), it is shown how the geometrical configuration with H_g=10m tends to amplify a frequency range larger than that with H_g=20m. The frequencies in the range f=1Hz÷3Hz are amplified, for H_g=10m, in terms of energy transmitted upward to the ground surface; in the same range, the scheme with H_g=20m shows a de-amplification. It is therefore noted that the geometrical configuration with H_g=20m is generally effective, with the exception of f=0.5Hz and 1Hz, whereas the scheme with H_g=10m leads to a decrement of the dynamic actions only for the highest frequencies.

Figures 2.3.4.5 and 2.3.4.7 report the maximum accelerations, respectively along the central vertical and at the ground surface for the soil layer, for H_g equal to 20m or 10m, for different Ricker wavelets. As expected, the scheme with H_g=10m determines higher maximum acceleration values both along the central vertical and at ground surface. As previously reported in §2.3.3.1, the presence of soft layers does not directly involve an increment of the displacement values (see Figures 2.3.4.6 and 2.3.4.8): at lower fundamental signal periods, a decrease in displacements at ground surface is observed. The displacements are larger for H_g=10m, confirming the considerations on amplitude effects.

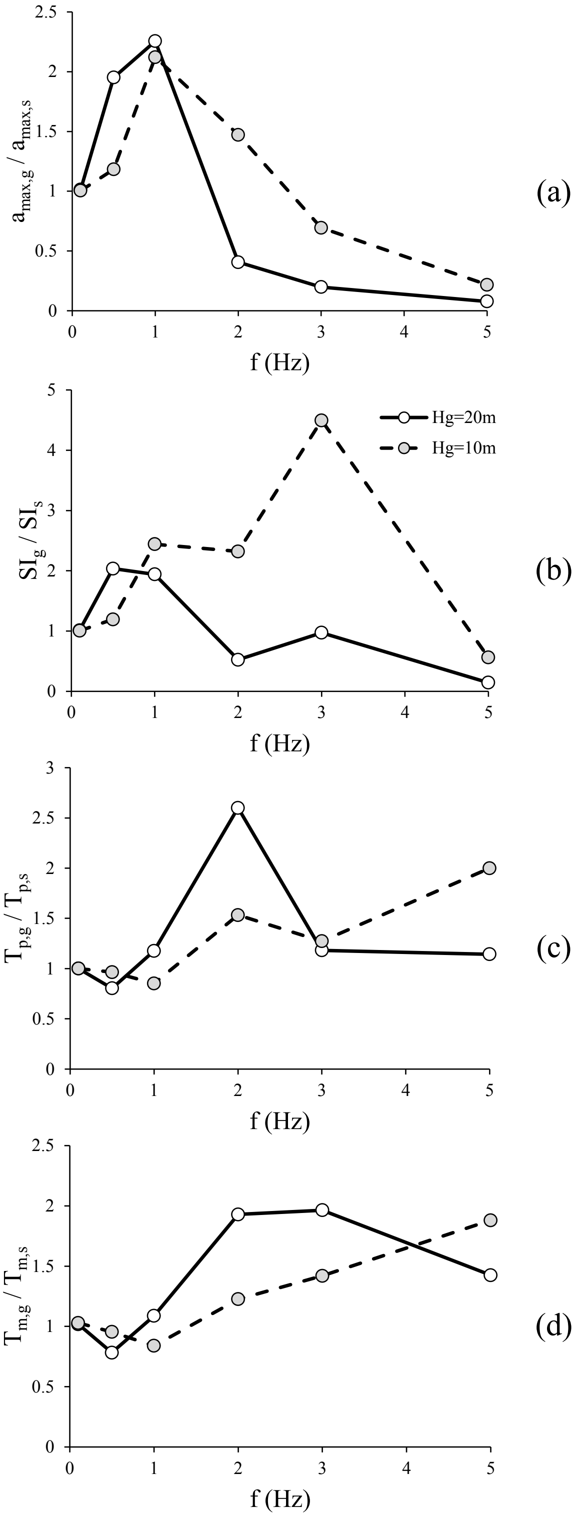

Figure 2.3.4.3 *Effects in the control point in terms of maximum accelerations (a), spectral intensities (b), predominant (c) and mean periods (d), assuming* $\iota=45°$, $V_{s,g}=20m/s$, H_g *equal to 20m or 10m and* $V_{s,s}=300m/s$ *and by varying the fundamental frequencies of the propagated Ricker wavelet.*

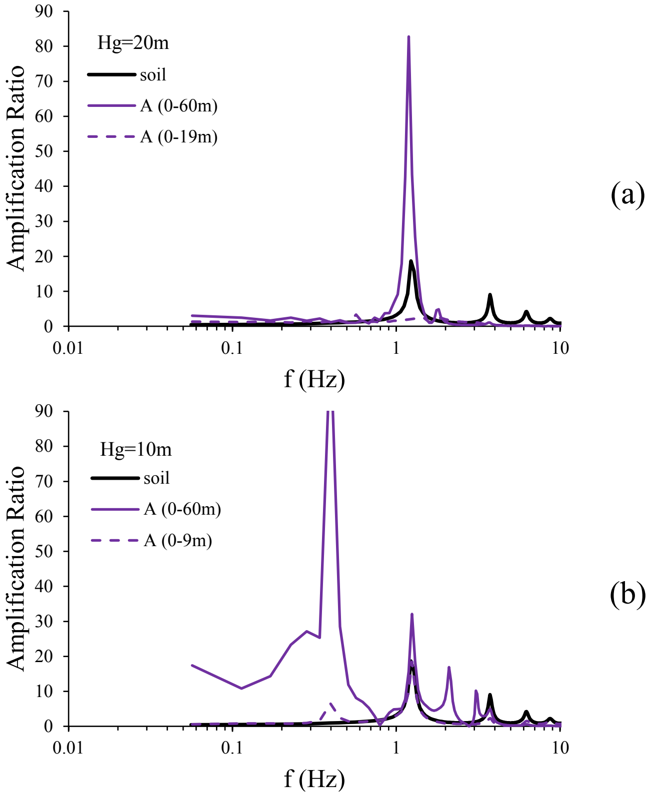

Figure 2.3.4.4 *Amplification ratio in the control point, assuming ι=45°, $V_{s,g}$=20m/s, H_g equal to 20m (a) or 10m (b) and $V_{s,s}$=300m/s and by varying the fundamental frequencies of the propagated Ricker wavelet.*

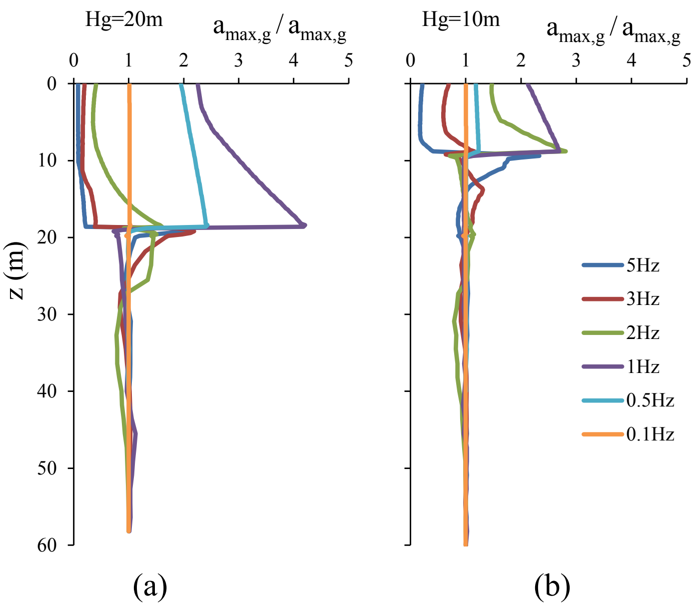

Figure 2.3.4.5 *Maximum acceleration along the central vertical for H_g equal to 20m (a) or 10m (b) with respect to the case of no treatment, by varying the fundamental frequencies of the propagated Ricker wavelet.*

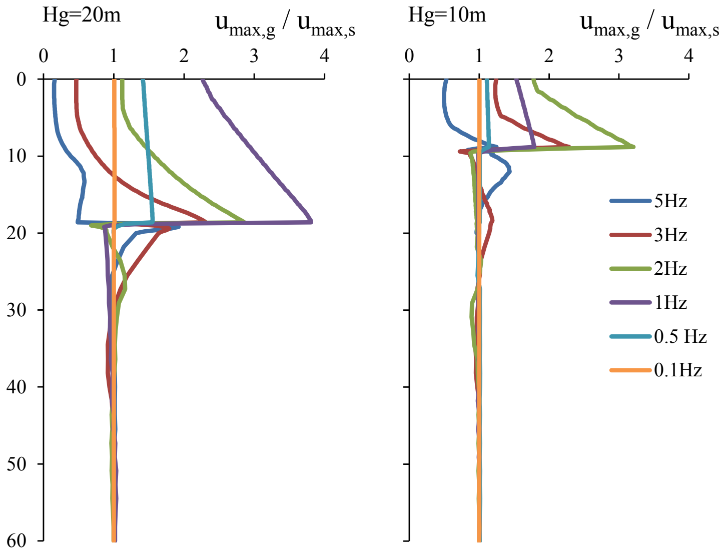

(a) (b)

Figure 2.3.4.6 *Maximum displacements along central vertical for H_g equal to 20m (a) or 10m (b) with respect to the case of no treatment, by varying the fundamental frequencies of the propagated Ricker wavelet.*

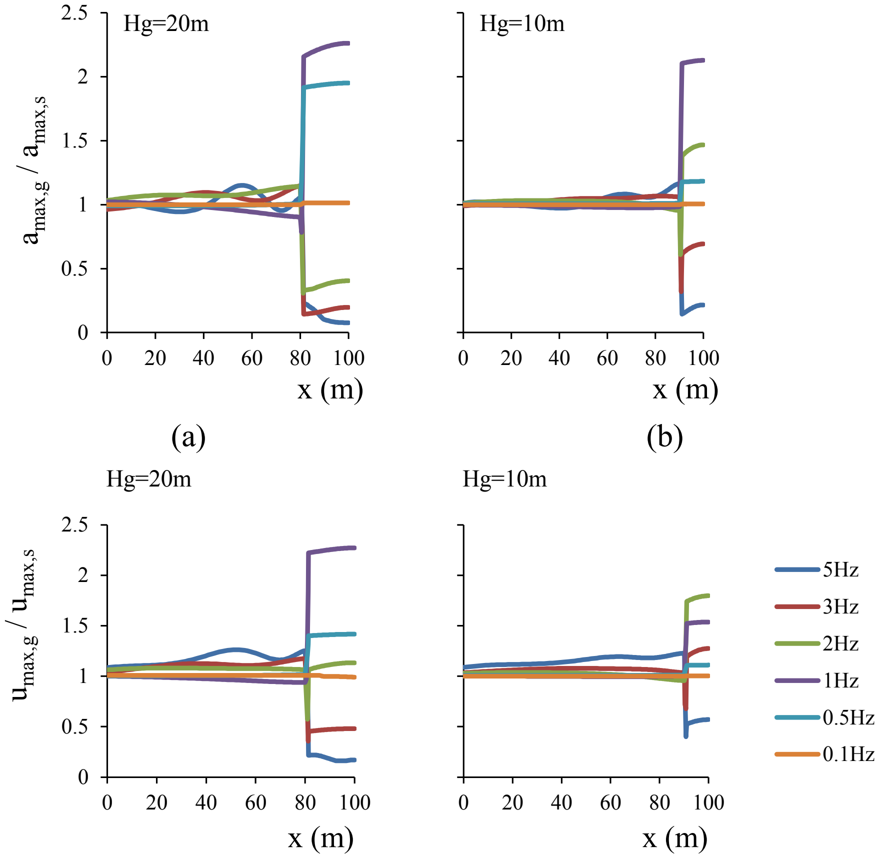

(c) (d)

Figure 2.3.4.7 *Maximum acceleration and displacement at ground surface for H_g equal to 20m (a and c) or 10m (b and d) with respect to the case of no treatment by varying the fundamental frequencies of the propagated Ricker wavelet.*

In terms of efficiency, the two schemes consequently exhibit different behaviours: for H_g=10m, the system is ineffective in reducing the maximum spectral actions in the control point, with the eception of f=5Hz, where a positive efficiency is shown on a large range of the simple oscillator periods. For H_g=20m and for $1 < f \leq 5$Hz, the efficiency E_I constantly assumes positive values for periods lower than 0.3s. For f=5Hz the maximum spectral effects in the control point are definitely reduced, with E_I variable in the range 0.4÷0.9.

With respect to the rectangular section (see §2.3.3), the effects at ground surface due to the inclined injections may be more variable with the considered position: since the thickness of the soil above the isolating layer varies between 0 and H_g, the response is more complex and differences in different points may be expected.

Therefore, a variability of efficiency at different x-axes points must be expected.

This is confirmed by Figure 2.3.4.9, which reports the values of efficiency E_I and the domain S_d-S_a for different positions at ground surface, for f=5Hz and H_g=20m. The efficiency seems to be sensible to the position at ground surface (Figure 2.3.4.9a), with a variation which is higher close to the intersection between the inclined soft layers and the ground level (in the following named edges), i.e. x=85m. For the inner position, a constant behaviour is observed, above all for the periods for which the treatment is more effective. The domain S_d-S_a (see Figure 2.3.4.9b) confirms the observations on efficiency E_I; in fact the domain for x=85m is the only one exhibiting important variations in accelerations and displacements, as confirmed by intersecting the segments related to given periods with the different curves. Similar observations may be done for amplification ratio variations at ground surface. Figure 2.3.4.10 reports the amplification ratio between the ground surface and the bedrock, A(0-60m), for different positions at ground surface and for H_g=20m. The differences in the energy distribution with frequencies are limited and larger for higher periods of the signals.

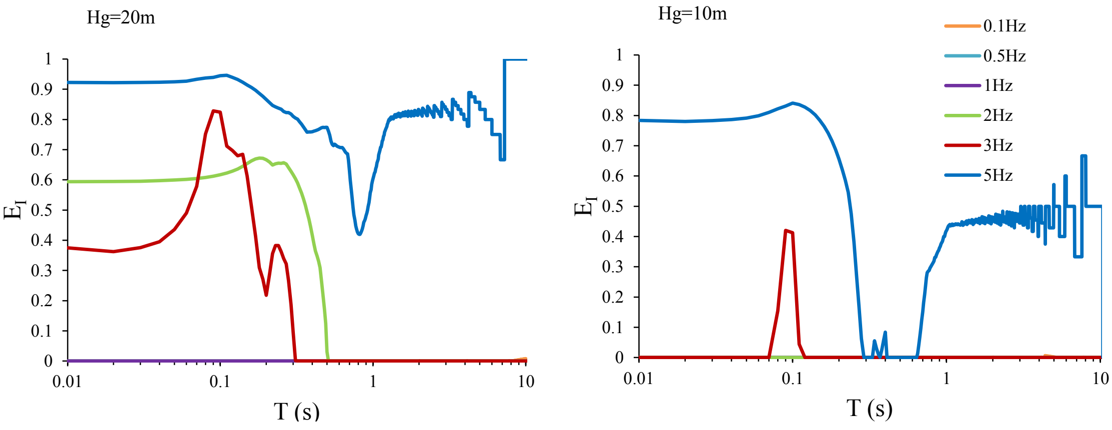

(a) (b)

Figure 2.3.4.8 *Efficiency parameter E_I in the control point by varying the fundamental signal frequency and for H_g=20m (a) and 10m (b).*

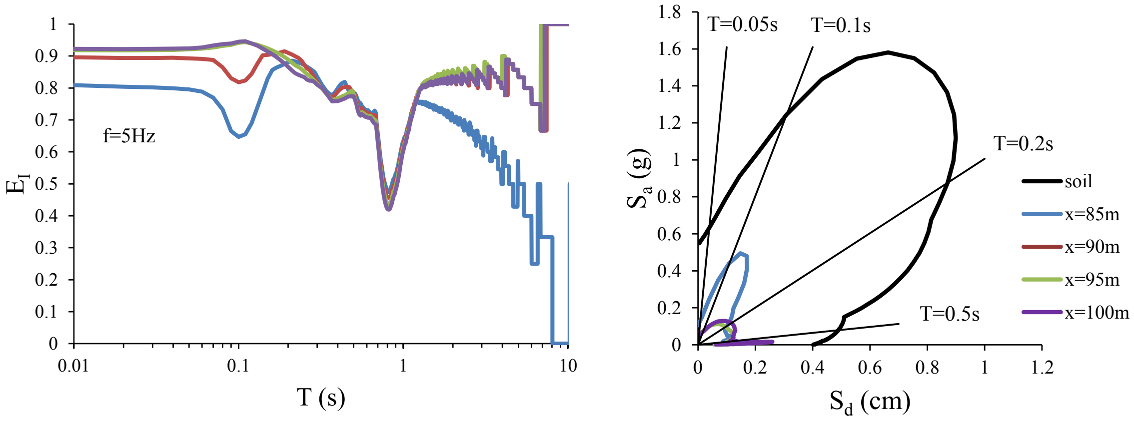

(a) (b)

Figure 2.3.4.9 *Efficiency parameter (a) and domain S_d -S_a (b) for different positions at ground surface for f=5Hz and H_g=20m.*

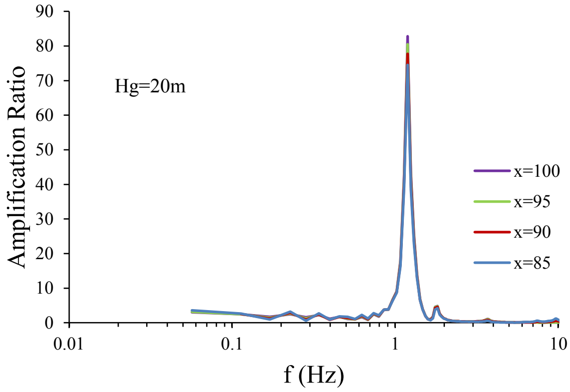

Figure 2.3.4.10 *Amplification ratio, A(0-60m), for different positions at ground surface for H_g=20m.*

In Figure 2.3.4.11, the accelerograms calculated at ground surface for f=1Hz and 5Hz, in absence of any treatment, are reported. They can be compared with the accelerograms reported for the case of a geometrical configuration with H_g=20m and f=1Hz (see Figure 2.3.4.12) and f=5Hz (see Figure 2.3.4.13). These figures show the x and y accelerations at different position at ground surface.

For f=1Hz, which is close to the resonance frequency of the soil deposit (see Figures 2.3.4.4), the signal amplitudes are increased inside the caisson; for f=5Hz (a frequency far from resonant conditions), on the contrary, sensible reductions are observed.

The y-accelerations develope close to the edges of the caisson, and tend to rapidly decrease in the inner zone of the caisson, when the treatment system is effective, as observed for the analyses on caissons having a rectangular section (see §2.3.3.1). Furthermore, the signal duration has been amplified by inserting the soft layers into the soil embankment.

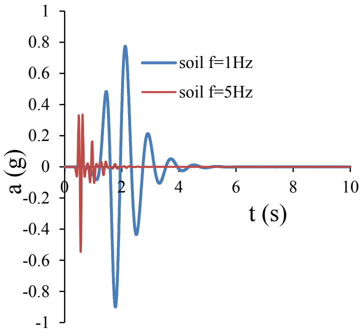

Figure 2.3.4.11 *Accelerations at ground surface without any treatment, for f=1Hz and 5Hz.*

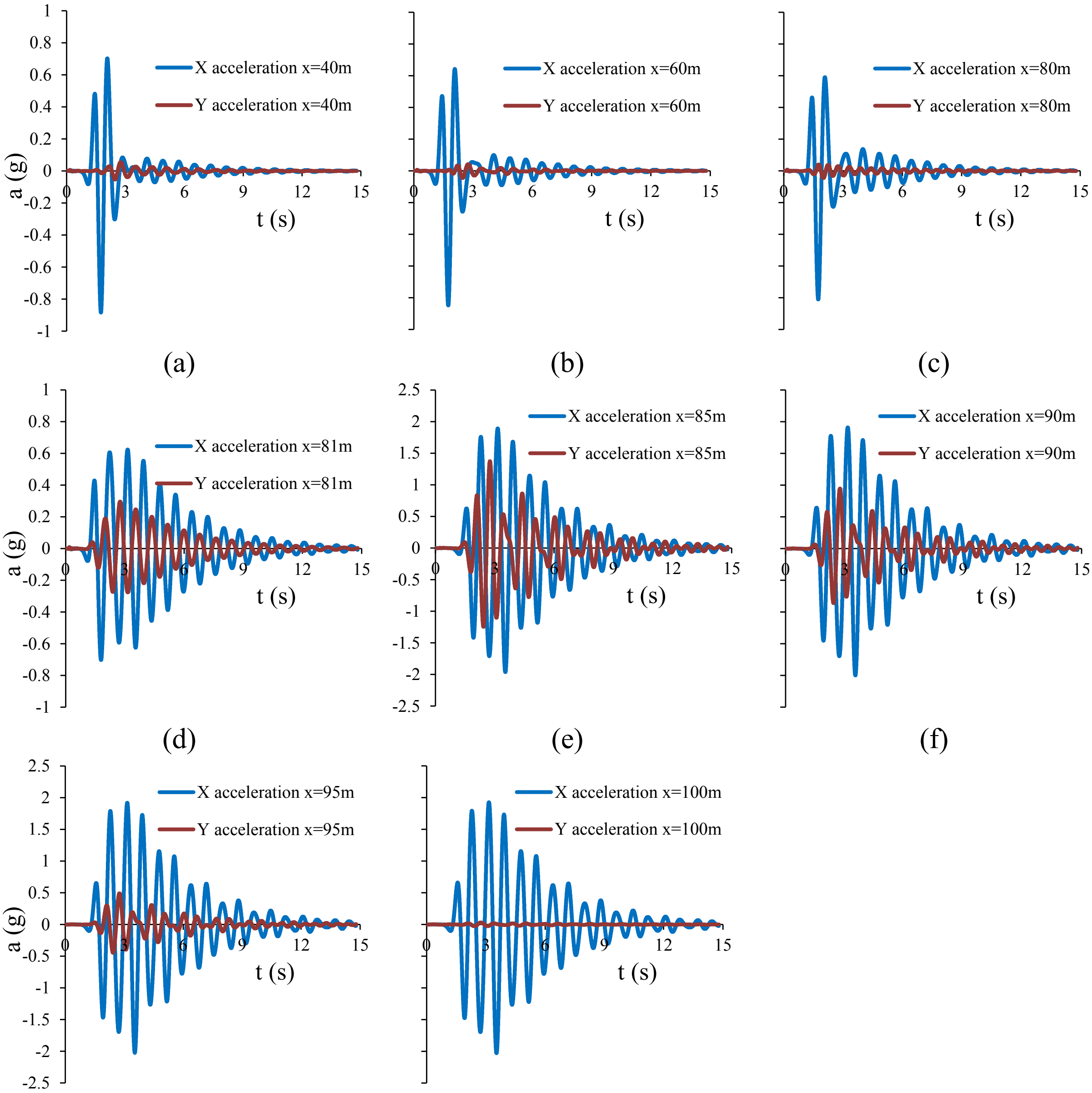

(a) (b) (c)

(d) (e) (f)

(h) (h)

Figure 2.3.4.12 *Accelerations, in different positions at ground surface, for f=1Hz and inclined injections.*

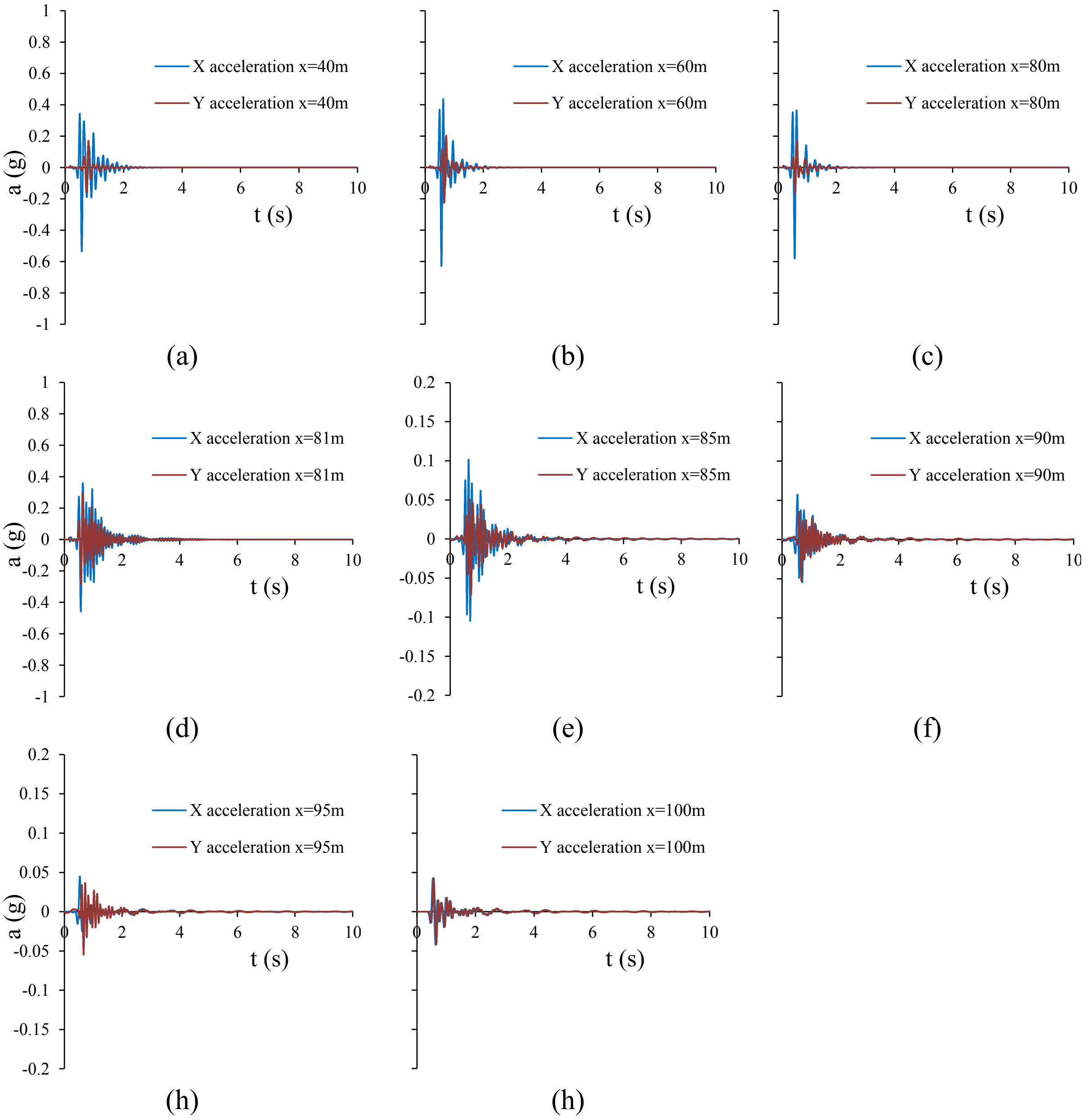

(a) (b) (c)

(d) (e) (f)

(h) (h)

Figure 2.3.4.13 *Accelerations, in different positions at ground surface, for f=5Hz, and inclined injections.*

Similar results are reported in terms of accelerograms, at different depths, along the central vertical (see Figures 2.3.4.14). For f=5Hz the inner part of the soft caisson exhibits lower accelerations, whereas, for f=1Hz, the behaviour changes completely, due to resonance problems.

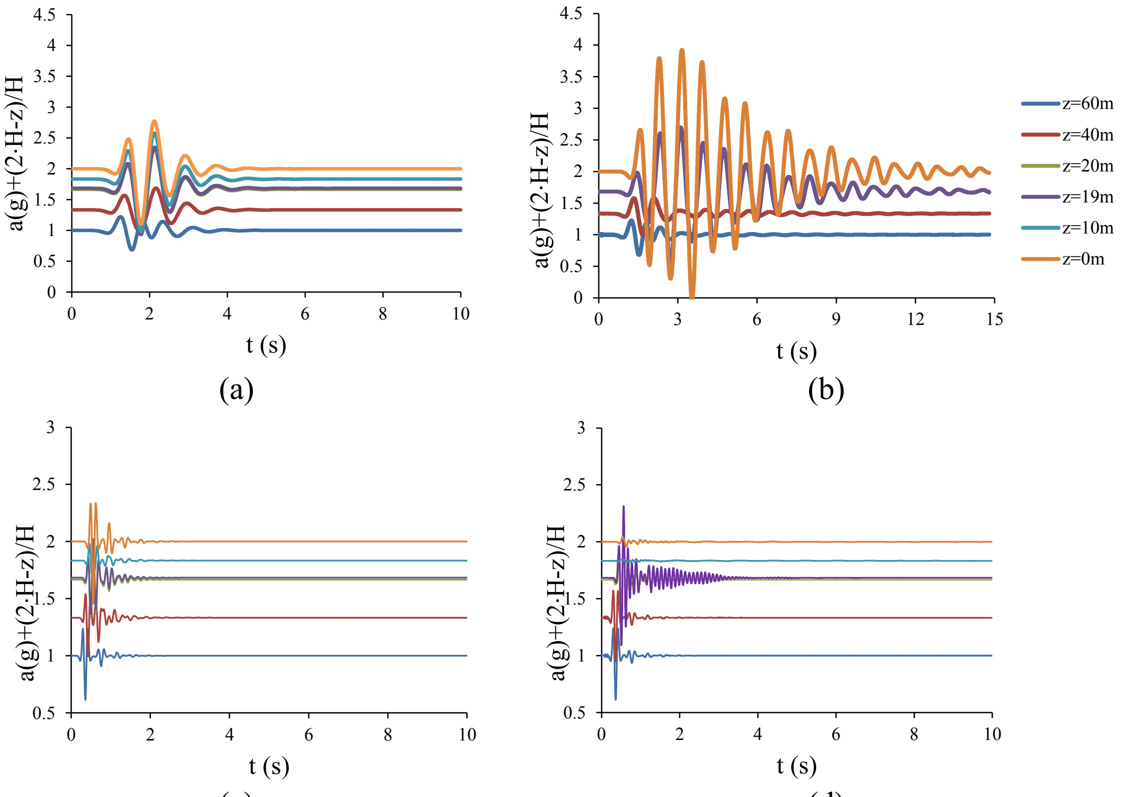

(a) (b)

(c) (d)

Figure 2.3.4.14 *Accelerations along the central vertical for f=1Hz without any treatment (a) and with inclined injections (b) and for f=5Hz without any treatment (c) and with inclined injections (d).*

In this sense, Figures 2.3.4.15 report the acceleration spectra at different depths from ground level, along the central vertical, by propagating a Ricker wavelet with f=5Hz both in the soil deposit without treatment and with inclined injections. By varying the depth z, large differences are observed. In the inner part of the soft caisson (i.e. z=10m and z=0m), a clear acceleration decrement is detected.

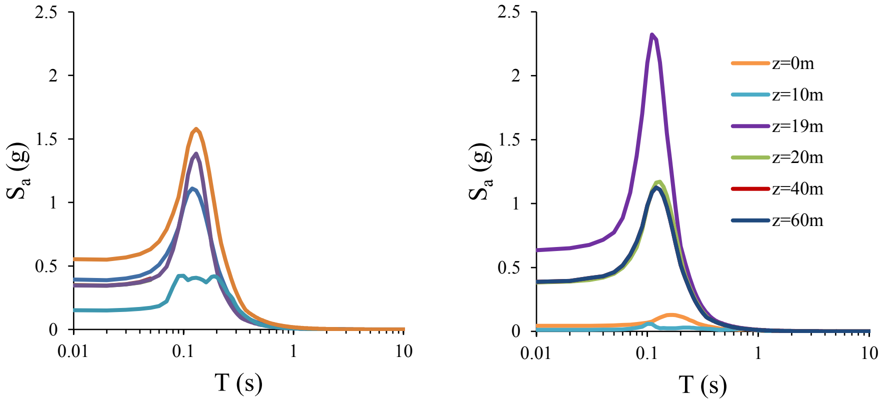

(a) (b)

Figure 2.3.4.15 *Acceleration spectra along the central vertical by propagating a Ricker wavelet for f=5Hz without any treatment (a) and with inclined injections (b).*

2.3.4.2 Effects of the variation of the treatment inclination and of the different depth

Different geometrical configurations have been considered, by varying both the depth H_g and the inclination ι of the soft layers (see Table 2.3.4.2.1).

H_g (m)	ι (°)			
10	30	40	45	55
20				

Table 2.3.4.2.1 *Values of the parameters varied in the analyses.*

Figures 2.3.4.2.1 show the predominant and mean periods, the spectral intensities and the maximum accelerations with respect to the case of no treatment, with reference to the control point, for H_g=20m and 10m, different inclinations ι (from 30° to 55°), for different fundamental frequencies of the transmitted signal. The most efficient geometrical configurations seem to be the deeper ones, as clearly shown in Figures 2.3.4.2.1, from i to h. Assuming a given inclination, the spectral intensities and the maximum accelerations are larger for H_g=10m. By considering a constant depth H_g, a dependence of such parameters from the inclination is also observed.

Lower inclinations seem to provide lower dynamic effects in the control point (i.e. better efficiencies). Along with the previously reported observation on the major efficiency of the deeper treatment, larger and deeper soft caissons are therefore the most efficient ones.

This is probably due both to the interaction of the dynamic wavefront propagating upwards with the soft layers, and to the material damping of the soil contained into the soft caisson. In fact, if the inclination in larger, the signal entrapped into the soft caisson is damped more by passing through a larger quantity of soil.

As far as the periods variations of the signals calculated in the control points are concerned, with the exception of ι=30°, deeper treatments lead to larger values, especially for lower Ricker signal fundamental frequencies. This is probably due to the fact that, by reducing H_g, smaller volumes of soils are surrounded by the V-shaped caisson. Such smaller volumes have stiffer lateral constraints and thus a reduced capacity of modifying the fundamental period.

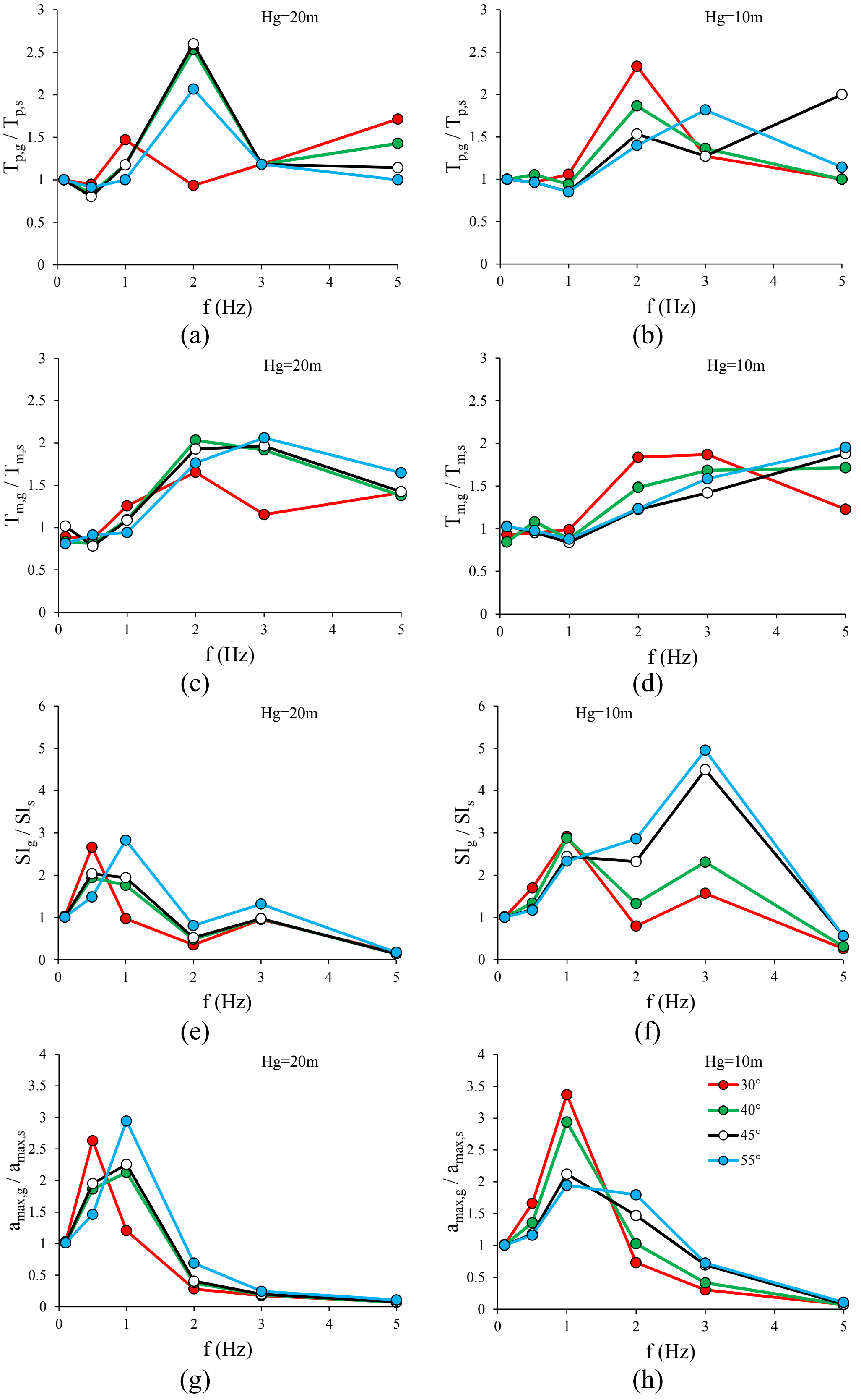

(a) (b) (c) (d) (e) (f) (g) (h)

Figure 2.3.4.2.1 *Predominant period (a and b) and mean period (c and d), spectral intensity (e and f) and maximum acceleration with respect to the case of no treatment, in the control point, for* H_g*=20m and 10m and different inclinations ι (from 30° to 55°).*

In conclusion, among the analysed schemes, the most efficient geometrical configuration has an inclination of 30° and a depth H_g of 20m. This is also reported in Figures 2.3.4.2.2 and Figures 2.3.4.2.3, where the amplification ratios in the control point describe the way in which the signal energy is distributed on the different frequencies, for the different geometrical configurations. The treatment with an inclination of 30° and a maximum depth of 20m leads to the de-amplification of all the frequencies higher than 2Hz; other geometrical configurations tend to have higher amplification ratios for a number of frequencies, above all the ones larger than 1Hz, which are the most crtical ones for squat buildings. Figures 2.3.4.2.4 and 2.3.4.2.5 confirm this behaviour, because the horizontal accelerations for ι equal to 30° and H_g of 20m are the lowest.

The efficience E_I of the treatment is consequently higher for the treatment with ι equal to30° and H_g of 20m (see Figures 2.3.4.2.6), with a larger range of periods of the simple oscillator whose dynamic safety conditions are improved by increasing the soft layers inclination.

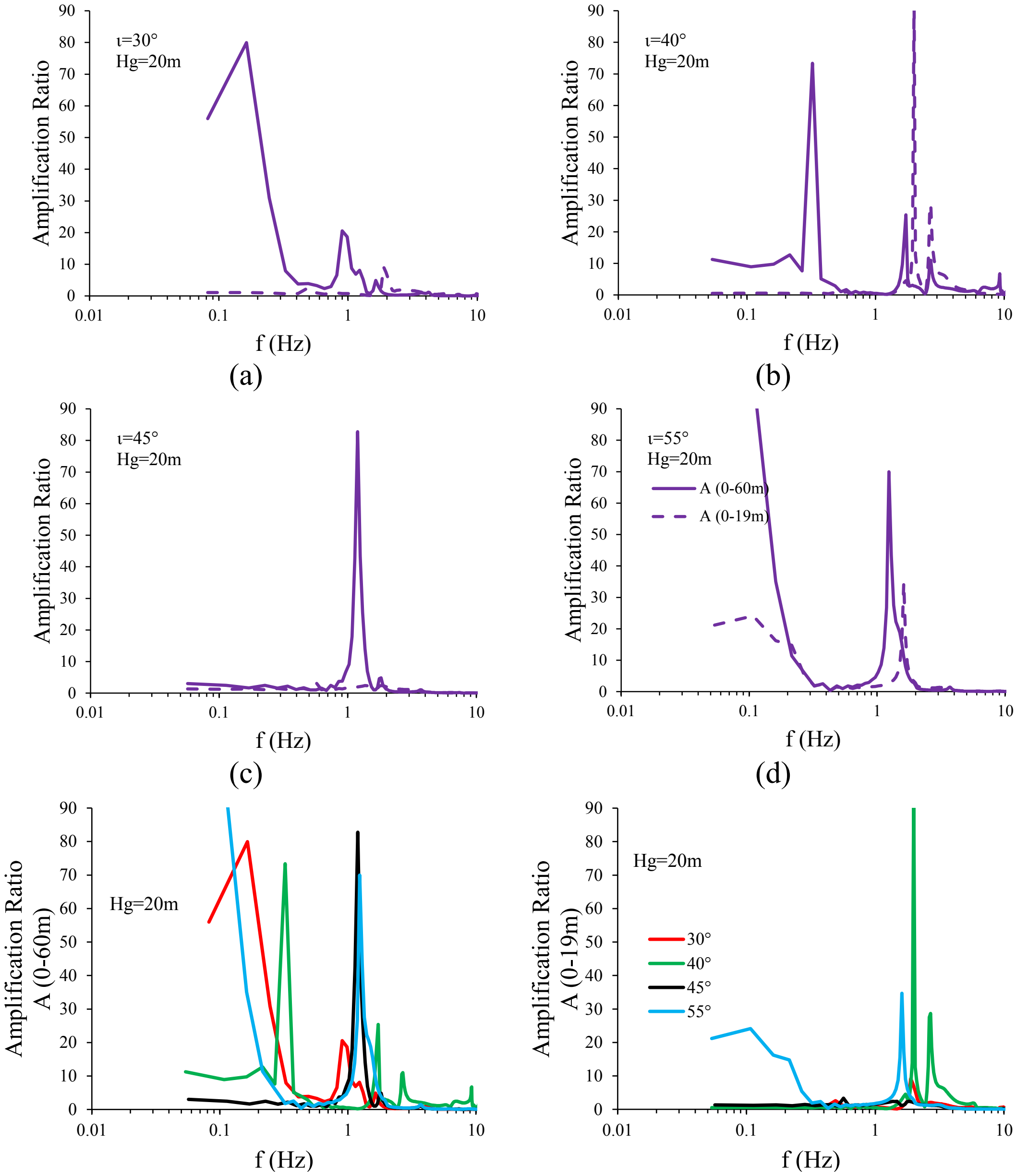

(a) (b) (c) (d) (e) (f)

Figure 2.3.4.2.2 *Amplification ratios A (0-60m) and A (0-19m), in the control point, for* H_g*=20m and different inclinations ι (from 30° to 55°).*

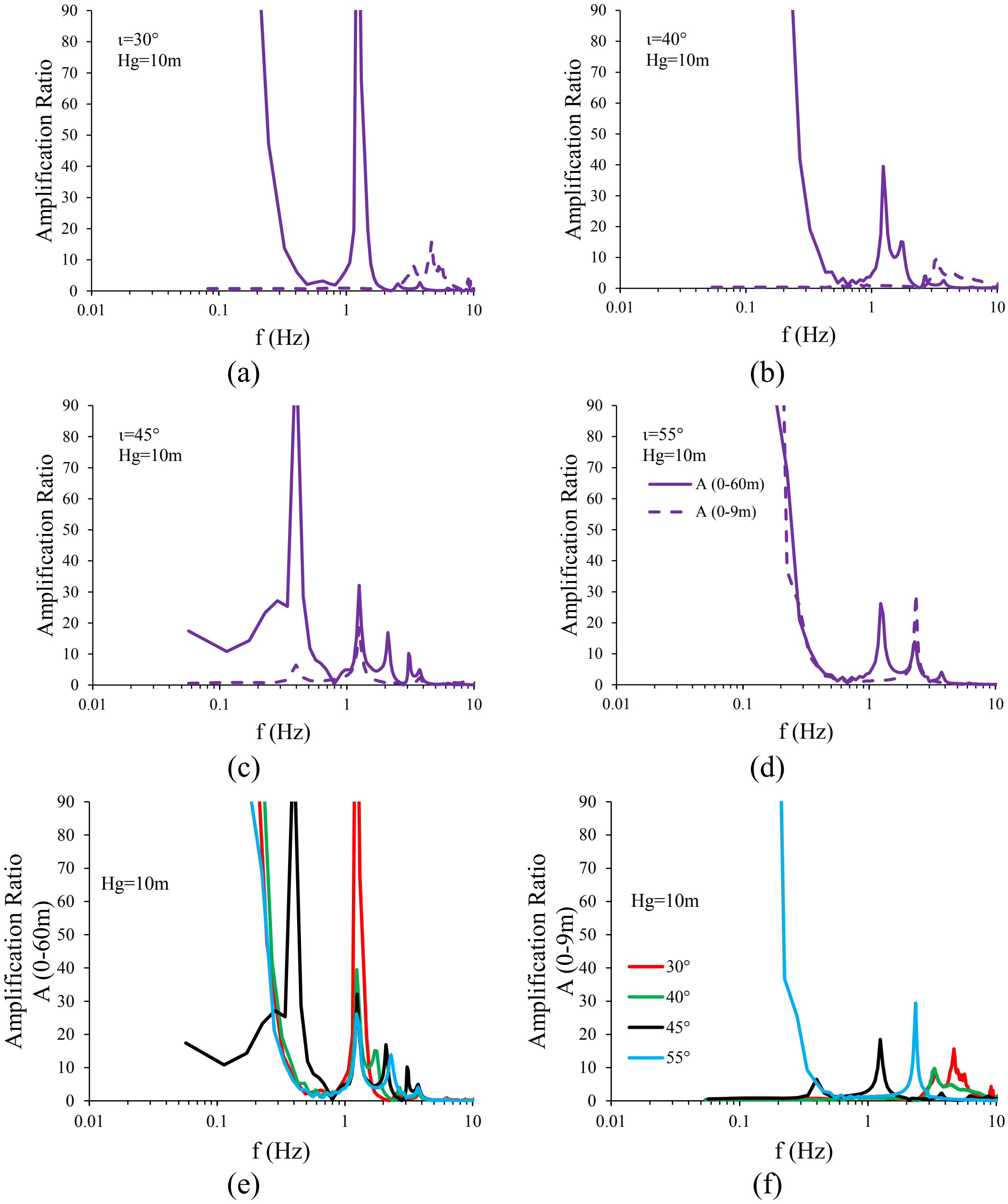

(a) (b) (c) (d) (e) (f)

Figure 2.3.4.2.3 *Amplification ratios A (0-60m) and A (0-9m), in the control point, for H_g=10m and different inclinations ι (from 30° to 55°).*

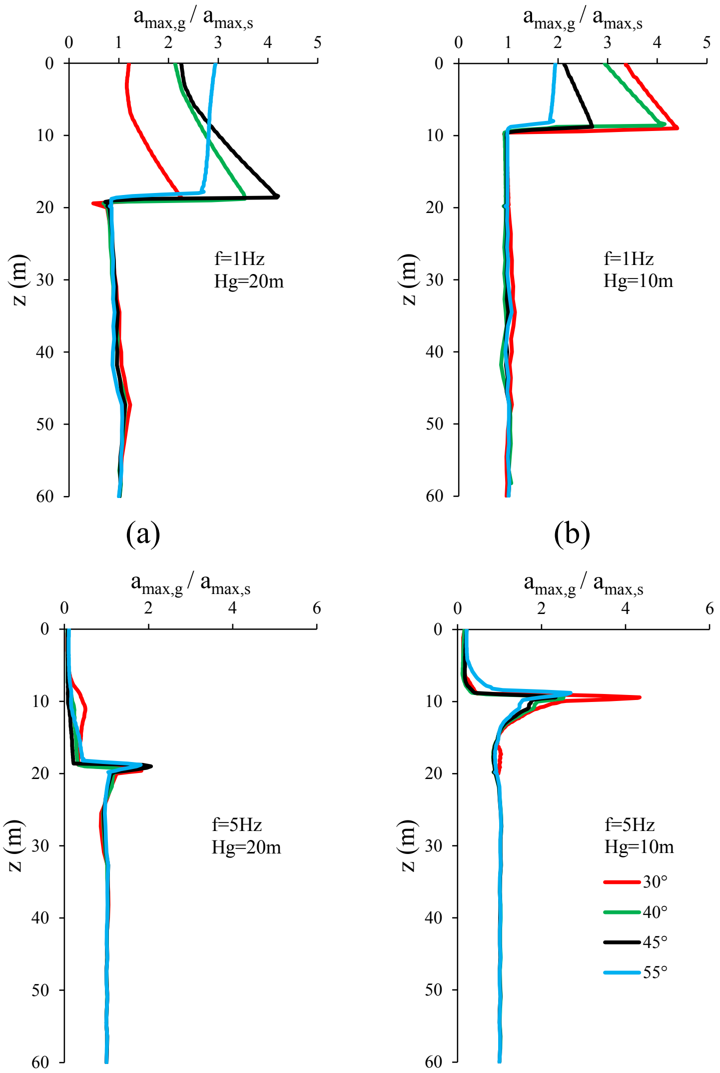

(a) (b)

(c) (d)

Figure 2.3.4.2.4 *Horizontal accelerations with depth along the central vertical for H_g equal to 20m (a and c)and 10m (b and d), different inclinations ι (from 30° to 55°) and f=1Hz (a and b) and 5Hz (c and d).*

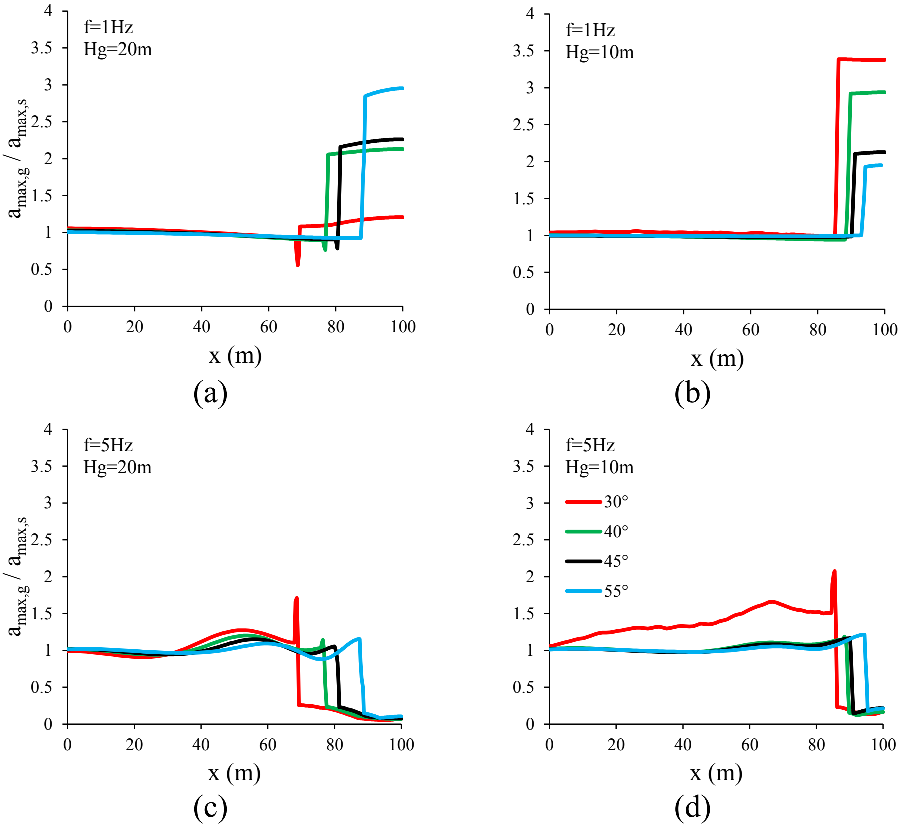

(a) (b)

(c) (d)

Figure 2.3.4.2.5 *Horizontal accelerations at ground surface for* H_g *equal to 20m (a and c) and 10m (b and d), different inclinations ι (from 30° to 55°) and f=1Hz (a and b) and 5Hz (c and d).*

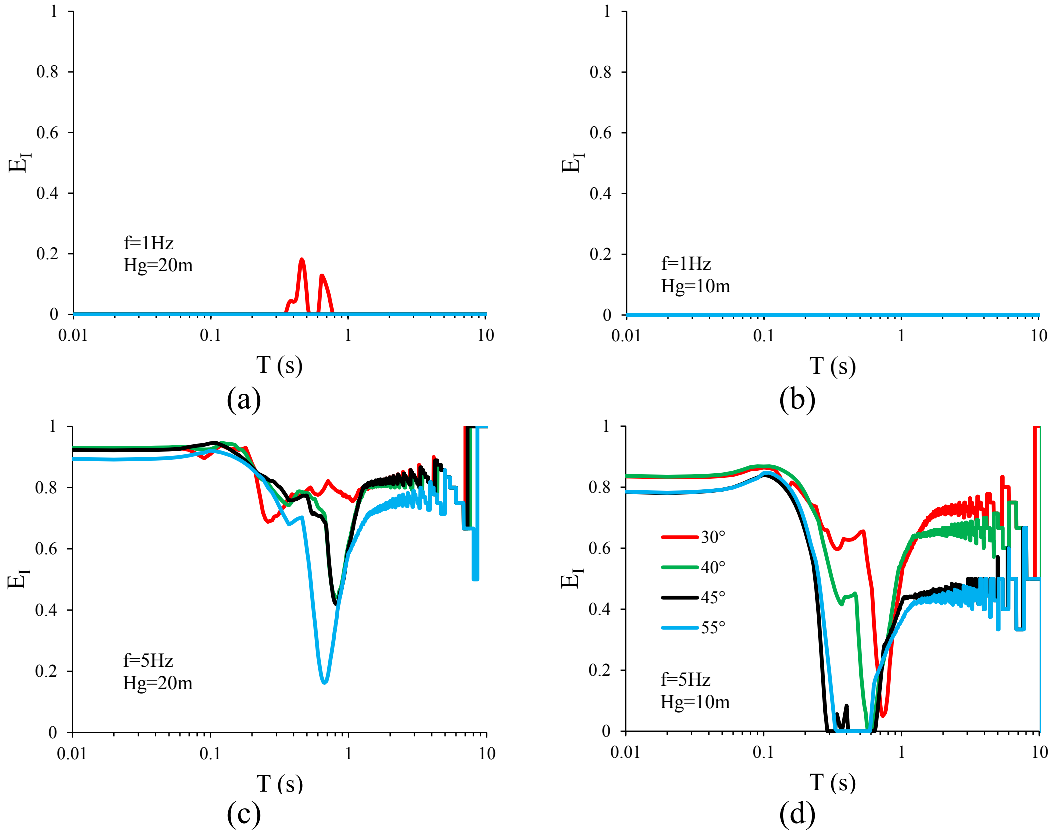

(a) (b)

(c) (d)

Figure 2.3.4.2.6 *Efficiency in the control point for H_g equal to 20m (a and c)and 10m (b and d), different inclinations ι (from 30° to 55°) and f=1Hz (a and b) and 5Hz (c and d).*

2.3.4.3 Effects of the variation of the volumetric stiffness of the soft layers

A geometrical configuration with a soft layer inclination ι equal to 45° and a treatment depth H_g equal to 20m has been assumed in this series of analyses. The soil deposit is 60m thick, with a shear velocity $V_{s,s} = 300$m/s; the shear wave velocity of the soft layers is $V_{s,g} = 20$m/s.

In the previous paragraphs, the only mechanical property parametrically changed has been the shear wave velocity. This is because it is well known that the site seismic amplification depends on materials impedances and impedance ratio. However, it is very interesting to check if the volumetric stiffness may have an effect as well: it will certainly affect the static behaviour, but it may also change the isolating efficiency. Therefore, in order to verify the variation in efficiency due to the volumetric stiffness K of the soft layers, three different values have been considered in the analyses, in accordance to the indications of Table 2.3.4.3.1.

			Soft layers		
Scheme	$V_{s,g}$ (m/s)	G (Pa)	ν	K (Pa)	G/K
K	20	$4.079 \cdot 10^5$	0.300	$8.838 \cdot 10^5$	0.46
0.5K	20	$4.079 \cdot 10^5$	0.147	$4.419 \cdot 10^5$	0.92
10K	20	$4.079 \cdot 10^5$	0.477	$88.38 \cdot 10^5$	0.05

Table 2.3.4.3.1 *Schemes adopted for studying the influence of the variation of the volumetric stiffness of the soft layers*

Since in all analyses $V_{s,g}$ has been kept constant, the ratio G/K varies.

Three values of K have been chosen consistently with the constitutive limits imposed by the theory of elasticity ($0 < \nu < 0.5$, being ν the Poisson ratio).

Figures 2.3.4.3.1 report the effects, calculated in the control point, in terms of maximum accelerations, spectral intensities, predominant and mean periods by varying the fundamental frequencies of the propagated Ricker wavelet.

As observed in §2.3.3.9, by increasing the soft layer volumetric stiffness, the efficiency of the system decreases, in terms of both maximum acceleration and spectral intensity.

The volumetric stiffness greatly affects the predominant and mean period values: by increasing K, the periods tend to be reduced on the whole range of frequencies (see Figures 2.3.4.3.1 c and d).

The worse efficiency of the system due to a higher volumetric stiffness can be observed in Figures 2.3.4.3.2 and 2.3.4.3.3 too. Figures 2.3.4.3.2 report the amplification ratios A(0-60m) and A(0-9m), in the control point; the A(0-60m), for the scheme 10K, indicates important increases in the frequency range from 0.1Hz to 10Hz, with the exception of f=1Hz. This trend explains the observed low efficiency. The results in terms of maximum acceleration along the central vertical and at ground surface due to the propagation of a Ricker wavelet with f=1Hz are reported in Figure 2.3.4.3.3a and 4a: the 10K scheme exhibits lower accelerations at ground surface with respect to the other ones.

Generally speaking, by increasing the volumetric stiffness, the soft caisson is less effective, due especially to the low compressibility of the inclined soft layers (see §2.3.2.9), which are subjected to compression because of vertical shear wave propagation.

The higher the compressibility of the lateral layers the larger the decrease in horizontal dynamic actions in the soft caisson.

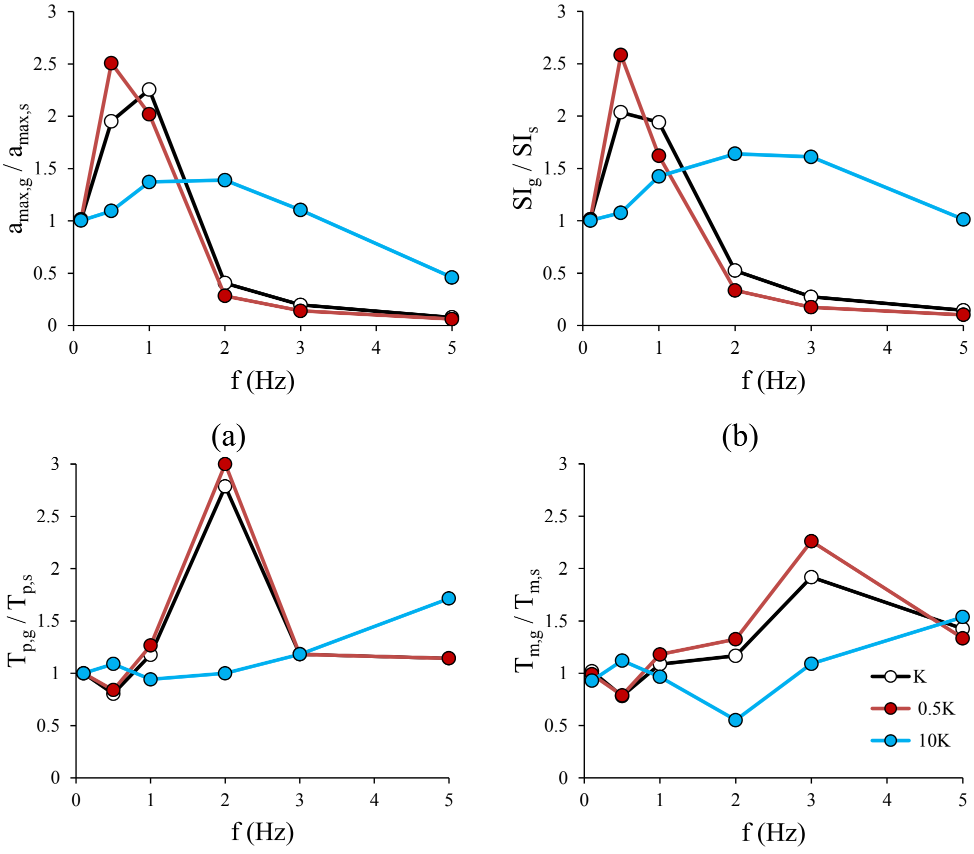

(a) (b)

(c) (d)

Figure 2.3.4.3.1 *Effects in the control point in terms of maximum accelerations (a), spectral intensities (b), predominant (c) and mean periods (d), by assuming* $V_{s,g}$*=20m/s,* H_g*=20m, ι=45° and* $V_{s,s}$*=300m/s.*

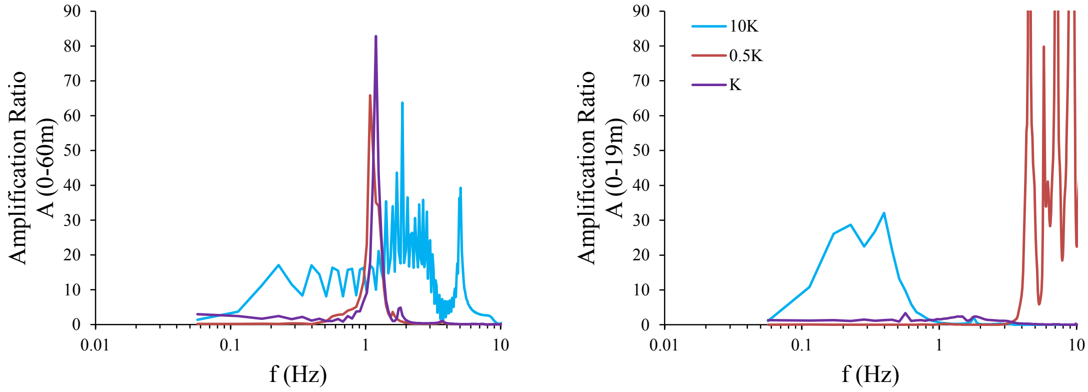

(a) (b)

Figure 2.3.4.3.2 *Amplification ratios A (0-60m) and A (0-9m), in the control point.*

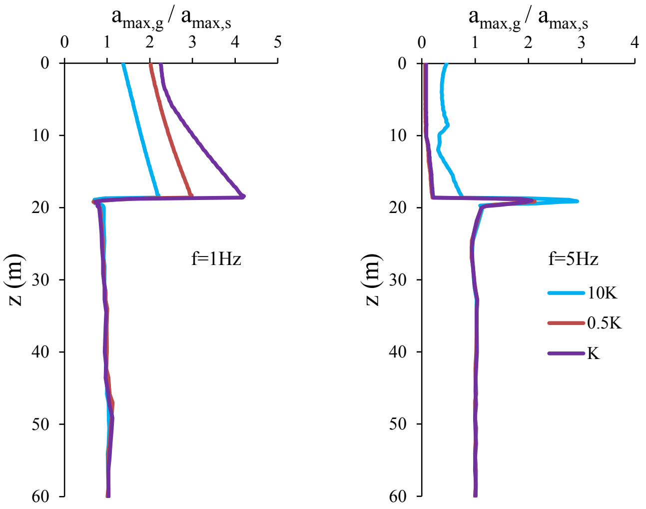

(a) (b)

Figure 2.3.4.3.3 *Maximum acceleration along the central vertical, by assuming $V_{s,g}$=20m/s, H_g=20m, ι=45°and $V_{s,s}$=300m/s, for f=1Hz (a) and 5Hz (b).*

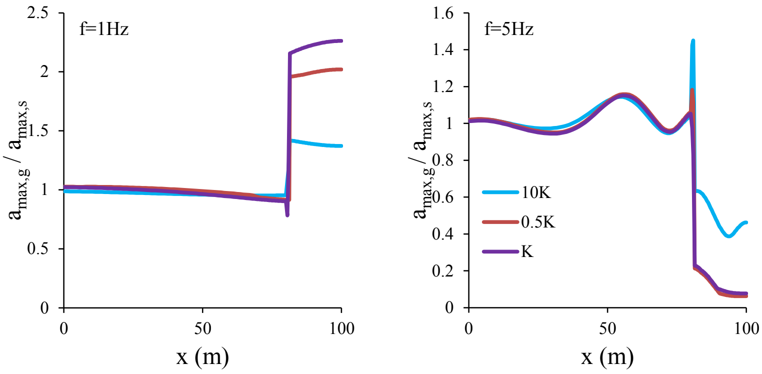

(a) (b)

Figure 2.3.4.3.4 *Maximum acceleration at ground surface, by assuming $V_{s,g}$=20m/s, H_g=20m, ι=45°and $V_{s,s}$=300m/s, for f=1Hz (a) and 5Hz (b).*

2.3.4.4 Effects of the constitutive model on the efficiency of the isolating box

A geometrical configuration with a soft layer inclination ι equal to 45° and a treatment depth H_g of 20m has been assumed in this series of analyses (see Table 2.3.4.4.1). The soil deposit thickness H is equal to 60m, with a soil shear velocity $V_{s,s}$ of 300m/s; the shear wave velocity of the soft layers is equal to 20m/s.

In §2.3.3.10, discussing the efficiency of rectangular soft caissons, it has been pointed out that the choice of the constitutive model adopted in the analyses is of great relevance in terms of the isolating efficiency. In particular, it has been shown that, with a more realistic elasto-plastic model, the efficiency of the isolating system tends to increase even for input signals having low predominant frequencies. In other words, if the signal has an amplitude large enough to involve plastic deformations, local plasticization (which in the case of a simple elastic-perfectly plastic model coincides with local shear failure) helps in attenuating the seismic effects in the isolated soil volume. This is mostly due to the plasticization within the grouted layers and at their interface with the surrounding soil. It is therefore of great interest to see if the same conclusions hold also for the more realistic V-shaped soft caisson scheme.

Therefore, an elasto-plastic behaviour has been assumed for the materials, whose mechanical characteristics are reported in Table 2.3.4.4.2. As previously reported, the values of the shear strength angles for the grouted layers have been assumed on the basis of the preliminary results obtained in laboratory. The amplitude of the Ricker wavelet applied to the bedrock base is, in this case, equal to 0.5g.

Scheme	Model	Maximum Ricker wavelet Amplitude (g)
S	Linear Elastic	0.5
E		
SP	Elastic Plastic	
EP D5		
EP D15		

Table 2.3.4.4.1 *Scheme of the performed analyses.*

Material	V_S (m/s)	ν	G (MPa)	K (MPa)	φ’ (°)
Soil	300	0.3	183.6	397.7	30
Soft layer	20	0.3	0.407	0.884	5/15

Table 2.3.4.4.2 *Materials mechanical properties.*

The observations reported in §2.3.3.10 have been confirmed: the adoption of a more realistic model leads to a reduction in terms of the maximum accelerations and of the spectral intensities calculated in the control point (see Figures 2.3.4.4.1). Furthermore, the lower the shear strength angle the higher the reductions. In terms of mean and predominant periods, the introduction of the failure conditions does not have a relevant effect, as they are mostly controlled by the soil mass contained into the soft caisson and by the constraint effect of the surrounding soil. The higher system efficiency is shown in terms of amplification ratios too, as reported in Figures 2.3.4.4.2. In these figures, the amplification ratios for two different frequencies, f=1Hz and 5Hz are shown. The A(0-60m) trends indicate lower maximum amplitudes with respect to the linear-elastic case, with the presence of peak values for lower frequencies. The elastic-plastic schemes EP-D5 and D15 show E_I values higher than the linear case E, as reported in Figures 2.3.4.4.3. By decreasing shear strength angle of the soft layers, larger simple oscillator periods have been protected. In fact, for f=1Hz, in the linear case E, the system does not provide any increment in safety condition. For the same signal frequency, the EP-D15 scheme shows slight improvement in the response, in the range 0.05s÷0.8s and the EP-D5 scheme shows a sharp increment in E_I values between 0.01s and 0.8s. Because of the propagation at the bedrock base of a dynamic signal with a maximum acceleration value of 0.5g, residual displacements are expected. Figures from 2.3.4.4.5 to 2.3.4.4.7 report the accelerations and the displacements at ground surface, both in the x and in y-directions, for the scheme without any treatment and for the configurations named EP-D15 and D5. Figure 2.3.4.4.4 shows the positions in which the signals have been calculated. These signals have been filtered with a lowpass Butterworth filter, with an order of 4, and a control frequency of 15Hz (see §2.3.3.10). The introduction of a soft caisson reduces the horizontal accelerations, with residual displacements that are of the same order of magnitude of the ones observed without any treatment. Inside the caisson, the amplitudes of the vertical accelerations and of the vertical displacements assume values similar to the ones calculated without treatment. Outside the isolated zone, the vertical accelerations have been amplified by the interaction of the wavefronts with the soft layers.

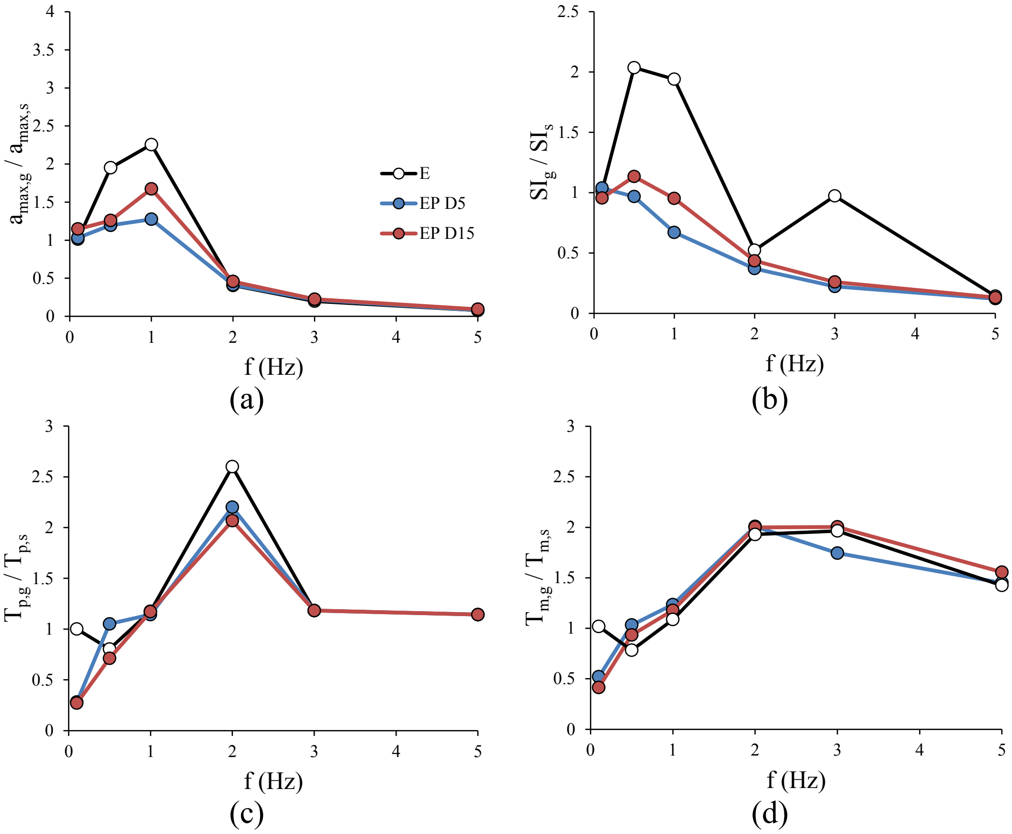

(a) (b) (c) (d)

Figure 2.3.4.4.1 *Effects in the control point in terms of maximum accelerations (a), spectral intensities (b), predominant (c) and mean periods (d), by assuming* $V_{s,g}$*=20m/s,* H_g *= 20m, ι=45°and* $V_{s,s}$*=300m/s and by varying the fundamental frequencies of the propagated Ricker wavelet.*

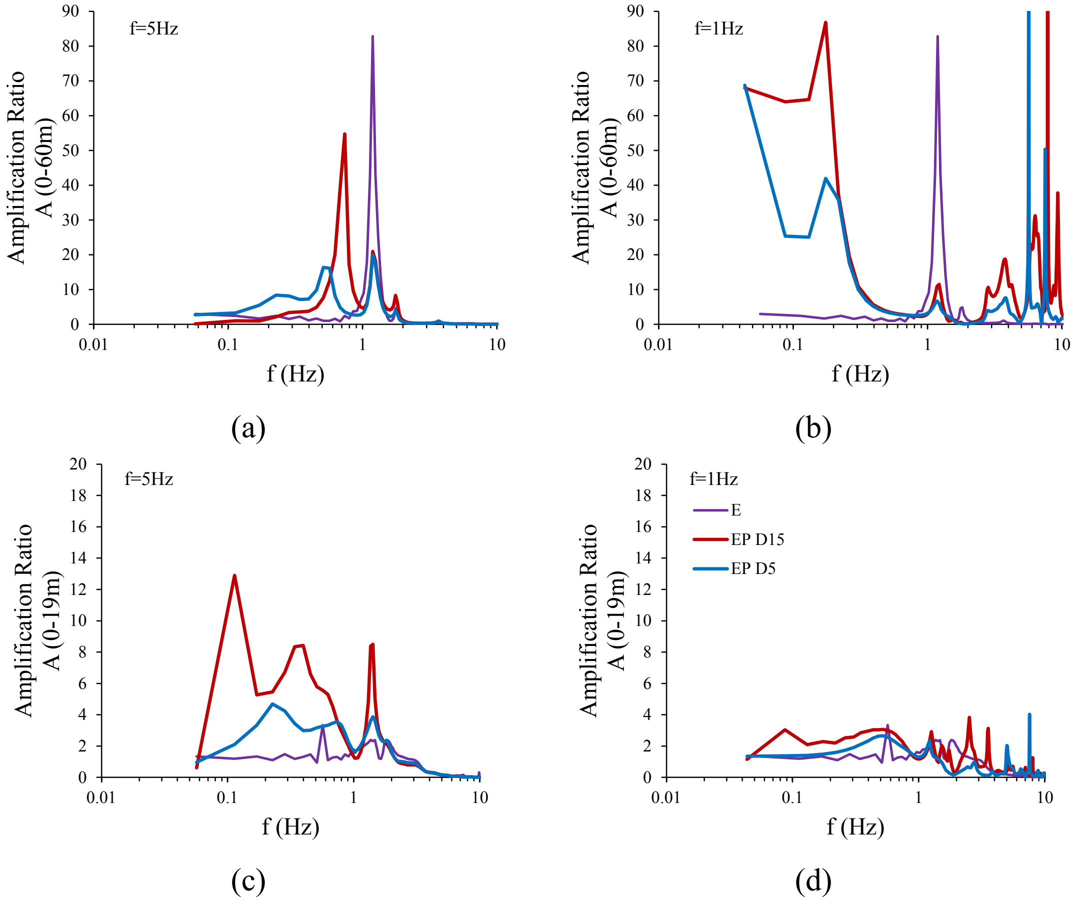

Figure 2.3.4.4.2 *Amplification ratios for two different frequencies, f=1Hz (a and c) and 5Hz (b and d).*

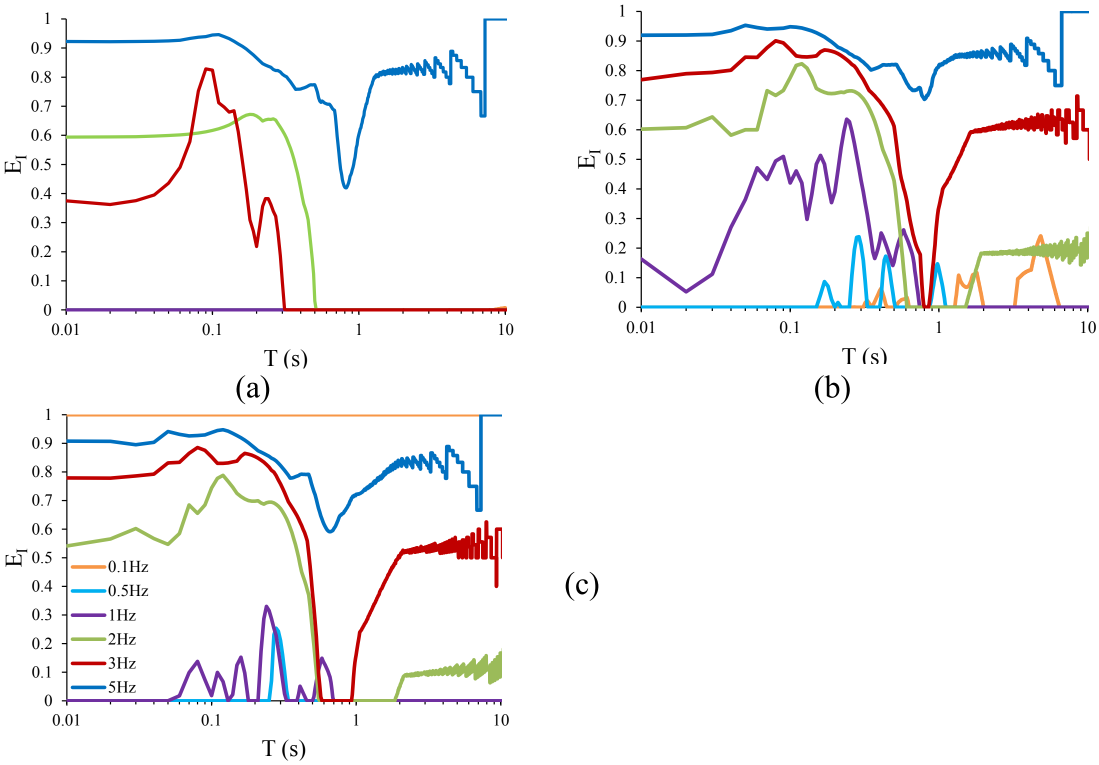

Figure 2.3.4.4.3 *Efficiency E_I for the linear-elastic E (a) and for the elasto-plastic ED-D5 (b) and EP- D15 (c) cases.*

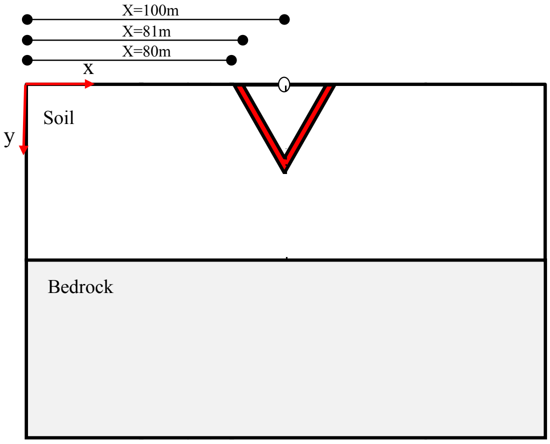

Figure 2.3.4.4.4 *Indications on the geometrical configuration.*

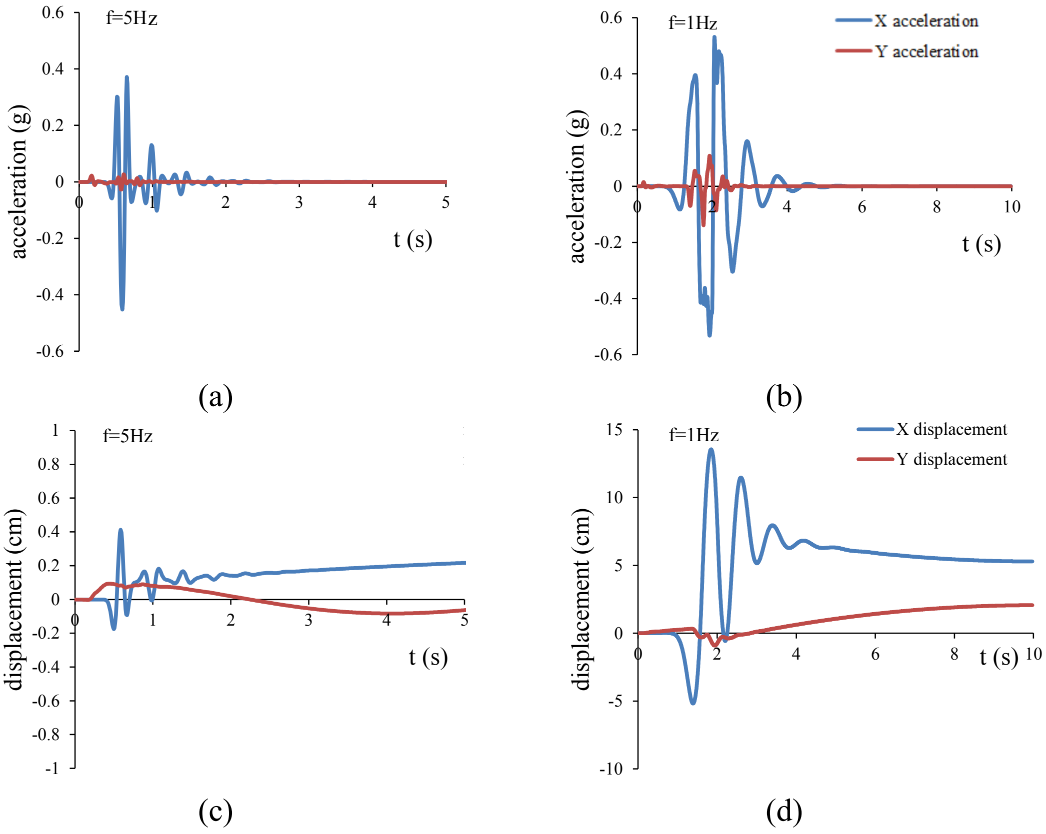

Figure 2.3.4.4.5 *X and y accelerations and displacements at ground surface due to the propagation of two different Ricker wavelet with f=1Hz and 5Hz, through the soil layer.*

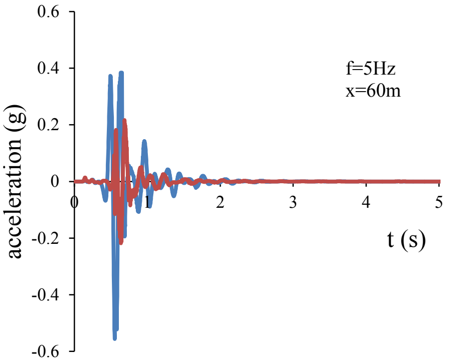
0.6
0.4
0.2
0
-0.2
-0.4
-0.6
acceleration (g)
0
1
2
3
4
5
t (s)
f=5Hz
x=60m

(a)

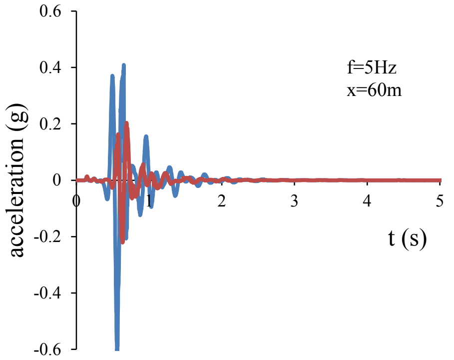
0.6
0.4
0.2
0
-0.2
-0.4
-0.6
acceleration (g)
0
1
2
3
4
5
t (s)
f=5Hz
x=60m

(b)

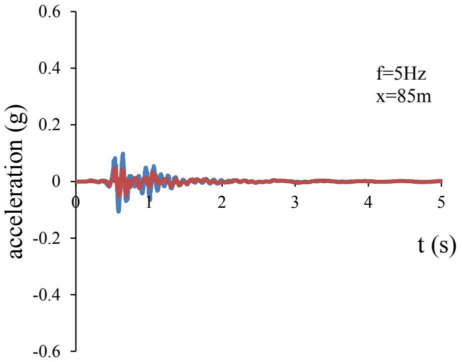
0.6
0.4
0.2
0
-0.2
-0.4
-0.6
acceleration (g)
0
1
2
3
4
5
t (s)
f=5Hz
x=85m

(c)

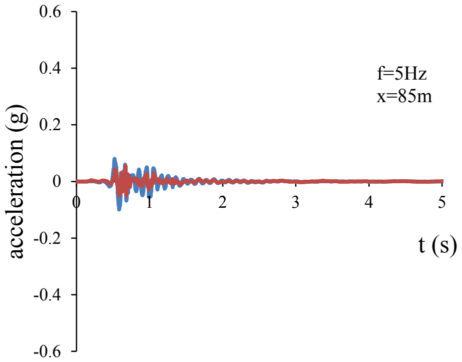
0.6
0.4
0.2
0
-0.2
-0.4
-0.6
acceleration (g)
0
1
2
3
4
5
t (s)
f=5Hz
x=85m

(d)

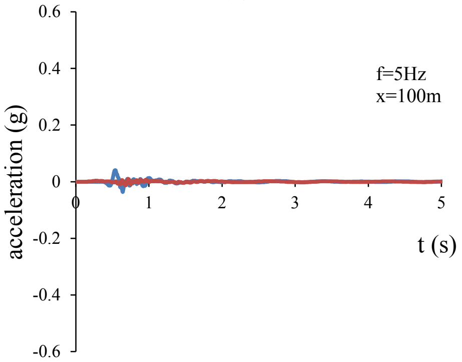
0.6
0.4
0.2
0
-0.2
-0.4
-0.6
acceleration (g)
0
1
2
3
4
5
t (s)
f=5Hz
x=100m

(e)

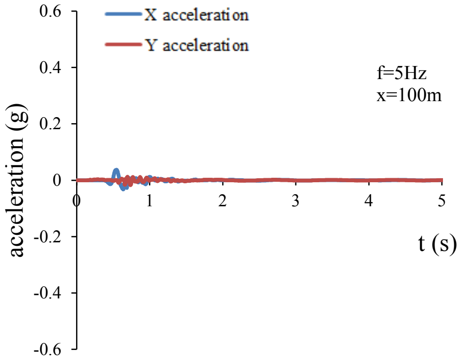
X acceleration
Y acceleration
0.6
0.4
0.2
0
-0.2
-0.4
-0.6
acceleration (g)
0
1
2
3
4
5
t (s)
f=5Hz
x=100m

(f)

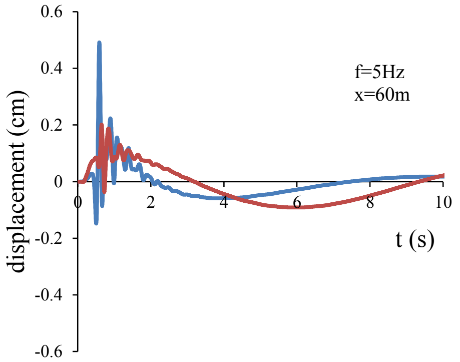
0.6
0.4
0.2
0
-0.2
-0.4
-0.6
displacement (cm)
0
2
4
6
8
10
t (s)
f=5Hz
x=60m

(g)

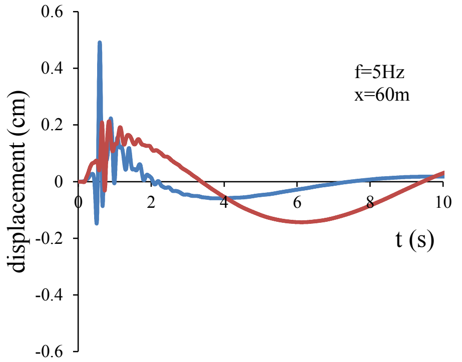
0.6
0.4
0.2
0
-0.2
-0.4
-0.6
displacement (cm)
0
2
4
6
8
10
t (s)
f=5Hz
x=60m

(h)

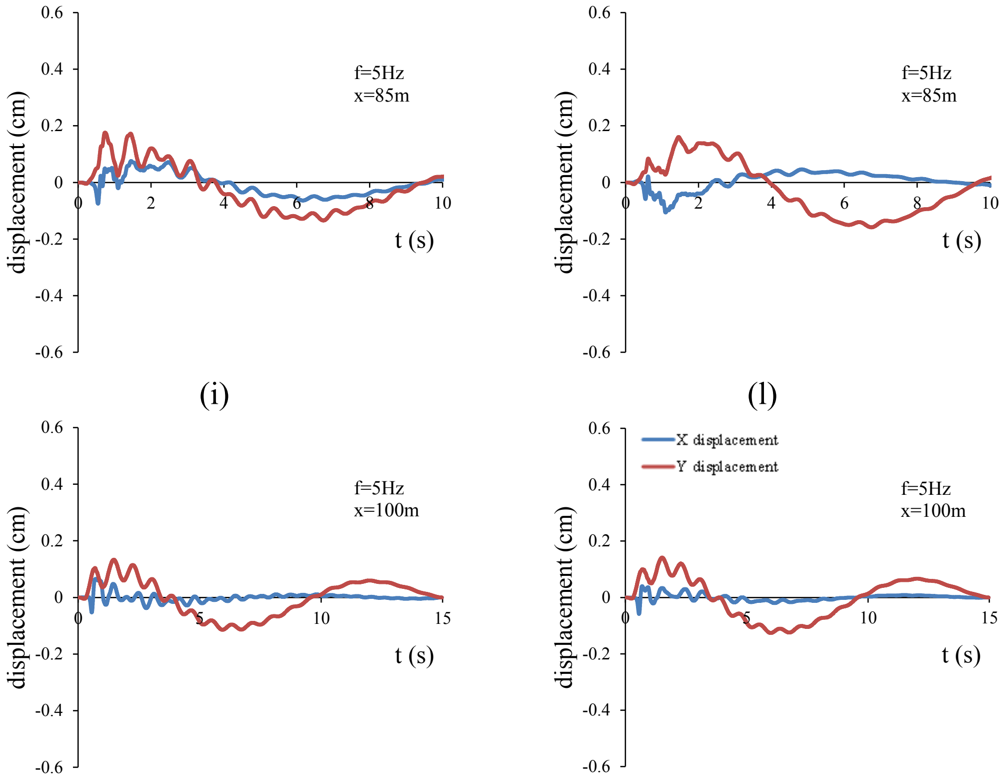

(m) (n)

Figure 2.3.4.4.6 *X and y accelerations and displacements at ground surface due to the propagation of a Ricker wavelet with 5Hz, for the EP-D15 (on the left side) and EP-D5 (on the right side) schemes.*

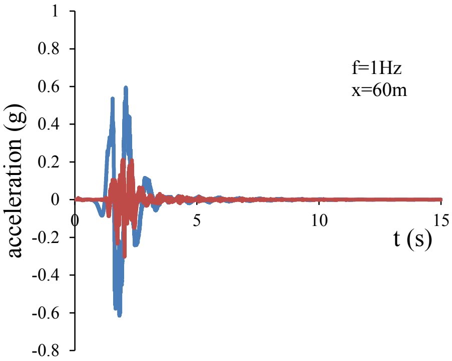
f=1Hz
x=60m
acceleration (g)
t (s)
1
0.8
0.6
0.4
0.2
0
-0.2
-0.4
-0.6
-0.8
0
5
10
15

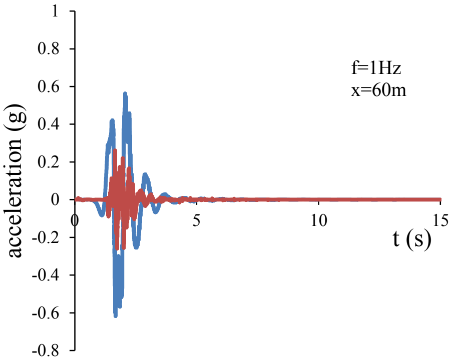
f=1Hz
x=60m
acceleration (g)
t (s)
1
0.8
0.6
0.4
0.2
0
-0.2
-0.4
-0.6
-0.8
0
5
10
15

(a)

(b)

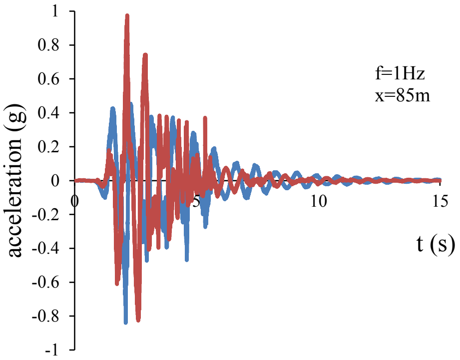
f=1Hz
x=85m
acceleration (g)
t (s)
1
0.8
0.6
0.4
0.2
0
-0.2
-0.4
-0.6
-0.8
-1
0
5
10
15

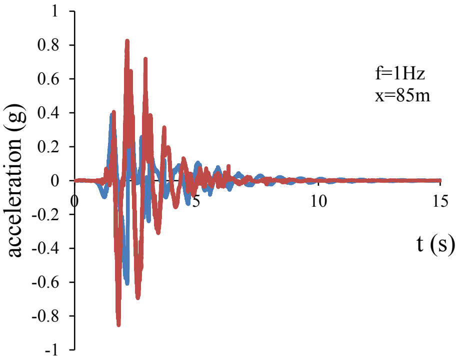
f=1Hz
x=85m
acceleration (g)
t (s)
1
0.8
0.6
0.4
0.2
0
-0.2
-0.4
-0.6
-0.8
-1
0
5
10
15

(c)

(d)

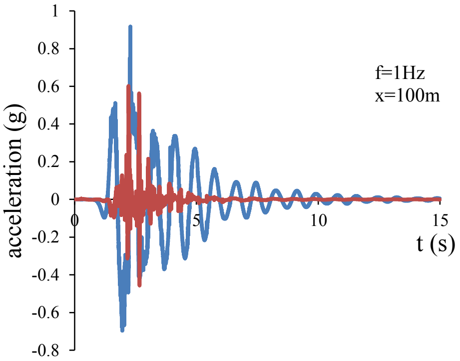
f=1Hz
x=100m
acceleration (g)
t (s)
1
0.8
0.6
0.4
0.2
0
-0.2
-0.4
-0.6
-0.8
0
5
10
15

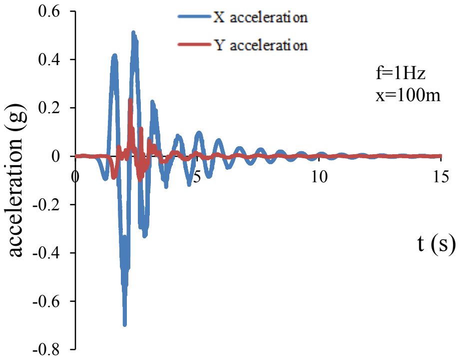
X acceleration
Y acceleration
f=1Hz
x=100m
acceleration (g)
t (s)
0.6
0.4
0.2
0
-0.2
-0.4
-0.6
-0.8
0
5
10
15

(e)1

(f)

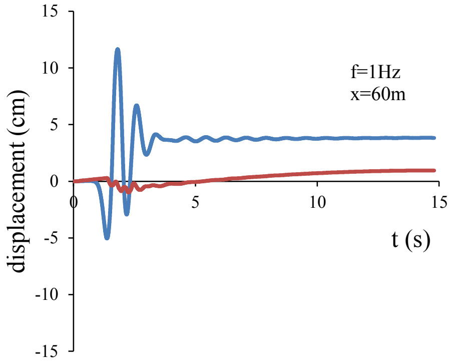
f=1Hz
x=60m
displacement (cm)
t (s)
15
10
5
0
-5
-10
-15
0
5
10
15

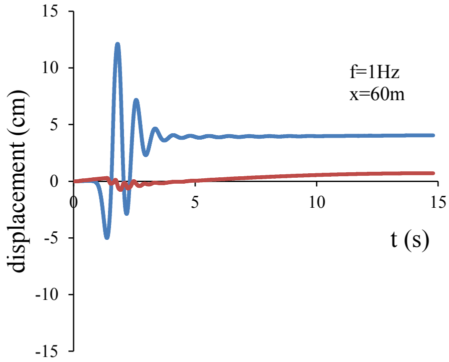
f=1Hz
x=60m
displacement (cm)
t (s)
15
10
5
0
-5
-10
-15
0
5
10
15

(g)

(h)

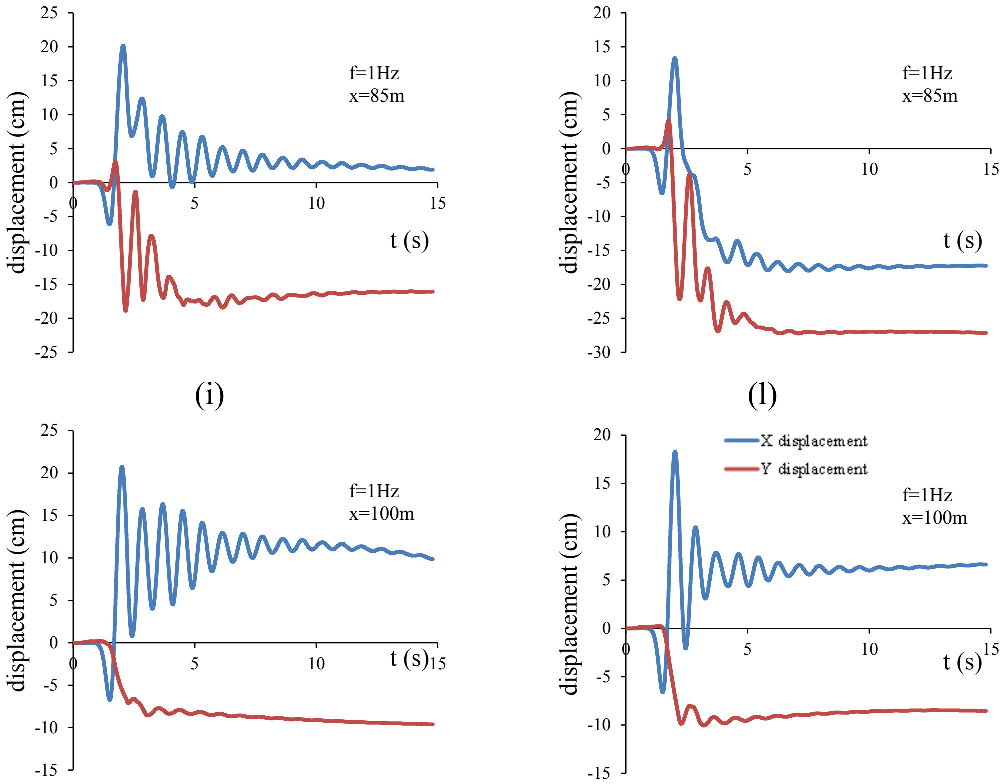

(i) (l)

(m) (n)

Figure 2.3.4.4.7 *X and y accelerations and displacements at ground surface due to the propagation of a Ricker wavelet with 1Hz, for the EP-D15 (on the left side) and EP-D5 (on the right side) schemes.*

2.4. References

Anastasopoulos I., Gazetas G., Loli M., Apostolou M., Gerolymos N. (2010) Soil failure can be used for seismic protection of structures. *Bulletin iof Earthquake Engineering, Vol.8, pp.309-326. Editor Springer, Berlin (Germany).*

Arias A. (1970). A measure of earthquake intensity. *Seismic Design for nuclear power plants.Robert J. Hansen editor. M.I.T. Press, Cambridge, Massachusetts (USA).*

Bardet J.P., Ichii K., Lin C.H. (2000). EERA a Computer Program for Equivalent-linear Earthquake site Response Analyses of Layered Soil Deposits. *Univ. of Southern California, Dep. of Civil Eng., Los Angeles, California (USA).*

Bardet J. P., Tobita T. (2001). NERA A computer program for nonlinear earthquake site response analyses of layered soil deposits. *Univ. of Southern California, Dep. of Civil Eng., Los Angeles, California (USA).*

Bathe K. J., WilsonE. L.(1976). Numerical Methods in Finite Element Analysis. *Englewood Cliffs, Prentice-Hall Inc., Upper Saddle River, New Jersey (USA), pp.528.*

Bouckovalas G., Papadimitriou A. (2006). Aggravation of seismic ground motion due to slope topography. *First European Conference on Earthquake Engineering and Seismology. Geneva (Switzerland), pp.1171.*

Born M., Wolf E. (1959). Principle of optics. *University Press Cambridge.*

Butterworth S. (1930). On the Theory of Filter Amplifiers.Experimental. *Wireless and the Wireless Engineer, Vol.7, pp.536–541.*

DM 14/1/2008. Norme Tecniche per le Costruzioni. *S.O. n. 30 - Gazzetta Ufficiale della Repubblica Italiana, No. 20 - 4/2/2008.*

EC8 (2004). Eurocode 8: Design of structures for earthquake resistance. *European Committee for standardization.*

FLAC Version 7.0 Manual (2011). Dynamic analyses. *5th Edition.*

Gazetas, G. (1982). Vibrational characteristics of soil deposits with variable wave velocity. *Int. Journal for Numerical and Analytical Methods in Geomechanics. Vol.6.*

Hashash, Y.M.A., Park D. (2002). Viscous damping formulation and high-frequency components in deep deposits. *Soil Dynamics and Earthquake Engineering, Vol.22(7), pp.611-624.*

Hardin B.O. (1978). The nature of stress-strain behaviour for soils-State of the art.*Proc.s Geotwechnical Eng. Division Specialty Conference onEarthquake Engineering and SoilDynamics ASCEE, Pasadena, California (USA).*

Hardin B.O., Black W.L. (1968). Vibration modulus of normally consolidated clay.*Journal of the Soil Mechanics and Foundation Division, ASCE, Vol.94, No.SM2. ASCEE, Pasadena, California (USA).*

INGV 2006. Interactive Seismic Hazard Maps. *Internet: http://esse1-gis.mi.ingv.it/.*

Iwan W.D. (1967). On a class of models for the yielding behaviour of continuous and composite systems. *J. Appl. Mech. (ASME), Vol.34, pp.612-617.*

Kelly J. (1999). The role of damping in seismic isolation. *Earthquake Engineering and Structural Dynamics, Vol.28, pp.3-20.*

Kirtas E., Pitilakis, K. (2009). Subsoil interventions effect on structural seismic response. Part II: parametric investigation. *Journal of Earthquake Engineering, Vol.13(2), pp.155-169.*

Kramer S.L. (1996). Geotechnical earthquake engineering. *Prentice-Hall Inc., Upper Saddle River, New Jersey (USA).*

Kuhlemeyer R. L., Lysmer J. (1973). Finite Element Method Accuracy forWave Propagation Problems. *J. Soil Mech. and Foundations, Div. ASCE, Vol.99(SM5), pp.421-427.*

Lysmer J., Kuhlemeyer R. L. (1969). Finite Dynamic Model for Infinite Media. *J. Eng. Mech., Vol.95(EM4), pp.859-877.*

Lombardi D., Flora A., Lirer S., Silvestri F. (2013). An innovative approach for reducing the seismic risk of existing buildings and historic sites. *Second Int. Symp. on geotechnical Engineering for the preservation of monuments and historic sites. Napoli (Italy. Viggiani C., Bilotta E., Flora A & Lirer S. Editors.*

Mroz Z. (1967). On the description of anisotropic workhardening. *J. Mech. Phys. Solids, Vol.15, pp.163-175.*

Ryan, H. 1994. Ricker, Ormsby, Klauder, Butterworth- A choice of wavelets. *CSEG.*

Semblat J. F., Pecker A. (2009). Waves and vibrations in soils: earthquakes, traffic, shocks, construction works. *IUSS press,Pavia (Italy), pp.499.*

Silvestri F., Tropeano G. (2008). Effetto del non sincronismo inclusa la risposta sismica locale sulla sicurezza dei ponti. *PRIN.*

Venditozzi D. (2013). Analisi numerica dell'interazione dinamica tra una fondazione superficiale ed il terreno. *Master Degree thesis, Università degli Studi di Napoli FedericoII, Dipartimento di Ingegneria Civile, Edile ed Ambientale (DICEA), Napoli (Italy).*

Vucetic M., Dobry R. (1991). Effects of the soil plasticity on cyclic response. *Journal of Geotechnical Engineering Division, ASCE, Vol.117, Pasadena, California (USA).*

3. Static analyses

The introduction of a soft caisson into a soil deposit may determine static problems to the structures eventually placed at ground surface. Absolute vertical settlements at ground surface, differential settlements and angular distortions of the building foundations should be valued to avoid incompatible displacements and collapse mechanisms due to the injections of soft layers. In this chapter, some evaluations of these critical aspects are reported.

3.1. Characteristics of the software Plaxis2D

Plaxis2D is a 2D finite element program used to perform deformation and stability analyses for various typologies of geotechnical applications (Plaxis2D Reference Manual). Plaxis2D is based on three different sub-programs, depending on the different stage of analysis, which are:

1. Input
2. Calculation
3. Output.

3.1.1. 1st phase: input

The model has to be large enough not to influence the results of the problem to be studied. Furthermore, it should include a representative discretization of the subsoil into distinct elements, of the construction stages and loadings. In these terms, Plaxis2D automatically generates a finite element mesh based on the composition of clusters and lines in the geometry model, where clusters are areas that are fully enclosed by lines and including homogeneous material properties.

During the generation of the mesh, clusters are divided into 15-node triangular elements, allowing an accurate calculation of stresses and failure loads. A 15-node element consists of 15 nodes (see Figure 3.1.1.1), where adjacent elements are connected through their common nodes. During a finite element calculation, the displacements are calculated at the nodes. In contrast with displacements, stresses and strains are calculated at individual Gaussian integration points (called stress points) rather than at the nodes. A 15-node triangular element contains 12 stress points as indicated in Figure 3.1.1.1b.

After the draft of the geometry, the finite element model (mesh) can be generated by a fully automatic mesh generation procedure, in which the geometry is divided into triangular elements. The generation process is based on a robust triangulation principle, which results in an unstructured mesh, not formed by regular patterns of elements.

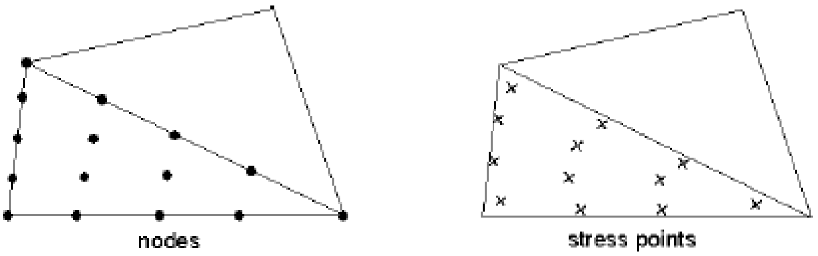

(a) (b)

Figure 3.1.1.1 *Nodes and stress points.*

As far as the mesh dimensions are concerned, a 200m wide and 60m depth calculation model has been assumed, locally varying the geometrical features of the zone where the different treatments (horizontal layers, soft caisson with a rectangular section, inclined injections) have been placed (see, for instance, Figure 3.1.1.2).

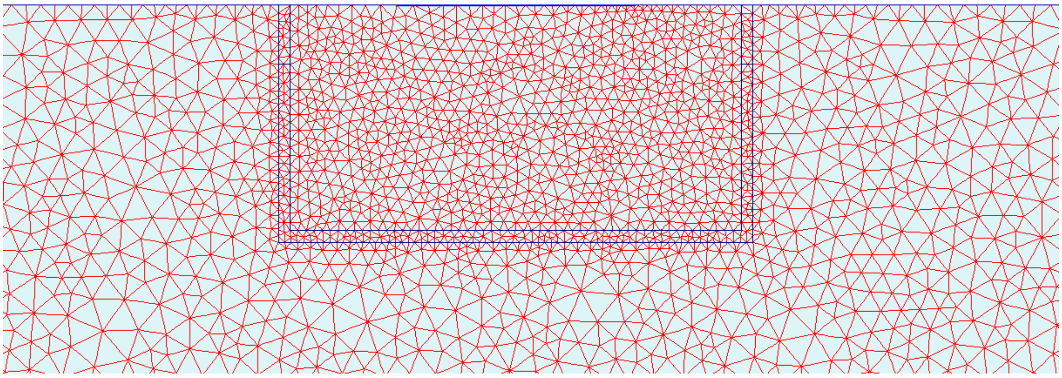

Figure 3.1.1.2 *A view of the mesh in the area close to the soft caisson with rectangular section.*

The mesh has been optimised by performing local refinements for tinier elements i.e. soft layers. The boundary conditions allow the vertical displacements of the lateral sides of the mesh, avoiding the horizontal ones. At the base, nil displacements are imposed.

The dynamic analyses shown in the previous chapters (§2) have been performed without considering any load distributions at ground surface (with the exceptions reported in §2.3.3.5), because dead loads were not relevant in the analyses. The effect of the building would have been relevant in inertial terms, but this was not considered in this thesis.

On the contrary, the results of the static analyses are sensible to the presence of load distributions at ground surface; consequently, different configurations both with and without constant gravity load distributions between 0 and 100kPa and with different extensions L_s at ground surface have been considered. For the sake of simplicity, the foundations are assumed infinitely deformable. In terms of differential settlements, this is a conservative assumption.

3.1.2. 2^nd^phase: calculation

Once the mesh has been generated, the initial conditions must be generated. They include the initial ground water condition, the initial geometry configuration and the initial effective stress state.

In the performed analyses, groundwater conditions have not been taken into account. The analyses require the generation of initial effective stress by using the so-called "k_0-procedure", which could be used for horizontally layered geometries with a horizontal ground surface (Plaxis2D Reference Manual). After the generation of the initial effective stress state, in some cases, a constant gravity load distribution of length L_s has been applied at ground surface. In these cases, the displacements, caused not only by the soil weight but also by the applied loads, have been set equal to zero, thus assuming the calculated stress state as the reference condition for the subsequent calculation phases.

The simulation of the injections is modelled by replacing the soil clusters with the soft layers, with a consequent modification of the stress and strain states. The injections are simulated by replacing the layers all in a sudden. So doing, the possible effects of non-symmetric grouting procedures are not taken into account.

Thefore, in the analyses the mechanical consequences due to the injections are due only to the replacement of the soil with softer layers; other consequences due to the installation techniques have not been simulated because of a totally lack of data or information on possible tested techniques for suitable soil softening procedures. This is an important, conservative assumption; as reported in §4.2.2.5, one of the tested materials shows an expansive behaviour when saturated, from the lowest vertical pressure to a vertical pressure of 200kPa. If a similar behaviour had been used for numerical analyses, the volumetric expansion would have taken into account, with a beneficial effect on vertical displacements.

3.1.3. 3^rd^ phase: output results

Once the calculation has been completed, results can be evalueted using the Plaxis Output sub-program. The static effects may be determinant; in fact, the compatibility of the treatment should be granted in terms of differential and absolute displacements at ground level. The displacements affect aspects such as the accessibility to the buildings, the presence of underground utilities and, above all, the stability of the structures.

Information on allowable values of absolute and differential settlements have been already widely reported by various authors (see Table 3.1.3.1 and 3.1.3.2, and Figure 3.1.3.1).

Usually the more restrictive criteria are considered if aesthetic and functional constraints prevail, for example in the case of valuable historical buildings.

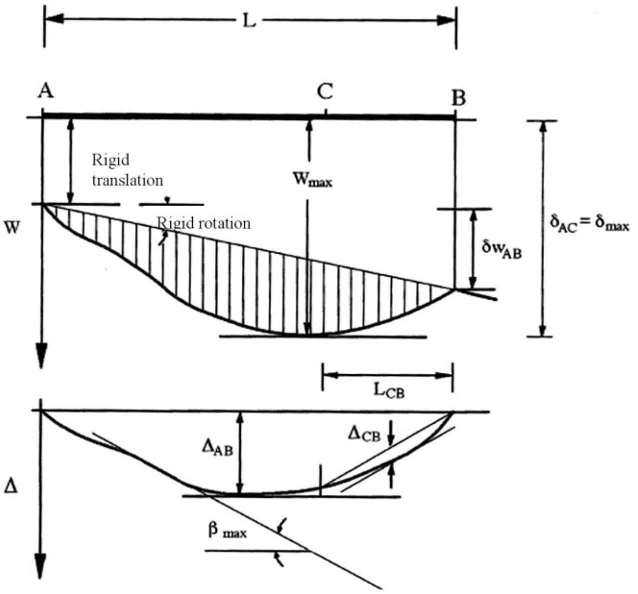

Figure 3.1.3.1 *Geometrical parameters for defining the foundation settlements profile (Viggiani, 1999).*

Motion type	Limitaton factor	Allowable value
Total settlements w_{max} (mm)	Connection to utilities networks	150÷300
	Accessibility	300÷600
	Possibility of differential settlements:	
	masonry walls	25÷50
	frame structures	50÷100
	smokestacks, silos	75÷300
Inclination δ/L	Overturning stability	
	Rotation of smokestacks and silos	≤ 0.04
	Machineries operability:	
	textile machines	0.003
	turbo-generators	0.0002
	overhead cranes	0.003
	Drainage of paved surfaces	0.01÷0.02
Relative rotation β	Multi-storeys masonry walls	0.0005÷0.001
	Mono-storey masonry walls	0.001÷0.002
	Plasters injuries	0.001
	Reinforced concrete frames	0.0025÷0.004
	Curtain walls of reinforced concrete frames	0.003
	Continuous steel frames	0.002
	Simple steel structures	0.005

Table 3.1.3.1 *Allowable values for settlements (Sowers, 1962).*

Structure	Damage typology	Allowable values for relative rotation β			
Frame structures and reinforced masonry walls	To resistant structures	Skempton and McDonald (1956)	Meyerhof (1974)	Polshin and Tokar (1957)	Bierrum (1973)
	To curtain walls	1/150	1/250	1/200	1/150
		1/300	1/500	1/500	1/500

		deflection ratio Δ/L		
		Meyerhof (1974)	Polshin and Tokar (1957)	Burland and Wroth (1974)
masonry walls	deformation with upward concavity	$0.4 \cdot 10^{-3}$	$0.3 \div 0.4 \cdot 10^{-3}$ ($L_l/H \leq 3$)	$0.4 \cdot 10^{-3}$ ($L_l/H = 1$) $0.8 \cdot 10^{-3}$ ($L_l/H = 5$)
	deformation with downward concavity			$0.2 \cdot 10^{-3}$ ($L_l/H = 1$) $0.4 \cdot 10^{-3}$ ($L_l/H = 5$)

Table 3.1.3.2 *Allowable values for relative rotation β and deflection ratio Δ/L, where Δ is the inflection ratio of the structure as defined by Viggiani (1999).*

3.1.4. Geometrical configurations

Three geometrical configurations have been considered:

1. schemes with a single horizontal soft layer;
2. schemes with a soft caisson with a rectangular section;
3. schemes with a soft caisson made of inclined injections.

3.1.4.1 Single horizontal soft layer

The Plaxis model assumed for analyses is shown in Figure 3.1.4.1.1a; the geometrical features and the displacements reference parameters are reported in Figure 3.1.4.1.1b.

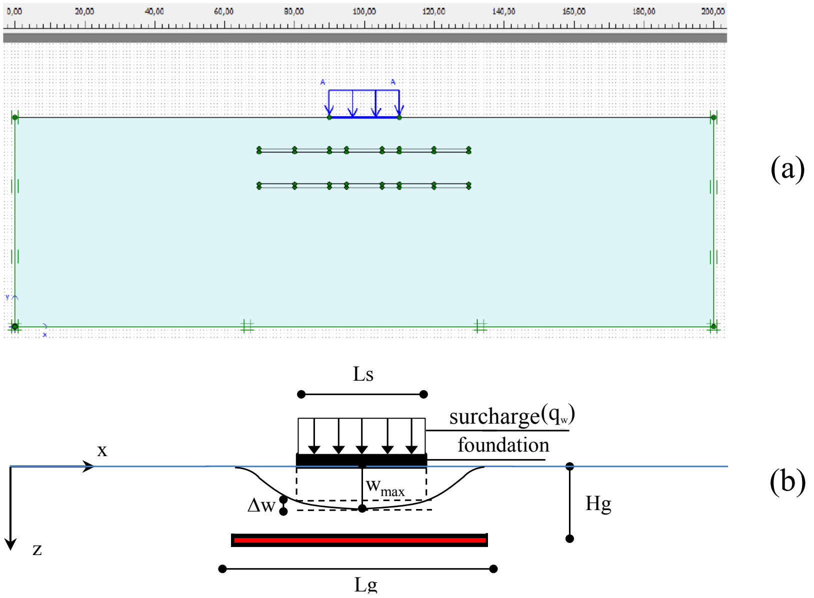

Figure 3.1.4.1.1 *Plaxis model (a), geometrical indications for horizontal soft layers (b) with indications on w_{max} and Δw as reference parameters for settlements.*

The length of the foundation, infinitely deformable, has been assumed equal to either 10m or 20m. The horizontal injections have been studied by varying their depth and their length, as reported in Table 3.1.4.1.1, by assuming, above the foundation, a distributed gravity load of 100kPa.

Parameters	Length L_g (m)	Depth H_g (m)	Thickness (m)
Horizontal soft layer	10; 20; 40; 60	10; 20	1

Table 3.1.4.1.1 *Parameters assumed for horizontal soft layer analyses.*

Three different hypotheses on the mechanical behaviour of the materials, i.e. soil and grouted layers, have been considered.

The first analyses were carried out with a linear elastic model for all the materials (see Table 3.1.4.1.2). As expected, a linear-elastic material exhibits physically meaningless results in terms of settlements. In fact, as reported in Figure 3.1.4.1.2, the vertical displacements at ground surface by assuming a linear elastic model for materials, show a swelling behaviour, with displacements directed upwards (Rainieri, 2013).

Material	Behaviour	γ_s (kN/m^3)	V_S (m/s)	G (kN/m^2)	E (kN/m^2)	K (kN/m^2)	ν
Soil	Linear elastic	20	300	183561	477259	397715	0.3
Soft layer	Linear elastic	10	10	102	265	221	0.3

Table 3.1.4.1.2 *Characteristics of the material assumed for linear elastic analyses.*

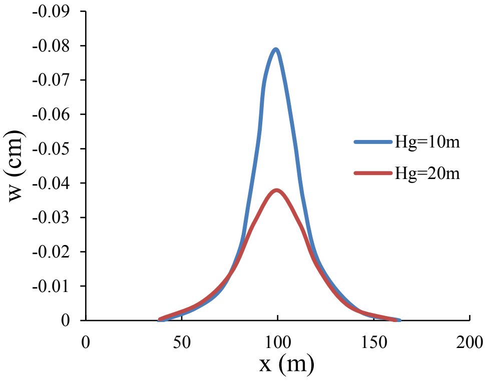

Figure 3.1.4.1.2 *Vertical displacements at ground surface for an elastic soft horizontal layer with H_g=10m or 20m.*

An analogous situation with upwards displacements due to gravity loads has occurred by assuming an elasto-plastic behaviour for the soil (with a Mohr –Coulomb failure criterion) and a linear elastic one for the grouted layers.

Neither the introduction of rigid plates to simulate a rigid foundation nor higher load amplitudes has led to physically acceptable results. The linear elastic model cannot be assumed for static simulations.

By assuming a Mohr-Coulomb failure criterion for both soil and soft layers, whose properties are reported in Table 3.1.4.1.3, analyses have been developed by assuming a 10m or 20m wide deformable foundation and a surcharge of 100kPa.

The foundation size and depth have been varied, as reported in Table 3.1.4.1.3:

Material	γ_s (kN/m^3)	V_S (m/s)	G (MPa)	E (MPa)	K (MPa)	φ (°)	ψ (°)	ν
Soil	20	300	184	477	398	30	0	0.3
Soft layer	10	10	0.102	0.265	0.221	5	0	0.3

Table 3.1.4.1.3 *Characteristics of the material assumed for elastic-plastic analyses.*

The geometrical configuration has been varied by changing the length of the foundation L_s (10m or 20m), the depth H_g (10m or 20m) and the length L_g of the soft layer.

The results have been reported in terms of maximum vertical displacement w_{max}, differential displacements Δw and maximum relative rotation β, where this parameter has been assumed as:

$$\beta_{max} = \frac{\Delta w}{L_s/2} \tag{3.1.4.2.1}$$

It must be preliminary observed that the case of a single horizontal layer (only theoretical) leads to extremely large differential settlements in most of the analysed cases and to relevant absolute displacements as soon as the ratio L_g/H_g exceeds the value 1.5.

The maximum vertical displacement w_{max} (see Figure 3.1.4.1.3 a), increases as the ratio between the length and the depth of the soft layer increases. As expected, the higher surcharge with the largest width of the foundation (i.e. L_s=20m) leads to larger vertical displacements. Deeper treatments result in lower differential settlements Δw (see Figure 3.2.1.1.3 b); the maximum relative rotation β increases as the width or the depth of the foundation decrease.

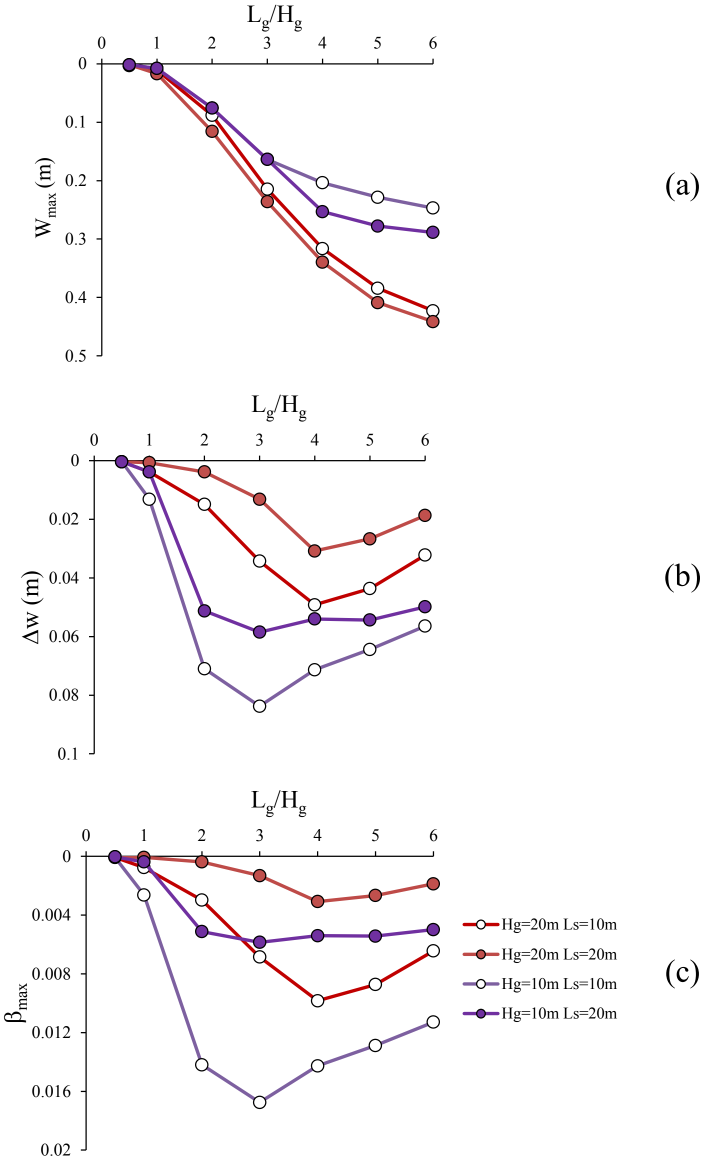

Figure 3.1.4.1.3 *Maximum displacements* w_{max} *(a), differential displacements* Δw *(b) and maximum relative rotation* β *(c) for different geometrical configurations of the horizontal soft layer.*

3.1.4.2 Soft caisson: rectangular section

With reference to a soft caisson with rectangular section (see Figures 3.1.4.2.1), in this paragraph, different geometrical and mechanical parameters have been considered, as reported in Table 3.1.4.2.1; furthermore, other analyses have been developed by varying the volumetric stiffness K, keeping G constant.

Material	γ_S (kN/m^3)	φ' (°)	ψ (°)	V_S (m/s)	G (MPa)	E (MPa)	K (MPa)	L_S (m)	q_W (kPa)
Soil	20	30	0	100/300	20/184	53/477	44/398	10/20	0/50/100
Soft layer	10	5/10/15	0	10	0.102	0.265	0.221		
				30	0.918	2.386	1.989		

Table 3.1.4.2.1 *Parameters varied in the static analyses.*

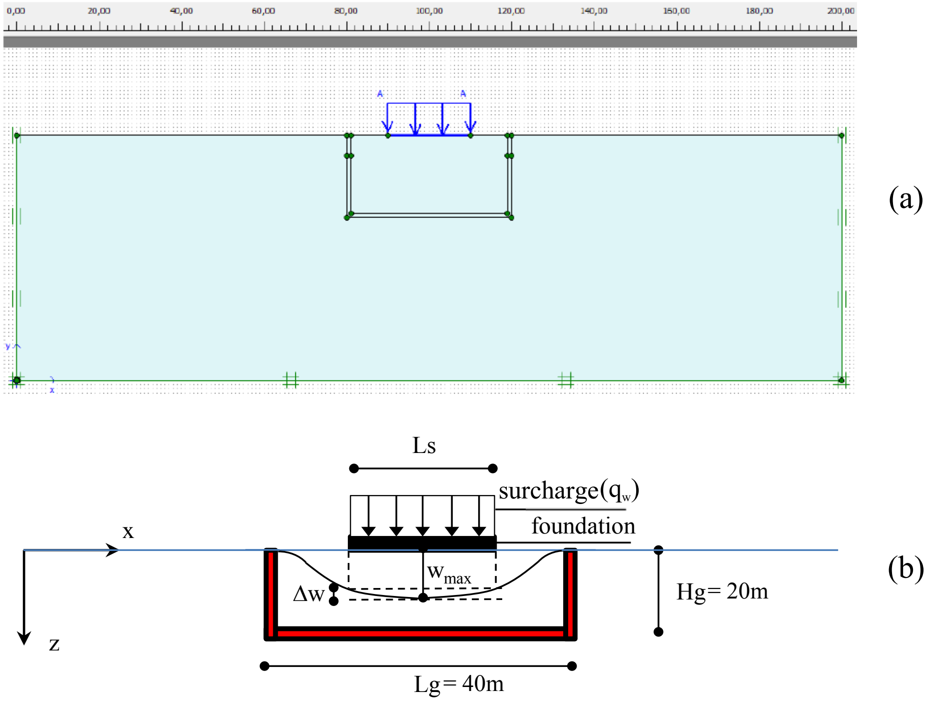

Figure 3.1.4.2.1 *Plaxis model (a) and geometrical indications for soft caisson (b) with indications on w_{max} and Δw as reference parameters for settlements.*

Figures 3.1.4.2.2 report the results in terms of maximum vertical displacements w_{max}, differential displacements Δw and maximum relative rotations β assuming a surcharge q_W of 100kPa and for different values of the shear strength angle.

As expected, the higher surcharge with the largest width of the foundation (i.e. L_s=20m) leads to larger vertical displacements; furthermore, a smaller L_s value determines a reduction in the differential settlements and in the maximum relative rotation.

For larger values of the shear strength angle of the grouted soil φ_g’, lower vertical settlements w_{max} and larger differential displacements Δw are observed. This is probably due to the smaller shear displacements at the soil-soft layer interfaces, which imply a reduction of the vertical settlements of the soft caisson. Figures 3.1.4.2.3 report a magnified picture of the settlements profile, and the position of the plastic points at the interfaces, i.e. the positions at which the failure conditions are reached.

The soil shear stiffness does not affect the maximum vertical displacements in a relevant way; in fact, the maximum vertical displacements and also the differential ones are significantly influenced by the soft layer shear stiffness.

The stiffness and the shear resistance of the grouted layer are extremely relevant, and they cannot be too low to avoid excessive settlements: Figures 3.1.4.2.2 seem to indicate that the shear strength angle φ_g’ should not be lower than 15° and the shear wave velocity $V_{s,g}$ cannot be lower than 30m/s.

Figure 3.1.4.2.4 reports the results of the static analyses developed by varying the surcharge (q_W= 0, 50kPa and 100kPa) as a function of the shear strength angle of the soft layers φ_g’, assuming the foundation length L_s equal to 20m, and the shear wave velocities of the soil $V_{s,s}$ and of the soft layers $V_{s,g}$ equal, respectively, to 300m/s and 10m/s.

A minor dependence of the maximum vertical displacements on q_w is observed, because the higher the load the larger the maximum vertical displacements because the larger the load amplitude the larger the maximum vertical displacements, but with small differences; what is really relevant is confirmed to be the shear strength angle of the grouted soil.

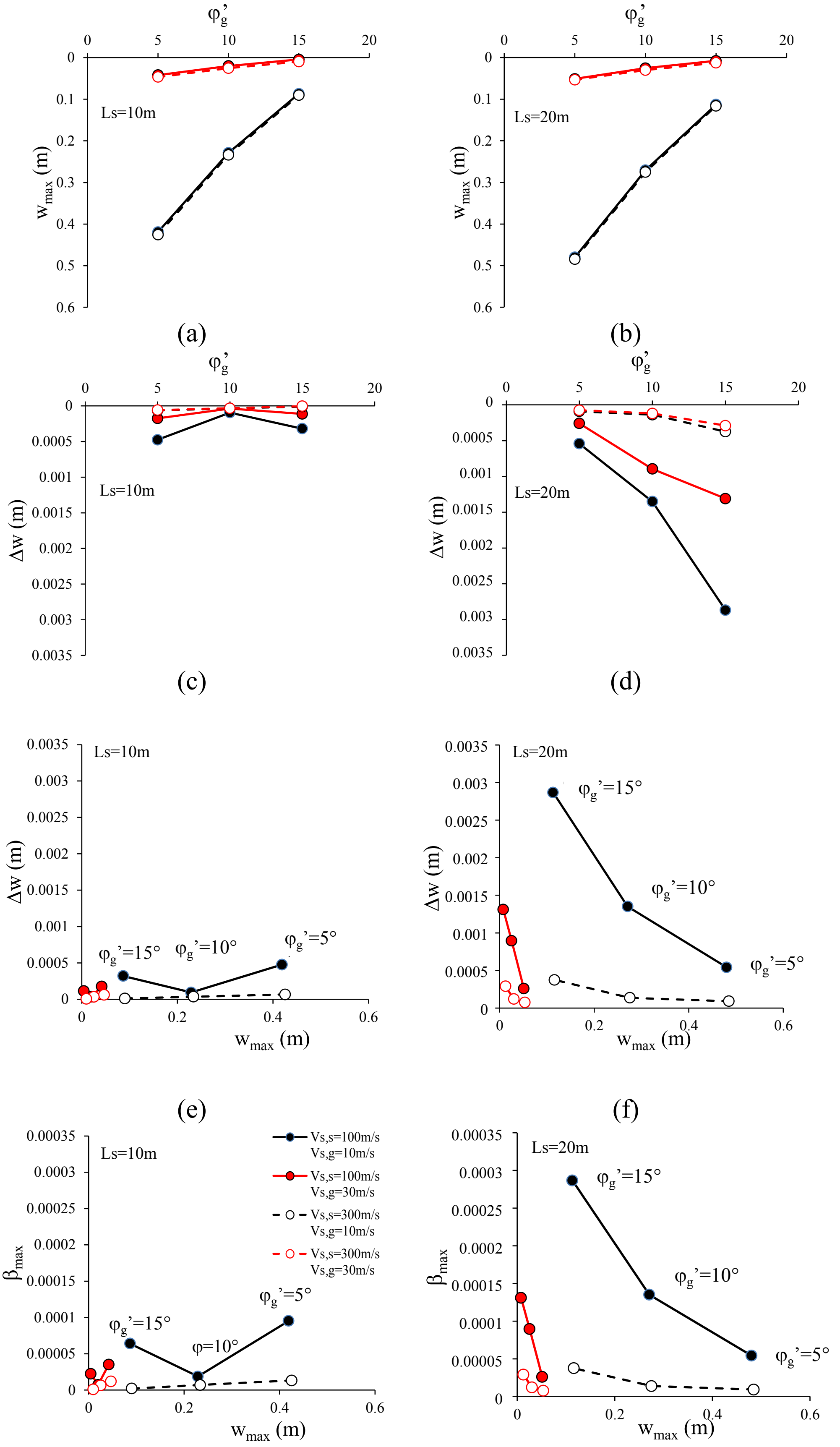

Figure 3.1.4.2.2 *Static analyses results:* w_{max} *(a and b) and* Δw *(c and d) with* φ_g*';* Δw *(e and f) and* β *(g and h) with* w_{max}*.*

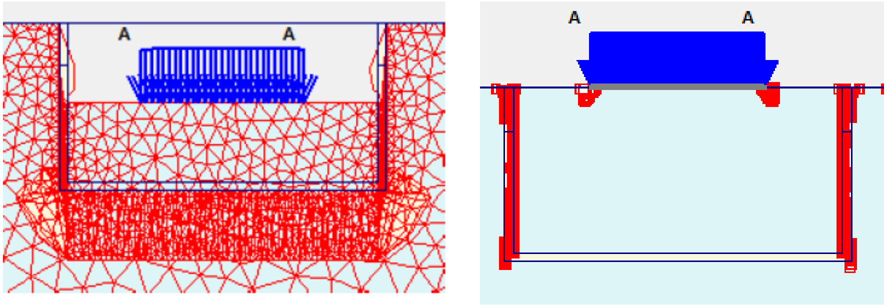

(a) (b)

Figure 3.1.4.2.3 *Magnified picture of the settlements profile (a) and position of the plastic points at the interfaces between the soft layers and the soil (b).*

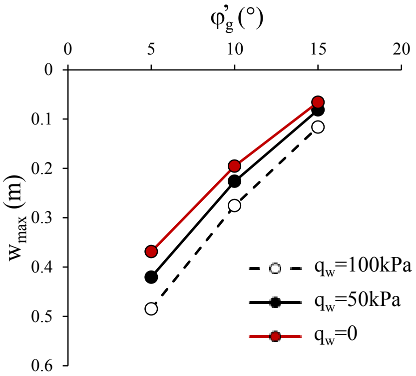

Figure 3.1.4.2.4 *Maximum displacements w_{max} by varying the q_w value.*

The maximum vertical displacements are largely influenced by the volumetric deformations taking place within the horizontal soft layer, and therefore by both the thickness and the volumetric stiffness of the grouted material.

In fact, if a certain scheme configuration with φ_g'=5°, $V_{s,g}$=10m/s, $V_{s,s}$=300m/s and q=100kPa is assumed, by increasing the thickness of the horizontal soft layer of the caisson from 1m to 2m, a doubled maximum vertical displacement is observed (see Table 3.1.4.2.2). As expected, this suggests that the settlements are due principally to the volumetric deformation of the horizontal soft layer.

Horizontal soft layer thickness	w_{max} (m)
2	0.93
1	0.49

Table 3.1.4.2.2 *Results from static analyses by increasing the thickness of the horizontal soft layer.*

On the other hand, the volumetric stiffness of the grouted soil is also significant in terms of displacements. With reference to the assumed soft caisson (see Figures 3.1.4.2.1) analyses have been developed by varying the volumetric stiffness K of the soft layers, as reported in Table 3.1.4.2.3.

Material	γ_s (kN/m^3)	φ' (°)	ψ (°)	V_S (m/s)	G (MPa)	ν	E (MPa)	K (MPa)	L_s (m)	q_w (kPa)
Soil	20	30	0	300	184	0.3	477	398	20	100
Soft layer	10	5	0	10	0.102	0.147	0.234	0.111		
						0.3	0.265	0.221		
						0.477	0.305	2.210		
				30	0.918	0.147	2.105	0.994		
						0.3	2.386	1.989		
						0.477	2.744	19.886		

Table 3.1.4.2.3 *Characteristics on the static analyses involved by varying the K value.*

In Figures 3.1.4.2.5, the maximum displacements w_{max}, the differential displacements Δw and the relative rotation β by varying the volumetric stiffness of the soft layers K are reported. As expected, the maximum displacements decrease with increasing the volumetric stiffness of the grouted soil, because of the lower compressibility of the horizontal soft layer.

By assuming a soft caisson with a rectangular section, potential damaging values for w_{max} are observed with reference to the lower shear strength angles and the lower volumetric stiffness ones (for $\varphi'_g = 5°$ and $V_{s,g} = 10$m/s, $w_{max} \approx 50$cm; see Figures 3.1.4.2.4).

The geometrical configuration of the treatment seems to be important, because by enlarging the soft caisson, a higher weight will load the horizontal soft layer up.

The differential displacements generally assume extremely low values, because the vertical displacements are regularly distributed along the soft caisson length. Consequently, the relative rotation β has generally a very low value, far from the ones that may produce structural damages or failures (see Table 3.1.3.2).

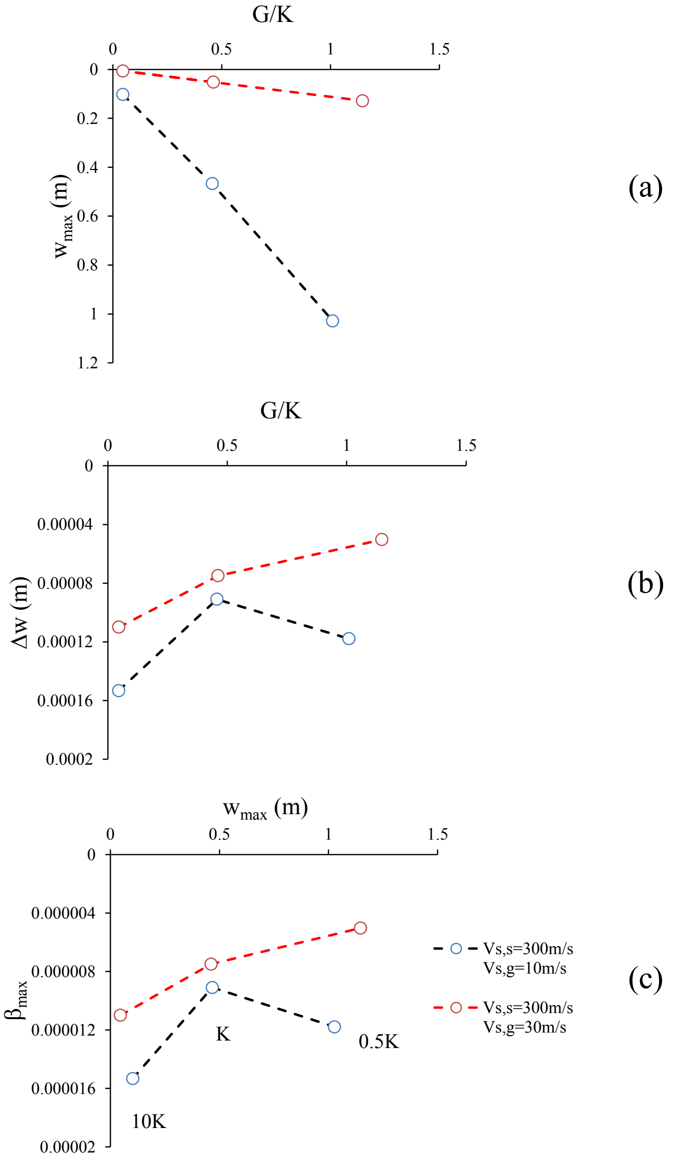

Figure 3.1.4.2.5 *Maximum displacements* w_{max}, *differential displacements* Δw *and relative rotation* β *by varying the volumetric stiffness of the soft layers K.*

3.1.4.3 Soft caisson: inclined injections

With reference to a soft caisson made of inclined injections (see Figures 3.1.4.3.1), the list of the carried out analyses is reported in Table 3.1.4.3.1. The maximum depth H_g of the treatment and the width of the foundations L_s are always equal to 20m.

Scheme	Material	γ_s (kN/m^3)	φ' (°)	V_S (m/s)	G (kPa)	ν	E (kPa)	K (kPa)	q_w (kPa)	ι (°)
1	Soil	20	30	300	184	0.3	477	398	0	45
	Soft layer	10	5/10/15	10	0.102	0.3	0.265	0.221		
2	Soil	20	30	100 300	20 184	0.3	53 477	44 398	100	45
	Soft layer	10	5/10/15	10 30	0.102 0.918	0.3	0.265 2.386	0.221 1.989		
3	Soil	20	30	100 300	20 184	0.3	53 477	44 398	100	45
	Soft layer	10	5	10	0.102	0.147 0.3 0.477	0.234 0.265 0.305	111 221 2210		
	Soft layer	10	5	30	0.918	0.147 0.3 0.477	2.105 2.386 2.744	0.994 1.989 19.886		
4	Soil	20	30	100	20	0.3	53	44	50	30/40 45/55
	Soft layer	10	5/10/15	10	0.102	0.3	0.265	221		

Table 3.1.4.3.1 *Schemes of the performed analyses.*

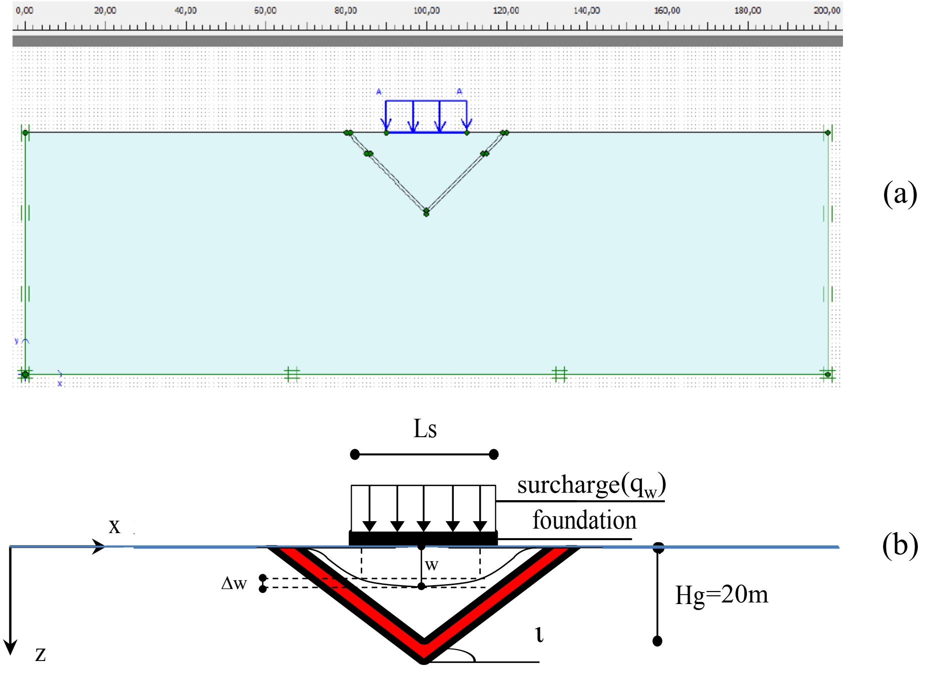

Figure 3.1.4.3.1 *Plaxis model (a) and geometrical indications for soft caisson (b) with indications on w_{max} and Δw as reference parameters for settlements.*

As for the rectangular soft caisson, the soft layers highly affect the tensional and deformative state. Figures 3.1.4.3.2 report the vertical displacements calculated both along the vertical passing for the centre of the model and at ground surface adopting the Scheme 1 (see Table 3.1.4.3.1). As observed for the rectangular section soft caisson, vertical displacements are concentred in the soft layer (see Figure 3.1.4.3.2a) and are essentially caused by the deformation of the soft layer (the value is in fact basically constant within the box). The vertical displacements are extremely sensitive to the value of the shear strength angle of the soft layers, increasing as it decreases. Again, these results indicate φ'_g=15° as a minimum value to avoid excessive settlements at ground level.

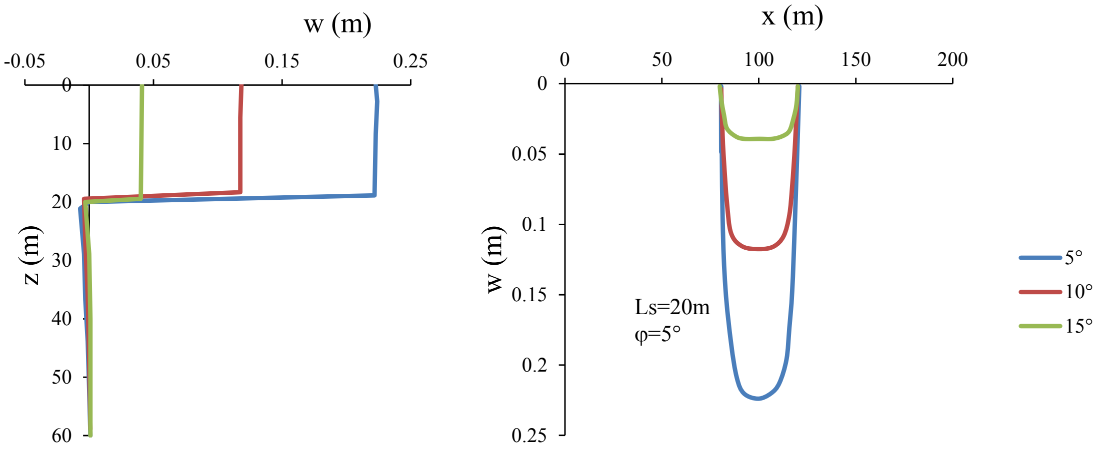

(a) (b)

Figure 3.1.4.3.2 *Vertical displacements, due to the injection of soft inclined soft layers into a soil embankment, along the vertical section for the centre of the model assumed for analyses (a), and at ground surface (b).*

As for the soft caisson with rectangular section (§3.1.4.2), the Scheme 2 (see Table 3.1.4.3.1) has been assumed to identify the dependence of the maximum displacements and of the differential displacements on the value of the shear strength angle φ'_g. In Figures 3.1.4.3.3, the results of the static analyses are reported. The maximum vertical displacements w_{max} increase as the shear strength angle increases, being influenced by the stiffness of the soft layers as well. The higher the stiffness of the soft layer the lower the maximum displacements. For the lower values of the soft layer stiffness, the maximum displacements are more sensitive to the shear strength angle.

Differential displacements Δw and relative rotations β show a dependence on the shear strength angle similar to the one observed in terms of maximum displacements. As expected, they also depend a lot on the stiffness of the soft layer. The maximum relative rotations β

always have very low values. Figure 3.1.4.3.3c summarizes in a neat way the combined effect of the shear strength angle and the stiffness of the soft layers, which results in an almost linear relation between w_{max} and β. Likely, this relationship depends on the inclination of the layers. The soil displacement profile at ground surface is shown, for φ'_g equal to 5° and 15°, in Figures 3.1.4.3.4; the relevance of the shear strength angle and of the soft layer stiffness is evident. The soil stiffness does not play a significant role.

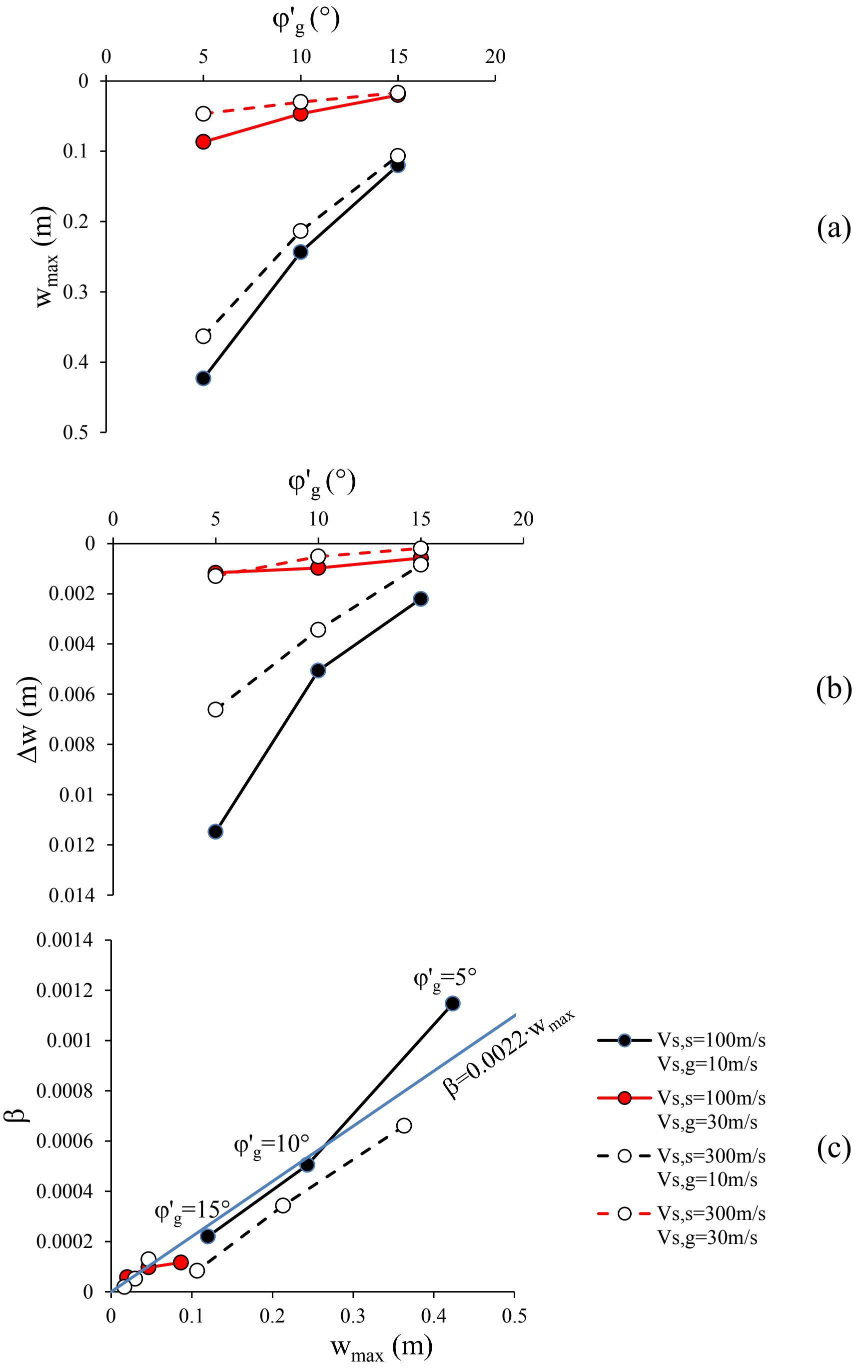

Figure 3.1.4.3.3 *Maximum vertical displacement* w_{max} *(a) and differential displacements* Δw *(b) by varying the shear strength angle* φ'_g*; maximum relative rotation* β *(c) wersus the maximum vertical displacement* w_{max}.

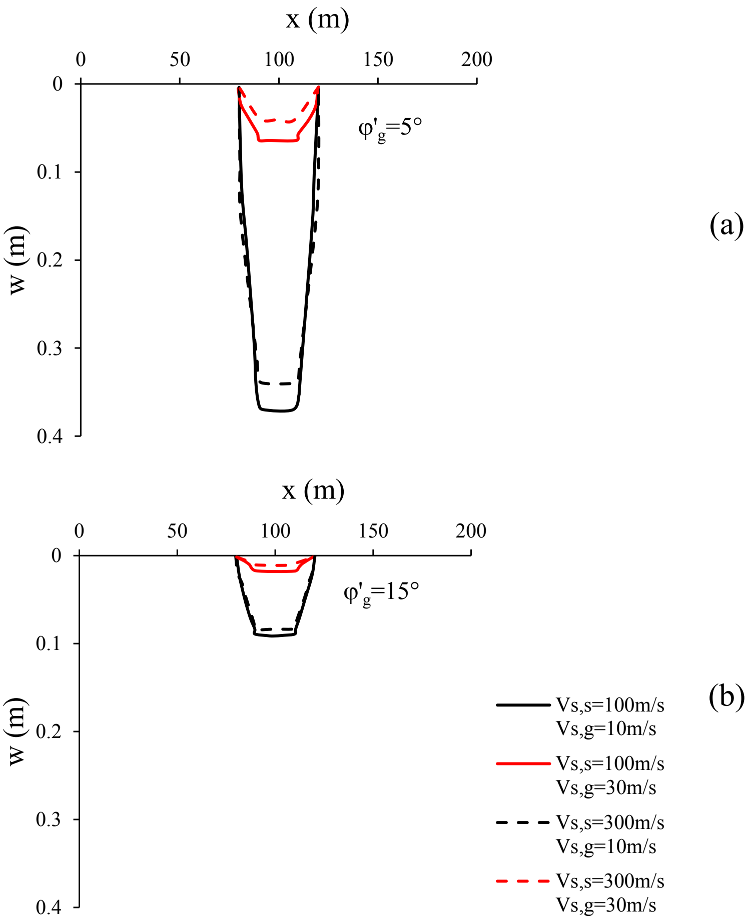

Figure 3.1.4.3.4 *Vertical displacements at ground surface for* $\varphi'_g=5°$ *(a) and* $\varphi'_g=15°$.

With reference to the Scheme 3 (see Table 3.1.4.3.1), the volumetric stiffness has been varied assuming a constant value of the shear stiffness.

Figures 3.1.4.3.5 report the maximum displacements w_{max}, the differential displacements Δw and the relative rotation β by varying the volumetric stiffness K of the soft layers. These curves confirm the observations reported in §3.2.1.2 on soft caissons of rectangular section: the maximum vertical displacements at ground level increase as the ratio G/K increases. This effect is not so clear for differential settlements.

The numerical analyses carried out varying the shear stiffness of the soft layers for a given value of their volumetric one have confirmed these conclusions.

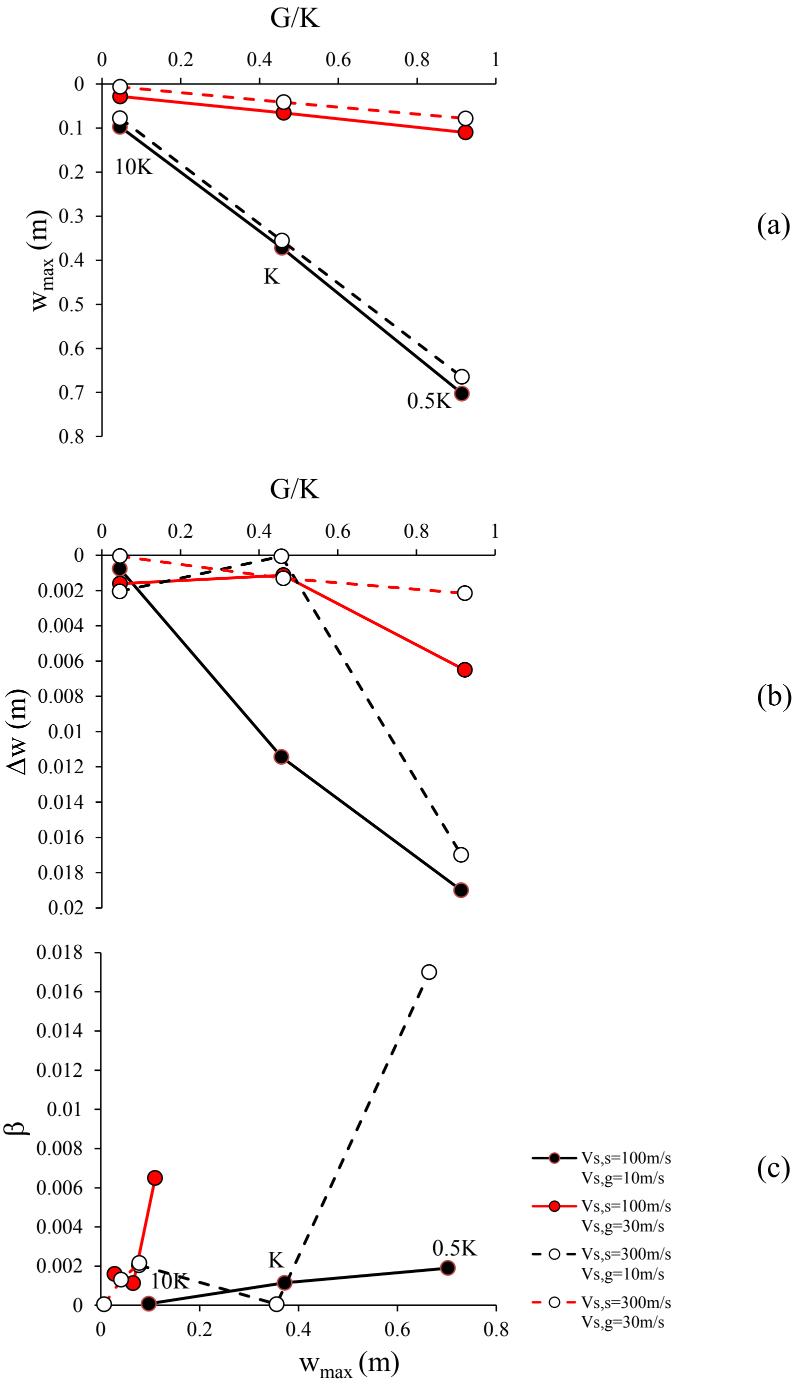

Figure 3.1.4.3.5 *Maximum displacements w_{max} (a), differential displacements Δw (b) and relative rotation β (c) by varying the volumetric stiffness K of the soft layers.*

In particular, inclination angles of 30°, 40°, 45° and 55° have been assumed, adopting the Scheme 3 (see Table 3.1.4.3.1).

By varying the inclination, a trend of the settlement has been observed, due to the differences among the vertical displacement distributions. Increasing the inclination from 30° to 55°, a concentration of displacement in the centre of the soft caisson can be observed.

The inclination of treatments clearly influences the displacements at the ground level, even though the shear strength angle and the treatment stiffness still seem to be the most relevant parameters, as stated in Figures 3.1.4.3.7.

Figure 3.1.4.3.7a suggests that, increasing the soft layer shear velocity from 10m/s to 20m/s, lower maximum and differential displacements are observed, with higher values for the larger treatment inclinations ι.

Figures 3.1.4.3.8 summarize the results in terms of differential displacements versus w_{max}. Increasing the treatment depth, higher maximum displacements are observed due to the larger stresses caused by the weight of the soil contained in the soft caisson.

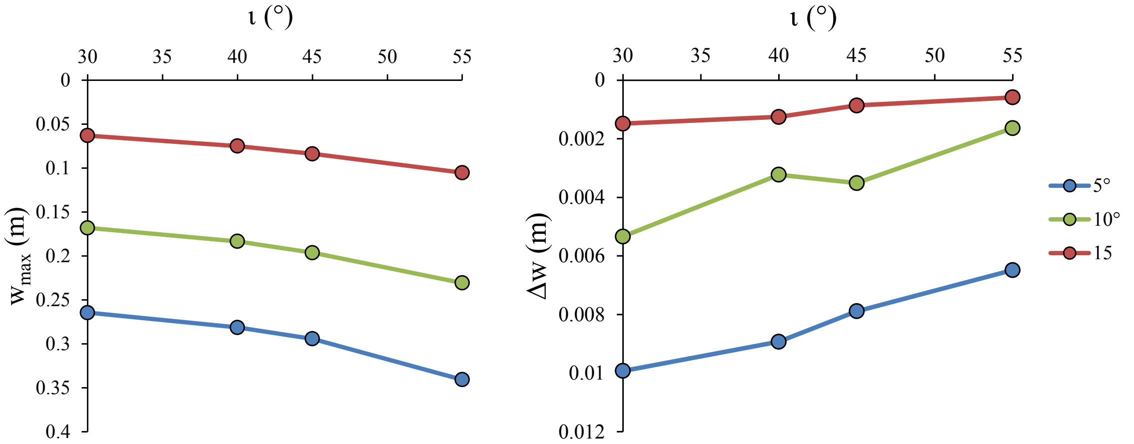

(a) (b)

Figure 3.1.4.3.6 *Maximum displacements w_{max} (a) and differential displacements Δw (b) by varying the inclination ι and the shear strength angle φ'_g from 5° to 15°.*

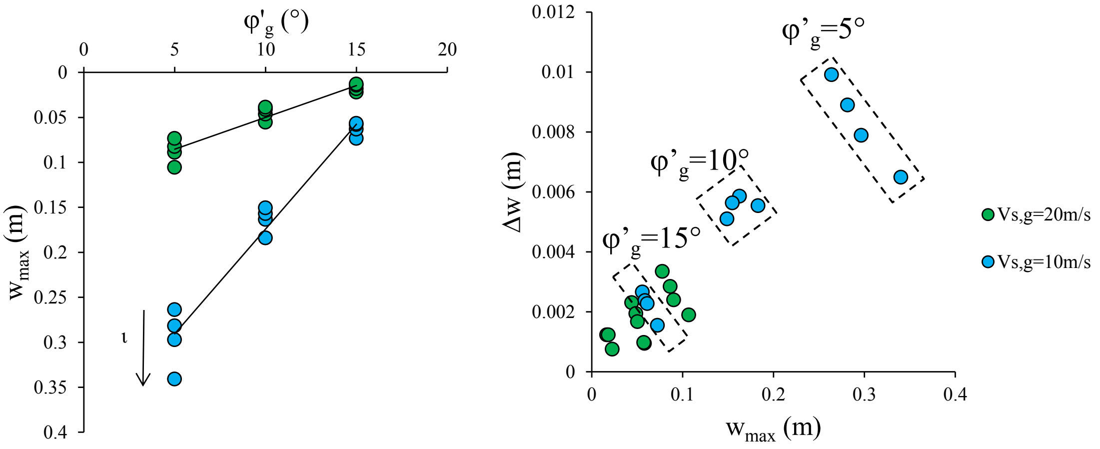

(a) (b)

Figure 3.1.4.3.7 *Maximum displacements w_{max} (a) and differential displacements Δw versus the maximum ones (b) by varying the shear strength angle φ'_g, the shear stiffness $V_{s,g}$ of the soft layers and the inclination ι.*

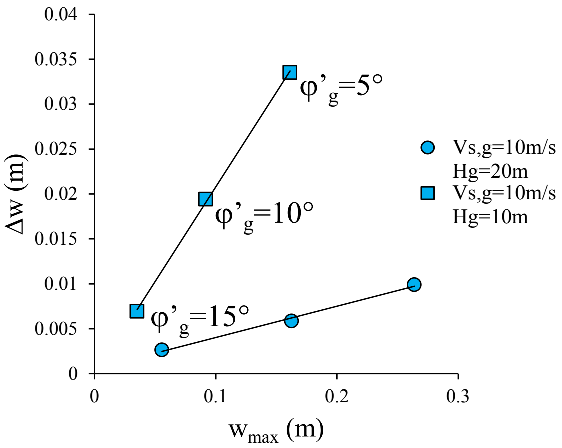

Figure 3.2.1.3.8 *Differential displacements versus the maximum ones by varying the shear strength angle* φ'_g*, and the maximum depth* H_g *of the soft layers, by assuming an inclination* $\iota=30°$*.*

3.1.5. Effect of the treatment on the ultimate load value

The introduction of the soft layers may cause a decrement of the ultimate load value. In Figure 3.1.5.1 the load-displacement curves related to a geometrical configuration made of injections with inclination ι equal to 45°, whose characteristics have been described in Table 3.1.5.1, are reported. The load-displacement curves have been calculated by imposing a rigid vertical displacement to the foundation.

In order to calibrate the model, the numerical limit load with no treatment has been compared to the value obtained with Terzaghi's formulation (Terzaghi, 1948) for shallow. For the assumed model with a shallow foundation placed at ground level, and for purely friction resistant materials, the Terzaghi formula leads to:

$$Q_{\lim,Terzaghi} = \left(\frac{1}{2} \cdot L_s \cdot \gamma_2 \cdot N_\gamma \right) \cdot L_s \qquad (3.1.5.1)$$

where N_γ is a parameter linked to the shear strength angle (Viggiani, 1999).:

$$N_\gamma = 2 \cdot \left(\frac{1+\sin\varphi'_g}{1-\sin\varphi'_g} \cdot e^{\pi \cdot tg\varphi'_g} + 1 \right) \cdot tg\varphi'_g \qquad (3.1.5.2)$$

N_γ is equal to 22.40; the ultimate load value derived with Terzaghi's formulation is therefore:

$Q_{lim,Terzaghi}$ = 89600kN/m.

$V_{s,s}$ (m/s)	$V_{s,g}$ (m/s)	H_g (m)	ι (°)	φ_g' (°)	L_s (m)
300	10	20	45	5/10/15	20

Table 3.1.5.1 *Characteristics of the scheme considered for ultimate load curves.*

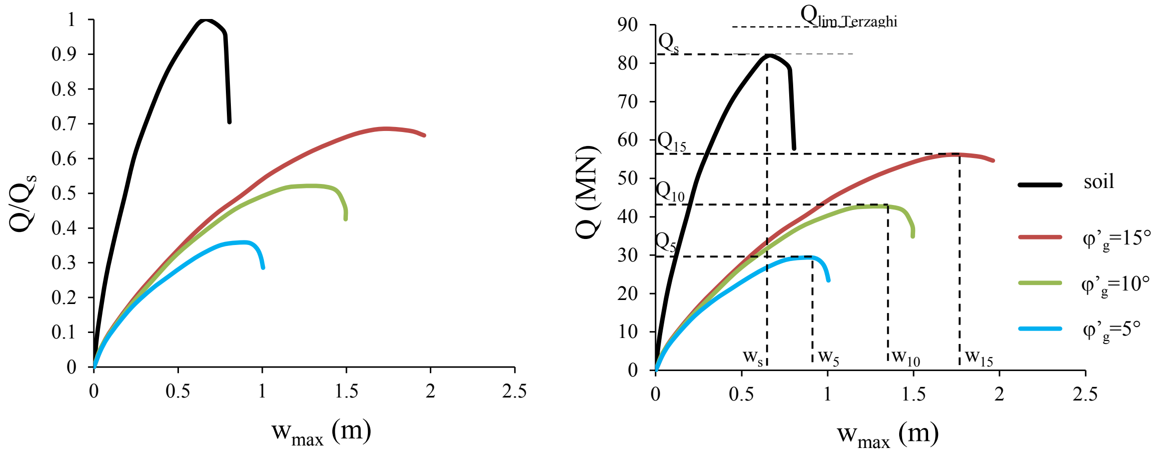

(a) (b)

Figure 3.1.5.1 *Ultimate load curves for different shear strength angle degrees φ'$_g$: normalized (a) and absolute values (b).*

The insertion of layers with low stiffness and shear strength causes a significant reduction of the ultimate bearing capacity of the shallow foundation, which may be unacceptable for structure at ground level to protect.

The reduction observed in Figures 3.1.5.1 depends on the value of the shear strength angle of the soft layers φ'$_g$: the ultimate load decreases as the shear strength angle decreases. In particular, it is observed a variation of the ultimate load value from Q_s=82MN/m in the case of no treatment to 30MN/m for φ'$_g$=5°. Furthermore, by decreasing the φ'$_g$ value from 15° to 5°, the ultimate load value is halved.

Moreover, the insertion of the soft layers causes a large increment of the vertical displacement observed when the ultimate condition occurs. In fact, the pre-existent value w_s (i.e. with no treatment) can be compared to the values obtained for φ'$_g$ equal to 5°, 10° and 15° (i.e. w_5, w_{10} and w_{15}): the vertical displacements increases as the shear strength angle φ'$_g$ increases. For instance, the vertical displacement varies from 0.67m, in the case of no treatment, to 1.73m for φ'$_g$=15°.

If the bearing capacities exhibited by the shallow foundation when the displacements are equal to w_s are taken into account, it is noted that, by varying φ'_g, the ultimate load values are included in a restricted range between 28MN/m and 33MN/m.

By assuming w_s as reference displacement, the ultimate load is reduced from Q_s=82MN/m to $Q_5 \cong$30MN/m: the numerical results pose a significant warning, especially because the soft caisson has been conceived with the aim to protect strategic buildings, whose integrity has to be necessarily preserved.

3.2. References

Burland J. B., Wroth C. P. (1974). Settlement of buildings and associated damage. *State of the Art review, Proc. Conf. on Settlement of Structures, Cambridge, Pentech Press, London pp.611-654.*

Bjerrum L. (1973). Problems of soil mechanics and construction on soft clays. *State of the Art Report, VIII Int. Conf. Soil. Mech. Found. Eng., Moscow (Russia), Vol.3, pp.111-159.*

Meyerhof G. G. (1974). Ultimate bearing capacity of footings on sand layer overlying clay. *Canadian Geotechnical Journal, Vol.11, pp.223-229.*

Skempton A. W., McDonald D. H. (1956). Allowable settlement of buildings. *Proc. ICE, part.3, Vol.5, pp.727-768.*

Plaxis2D Reference manual http://www.plaxis.nl/files/files/2DAnniversaryEdition-2-Reference.pdf

Polshin D. E., Tokar R. A. (1957). Maximum allowable non-uniform settlement of structure. *Proc. 4th ICSMFE, London (Great Britain) Vol.1, pp.402-405.*

Rainieri G. (2013). Fattibilità di Interventi di mitigazione del rischio sismico per edifici esistenti con iniezioni profonde nel terreno. *Tesi di laurea in Ingegneria Strutturale e Geotecnica presso il Dipartimento di Ingegneria Idraulica, Geotecnica e Ambientale dell'Università degli Studi di Napoli Federico II, Napoli (Italy).*

Sowers G. F. (1962). Shallow foundations Foundation Engineering. *G.A. Leonards (ed.), McGraw-Hill Book Co., New York, New York (USA), pp.525-632.*

Viggiani C. (1999). Fondazioni. *Hevelius Edizioni, Benevento (Italia), pp.565.*

Terzaghi K., Peck Peck R. B.(1948). Soil Mechanics in Engineering Practice. *John Wiley and Sons, New York, New York (USA), pp.566.*

4. Laboratory tests

The basic idea is to obtain a mixture with mechanical characteristics able to ensure a low dynamic impedance. Several materials could, in principle, be suitable as soft worsening grouts; in this chapter, the results of some tests carried out on two different materials are reported, i.e. a polyurethane foam and a superabsorbent polymer (SAP).

The polyurethane foams can be considered an interesting class of material; they are polymers that have a molecular backbone containing carbamate groups (-NHCO2). These groups, called urethane, are produced through a chemical reaction between a diisocyanate and a polyol. Developed in late 1930s, polyurethanes are some of the most versatile polymers; they are broadly used in the construction field and for the geotechnical industry (Naudts, 2003). They are used in building insulation, surface coatings, adhesives, solid plastics, and athletic apparel. The polyurethane rigid foams (PF) are of potential interest; the mechanical features of the PF are primarily derived by a highly cross-linked network structure in the polyurethane matrix. The polyurethane rigid foams are usually prepared by mixing diphenylmethane diisocyanate or its derivatives with a polyol blend which contains polyols, blowing agents, surfactants, catalysts, and other additives such as, flame retardants. Polymeric diphenylmethane diisocyanate is most commonly used to make polyurethane rigid foams, while a very broad range of polyols can be selected to achieve different properties.

Another tested material is a superabsorbent polymer (SAP), i.e. a polymer that can absorb and retain extremely large amounts of a liquid with respect to its own mass. Water absorbing polymers, which are classified as hydrogels when cross-linked (Kabiri, 2003), absorb aqueous solutions through hydrogen bonding with water molecules. The ability of the SAP to absorb water is a factor of the ionic concentration of the aqueous solution. In deionized and distilled water, a SAP may absorb 500 times its weight (from 30÷60 times its own volume) and can become up to 99.9% liquid, but when put into a 0.9% saline solution, the absorbency drops to maybe 50 times its weight. The presence of valence cations in the solution will inhibit the ability of the polymer to bond with the water molecule. The total absorbency and swelling capacity are controlled by the type and degree of cross-linkers used to make the gel. Low density cross-linked SAP generally has a higher absorbent capacity and swells to a larger degree. This type of SAP also has a softer and more sticky gel formation. High cross-link density polymers exhibit lower absorbent capacity, but the gel strength is firmer and can maintain particle shape even under modest pressure.

4.1. Laboratory activity on a polyurethane foam

The Polyurethane foam used in the laboratory activity (Bostik-Construct PU-Universale; see:http://www.bostik.it/bostik/prodotti/sigillanti/1480/construct-pu-universale) is a self-expanding polyurethane insulating foam generally used to fills joints and fissures. It expands up to 50÷60 times its original volume and it is essentially a hydrophobic material.

The laboratory tests have tried to determine the density and the shear stiffness of this foam when injected to pressure higher than the atmospheric one. It is a matter of interest the capacity of the foam to expand at a given depth into a soil deposit, preserving its low dynamic impedance.

A test equipment has been designed to inject the foam at given pressures, to define the volume variation and the density of the material, and to obtain a certain number of specimens (formed at high pressures). The specimens extracted by the density test equipment have been then tested in the Thor cell (D'Onofrio, 2006), to perform resonant column tests (RCT).

Figure 4.1.1 shows the equipment scheme used to determine the density of the specimens.

The foam is injected into a soft latex box placed into a cell with water at a given pressure. The volumetric expansion of the self-expanding polyurethane foam varies the water volume. A volume gauge linked to the cell assures accurate measurements of the variations of volume due to the foam injection. The air eventually lying in the injection circuits is expelled by an air drainage placed at the final side of the equipment.

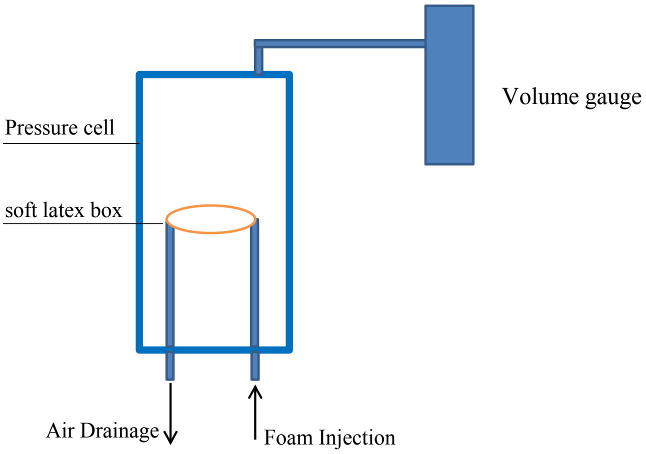

Figure 4.1.1 *Test equipment scheme.*

Figure 4.1.2a shows the variations of the mass density value ρ with the pressure p. Figure 4.1.2b reports the results of the RCT in terms of decay curves of the shear stiffness G/G_0 and damping ratio D versus the shear strains γ. The density assumes extremely low values, which varies from 5kg/m^3 to 50kg/m^3 in the pressure range 0÷150kPa.

The shear stiffness decay curves and the variations of the damping ratio have been measured on two specimens, formed at two different pressures of 0 and 150kPa. The isotropic pressures of the Thor cell during the tests have been assumed equal to the ones at which specimens have been formed. The shear stiffness decay curves are well described by the Ramberg-Osgood relationships (Ramberg and Osgood, 1943), defined by the following equation:

$$\gamma = \left(\frac{1-\frac{G}{G_0}}{C_a \cdot \left(\frac{G}{G_0}\right)^{R_a}} \right)^{\frac{1}{R_a-1}} \tag{4.1.1}$$

where the parameters C_a and R_a are assumed, respectively, equal to 2.6 and 2.

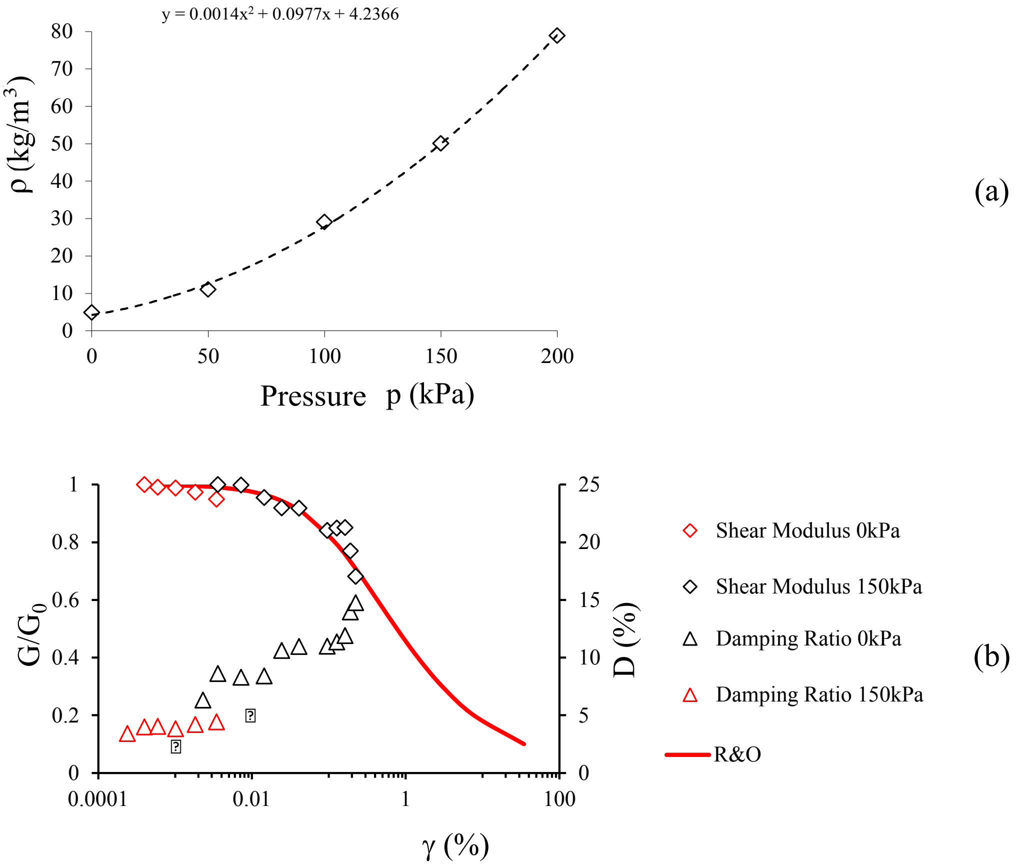

Figure 4.1.2 *Density measurements (a), decay curves G/G$_0$ and variations of the damping ratio D (b) from RCT.*

The values of the measured initial shear stiffness G_0 are:

G_0 (p=0) = 2.4MPa
G_0 (p=150kPa) = 28MPa

Considering the previous density values, in the range 0÷150kPa, the following values of the dynamic impedance at low shear strain have been calculated:

$\eta=\rho\cdot V_S=3400\div38000\text{kN}/(\text{m}^2\text{s})$

These values are extremely high with respect to the ones which result numerically effective (1000÷3000kN/(m^2s); see §2.3); as a consequence, the polyurethane foams cannot be considered suitable as soft layers.

4.2. Laboratory activity on a Super Absorbent Polymer (SAP)

The SAP used in this research activity is a polyacrylic acid partial sodium salt (see: http://www.sigmaaldrich.com/catalog/product/aldrich/436364?lang=it&region=IT).

The characteristics of the Super Absorbent Polymers depend on the chemical formulation, and could be useful in employing these materials as softening grouts, thanks to their low shear stiffness due to the extremely high content of water mixable with the polymers. In this regard, some different mixtures have been tested. In the following paragraphs, some results are reported in terms of the features of the mixtures and of the sand used for the mixtures.

4.2.1. Tests on Sand

4.2.1.1 Grain size distribution

A series of laboratory tests on a sand with a unit weight γ_s equal to 28.3kN/m^3 have been made, starting from the grain size distribution, whose results are reported in Table 4.2.1.1.1 and Figure 4.2.1.1.1.

The sand has an almost medium uniform granulometry (see Figure 4.2.1.1.1) as indicated by the coefficient of uniformity C_u calculated using the following equation:

$$C_u = \frac{D_{60}}{D_{10}} \qquad (4.2.1.1.1)$$

where D_{60} is the grain diameter at 60% passing, and D_{10} is the grain diameter at 10% passing. This sand assumes C_u equal to 1.8; being less than 2, the sand is classified as uniform (Holtz and Kovacs, 1981).

Diameter, d (mm)	Retained quantity (gr)	Σ Retained quantities (gr)	Passed materials (gr)	Passed materials, P (%)
2	0	0	100	100
1	0.07	0.07	99.93	99.93
0.5	7.85	7.92	92.08	92.08
0.3	58.7	66.62	33.38	33.38
0.15	31.23	97.85	2.15	2.15
0.075	1.07	98.92	1.08	1.08
0.074	0.18	99.1	0.9	0.9

Table 4.2.1.1.1 *Sand grain size distribution.*

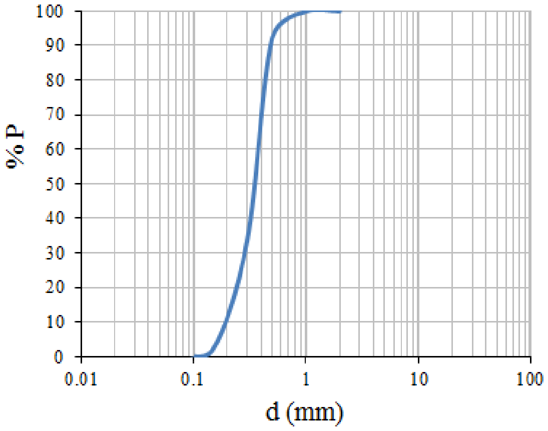

Figure 4.2.1.1.1 *Sand grain size distribution.*

4.2.1.2 Oedometer test

An oedometer test is a kind of geotechnical investigation performed in geotechnical engineering that measures the consolidation properties of the soil. Oedometer tests are performed by applying different loads to a soil specimen and measuring the deformation response by an automatic acquisition method (l.v.d.t.).

The test has been made on a dry specimen with an initial void ratio e equal to 0.86.

The oedometer test results have been examined taking into account two parameters, i.e. the volumetric deformation and the Oedometric modulus of the specimen, respectively defined as:

$$\varepsilon_v = \frac{\Delta H}{H_0} \tag{4.2.1.2.1}$$

$$E_{ed} = \frac{\Delta \sigma_v^{'}}{\Delta \varepsilon_v} \tag{4.2.1.2.2}$$

where ΔH is the whole settlements at the end of a certain load increment, and H_0 is the specimen height before the load step, $\Delta\sigma'_v$ is the vertical load increment and $\Delta\varepsilon_v$ is the consequent volumetric deformation. Table 4.2.1.2.1 and Figures 4.2.1.2.1 report the oedometer test results, from which a series of mechanical index could be derived:

- the re-compression ratio RR in the ε_v-logσ'_v plane, which is the curve gradient in the re-compression path:

$$RR = \frac{\Delta \varepsilon_v}{\Delta \log \sigma_v^{'}} = 0.15 \tag{4.2.1.2.3}$$

- the re-compression index c_{rc} in the e-logσ'_v plane:

$$c_{rc} = -\frac{\Delta e}{\Delta \log \sigma_v^{'}} = 0.003 \tag{4.2.1.2.4}$$

- the compression ratio CR in the ε_v-logσ'_v plane, which is the curve gradient in the compression path:

$$CR = \frac{\Delta \varepsilon_v}{\Delta \log \sigma_v^{'}} = 5.78 \tag{4.2.1.2.5}$$

- the compression index c_c in the e-logσ'_v plane:

$$c_c = -\frac{\Delta e}{\Delta \log \sigma_v^{'}} = 0.11 \tag{4.2.1.2.6}$$

- the unloading ratio SR in the ε_v-logσ'_v plane, which is the curve gradient in the unloading path:

$$SR = \frac{\Delta \varepsilon_v}{\Delta \log \sigma_v^{'}} = 0.48 \qquad (4.2.1.2.7)$$

- the unloading index c_s in the e-logσ'_v plane:

$$c_s = -\frac{\Delta e}{\Delta \log \sigma_v^{'}} = 0.01 \qquad (4.2.1.2.8)$$

Pressure	Total Displacement	Vertical deformation	E_{ed}	e_0 =0.86
(MPa)	(mm)	(%)	(MPa)	e
0.0010	0.156	0.8	384	0.01
0.0098	0.187	0.9	5.69	0.84
0.0196	0.195	1.0	24.50	0.84
0.0392	0.222	1.1	14.52	0.84
0.0784	0.266	1.3	17.82	0.83
0.1470	0.323	1.6	24.07	0.83
0.2940	0.404	2.0	36.30	0.82
0.5880	0.507	2.5	57.09	0.81
1.1761	0.617	3.1	106.92	0.80
2.4502	0.829	4.1	120.20	0.78
4.9	1.177	5.9	140.81	0.75
4.9	1.177	5.9	140.8	0.75
1.1761	1.083	5.4	792	0.76
0.2940	1.013	5.1	252	0.76
0.0784	0.952	4.8	71	0.77
0.0196	0.913	4.6	30	0.77

Table 4.2.1.2.1 *Oedometer test results on sand.*

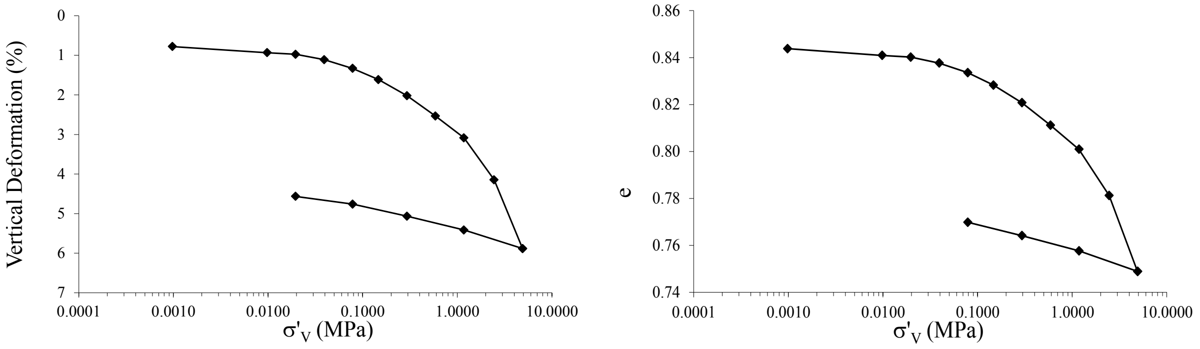

(a) (b)

Figures 4.2.1.2.1 *Oedometer test on sand: vertical deformations (a) and void ratio (b) by varying the applied loads.*

4.2.1.3 Direct shear test

A direct shear tests has been performed on a sand specimen (see Figure 4.2.1.3.1) with a square base (60mm·60mm) and 20mm thick.

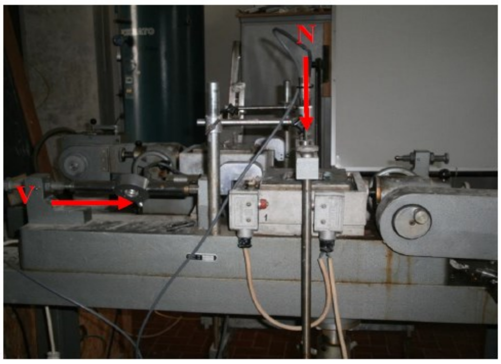

Figure 4.2.1.3.1 *Direct shear test equipment.*

The direct shear test has been performed on a dry sand, with a relative velocity v_r of 0.0366mm/m, and an axial load equal to 50kPa. The test is made of two steps:

- a consolidation phase, with a duration of a few minutes, in which the whole load is transferred to the solid skeleton;
- a failure phase, where a vertical shear force is gradually increased, until reaching the failure condition.

The soil specimen has been made up with the same initial void ratio of the oedometer test specimen (see §4.2.1.2). To obtain a certain void ratio, by referring to the unit weight γ_s and to the shear box volume V_l, the soil mass to put into the shear test box has been calculated.

The direct shear test results are shown in Figures 4.2.1.3.2, where the shear stress τ and the vertical displacements s_v versus the horizontal displacements s_h are reported.

In Figure 4.2.1.3.2a, the shear stress τ increases until failure is reached. Its trend firstly shows a peak and, subsequently, a decrement to a constant value. Figure 4.2.1.3.2b shows a dilatant behaviour; the sand is still loose after the consolidation phase (the void ratio varies from 0.80 to 0.78). The physical features of the direct shear test, which imposes a failure plane, should cause the dilatant behaviour. This is a reason for which the direct shear test overestimates the shear strength angle (Lancellotta, 2004). Considering the Mohr-Coulomb failure criterion, written as:

$$\tau = c' + \sigma_n' \cdot \tan\varphi' \qquad (4.2.1.3.4)$$

where c’ is the effective cohesion and σ'_n is the tension acting normally to the horizontal plane. Assuming c’=0, the shear strength angles φ' in the peak condition (φ'_{peak}) and at constant volume (φ'_{cv}) are equal respectively to φ'_{peak}=38° and φ'_{cv}=35°.

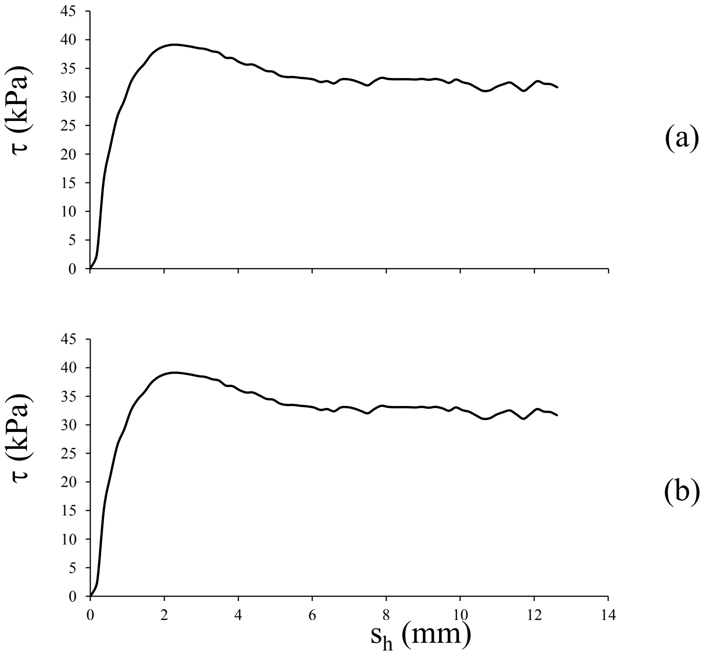

Figure 4.2.1.3.2 *Direct shear test on sand: shear stress τ (a) and vertical displacements (b) by increasing the horizontal displacements.*

4.2.1.4 Triaxial test

The triaxial test equipment (Figure 4.2.1.4.1a) is constituted by a cell within which is positioned a cylindrical specimen of height h = 76 mm and diameter d = 38 mm protected by a latex membrane. This membrane aids to transform the pressure of the liquid placed into the cell in total stress σ_c on the specimen. This pressure produces an isotropic stress, and, in order to reach the failure conditions, an axial vertical stress σ'_a has to be applied. The test has been carried out on a specimen of loose sand (see Figure 4.2.1.4.1b) with the following features:

Height:	h = 95.5mm
Effective diameter:	$d_{eff} = d - 2 \cdot s = 35.5$mm
Unit weight:	$\gamma_s = 28.3$kN/m^3
Weight:	P = 147.63gr
Volume:	$V_l = 94.48$cm^3
Void ratio:	e = 0.81

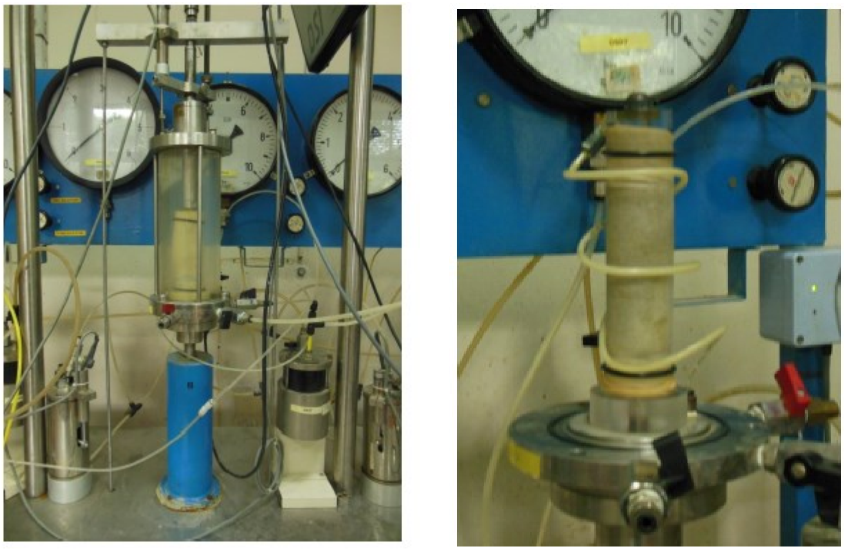

(a) (b)

Figure 4.2.1.4.1 *Triaxial test equipment (a) and sand specimen (b).*

Once the specimen is realized, the cell pressure σ'_c is gradually applied and simultaneously the negative pressure is decreased; in such a way that material does not suffer unloading and reloading effects. During this phase, it is possible to measure the specimen volume changes ΔV_l. It has been recorded a $\Delta V_l = 0.341 cm^3$ which is considered to be distributed along the three directions. After this phase, the specimen has new sizes and a new void ratio:

Final Volume: $V_{l,fin} = 94.14cm3$

Final height: $h_{fin} = 95.3mm$

Final diameter: $d_{fin} = 35.4mm$

Final void ratio: $e = 0.80$

Once the cell pressure σ'_c of 50kPa is reached, the specimen has been subjected to a short time phase of consolidation in which the load applied by the fluid to the specimen has been transferred as effective stresses to the soil skeleton. After that, a deviatoric load has been applied in drained condition.

The equipmnet has automatically recorded the force F(t) applied at failure, the variation of the height $\Delta h(t)$ and the volume $\Delta V_l(t)$. From these measures, it was possible to carry out a series of profiles by applying the eq.s from (4.2.1.4.1) to (4.2.1.4.9):

Volume variation with time of the piston coming into cell:

$$\Delta V_{l,pist}(t) = \Delta h_{pist} \cdot A_{pist} \qquad (4.2.1.4.1)$$

Volume variation of the specimen with time:

$\Delta V_{l,spec}(t) = \Delta V_l(t) - \Delta V_{l,pist}(t)$ (4.2.1.4.2)

Volumetric deformation with time:

$\varepsilon_v(t) = \Delta V_{l,spec}(t) / V_{l,fin}$ (4.2.1.4.3)

Axial deformation with time:

$\varepsilon_a(t) = \Delta h(t) / h_{fin}$ (4.2.1.4.4)

Heigth of the specimen:

$h_{spec} = h_{fin} - \Delta h(t)$ (4.2.1.4.5)

Area of the specimen:

$A_{spec} = (V_{l,fin} - \Delta V_{l,spec}(t)) / h_{spec}$ (4.2.1.4.6)

Effective axial stress with time:

$\sigma'_a = F(t) \cdot A_{spec}$ (4.2.1.4.7)

Deviatoric stress with time:

$q(t) = \Delta\sigma'_a(t) \cdot A_{spec}$ (4.2.1.4.8)

Isotropic effective pression with time:

$p'(t) = \sigma'_c + q\,(t) / 3$ (4.2.1.4.9)

where A_{spec} is the area of the sand specimen; A_{pist} and $\Delta V_{l,pist}$ are respectively the area and the volume of the piston which slides inside the cell. Figures 4.2.1.4.2 show the results of the triaxial test.

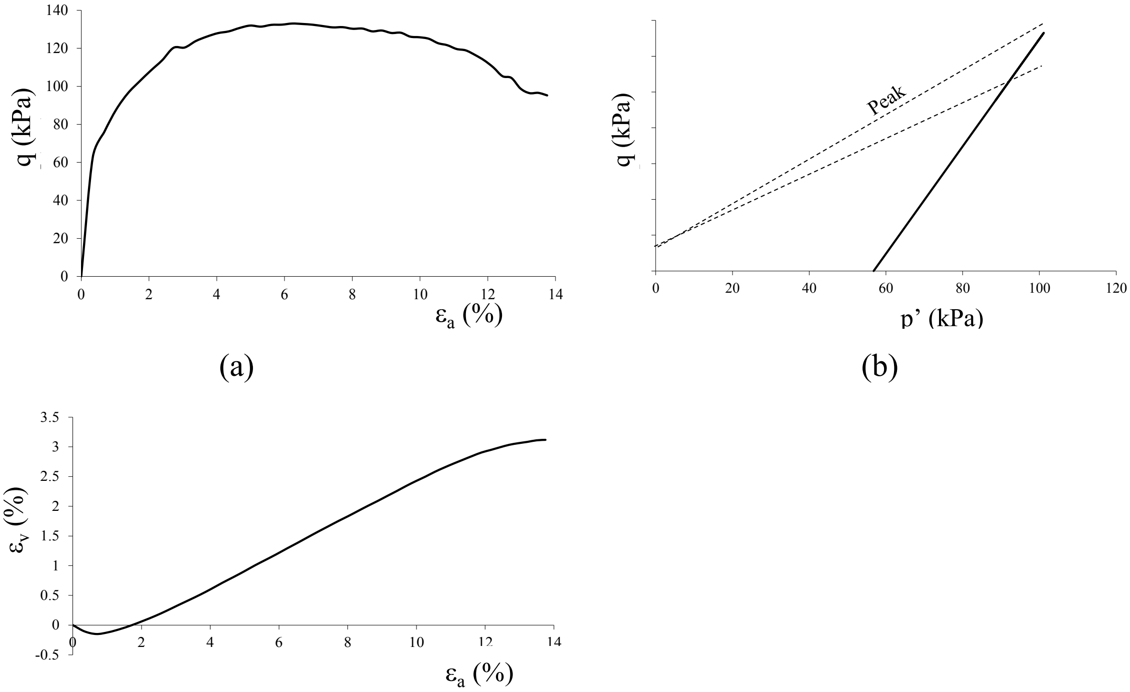

(a) (b)

(c)

Figure 4.2.1.4.2 *Results from the triaxial sand on sand.*

A dilatant, unstable behaviour of the tested sand is observed, as clarified by Figure 4.2.1.4.3 in which a picture of the specimen at failure condition is reported. This dilatant behaviour is probably due to the low tensional isotropic state and slightly to the initial vacuum, which has been applied in phase of realization of the specimen. This vacuum has probably make the sand denser and, consequently, allowed a fragile failure.

To obtain the failure envelope of the material, other triaxial tests at different isotropic stresses should be necessary. The shear strength angle has been obtained by referring to the modulus M (Lancellotta, 2004), as reported:

$$\begin{aligned} M &= \frac{q}{p'} \\ \varphi' &= arcsen\frac{3 \cdot M}{M+6} \end{aligned} \tag{5.2.1.4.1}$$

As expected, the shear strength angle at constant volume is equal to 27°, lower than the one derived by the direct shear test.

Figure 4.2.1.4.3 *Failure phase of the sand specimen in a triaxial test.*

4.2.2. Tests on Poly (acrylic acid) partial sodium salt (SAP)

The SAP is a polymer that can physically be in the form of a powder, crystals or granules. The adopted SAP has granular particles with a diameter less than 1000 microns and a density equal to 0.69gr/ml at environmental temperature.

SAP is able to absorb high amount of aqueous liquids; therefore, in the performed tests, SAP and distilled water have been mixed, with a ratio 99.4% by weight of distilled water and 0.6% of SAP. The resulting material has been named "Saturated SAP" (whose acronym is "Sat SAP"). The saturated SAP and the sand have been jointed together in order to make soft and spongy mixtures. Some mechanical tests have been carried out on these mixtures to analyse the variation of the mechanical characteristics with respect to the percentages by weight of saturated SAP.

4.2.2.1 Grain size distribution

The grain size distribution of a sample of SAP has been done by using sieves with diameters from 0.074mm to 1 mm (see Figure 4.2.2.1.1).

For each sieve, the weight of retained weight P, the passed material weight and the percentages of passed weight have been measured (see Table 4.2.2.1.1). These percentages have been then plotted as a function of the diameter of the corresponding sieve (see Figure 4.2.2.1.2). Also in this case it is possible to determine the uniformity coefficient C_u , equal to 4, revealing the uniformity of the material. By overlaying the curves referring to the sand and to the SAP (Figure 4.2.2.1.3), it can be noted that both curves belong to the same granulometric zone.

Figure 4.2.2.1.1 *Grain size distribution on SAP.*

d (mm)	P (gr)	ΣP (gr)	Passed weight (gr)	Percentages of passed weight (%)
1	0	0	63,29	100,00
0,5	28,29	28,29	35,00	55,30
0,3	23,9	52,19	11,10	17,54
0,15	9,7	61,89	1,40	2,21
0,075	1,14	63,03	0,26	0,41
0,074	0,26	63,29	0,00	0,00

Table 4.2.2.1.1 *SAP grain size distribution.*

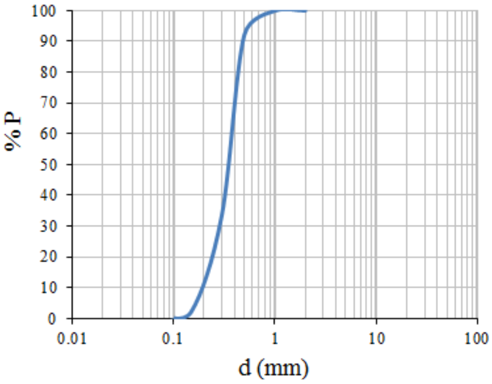

Figure 4.2.2.1.2 *SAP grain size distribution.*

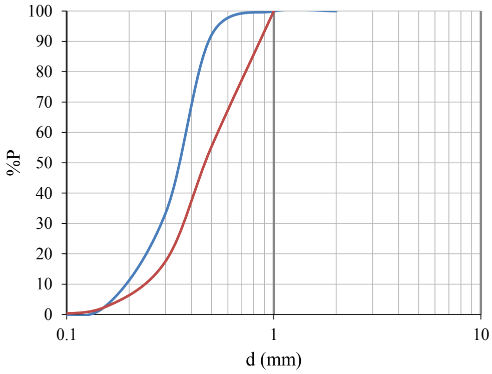

Figure 4.2.2.1.3 *Comparison between the grain size distributions of the two materials.*

4.2.2.2 Water absorbing features

Water absorbing tests have been carried out on SAP specimens, at atmospheric pressure, entering both distilled water and tap water, with the following results:

- 1 gr of SAP absorbs approximately 240gr of distilled water;
- 1 gr of SAP absorbs about 138gr of tap water.

Then the mixture has been placed into an oven for 24 hours at 105°C to release all the water absorbed. By repeating the swelling tests, it is noted that the SAP loses part of its absorbing capacity. In fact:

- 1 g of dehydrated SAP absorbs about 180 grams of distilled water;
- 1 g of dehydrated SAP absorbs about 97 gr of tap water.

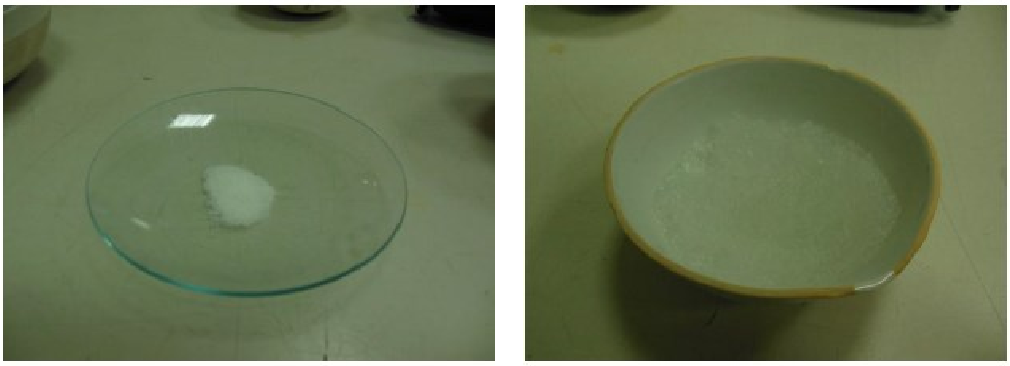

(a) (b)

Figure 4.2.2.2.1 *Dry SAP (a) and Saturated SAP (b).*

4.2.2.3 Oedometer tests

Three edometer tests have been performed on different mixtures by increasing their saturated SAP content. The mixtures characteristics are reported in Table 4.2.2.3.1. The mixture SAP0.33 has not a void ratio equal to the ones of SAP0.09 and SAP0.23 cause to the compaction of the material during the specimen preparation.

An average unit weight value has been calculated between the unit weight of the sand (γ_{Sand}) and the one of the saturated SAP (γ_{SatSAP}) , which has been considered equal to the water unit weight, (γ_{SatSAP}=10kN/m^3):

$$\bar{\gamma}_{SAP0.09} = \alpha_{sand} \cdot \gamma_{sand} + \alpha_{SatSAP} \cdot \gamma_{SatSAP} \qquad (4.2.2.3.1)$$

where α_{sand} is the percentage by weight of sand and α_{SatSAP} is the percentage by weight of saturated SAP. Figure 4.2.2.3.1 reports the results of the tests on the SAP specimens; because of the significant creep deformation undergone by the specimens, the deformations reported in Figure 4.2.2.3.1 correspond to the values recorded after 100s from the beginning of each loading step. Figure 4.2.2.3.1 reports a comparison among the different mixtures in terms of the vertical axial deformation ε_a with the applied load.

Mixture	α_{SAP}	α_{Sand}	$\bar{\gamma}_{SAP}$ (kN/m^3)	e_0
SAP0.09	9	91	26.7	0.8
SAP0.23	23	77	24.1	0.8
SAP0.33	33	67	22.61	0.46

Table 4.2.2.3.1 *SAP mixtures.*

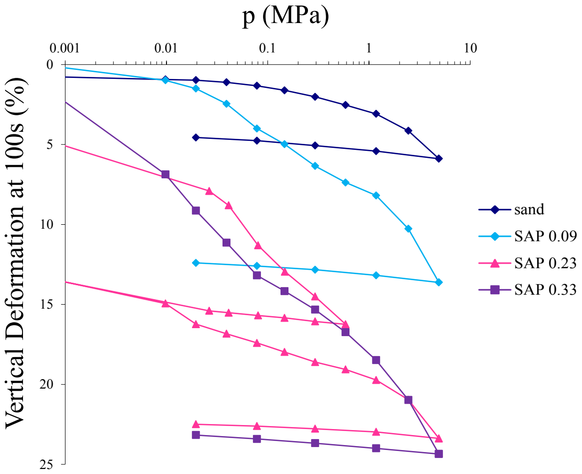

Figure 4.2.2.3.1 *Results of the oedometer tests on SAP specimens.*

The saturated SAP increases the compressibility of the natural soil, but, if the SAP amount is increased over the 20% with respect to the soil quantity, the compressibility does not significantly change. It is possible to define, from the curve e-logσ'_v, the values of the re-compression (c_{rc}), compression (c_c) and unloading (c_s) indices for each mixture. They are reported in Table 4.2.2.3.1:

Material	c_{rc}	c_c	c_s
Sand	0.003	0.11	0.01
SAP0.09	0.02	0.12	0.01
SAP0.23	0.04	0.13	0.01
SAP0.33	0.08	0.10	0.01

Table 4.2.2.3.1 *Values of the recompression index c_{rc}, the compression index c_c and the unloading c_s for the the sand and the SAP mixtures.*

Cause the specimens have been obtained by mixing the saturated SAP with sand, the oedometer tests are not influenced by possible swelling phenomena that could affect the mixtures behaviour. On the contrary, in engineering practice, the idea is to inject the soil mixed with dry SAP at a certain depth into the soil deposit, so that groundwater may induce the injected material to swollen. On this aspect, some swelling tests, under constant loads, have been made (see §4.2.2.5).

4.2.2.4 **Direct shear tests**

On the three SAP-sand mixtures previously defined (see §4.2.2.4), some direct shear tests have been carried out, trying to preserve the same void ratios used for the oedometer tests. Consequently, the mixtures have the following void ratios:

SAP0.09: e=0.80;

SAP0.23: e=0.80;

SAP0.33: e=0.46.

Only one test has been carried out for each type of mixture, under an isotropic pressure of 50kPa, in order to give a first valuation of the shear strength. The adopted displacement rate in the direct shear test is the same of the one for the test on sand (v_r = 0.0366 mm/min). The results of the shear tests are reported in Figures 4.2.2.4.1, which show that, even for small percentages of saturated SAP, the mechanical behaviour of the mixture changes with respect to the sand; from Figure 4.2.2.4.1b, the behaviour of the sand, previously dilatant, becomes contracting. Furthermore, the higher the percentage by weight of Saturated SAP the higher the reduction of the mixture shear strength (see Figure 4.2.2.4.2).

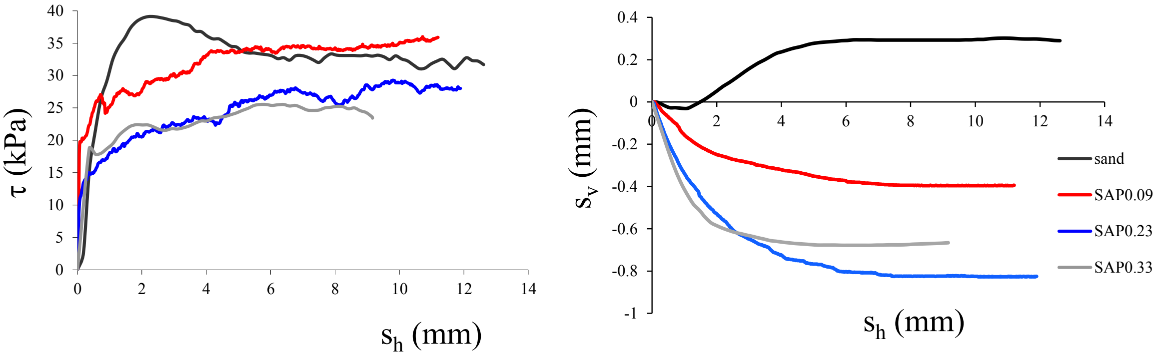

(a) (b)

Figure 4.2.2.4.1 *Results of direct shear tests, in terms of shear stress τ (a) and vertical displacements (b).*

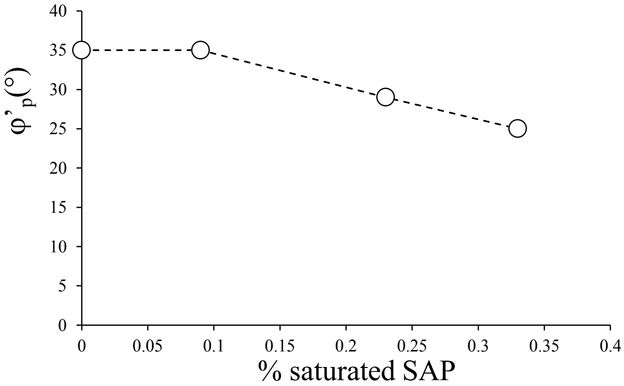

Figure 4.2.2.4.2 *Shear strength angle by varying the percentages by weight of the saturated SAP.*

In order to verify the shear resistance of specimens with higher SAP contents, some ring shear tests (Raviolo, 1993) have been performed on different mixtures subjected to a vertical load equal to 200kPa. These mixtures have the characteristics reported in Table 4.2.2.4.1.

Mixture	α_{SAP}	α_{Sand}	$\bar{\gamma}_{SAP}$ (kN/m^3)
SAP0.50	50	50	19.15
SAP0.70	70	30	15.49
SAP0.90	90	10	11.83

Table 4.2.2.4.1 *SAP mixtures.*

Figures 4.2.2.4.3 report the results of the ring shear tests, in terms of shear stress τ (a) and vertical displacements (b). It can be observed that, by increasing the SAP content, extremely low values in terms of shear stress are shown. In particular, the mixture named SAP0.9 does not show an appreciable shear resistance (see Figure 4.2.2.4.3a).

These observations are confirmed by looking at Figure 4.2.2.4.4, where the results from direct and ring shear tests are reported in terms of normalized shear stress τ/σ versus the horizontal displacements s_h: by increasing the SAP content, the shear resistance decreases.

Figure 4.2.2.4.5 reports the values of the shear strength angle at constant volume of the different mixtures: a rather linear variation is shown.

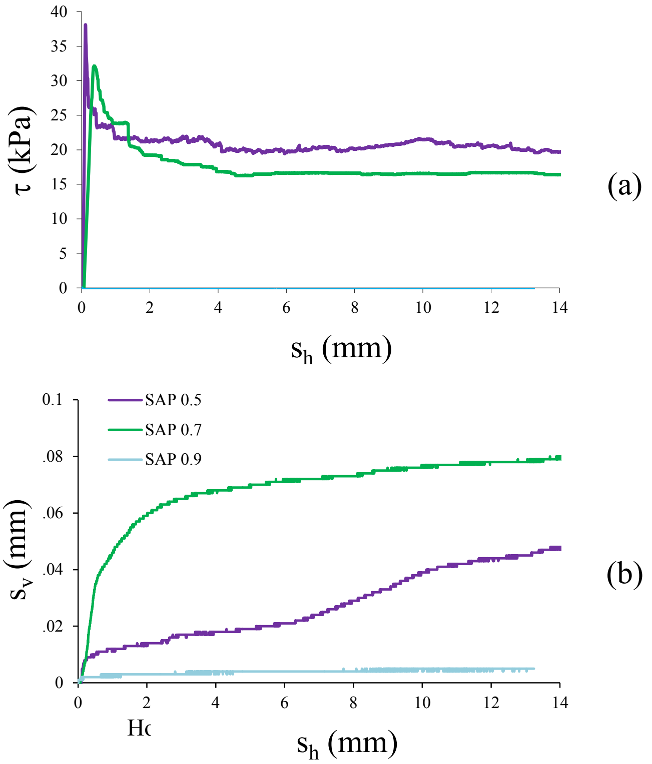

Figure 4.2.2.4.3 *Results from ring shear tests, in terms of shear stress τ (a) and vertical displacements s_v (b) versus the horizontal displacements s_h.*

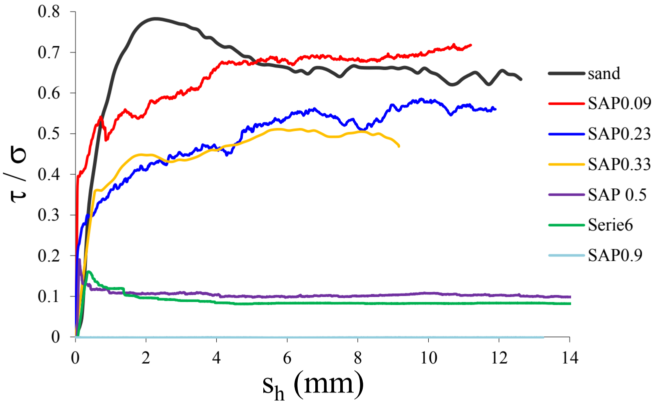

Figure 4.2.2.4.4 *Results from direct and ring shear tests, in terms of normalized shear stress τ/σ versus the horizontal displacements s_h.*

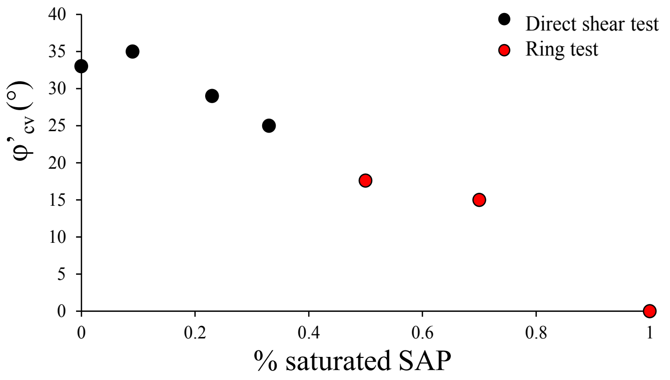

Figure 4.2.2.4.5 *Shear strength angle at constant volume of the mixtures by varying the percentages of the saturated SAP.*

4.2.2.5 Swelling tests

Some tests have been carried out to analyse the capacity of the mixture to swell under given loads. Three tests under the axial loads of 50kPa, 100kPa and 200kPa have been performed on a mixture with the characteristics reported in Table 4.2.2.5.1.

Mixture	α_{SAP}	α_{Sand}	$\bar{\gamma}_{SAP}$ (kN/m^3)
SAP0.50	50	50	19.15

Table 4.2.2.5.1 *SAP mixtures.*

At the base of the specimen, a latex disk has been placed instead of a filter paper. To inject the quantity of water required for the SAP swelling, the oedometer cell has been isolated with silicon foam. To avoid the water evaporation, the oedometer cell has been then covered with a waterproof film (Figure 4.2.2.5.1).


(a)
(b)

Figure 4.2.2.5.1 *Swelling tests: some details of the test equipment: waterproof film (a) and latex disk at the base of the cell (b).*

In the first phase of the swelling tests, a vertical load is applied to the specimens, and the subsequent settlements are recorded. After 10 minutes, distilled water has been added to allow swelling.

The volumetric expansions (ε_v), due to the load increments and to the saturation of the specimens, are reported in Table 4.2.2.5.1 and Figure 4.2.2.5.2, where the volumetric compression assumes, conventionally, the positive sign.

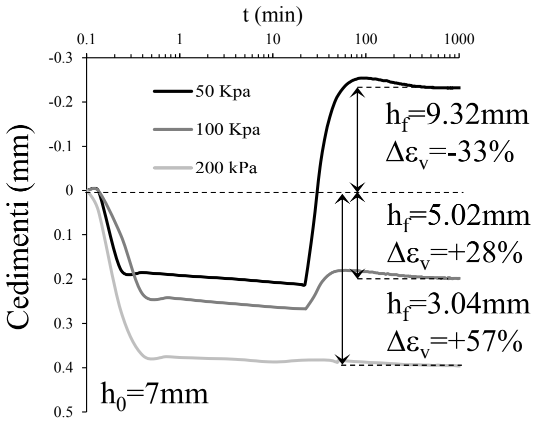

Figure 4.2.2.5.2 *Swelling tests by varying the load applied to the specimens.*

As expected, it can be observed that the initial settlements increase by increasing the load. Injecting water into the specimens, it is shown a volumetric expansion in the cases of load amplitudes lower than 200kPa.

Vertical loads (kPa)	ε_v (%)
50	-33
100	+28
200	+57

Table 4.2.2.5.1 *Volumetric expansions due to the swelling tests performed on SAP0.50 specimens (the positive sign refers to the volumetric compression).*

4.2.2.6 S-wave velocity measurements

A series of tests in a large triaxial cell has been made with the aim to measure, in a large specimen, the shear wave velocity $V_{s,g}$ of the treated soil and, consequently, its shear modulus at small strain levels G_0.

The experimental activity was carried out in a stress-path triaxial apparatus (TX; Flora and Lirer, 2013; see Figure 4.2.2.6.1) designed to accommodate a large specimen (diameter d=20cm, height h=40cm). The apparatus is controlled via a PC and is equipped with: two pressure transducers to measure cell and pore pressures, an internal load cell to measure the deviatoric stress, a volume gauge and two internal LVDTs to measure the specimen volumetric and axial strains. The TX cell is equipped with a special device conceived for dynamic measurements: on both the specimen pedestal and cap (Figure 4.2.2.6.2b), two electromagnetic systems can be excited, and two pistons hit two steel plates, placed to generate respectively shear (S) and compression waves (P) (Figure 4.2.2.6.2 b/c). To be sure that the signal would be easily read at the receiving end, the piston was designed to give a significant energy to the shear or compression plate. As a consequence, the input wave is more complex than the usual impulsive or sinusoidal ones. The input and output waveforms are automatically recorded by a digital oscilloscope (Figure 4.2.2.6.2a). Close to the exciting plates, a very sensitive tridimensional accelerometer is placed to detect the starting time (on the specimen end at which the waves are generated) and the arrival time (at the opposite end).

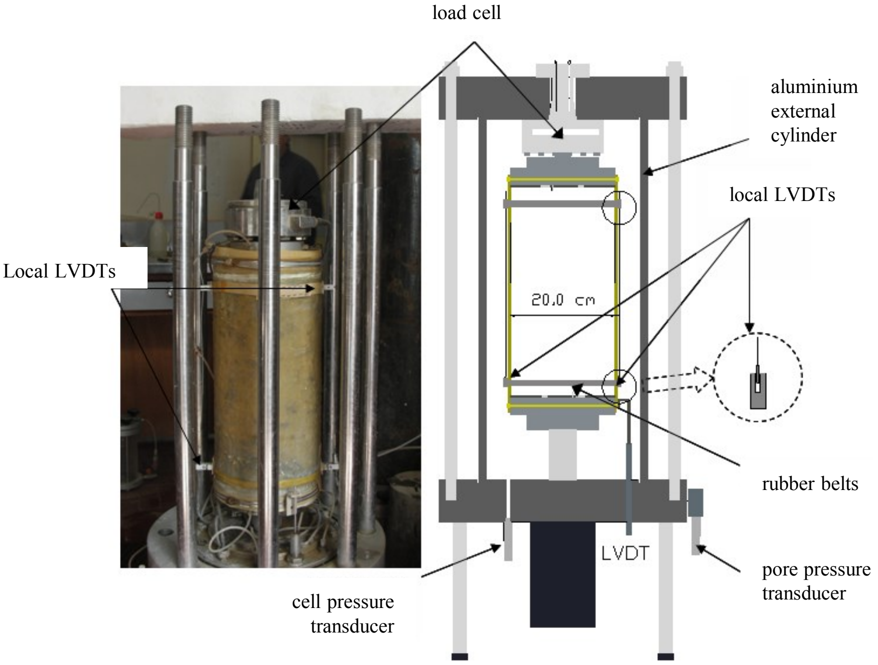

Figure 4.2.6.1 *Triaxial cell adopted in the experimental activity (Flora and Lirer, 2013).*

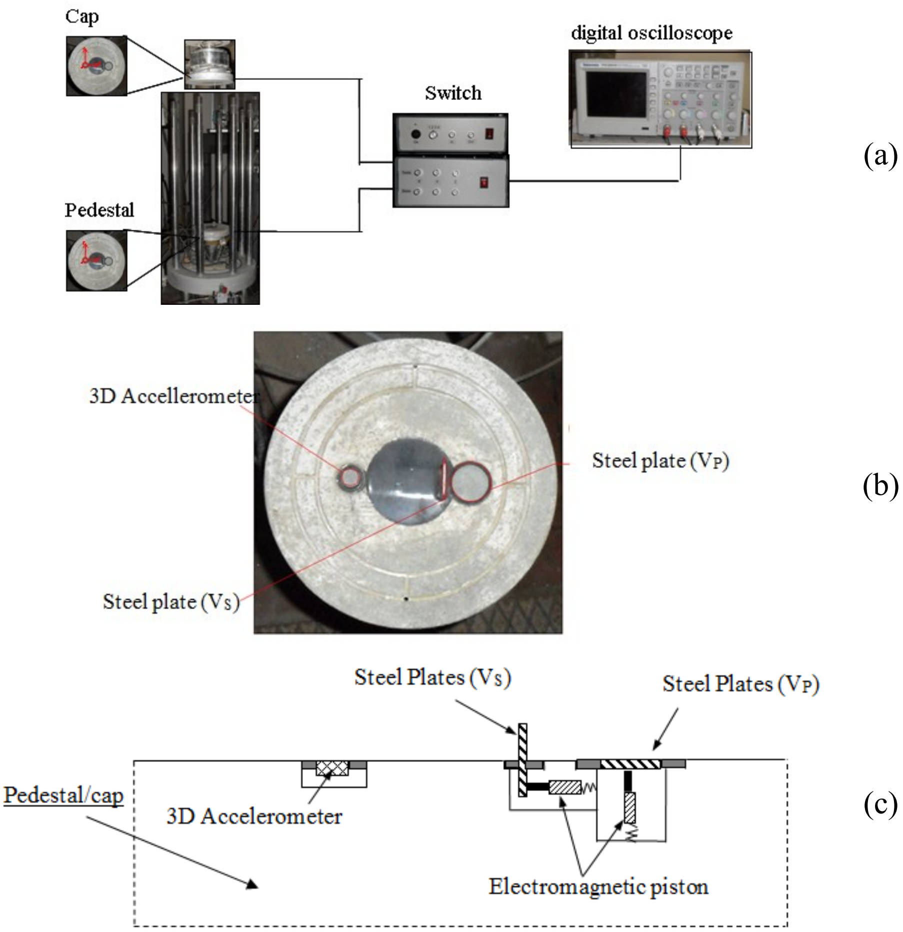

Figure 4.2.6.2 *System for dynamic measurements (a) and wave generating system (b,c) (Flora and Lirer, 2013).*

A first test has been made on a sand specimen with void ratio equal to 0.65. The different isotropic stresses applied to the specimen and the average values of the shear wave velocities of the sand $V_{s,s}$ are reported in Table 4.2.2.6.2.

Sand	
p' (kPa)	$V_{s,s}$ (m/s)
20	228
40	260
60	277

Table 4.2.2.6.1 *Average $V_{s,s}$ values of the sand.*

A second test has been carried out on a specimen made of three different parts: the upper and the lower parts are made of sand; the central part is made of a layer of SAP0.33 (see Figure 4.2.2.6.3).

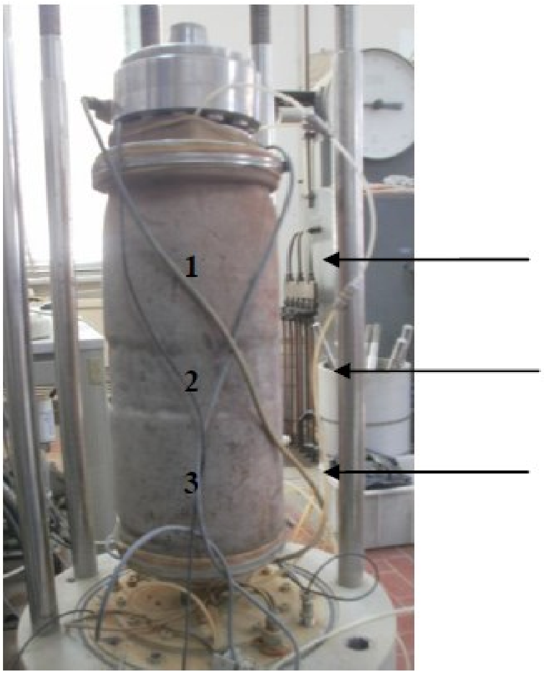

$d_1 = 19.6\,cm\ \ h_1 = 20{,}5\,cm\ \ e_1 = 0.78$ $\rho_1 = 1622\,kg/m^3$
$d_2 = 19.4\,cm\ \ h_2 = 4{,}5\,cm\ \ e_2 = 0.23$ $\rho_2 = 1847\,kg/m^3$
$d_3 = 20.1\,cm\ \ h_3 = 15\,cm\ \ e_3 = 0.77$ $\rho_3 = 1630\,kg/m^3$

Figure 4.2.2.6.3 *Dimensions and physical characteristics of the specimen with SAP0.33.*

Even in this case, some tests were carried out for each applied confining pressure, obtaining some average values of $V_{s,g}$ (Table 4.2.2.6.2):

SAP0.33	
p' (kPa)	$V_{s,g}$ (m/s)
20	132
40	142
60	216

Table 4.2.2.6.2 *$V_{s,g}$ values for different confining pressures.*

A third test has been conducted on a specimen where the inner part was made of SAP0.33 (see Figure 4.2.2.6.4).

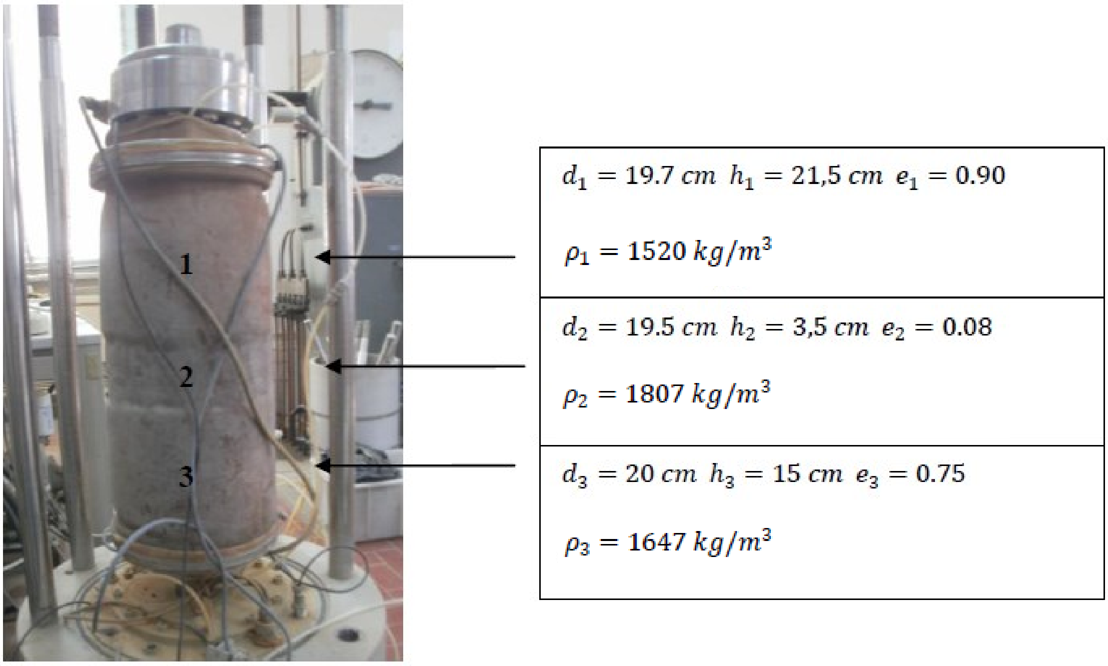

$d_1 = 19.7\ cm\ \ h_1 = 21{,}5\ cm\ \ e_1 = 0.90$

$\rho_1 = 1520\ kg/m^3$

$d_2 = 19.5\ cm\ \ h_2 = 3{,}5\ cm\ \ e_2 = 0.08$

$\rho_2 = 1807\ kg/m^3$

$d_3 = 20\ cm\ \ h_3 = 15\ cm\ \ e_3 = 0.75$

$\rho_3 = 1647\ kg/m^3$

Figure 4.2.2.6.4 *Dimensions and physical characteristics of the specimen with SAP0.50.*

Some tests were conducted for each applied confining pressure, obtaining some average values of $V_{s,g}$ (Table 4.2.2.6.3):

SAP0.50	
p' (kPa)	$V_{s,g}$ (m/s)
20	58
40	82
60	176

Table 4.2.2.6.3 *$V_{s,g}$ values for different confining pressures.*

Another test has been made on a specimen with an inner part made totally of SAP (see Figure 4.2.2.6.5).

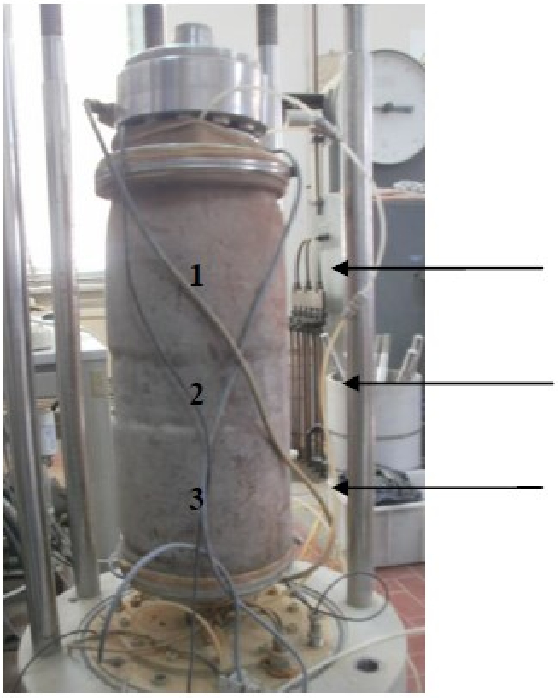

$d_1 = 19.7\ cm\ \ h_1 = 21{,}5\ cm\ \ e_1 = 0.82$

$\rho_1 = 1587\ kg/m^3$

$d_2 = 19.5\ cm\ \ h_2 = 3{,}5\ cm$

$\rho_2 = 1000\ kg/m^3$

$d_3 = 20\ cm\ \ h_3 = 15\ cm\ \ e_3 = 0.75$

$\rho_3 = 1647\ kg/m^3$

Figure 4.2.2.6.5 *Dimensions and physical characteristics of the specimen with SAP.*

By placing a SAP stratum, it is observed that the shear wave velocity does not significantly depend on the confining pressure p'as reported in Table 4.2.2.6.4.

SAP	
p' (kPa)	$V_{s,g}$ (m/s)
20	27
40	26
60	27

Table 4.2.2.6.4 $V_{s,g}$ *value for different confining pressures.*

The $V_{s,g}$ values versus the SAP percentages are reported in Figure 4.2.2.6.6: it is clear that $V_{s,g}$ significantly decreases by increasing the SAP percentages.

As expected, the higher the confining pressure the higher the values of $V_{s,g}$ of the mixtures, with the exception of the layer made only of SAP, whose stiffness sem not to be affected by the confining pressure value.

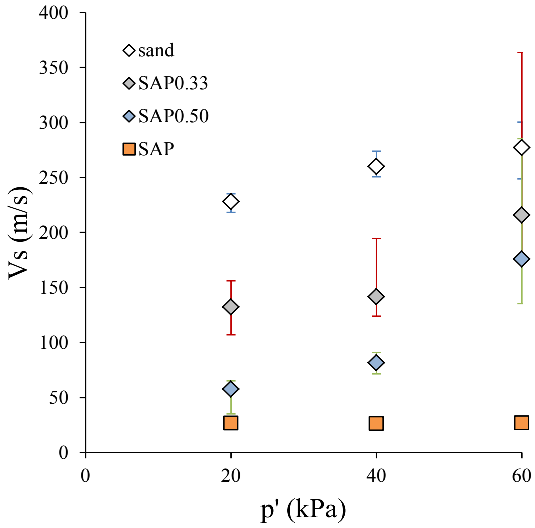

Figure 4.2.2.6.6 *Average values of* $V_{s,g}$ *by varying the SAP percentages.*

Tests results indicate that the saturated SAP, having a density ρ close to 1000kg/m^3 and a shear wave velocity $V_{s,g} \cong 30$m/s, has a dynamic impedance similar to the ones suggested as effective in numerical analyses (see §2.3.3).

Furthermore, the saturated SAP reveals a capacity of swelling under load, as observed in §4.2.2.5, which could be useful in reducing the settlements caused by its high compressibility when injected deep into a soil deposit to form a soft layer. Other tests will be carried out to improve the knowledge on the SAP mechanical behaviour, but this material seems to be potentially suitable as soft worsening grout.

4.2.3. References

D'Onofrio A. (2006). Thor. Apparecchiatura di taglio torsionale ciclico e dinamico. *Centro Regionale di Competenza AMRA, Manuali tecnici di strumentazione, pp.17.*

Flora A., Lirer S. (2013). Small strain shear modulus of undisturbed gravelly soils during undrained cyclic triaxial tests. *Geotechnical and Geological Engineering, Vol. 31(4), pp.1107-1122.*

Holtz R., Kovacs W. (1981). An Introduction to Geotechnical Engineering. *Prentice-Hall Inc., Upper Saddle River, New Jersey (USA).*

Kabiri K. (2003). Synthesis of fast-swelling superabsorbent hydrogels: effect of crosslinker type and concentration on porosity and absorption rate. *European Polymer Journal, Vol.39(7), pp.1341-1348.*

Lancellotta R. (2004). Geotecnica. *Zanichelli, pp.544.*

Naudts A. (2003). Irreversible Changes in the Grouting Industry Caused by Polyurethane.Grouting: An overview of 30 years of polyurethane grouting.*Geotechnical. Special Publication.*

Ramberg W., Osgood W. R. (1943). Description of stress-strain curves by three parameters. *Technical Note n°902, National Advisory Commettee for Aeronautics, Washington D.C (USA).*

Raviolo L. (1993). Il laboratorio geotecnico: procedure di prova, elaborazione, acquisizione dati. *Editrice Controls, Novara (Italy), pp.608.*

Zohuriaan-Mehr M.J., Omidian H., Doroudiani S., Kabiri K. (2010). Advances in non-hygienic applications of superabsorbent hydrogel materials. *Journal of Materials Science, Vol.45(21), pp.5711-5735.*

5. Results and future perspectives

This thesis reports the results of a comprehensive research program on an innovative ground treatment approach for the mitigation of the seismic risk of existing structures, especially with reference to squat (i.e. rigid) structures.

1D and 2D dynamic and static numerical analyses have been performed in order to study the efficiency of different treatment schemes, whose geometrical and mechanical configurations have been varied with the aim to get an insight on their potentials and limits.

Even though most of the work has focused on numerical simulations of the performance of some possible configurations of the soft caisson, some very preliminary laboratory tests have been carried out on sand mixed with two different industrial products. Their characteristics seemed, at least initially, well suited to the problem under study, because of their either low density or low shear stiffness.

5.1. Dynamic Analyses

5.1.1. 1D analyses

The 1D analyses have been carried out using either EERA or NERA, supposing the soil layers to be horizontally homogenous, horizontally unlimited, and subjected only to a horizontal excitation from the bedrock.

As far as the 1D results are concerned, the insertion of a soft grouted layer at a given depth into the soil deposit is extremely effective in reducing the peak ground accelerations. The maximum acceleration strongly reduces above the soft layer, and such a reduction increases as the impedance ratio between the grouted and the soil layer increases.

The proposed deep ground treatment has demonstrated to be effective for the attenuation of the spectral intensity in the range of periods pertaining to medium stiff constructions, including masonry buildings i.e. 0.1÷0.5s.

The insertion of the soft layer causes the shrinkage and rotation of the S_d-S_a domain: the higher the impedance ratio of the treatment to the surrounding soil the larger the shrinkage and the rotation of the maximum responses in terms of accelerations and displacements to higher periods. Therefore, the introduction of a soft layer at a given depth into a soil column leads to a global system response that moves to higher periods.

In some cases, the insertion of a soft grouted layer may increase the spectral acceleration for large periods, which may be critical for slender structures such as, for instance, tall towers.

Most of the 1D analyses have been performed considering no damping in the grouted layer. Increasing it, the effects above the soft layer are reduced. However, the impedance ratio is by far the most relevant parameter.

5.1.2. 2D analyses

2D dynamic analyses have been used to study the effects of a soft caisson having a rectangular section or made of inclined injections on the dynamic response of a soil deposit subjected to the propagation of shear waves.

The 2D dynamic analyses have been carried out using FLAC7. Different geometrical and mechanical configurations of the soft caisson have been considered. In the analyses, the materials have been assumed either linearly elastic or elasto-plastic. In such a way, the relevance of the choice of the constitutive model has been highlighted. Such a choice may be relevant for large amplitude seismic inputs. The interaction of the wavefront with the boundaries of the soft caisson may generate secondary wavefronts, whose effects on ground surface are difficult to foresee. The interaction between the soft layers and the dynamic signals is in the 2D analyses much more complex than the 1D wave propagation. The 2D analyses confirm the 1D observations, with significant differences based on the different signal propagation conditions and on the constraint effect due to the surrounding soil.

In the elastic analyses, it is noted that, varying the geometrical and mechanical configurations of the soft caisson, the lower frequencies are amplified, and the higher ones are reduced. Observing, for instance, the results in terms of acceleration at ground surface (see §2.3.3.1), when the soft caisson produces a reduction in the dynamic effects for the soil within the caisson, an increase in the effects outside it is observed.

This is due to the reflecting effect of the waves impacting on the lateral soft screen, which are reflected back. Consistently, when this kind of mitigation system does not reduce the effects in the zone to be protected, no significant increase of the accelerations outside the caisson are observed.

The beneficial screening effect in terms of acceleration, in the case where it takes place, does not necessarily correspond to an increase in displacements in the soil within the soft caisson (see, for instance, Figures 2.3.3.1.3 e-h and Figures 2.3.3.1.4 e-h). This depends on both the fundamental frequency of the propagated signal and the shear stiffness of the soft layers, especially when the treatment is effective in mitigating seismic effects at ground level. For the lowest value of $V_{s,g}$, actually, both accelerations and displacements are reduced within the soft caisson.

In the effective cases, the dynamic signals are clearly and sharply modified in amplitude by impacting the soft layers. At ground surface, an increase in the duration of the signal can be also observed (see, for instance, Figure 2.3.3.1.5 a and b).

The peaks of the signal over the soft layer decrease in amplitude and are shifted to lower frequencies; the response spectra also point out that the peaks of acceleration are not only reduced, but also shifted towards higher periods. The introduction of a soft caisson, then, modifies the resonance frequencies of the deposit in which it is inserted; if the signal fundamental frequency is close to a natural frequency of the modified deposit, resonance phenomena may occur. Since the soft caisson generally tends, when detrimental, to amplify the lower frequencies, it is confirmed that this system can be effective in reducing the maximum dynamic effects on squat structures, which have lower natural frequencies. It is then confirmed that the maximum detrimental effects, as observed in 1D analyses, will be for slender structures, which have higher natural periods.

The proposed seismic mitigation system may induce further effects in the vertical direction. The soft caisson has the negative effect of causing vertical accelerations at ground level, obviously not observed in the case with no treatment, whose amplitude may be extremely detrimental inside the caisson. When a resonance phenomenon occurs, the generation inside the caisson of vertical accelerations of the same order of magnitude of the horizontal ones can be observed, whereas, outside the box, they rapidly decrease (see, for instance, Figure 2.3.3.1.11). When the propagated signal does not induce resonance of the whole system, significant values of vertical accelerations are relegated outside the caisson (see, for instance, Figure 2.3.3.1.12); in such cases, in the inner part, the accelerations in the two directions are extremely low, of the same order of magnitude. The system seems therefore to be able to isolate the interior part from effects in terms of accelerations both in the vertical and horizontal directions. It must be pointed out, again, that the soft barrier may increase the seismic effects immediately outside the caisson, and thus possible negative effects on buildings adjacent to the one to protect have to be carefully evaluated.

In §2.3.3.2, it has been pointed out that the response of the system depends more on the absolute value of the shear wave velocity $V_{s,g}$ (and therefore its shear stiffness G) of the grouted layers than on the impedance ratio, and this is somehow an unexpected and certainly original result. In particular, it seems that both the shear wave velocity of the soft layers and the impedance ratio are relevant parameters in the propagation of the signal through the insulating box, but the former plays a more significant role. To mitigate the seismic risk, it is therefore more convenient the injection of soft layers with a very low shear wave velocity, whatever the shear stiffness of the surrounding soil.

Different geometrical configurations have been studied both for the rectangular section (see §2.3.3.6 and §2.3.3.7) and for the inclined injections (see §2.3.4.1 and 2.3.4.2). The geometrical parameters of the soft caisson with a rectangular section are the maximum depth H_g, the width L_g and the thickness of the layers. An enlargement of the soft caisson leads to lower maximum accelerations and spectral intensities values (see for instance Figures 2.3.3.6.6 and 2.3.4.2.1). In terms of spectral intensities and maximum accelerations (see Figures 2.3.3.6.1 c and d), the more shallow schemes tend to amplify the effects in correspondence of some frequencies more than the deeper schemes. This result is consistent with 1D analyses results. This behaviour is due both to frequencies amplification distribution, to material damping (which is more impacting by considering a deeper or larger soft caisson) and to the coupled effects of the soil mass contained into the soft caisson with the constraint effects of the surrounding soil.

Furthermore, increasing the thickness of the soft layers, the system has larger efficiencies E_I for higher SDOF period ranges; in this sense, the increase of thickness seems to correspond to a better response of the system under dynamic excitation.

In this work, schemes not fully continuous have also been analysed, to check if such scheme may have similar dynamic effects but lower impact on the static behaviour of the structure to protect. The results have shown that open caissons are never effective, and the waves penetrate through the discontinuities wherever they are.

By changing the damping ratio of the soft layers (see §2.3.3.8), only a tiny variation in the distribution of results is observed (see for instance Figure 2.3.3.8.1). This is physically consistent, as the small thickness of the soft layer (assumed equal to 1m) reduces the possibility to dissipate energy within it, regardless of the value of the damping ratio.

For the sake of simplicity, the existence of a structure at ground level has not been considered in terms of dynamic interaction between the soil and structure behaviour in this work, even though it is expected to play a relevant role. This is certainly a limit of the research at this stage, and it should be faced in the next future. By considering the existence of a structure at ground level only as a supplementary dead weight, analyses have confirmed that such a weight does not play a relevant role (see §2.3.3.5) on the dynamic response of the system. As will be recalled in the following, the effect of dead weight is on the contrary relevant for the static response of the system.

By increasing the volumetric stiffness of the grouted layers, the soft caisson is less effective (see §2.3.3.9 and §2.3.4.3), due especially to the low compressibility of the lateral soft layers which undergo lateral deformation because of vertical shear wave propagation outside the caisson. The higher the compressibility of the lateral layers the larger the decrease in horizontal dynamic actions in the soft caisson.

In the elasto-plastic analyses, two maximum amplitudes (0.05g and 0.5g) of the signals have been considered, in order to check the influence of the plastic behaviour of the natural and treated soil on the effectiveness of the reference soft caisson in filtering and reducing the dynamic effects in the protected soil mass. Two values of the shear strength angle φ'_g have been assumed (5° and 15°). The attainment of plasticization at the interface between the soft layers and the soil, as well as within the soft layers, act as a “safety valve” (Anastasopoulos, 2010). In terms of accelerations, it is very interesting to note that the more realistic elasto-plastic model leads to a more efficient behaviour of the isolating caisson for the most critical frequencies. In particular, for such frequencies, even though the signal is not largely reduced, at least it is not as amplified as in the linear elastic analyses. This result is encouraging because, also in resonance conditions, the proposed treatment has not detrimental effects. Moreover, the residual displacements due to the introduction of the soft caisson show amplitudes similar to the condition of no treatment.

5.2. Static analyses

As far as static analyses are concerned (see §3), vertical displacements have been calculated taking into account only some schemes for the caisson. Some geometrical and mechanical parameters have been varied, i.e. the length L_g or the inclination ι, the depth H_g, the shear and the volumetric stiffness and the shear resistance of the soft layers. At ground level, a gravity load distribution has been also considered, whose amplitude q_w and length L_s have been varied.

It is noted that, as largely expected, the vertical displacements are increased by assuming a larger value of the distributed load q; furthermore, a smaller load length L_s value determines a reduction in the differential settlements Δw and in the maximum relative rotation β.

By increasing the shear strength angle φ_g', lower vertical settlements w_{max} are calculated. On the other hand, soil shear stiffness does not affect the maximum vertical displacements, which are largely influenced by the volumetric deformations taking place within the horizontal soft layer, and therefore by both the thickness and the volumetric stiffness of the grouted material.

The differential displacements Δw and the relative rotations β are significantly influenced by the soft layer stiffness and the shear resistance too.

Moreover, the introduction of soft layers causes a significant reduction of the ultimate bearing capacity of the shallow foundation (see §3.1.5), which may be unacceptable for structure at ground level to protect. The reduction depends on the value of the shear strength angle of the soft layers: the ultimate load decreases as the shear strength angle decreases. Furthermore, the insertion of the soft layers causes a large increment of the vertical displacement when the ultimate condition occurs.

In the static analyses reported in this thesis (see §3.1.4), maximum vertical displacement w_{max} as large as 50cm can be observed (see Figures 3.1.4.2.2 and 3.1.4.3.3). These extremely high values are incompatible with usual structures at ground level. Anyway, these values have been calculated by considering the worst conditions of soft layers having the lowest stiffness and, contemporary, the lowest shear resistance, for an infinitely deformable foundation. Moreover, the static analyses have taken into account the deformability and the resistance of the soft grout, without considering its possible expanding capacity after injection. A last, general comment has to be done on the static effects of the soft caisson: the insertion of layers with low stiffness and shear strength angle causes displacements, distortions and a reduction of the ultimate limit load that seem to be most times unacceptable.

The results have been obtained in very conservative hypothesis, but this is not sufficient to overlook the warning posed by the numerical results, specially because the soft caisson analysed in this thesis has been conceived as a means to protect strategic buildings, often very sensitive from a structural point of view.

5.3. Laboratory activity

Two materials have been tested, in order to look for a potentially suitable soft grout.

The first material is a self-expanding polyurethane insulating foam, essentially a hydrophobic material, resistant to water, chemicals and moisture (see §4.1). Laboratory tests have been carried out to quantify its density and its shear stiffness when injected to pressures higher than the atmospheric one. The foam has shown a capacity to expand under large confining pressures keeping a very low density. Some resonant column tests have been performed to quantify the shear stiffness at low shear strains as well. Tests results indicate that the polyurethane foam cannot be considered a suitable material for soft layers, because even though it shows a low density even under high pressures, it is rather stiff, having therefore a dynamic impedance ($\eta=\rho\cdot V_s=3400\div38000$kN/(m^{2}s)) which is much larger than the one needed on the base of the results of the numerical analyses (1000÷3000 kN/(m^{2}s); see §2.3).

The second tested material is a super absorbent polymer (SAP), which is a hydrophilic network being able to absorb and retain huge amounts of water or aqueous solutions (see §4.2.2). The SAP used in this research activity is a polyacrylic acid partial sodium salt. The SAP, previously saturated with distilled or tap water has been mixed with sand, obtaining specimens characterized by different SAP percentages by weight. These specimens have been subjected to a few traditional laboratory tests (direct shear tests, ring tests, oedometer tests, triaxial tests). Even though the extremely low shear stiffness of this jelly material caused a number of difficulties in laboratory activities, starting from the preparation of the specimens, some results could be obtained: increasing the SAP quantities, a significant reduction of both the shear and the volumetric stiffness has been observed, and dynamic impedances similar to the ones suggested by the numerical analyses could be obtained.

Furthermore, the SAP reveals a capacity of swelling under load when saturated. This is an interesting result, because a potential volumetric expansion of the material, when injected deep into a soil deposit to form a soft layer, could reduce the settlements caused by its low volumetric stiffness.

5.4. Final Considerations

It has been observed that high values of the shear and volumetric stiffness of the grouted soil are detrimental for the dynamic efficiency of the treatment, but lead to lower vertical displacements. For the soft caisson with a rectangular section, this problem can be partially overcame by using a stiffer horizontal layer and very soft lateral sides (see §2.3.3.9). In terms of shear resistance of the soft layers, lower shear strength angles lead to higher efficiencies, but, on the other hand, to larger settlements. The best solution should be certainly conceived to find a smart intersection between the two requirements, which will be a function of the specific structural issue.

This new approach to the seismic risk mitigation appears a potentially valid alternative to other more conventional and invasive solutions, such as the structural reinforcement and the base isolation, and can result suited for the historical constructions for which integrity has to be preserved.

Based on these first results, it is obvious that the soft caisson must be designed taking into account also the natural frequency of the structure to be protected, considering the dynamic coupling of the input motion with the subsoil and the building response, whose dynamic interaction with the foundation soil has not been taken into account in this thesis.

Since the effectiveness of the grouting depends on the mechanical properties of the grouted layer, a much more detailed laboratory testing program is needed to characterize the behaviour of the material to be used. As previously discussed, at the moment SAP seems a good solution, but a joint research work has been recently undertaken with chemical engineers to check possible alternatives.

The research presented in this thesis has pointed out that the intriguing idea of a soft caisson may be feasible. Much more needs to be done to reach the engineering design level. The hope of the writer is to have given at least a little contribution to the aim of the final solution of the engineering problem.

List of Symbols

a = acceleration
a_y = vertical acceleration
a_{max} = maximum horizontal acceleration
$a_{max,g}$ = maximum horizontal acceleration at ground level for a given treatment
$a_{max,s}$ = maximum horizontal acceleration at ground level in the case of no treatment
$a(t)$ = accelerogram
A_{loop} = area of the hysteretic loop
A_i = Fourier amplitude
A_I = amplitude of the incident wave
A_{pist} = area of the piston
A_{spec} = area of the specimen
A_R = amplitude of the reflected wave
A_T = amplitude of the refracted (transmitted) wave
A_Δ = area of the triangular subzone of the FLAC7 mesh
$A()$ = amplification ratio
B = characteristic dimension of the foundation
c = viscous-damping coefficient
c' = cohesion
c_c = compression index
c_r = coefficients of reflexion and of
c_{rc} = re-compression index
c_s = unloading index
c_t = coefficients of transmission
$\hat{C}$ = damping matrix
C_a = Ramberg-Osgood parameter
C_u = coefficient of uniformity
CR = compression ratio
d = diameter
d_{eff} = effective diameter of the specimen
d_{fin} = final diameter of the specimen
D = damping ratio
D_{ef} = effective damping ratio
D_i = damping ratio of the ith-material
Dr = radiative damping ratio
D_{10} = grain diameter at 10% passing
D_{60} = grain diameter at 60% passing
e = void ratio
e_0 = initial void ratio
E = Young modulus
E = exposure
E_{ed} = oedometric modulus

$E_I(T)$ = efficiency parameter
f = frequency
$\overline{f}$ = frequency of the applied loading
f_n = natural frequency
F = force amplitude
$\hat{F}(t)$ = force matrix
G = shear stiffness modulus
G_0 = initial shear stiffness modulus
G_{secant} = secant shear modulus
$G_{tangent}$ = tangent shear modulus
h = height of a specimen
h_{fin} = final height of a specimen
h_{norm} = normalized value of the structural height
h_{str} = superstructure height
H = depth
H = hazard
H_B = masonry building height
H_g = maximum treatment depth
H_0 = specimen height before the load step in an oedometric test
I_a = Arias intensity
IP = plastic index
k = elastic stiffness
k^* = equivalent stiffness
k_{ni} = wave number in the i-material.
K = volumetric stiffness modulus
$\hat{K}$ = stiffness matrix
L = length
L^{max} = maximum edge-length of the triangular subzone of the FLAC7 mesh
L_g = maximum treatment length
L_s = foundation width
L_w = wavelength
m = mass
m^* = equivalent elastic spring
m_{str} = superstructure mass
M = ratio between the deviatoric stress and the effective isotropic stress
p = pressure
P = weight
q = deviatoric stress
q_w = surcharge
Q = surcharge for unit length
Q_f = quality factor
$Q_{lim,Terzaghi}$ = ultimate load for a shallow foundation as reported by the Terzaghi’s formula
Q_s = numerical ultimate load in the case of no treatment

Q_5 = numerical ultimate load in the case of $\varphi'_g=5^\circ$
Q_{10} = numerical ultimate load in the case of $\varphi'_g=10^\circ$
Q_{15} = numerical ultimate load in the case of $\varphi'_g=15^\circ$
m = Hardin constant
m_{norm} = normalized values of structural mass
$\hat{M}$ = mass matrix
M_W = moment magnitude
N = wave number
N_γ = Terzaghi's capacity factort
P = P-wave
r = radius
R = seismic risk
R_a = Ramberg-Osgood parameter
RR = re-compression ratio
s_h = horizontal displacements
s_v = vertical displacements
S = S-wave
SI = spectral intensity
$S_a(T)$ = spectral acceleration
$S_d(T)$ = spectral displacement
$Sv(T)$ = spectral velocity
SR = unloading ratio
t = time
t_g = grouted soil thickness
T = period
T^* = equivalent fundamental period
$\overline{T}$ = period of the applied loading
$\underline{T}$ = out-of-plane dimension in FLAC7 analyses
T_B = masonry building natural period (NTC, D.M. 14.I.2008)
T_m = mean period
$T_{m,g}$ = mean period for a given treatment
$T_{m,s}$ = mean period in the case on no treatment
T_p = predominant period
$T_{p,g}$ = predominant period for a given treatment
$T_{p,s}$ = predominant period in the case on no treatment
T_{str} = structural (SDOF) natural period
u = displacements in the x-directions
u_{max} = horizontal maximum displacement
v_r = relative velocity of the direct shear test equipment
V = wave velocity
V = vulnerability
V_b = base shear force
V_l = volume

$V_{l,fin}$ = final volume

V_L = Love wave velocity

V_P = compression wave velocity

V_R = Rayleigh wave velocity

V_S = shear wave velocity

V_{S30} = equivalent velocity according to EC8

$V_{S,i}$ = shear wave velocity of the i^{th}-material

$V_{s,g}$ = shear wave velocity of the soil

$V_{s,s}$ = shear wave velocity of the grouted soil

S = Hardin constant

SV = shear wave confined in the vertical plane

SH = shear wave confined in a horizontal plane

v = displacement in the y-directions

w = displacement in the z-directions

w_{max} = maximum vertical displacement

w_s = vertical displacement when the ultimate load condition occurs, in the case of no treatment

w_5 = vertical displacement when the ultimate load condition occurs, in the case of $\varphi'_g=5°$

w_{10} = vertical displacement when the ultimate load condition occurs, in the case of $\varphi'_g=10$

w_{15} = vertical displacement owhen the ultimate load condition occurs, in the case of $\varphi'_g=15°$

W_D = dissipated energy in a hysteretic loop

W_S = maximum strain energy in a hysteretic loop

α = impedance ratio

α' = the mass-proportional damping damping constant

α_{sand} = weight percentage of sand

α_{SatSAP} = weight percentage of saturated SAP

β = relative rotation

β' = stiffness-proportional damping constant

γ = Shear strain

γ_c = maximum shear strain in a hysteretic loop

γ_s = unit weight

γ_l = linear threshold

γ_v = volumetric threshold

$\bar{\gamma}_{SAP}$ = average unit weight of saturated SAP-sand mixtures

γ_{Sand} = unit weight of the sand

γ_{SatSAP} = unit weight of saturated SAP

Γ_P = transmission coefficient

Γ_{VS} = transmission coefficient

Δ = reference displacement

Δe = void ratio increment

Δh = height variation
ΔH = whole settlements at the end of a certain load increment in an oedometric test
Δl = spatial element size
Δt_d = FLAC7 explicit method time step
ΔV_l = volume variation
$\Delta V_{l,spec}\,(t)$ = volume variation of the specimen
$\Delta V_{l,pist}\,(t)$ = volume change with time of the piston coming into cell
Δw = differential displacements
$\Delta \varepsilon_v$ = volumetric deformation increment
$\Delta \sigma'_v$ = vertical load increment
Δ / L = deflection ratio
εi = linear strain in the i-direction
ε_v = volumetric deformation
η = dynamic impedance
η' = viscosity
ι = Inclination of the inclined soft layers
λ = Lamé’s constants
μ = dynamic impedance
μ_i = dynamic impedance of the i^{th}-material
ν = Poisson ratio
ϕ = phase angle
φ' = shear strenght angle
φ'_{peak} = shear strenght angle in the peak condition
φ'_{cv} = shear strenght angle at constant volume
φ'_g = shear strength angle of the grouted soil
φ'_s = shear strength angle of the soil
Φ = potential function
ξ = damping ratio
ξ_s = soil damping
ξ_g = grouted soil damping
ξ_P = equivalent damping ratio
ρ = mass density
ρ_i = mass density of the i^{th}-material
σ = normal stress
σ' = effective normal stress
σ'_a = effective axial vertical stress in a triaxial test
σ_c = cell pressure in a triaxial test
σ_i = stress amplitude of the i^{th}-wave
σ'_{v0} = vertical geostatic normal stress
σ'_{h0} = horizontal geostatic normal stress
τ = shear stress

χ_S = velocity ratio
ψ = dilatancy
Ψ = potential function
ω = angular frequency
ω_P = equivalent angular frequency
ω_x = rotation around the x-directions
ω_y = rotation around the y-directions
ω_z = rotation around the z-directions
$\bar{\omega}$ = circular frequency of the applied loading

Notes about subscripts:

∇^2 is the Laplacian operator
x, y and z refer to Cartesian coordinates
i, j, k represent general coordinate directions